The Eukaryotic Flagellum in Health and Disease

A thesis submitted for the degree of Doctor of Philosophy in the University of Oxford

Trinity Term 2007

Helen Katherine Farr

Sir William Dunn School of Pathology



Abstract

The 9 + 2 microtubule axoneme of flagella and cilia represents one of the most iconic structures built by eukaryotic cells and organisms. Some cilia are motile, whilst others serve as sensory organelles, and can variously possess 9+2, 9+0 axonemes and other associated structures. The recent emergence of ciliary dysfunction as a cause of human disease has renewed interest in these organelles, with several genomic and proteomic studies of cilia and flagella now published from various systems. I identified ten genes from such screens, and functionally characterised them in the flagellate protozoan parasite *Trypanosoma brucei*. One further gene was identified by searching a gene locus for polycystic kidney disease, a disease linked to malfunction of the primary cilium. I carried out a bioinformatic screen on the selected genes to determine their phylogenetic distribution. Cell lines expressing GFP fusion proteins were made to assess the localisation of this set of proteins, which were found to localise to a range of flagellar compartments including the axoneme and regions of the basal body. The well established inducible RNA interference system in *T. brucei* was then used to assess function of this set of proteins. In procyclic form trypanosomes the ablation of five proteins produced motility phenotypes when ablated; in some, but not all, this was accompanied by defects in axonemal ultrastructure. Two of these are closely related homologues and showed functional redundancy; when ablated independently there was no difference in motility, however simultaneous ablation produced flagellar paralysis. RNAi-mediated ablation of proteins affecting flagellar motility in bloodstream form trypanosomes produced rapid cytokinesis defects, suggesting that impairment of flagellar function may provide a novel avenue for disease control.

Acknowledgments

I would like to thank my supervisor Professor Keith Gull for his invaluable help and support. I would also like to thank Helen Dawe for all her help, Bill Wickstead for knowing everything about everything, and all the members of the Gull lab, both past and present, for all their help and for making the last four years so enjoyable and memorable. I would also like to thank Steve Kelly and my family for their support.

This work was supported by a BBSRC studentship and funding from the E. P. Abraham Trust.

Declaration

No portion of the work referred to in this thesis has been submitted in support of an application for another degree or qualification of this or any other university or other institute of learning.

Abbreviations

ATP	Adenosine triphosphate
BLAST	Basic local alignment search tool
bp	Base pair
cDNA	Complementary deoxyribonucleic acid
DAPI	4,6-diamidino-2-phenylinidole
ddH2O	Double-distilled water
DHC	Dynein heavy chain
DIC	Differential interference contrast
DNA	Deoxyribonucleic acid
dNTP	Deoxyribonucleoside triphosphate
DNA	Deoxyribonucleic acid
dsRNA	Double-stranded RNA
EDTA	Ethylenedinitrilo tetraacetic acid (disodium salt)
EGTA	Ethylenebis(oxyethylenenitrilo) tetraacetic acid
EM	Electron microscopy
FAZ	Flagellum attachment zone
FC	Flagella connector
FCS	Foetal calf serum
FLA	Flagellum adhesion glycoprotein
GFP	Green fluorescent protein
IC	Intermediate chain
IFT	Intraflagellar transport
kb	Kilobase
kDa	Kilo-dalton

kDNA	Kinetoplast DNA
LB	Luria broth
LC	Light chain
M	Molar (moles per litre)
mAb	Monoclonal antibody
MAP	Microtubule-associated protein
mRNA	Messenger ribonucleic acid
MTOC	Microtuble-organising centre
ORF	Open reading frame
pAb	polyclonal antibody
PAGE	polyacrylamide gel electrophoresis
PBS	Phosphate-buffered saline
PCR	Polymerase chain reaction
PFR	Paraflagellar rod
PIPES	Piperazine-N,N-bis (2-ethane sulphonic acid)
rRNA	Ribosomal RNA
RNA	Ribonucleic acid
RNAi	RNA interference
TEM	Transmission electron microscopy

Table of Contents

ABSTRACT **2**

ACKNOWLEDGMENTS **3**

DECLARATION **4**

ABBREVIATIONS **5**

TABLE OF CONTENTS **7**

1. INTRODUCTION **11**

1.1 PREFACE 11
1.2 EUKARYOTIC CILIA AND FLAGELLA 11
1.3 MULTIPLE PATHWAYS OF CILIOGENESIS 16
1.4 CENTRIOLE PRODUCTION 16
1.4.1 Centriole duplication *19*
1.4.2 Centriole multiplication *20*
1.5 CENTRIOLE MIGRATION AND ACQUISITION OF ACCESSORY STRUCTURES 25
1.6 DISEASES ASSOCIATED WITH DYSFUNCTIONAL CILIOGENESIS 26
1.7 TRYPANOSOMES AS A MODEL ORGANISM FOR STUDY OF FLAGELLA 28
1.7.1 Trypanosomiasis *28*
1.7.2 Life cycle of T. brucei *29*
1.7.3 Cell cycle *30*
1.8 CELL MORPHOGENESIS 32
1.8.1 Subpellicular microtubules *32*
1.8.2 Flagellum attachment zone *33*
1.8.3 Flagellar pocket *35*
1.8.4 Flagella connector *35*
1.9 THE EUKARYOTIC FLAGELLUM 37
1.9.1 Intraflagellar Transport (IFT) *37*
1.9.2 Dynein arms *39*
1.9.3 Paraflagellar Rod *43*
1.10 INVESTIGATING THE FLAGELLUM 44
1.10.1 Genomic methods *44*
1.10.2 Proteomes *46*
1.10.3 Mutants *48*

2. MATERIALS AND METHODS **52**

2.1 CELL LINES AND CELL CULTURE 52
2.1.1 Transformation of Trypanosomes *52*
2.1.2 Culture of trypanosomes *52*
2.2 MOLECULAR BIOLOGY 53
2.2.1 DNA constructs *53*
2.2.2 Bacterial cell lines and transformation *54*
2.2.3 Plasmid DNA isolation *55*
2.2.4 Genomic DNA isolation *55*
2.2.5 Restriction digests, Gel extraction of DNA fragments and DNA ligation *55*
2.2.6 Polymerase Chain Reaction (PCR) *56*
2.2.7 qRT-PCR *56*
2.3 LIGHT MICROSCOPY 57
2.3.1 Immunofluorescence *57*
2.3.2 Fluorescence microscopy of cells expressing GFP *58*
2.3.3 Videomicroscopy and analysis of motility *59*
2.4 ELECTRON MICROSCOPY 59
2.4.1 Preparation of samples for thin section Transmission Electron Microscopy (TEM) *59*
2.4.2 Scanning Electron Microscopy (SEM) *60*
2.5 PROTEIN BIOCHEMISTRY 61
2.5.1 Preparation of cell extracts *61*

2.5.2 SDS-polyacrylamide gel electrophoresis ... *62*
2.5.3 Western blotting and immunodetection ... *62*

3. SURVEY OF FLAGELLAR PROTEINS ... **67**

3.1 USING FLAGELLAR PROTEOMES TO IDENTIFY NOVEL FLAGELLAR PROTEINS ... 67
3.2 SELECTED GENE SET ... 68
3.3 APPLYING THE RNAI PHENOTYPE TEST ... 71
3.3.1 Localisation studies ... *74*
3.4 PROTEINS IDENTIFIED FROM A T. BRUCEI FLAGELLAR PROTEOME (TBFP) ... 74
3.4.1 TAX-3 ... *74*
3.5 PROTEINS THAT ARE PREDICTED TO BE ASSOCIATED WITH THE BASAL BODY ... 78
3.5.1 Cep164 ... *78*
3.5.2 Cep76 ... *80*
3.5.3 WDR16 ... *81*
3.5.4 TbWDR67 ... *83*
3.6 A PROTEIN IDENTIFIED IN SEARCHING A LOCUS LINKED TO CILIARY DISEASE ... 84
3.6.1 Meckelin ... *84*
3.7 CONCLUSIONS AND DISCUSSION ... 85

4. CHARACTERISATION OF THE PARKIN CO-REGULATED GENE PRODUCT, PACRG ... **91**

4.1 INTRODUCTION ... 91
4.2 TWO PACRG FAMILY MEMBERS IN TRYPANOSOMA BRUCEI ... 91
4.3 ABLATION OF BOTH TBPACRG MRNAS PRODUCES SLOW GROWTH AND PARALYSIS IN PROCYCLIC FORM TRYPANOSOMES ... 93
4.4 TBPACRG AB RNAI INDUCTION CAUSES LOSS OF OUTER DOUBLET MICROTUBULES ... 97
4.5 OUTER DOUBLET MICROTUBULE NUMBER DECREASES TOWARDS THE DISTAL TIP OF THE FLAGELLUM ... 99
4.6 GFP:TBPACRG FUSION PROTEINS LOCALISE TO THE AXONEME ... 102
4.7 RNAI ABLATION OF PACRG A AND B IN BLOODSTREAM FORM TRYPANOSOMES ... 104
4.8 CONCLUSIONS AND DISCUSSION ... 109

5. CHARACTERISATION OF TRYPANOSOME AXONEMAL PROTEIN-1 ... **118**

5.1 TAX-1 IS WELL CONSERVED IN FLAGELLATE EUKARYOTES ... 118
5.2 GFP:TY:TAX-1 FUSION PROTEIN LOCALISES TO THE AXONEME ... 120
5.3 RNAI AGAINST TAX-1 IN PROCYCLIC FORM T. BRUCEI CELLS REDUCES CELL MOTILITY ... 120
5.4 EXAMINATION OF RNAI INDUCED AXONEMES BY TRANSMISSION ELECTRON MICROSCOPY (TEM) 123
5.5 RNAI AGAINST TAX-1 IN BLOODSTREAM FORM T. BRUCEI CELLS CAUSES CYTOKINESIS DEFECTS 127
5.6 CONCLUSIONS AND DISCUSSION ... 131

6. CHARACTERISATION OF TRYPANOSOME AXONEMAL PROTEIN-2 ... **136**

6.1 TAX-2 IS EVOLUTIONARILY CONSERVED IN MANY FLAGELLATES ... 136
6.2 TAX-2 LOCALISES TO THE AXONEME OF T. BRUCEI ... 138
6.3 ABLATION OF TAX-2 AFFECTS MOTILITY IN PROCYCLIC FORM TRYPANOSOMES ... 139
6.4 LOSS OF GFP:TY:TAX-2 FROM THE AXONEME AFTER RNAI INDUCTION ... 139
6.4.1 GFP:TY:TAX-2 is lost from the distal tip of the axoneme ... *142*
6.4.2 Analysis of GFP:TY:TAX-2 loss indicates a post-cytokinesis flagellum growth phenomenon *145*
6.5 TAX-2 RNAI CAUSES A RANGE OF AXONEMAL DEFECTS ... 146
6.6 TAX-2 RNAI INDUCTION IN BLOODSTREAM FORM CELLS CAUSES DEFECTS IN GROWTH AND CYTOKINESIS ... 149
6.7 CONCLUSIONS AND DISCUSSION ... 149

7. CHARACTERISATION OF TBAAT-1 ... **156**

7.1 TBAAT-1 IS EVOLUTIONARILY CONSERVED IN MANY FLAGELLATES ... 156
7.2 GFP:TY:TBAAT-1 FUSION PROTEIN LOCALISES TO THE AXONEME IN T. BRUCEI ... 158
7.3 RNAI ABLATION OF TBAAT-1 IN PROCYCLIC FORM TRYPANOSOMES ... 158
7.4 TBAAT-1 RNAI INDUCTION DOES NOT AFFECT AXONEME STRUCTURE ... 161
7.5 RNAI ABLATION OF TBAAT-1 IN BLOODSTREAM FORM TRYPANOSOMES ... 164
7.6 CONCLUSIONS AND DISCUSSION ... 166

8. DISCUSSION **169**

8.1 IDENTIFYING THE COMPONENTS OF CILIA AND FLAGELLA 169
8.2 FROM COMPONENTS TO FUNCTION IN MORPHOGENESIS AND DISEASE 172

REFERENCES **176**

APPENDIX **176**

CHAPTER 1

INTRODUCTION

Eukaryotic cilia and flagella

1 1. Introduction

1.1 Preface

The first part of this introduction contains excerpts from a collaborative review written jointly by Helen Dawe and myself. The electron micrographs of rat trachea in Fig. 1.3 were contributed by Alison Faragher. This was published as: Dawe, H. R., Farr, H. and Gull, K. (2007) Centriole / basal body morphogenesis and migration during ciliogenesis in animal cells. *J Cell Sci* 120, 7-15

1.2 Eukaryotic cilia and flagella

Cilia are found on virtually all cells in the human body; yet despite the importance of these organelles many aspects of their formation and function have remained enigmatic. Cell biology textbooks usually pronounce that cilia and flagella are highly conserved structures containing a 9+2 microtubule axoneme made up of nine outer doublet microtubules and two single central pair microtubules (Fig. 1.1A) surrounded by a ciliary membrane. Whilst it is true that this basic structure is well conserved throughout eukarya, and that 9+2 and 9+0 (lacking the central pair) axonemes are the most common, there are many variations in either the axoneme itself or in the presence of extra-axonemal structures (Fig. 1.1D) that allow cilia, either motile or non-motile, and flagella to perform specialised functions in diverse organisms and cell types (Afzelius, 2004).

The terms cilia and flagella are sometimes used interchangeably but there are differences: first, only one or two flagella are usually present on cells while motile cilia are usually found in higher multiples. This is a generalisation, however, as the

Figure 1.1

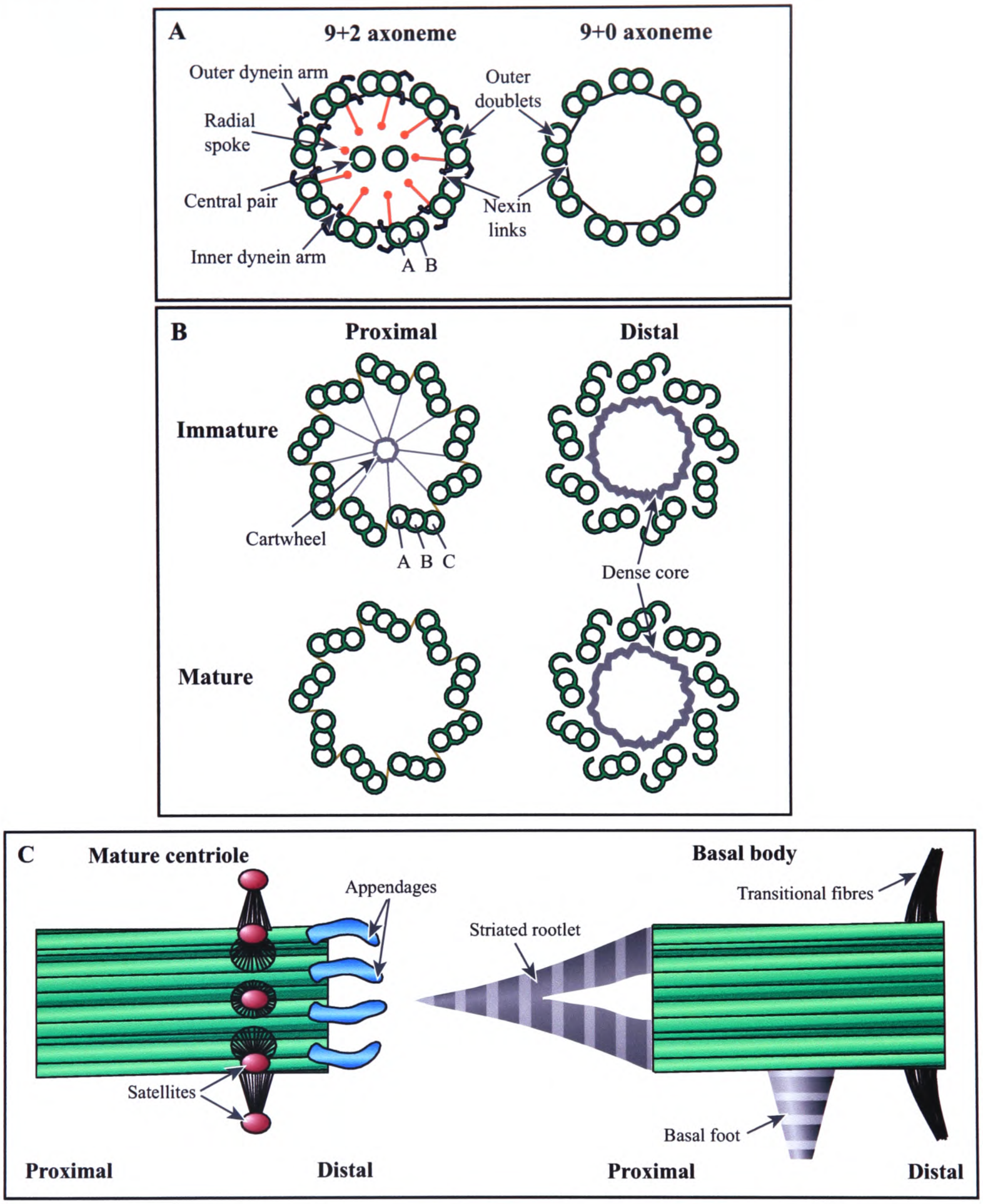


Figure 1.1 Structures of centrioles and cilia.
(A) The structure of the canonical motile 9+2 axoneme and its most common variation, the immotile 9+0 axoneme. (B) Schematic of a transverse section through the immature and mature centrioles. (C) Schematic of a longitudinal view of the mature centriole, showing the appendages, and a basal body with accessory structures.

sperm of the fern *Marsilea* and the gymnosperm Ginkgo are multiflagellate, with up to a thousand flagella (Myles, 1975; Vaughn and Renzaglia, 2006). Second, cilia move with a characteristic ciliary beat that is distinguished by an effective stroke followed by a recovery stroke, while flagellar motility usually consists of successive waves originating at either the base or the tip of the flagellum and propagated along its length. Again, there are exceptions to this and many cells, including the single-celled parasitic protozoan *Trypanosoma brucei*, are capable of both flagellar and ciliary beating (Gadelha et al., 2007). Third, cilia are often all of one developmental state while in cells the multiple flagella may often be at different stages of development. Fourth, the term cilium is usually used to describe structures shorter than flagella. Fifth, rows of cilia can fuse to form specialised cirri or membranelles.

Flagella often move individual cells, such as mammalian sperm and protists. Cilia can be motile or non-motile and occur singly or in multiples. Multiple cilia are generally motile. They move single-celled protists such as *Tetrahymena* and, in metazoa, material such as mucosal fluids past epithelial cell layers. Single cilia are normally non-motile - the primary cilia on the surface of most mammalian cells are the most common (Wheatley et al., 1996), and much evidence suggests these play pivotal roles in normal tissue homeostasis and disease (reviewed by Davenport and Yoder, 2005), cilium-generated Hedgehog and Wnt signalling being critical during development (reviewed by Scholey and Anderson, 2006). Certain tissues contain specialised cilia, including motile and non-motile nodal cilia (which are found exclusively in the embryonic node), the transient non-motile kinocilium of the inner ear and the long-lived, highly modified non-motile connecting cilium of the retina.

As rehearsed above, most axonemes consist of a ring of nine outer doublet microtubules held together by nexin linkages (Fig. 1.1); this is the basic structure of the primary cilium. Motile cilia and flagella generally additionally have two singlet central pair microtubules, radial spokes and dynein arms, which are the molecular motors that enable microtubule sliding and consequent cilia or flagella beating. The dynein arms are attached to the A-tubule of each doublet such that their motor head domains are in close proximity to the B-tubule of the neighbouring doublet (Brenner and Anderson, 1973; Gibbons and Gibbons, 1973). With the exception of early ultrastructural observations of cilia and flagella, much work has been carried out in single-celled organisms, particularly the green algae, *Chlamydomonas reinhardtii* (reviewed by Dutcher, 1995; Silflow and Lefebvre, 2001). Until recently the molecular composition of cilia and flagella was largely obscure. Using a combination of forward genetic mutational analysis and electrophoresis the *C. reinhardtii* flagella were predicted to contain 250 polypeptides (reviewed by Silflow and Lefebvre, 2001). More recent studies on a variety of model organisms have used proteomic (Ostrowski et al., 2002; Andersen et al., 2003; Keller et al., 2005; Pazour et al., 2005; Smith et al., 2005; Broadhead et al., 2006), transcriptomic (Blacque et al., 2005; Stolc et al., 2005) and genomic (Avidor-Reiss et al., 2004; Li et al., 2004; Efimenko et al., 2005) approaches and to suggest that the number is much greater. A central repository of cilia / flagella and basal body components identified in these studies can be found at the Ciliary Proteome Web Server (http://www.ciliaproteome.org/, Gherman et al., 2006).

Studies primarily in algae have led to a model of ciliary / flagellar motility where coordinate action of the central pair, radial spokes and dynein arms enable motility.

It has been proposed that the central pair signals through the radial spokes to provide an asymmetric stimulus of the dynein motors associated with each of the outer doublet microtubules that enables a flagellar bend to be generated. One hypothesis for how this stimulus is generated relies on the rotation of the central pair microtubules observed in *Chlamydomonas* and *Paramecium* (Omoto and Kung, 1979; Omoto and Kung, 1980; Mitchell, 2003). However, this paradigm does not work for all systems: central pair rotation is not found in all organisms (Tamm and Tamm, 1981; Sale, 1986; Gadelha et al., 2006), raising the question of how the central pair regulates motility in these systems.

All cilia are extended from a basal body. The Henneguy-Lenhossek theory, first postulated in 1898 and generally accepted today, proposed that these basal bodies are analogous to the mitotic centrioles (Henneguy, 1898; Lenhossek, 1898). Indeed the primary cilium is extended from a single basal body analogous to the pre-existing mature centriole in the cell. In contrast, in multi-ciliated epithelia, ciliogenesis begins with centriole multiplication that yields up to several hundred basal bodies. In both cases migration of the centrioles to the apical cell surface and acquisition of accessory structures follows. Once a centriole has docked with the cell membrane, it is known as a basal body. Finally, an axoneme is extended to form a cilium. Despite the overall similarities there are distinct differences in the mechanisms of formation of single cilia and cilia of multi-ciliated cells in terms of cell cycle regulation and control of centriole number. Our knowledge of the molecular mechanisms of ciliogenesis is largely restricted to intraflagellar transport (IFT), the bidirectional movement of particles along the doublet microtubules, which elongates and maintains the cilium. Many excellent reviews on IFT are available (e.g. Rosenbaum

and Witman, 2002; Scholey, 2003). I will cover IFT in later sections but here I will focus on the earlier stages of ciliogenesis, comparing the ultrastructural details and molecular events that occur during formation of ciliated epithelia and solitary primary cilia.

1.3 Multiple pathways of ciliogenesis

At least six mechanisms for generation of cilia and flagella exist and the resulting cilia or flagella can be transient or long-lived (Flock and Duvall, 1965; Sorokin, 1968; Anderson and Brenner, 1971; Brenner and Anderson, 1973; Lemullois et al., 1988; Sherwin and Gull, 1989; Sobkowicz et al., 1995). These enable the production of many kinds of cilia, as well as sperm flagella (Fig. 1.2). They require various mechanisms for accurate control of centriole number, and there are variations in cell cycle control, in the timing of cilium production in the cell cycle, in the timing of centriole maturation and in whether a probasal body is associated with the cilium or flagellum basal body. My focus here is on the five major mechanisms for formation of cilia; sperm flagella will not be dwelt upon further.

1.4 Centriole Production

The centriole is a cylindrical structure 0.4μm long and 0.2μm in diameter, composed of microtubule triplets with nine-fold radial symmetry. The triplets are positioned around a cylindrical core with a slight twist, and are composed of heterodimers of α- and β-tubulin. The immature centriole has a unique feature called the cartwheel (Vorobjev and Nadezhdina, 1987), made up of a central rod linked to the inner (A) tubule of each triplet by spokes (Fig. 1.1 B). The mature centriole also has distinct

Figure 1.2

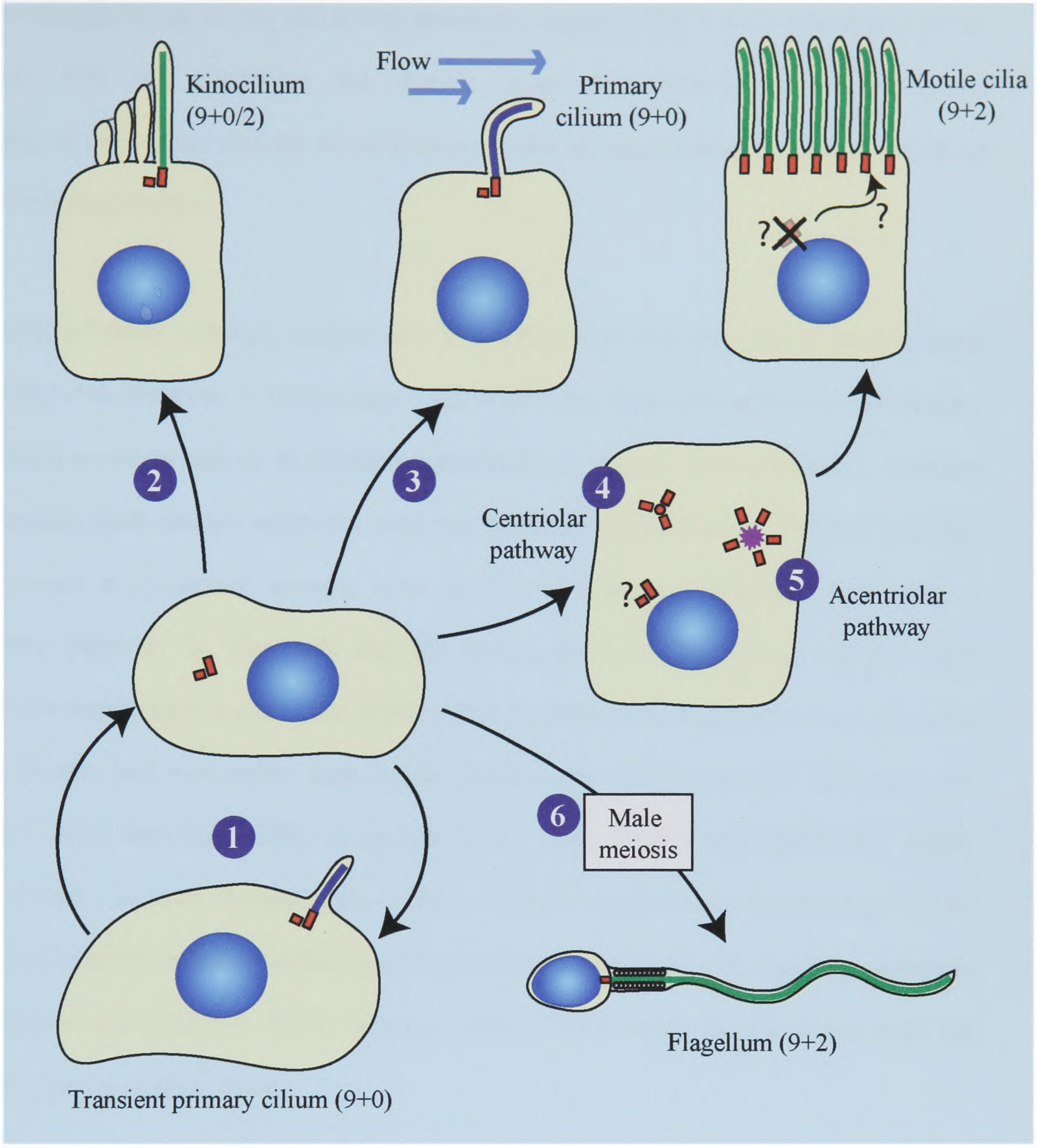


Figure 1.3 Multiple pathways of ciliogenesis.
Quiescent somatic cells use a single pre-existing mature centriole to subtend a transient primary cilium (Fig. 1 (1)) lacking central pair microtubules, which is lost as the cell re-enters the cell cycle. In differentiated cells, several different types of single cilia can be produced from a mature centriole, such as the temporary (9+2 or 9+0) kinocilium (2), which may or may not possess the central pair microtubules (Flock and Duvall, 1965; Sobkowicz et al., 1995) and the primary (9+0) cilium produced on the luminal epithelium of kidney tubules (3). (4) and (5) show the pathways that produce several hundred cilia in epithelial cells in the mammalian airway. Here, hundreds of centrioles are produced, duplicated either using the pre-existing centriole as a template (4), or formed via a non-templated method (5). (6) shows the sperm flagellum produced in male meiosis. Green denotes 9+2 axonemes; dark blue denotes 9+0 axonemes; centrioles are red; deuterosome is purple.

appendages found at the distal and subdistal regions (Fig. 1.1 C, (Paintrand et al., 1992). The two centrioles are closely associated, usually in an orthogonal configuration surrounded by an amorphous mass of pericentriolar material (PCM) to form the centrosome.

Most differences between ciliogenesis in primary cilia and the cilia of multi-ciliated epithelia are observed in centriologenesis: a primary cilium forms from a pre-existing centriole whereas cilia of multi-ciliated epithelia require de novo production of many centrioles. Multi-ciliated epithelial cells are terminally differentiated. Primary cilia can be formed in quiescent somatic cells, or in proliferating populations that make a primary cilium in G_1. For cells that will form a primary cilium (Fig. 1.2 (1) - (3)), centriole duplication is cell cycle related. The centriole pair duplicates once per cycle at S phase and maturation (see below) occurs later (Vorobjev and Chentsov Yu, 1982; Lange and Gull, 1996; Hinchcliffe et al., 1998; Sluder and Hinchcliffe, 1998). In contrast, centriole multiplication in cells that will become multi-ciliated (Fig. 1.2 (4) and (5)) is differentiation related and often independent of the pre-existing centrioles (Anderson and Brenner, 1971; Dirksen, 1991). In this case the centrioles that are made mature as they form.

Once formed, centrioles of ciliated cells migrate to the cell surface. For cells that form a primary cilium (Fig. 1.2 (1) and (3)), the centriole remains associated with its procentriole daughter throughout ciliogenesis (Sorokin, 1968; Hagiwara et al., 2002; Alieva and Vorobjev, 2004; Jensen et al., 2004); those in multi-ciliated epithelia and the centriole subtending the kinocilium of the inner ear do not have associated procentrioles (Sorokin, 1968; Anderson and Brenner, 1971; Dirksen, 1971; Kalnins

et al., 1972; Hagiwara et al., 1992; Sobkowicz et al., 1995; Abughrien and Dore, 2000). During maturation, centrioles acquire additional appendages such as transitional fibres and basal feet that stabilise the centriole/basal body, and IFT extends and maintains the axoneme. This occurs in both primary cilia and cilia of multi-ciliated cells (Rosenbaum and Witman, 2002).

1.4.1 Centriole duplication

During the cell division cycle the centrosome duplicates just before S phase; duplication requires the immature centriole-associated protein Centrobin (Zou et al., 2005). Several serine/threonine kinases are implicated in the process, including Polo-like and Aurora kinases (Lane and Nigg, 1996; Hannak et al., 2001; Berdnik and Knoblich, 2002). A procentriole (Gall, 1961; Andre and Bernhard, 1964; Renaud and Swift, 1964; Mizukami and Gall, 1966) forms from the side of each centriole and elongates throughout S phase so that the cell possesses two pairs of centrioles as it enters G2 phase. Only the mature centriole can produce a cilium. Maturation occurs over 1.5 cell cycles, the maturing centriole acquiring the unique fibrous distal and subdistal appendages mentioned above. Several protein components of these appendages have been identified, including ninein (Mogensen et al., 2000), ε-tubulin (Chang et al., 2003), centriolin (Gromley et al., 2003) and CEP110 (Ou et al., 2002). Cenexin is found exclusively at the mature mother centriole and its acquisition at the G2/M transition is a marker for maturation (Lange and Gull, 1995) and essential for appendage production (Ishikawa et al., 2005).

Centrioles are inherited by daughter cells in a semi-conservative manner (Kochanski and Borisy, 1990). Centrosome duplication and DNA regulation are coordinated by a

complex pathway involving cyclin-E-Cdk2 (Hinchcliffe et al., 1999; Karsenti, 1999; Meraldi et al., 1999). Centrosome duplication is stimulated by Cdk2. Factors required for entry into S phase, such as Cdk2 and E2F, are required for centrosome duplication, and phosphorylation of the tumour suppressor Rb is also needed (Meraldi et al., 1999). Unduplicated G1 centrosomes are duplication-competent, whereas G2 centrosomes placed under identical experimental conditions are not. This strongly suggests the centrosome itself blocks further centrosome duplication (Wong and Stearns, 2003); this might involve a physical connection between the mature and immature centrioles that prevents duplication until after mitosis (Tsou and Stearns, 2006). In most cell lines the centrosome will not re-duplicate during S phase, even in cells treated with hydroxyurea to prolong S phase (Balczon et al., 1995; Meraldi et al., 1999). However, in certain cell lines containing mutant p53, extended cell cycle arrest leads to centrosome accumulation (D'Assoro et al., 2004), suggesting that centrosome duplication is uncoupled from cell division checkpoints in these cells.

1.4.2 Centriole multiplication

Multi-ciliated epithelial cells such as those in the mammalian trachea can each produce 200-300 centrioles during ciliogenesis. Two mechanisms of centriole production have been identified: the centriolar and acentriolar pathways, both of which can occur in a single cell (reviewed by Beisson and Wright, 2003). In contrast to centriole duplication during the cell division cycle, these pathways are linked to differentiation rather than proliferation, and multiple procentrioles are produced simultaneously, making this process distinct from the centriole duplication described above. In the centriolar pathway (Fig. 1.2 (4)), new centrioles are produced around

an existing centriole. Unlike cell-cycle-dependent centriole duplication, however, more than one procentriole may be produced around a single centriole (Sorokin, 1968; Steinman, 1968; Anderson and Brenner, 1971; Chang et al., 1979; Hagiwara et al., 1992). Variations in the number of procentrioles observed could be attributable to the plane of the electron micrograph: among several procentrioles surrounding a centriole, two or three are seen only in glancing section (Sorokin, 1968); serial thin section electron microscopy will be necessary to resolve the exact number of procentrioles formed in the centriolar pathway. The origin of the core centriole that produces these procentrioles is unclear. Neither the cartwheel, a marker for immature centrioles, nor appendages, present around mature centrioles, appear to be present. Thus the identity of the core centriole is unknown.

In the acentriolar pathway (Fig. 1.2 (5)), centrioles form around intermediary structures rather than an existing centriole (Dirksen and Crocker, 1966; Sorokin, 1968; Steinman, 1968; Anderson and Brenner, 1971; Dirksen, 1971; Kalnins et al., 1972; Chang et al., 1979; Lemullois et al., 1988; Hagiwara et al., 1992). The terminology for these intermediary structures is confused in the literature. Here, I use the nomenclature system of Chang (1979) for the granular structures observed at the first stage of the acentriolar pathway. So-called dense granules (Fig. 1.3 A) form clusters that can be associated with the existing centriole. Some molecular components of these dense granules have been identified: PCM-1 has been detected in them (Kubo et al., 1999) in addition to the striated rootlet protein p195 (Hagiwara et al., 2000). Centrin proteins localise close to granules in ciliogenic epithelial cells, suggesting that they may be involved in an early stage of the acentriolar pathway (Laoukili et al., 2000). Dense granule clusters may condense to

produce deuterosomes (Fig. 1.3 B, arrowheads), around which procentrioles (Fig. 1.3 B, P) develop. Two types of deuterosome exist, classified as solid or hollow on the basis of their ultrastructural appearance; there are organismal and size differences between the two (Sorokin, 1968; Dirksen, 1971; Dirksen, 1991; Hagiwara et al., 1992). The number of procentrioles around a deuterosome correlates with its size (Sorokin, 1968; Anderson and Brenner, 1971; Kalnins et al., 1972; Chang et al., 1979; Hagiwara et al., 1992). Serial thin section electron microscopy reveals different numbers of procentrioles in each section (Anderson and Brenner, 1971), showing that not all procentrioles produced by the acentriolar pathway are visible in a single section. Thus the centriolar pathway may also produce more procentrioles than are seen in a single section, and there may be less variability in procentriole number in both the centriolar and acentriolar pathways in vivo than previously thought.

What happens to the pair of centrioles initially present in the cell during centriole multiplication? Several possible scenarios exist. First, the centriole pair could migrate to the surface and extend one of the motile cilia. This would imply that all centrioles are identical and that global control of ciliogenesis exists. Second, the two centrioles could migrate to the surface and extend a distinct, primary cilium prior to centriole multiplication and subsequent generation of the multiple motile cilia. This would suggest that an individual cell can form both 9+0 and 9+2 cilia, albeit at slightly different times. This phenomenon has been observed (Sorokin, 1968; Anderson and Brenner, 1971; Brenner and Anderson, 1973; Lemullois et al., 1988), and the presence of developing procentrioles around the mature basal body subtending a primary cilium (Sorokin, 1968; Anderson and Brenner, 1971) makes it

Figure 1.3

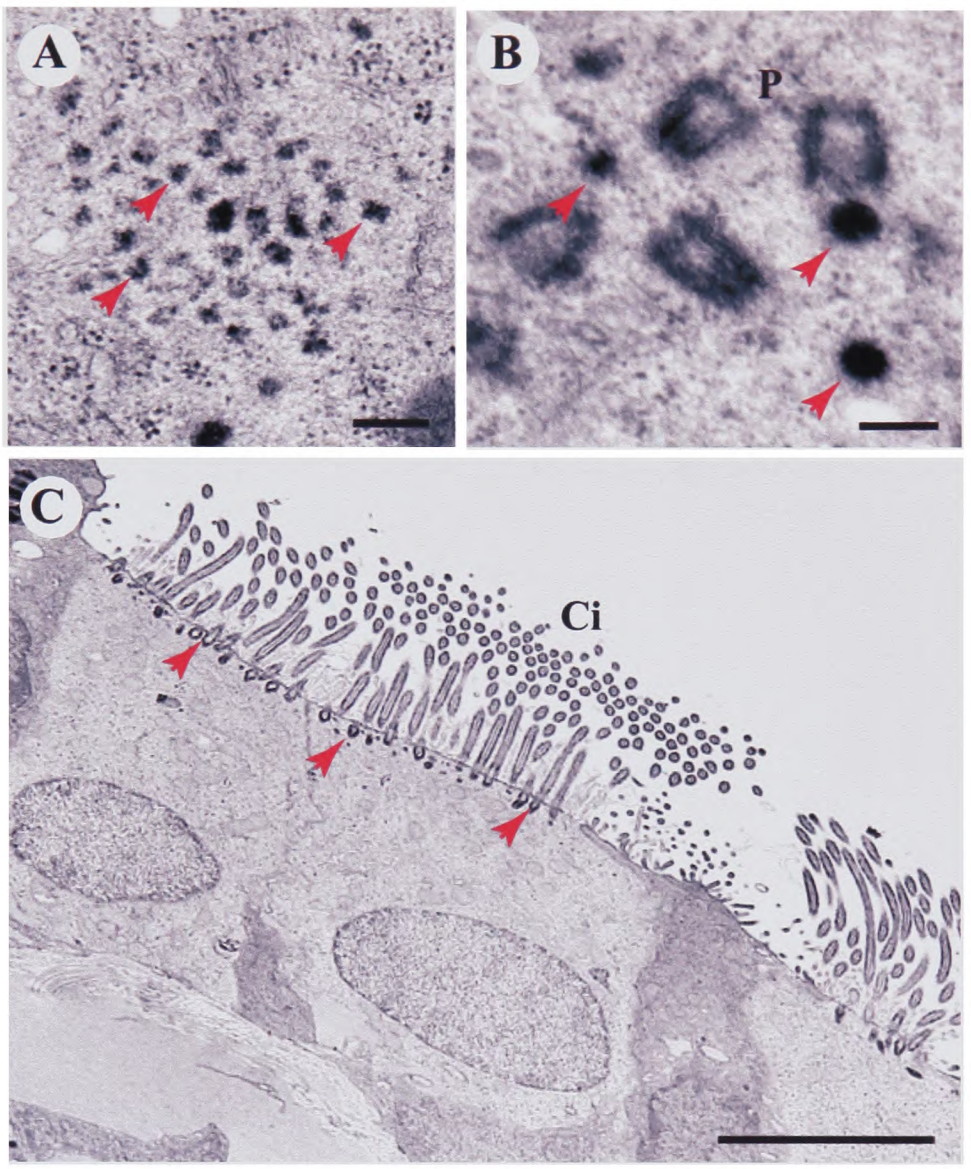


Figure 1.3 Ciliogenesis in rat trachea.
(A) The first visible stage in the acentriolar pathway is the appearance of dense granules (arrowheads). (B) Procentrioles (P) form around deuterosomes (arrowheads). (C) Mature ciliated cells. The procentrioles have docked with the apical membrane to become basal bodies (arrowheads) and have extended cilia (Ci). Scale bars (A) and (B) = 200nm; (C) = 5µm.

likely that the same cell goes on to produce multiple cilia. In this case, the primary cilium is probably only transient, because none has been found in mature ciliated cells (Lemullois et al., 1988); it may function to pattern the apical surface in preparation for formation of motile cilia. The ultimate fate of its basal body – whether it later subtends a motile cilium or returns deeper into the cytoplasm - is unknown, but if it goes on to subtend a 9+2 cilium it is likely that the information needed to template a 9+0 cilium versus a 9+2 cilium does not lie within the centriole. Third, the mature centriole could remain in the cytoplasm. This would imply that existing centrioles are different from those produced by the centriolar and acentriolar pathways and that ciliogenesis is controlled at the level of individual centrioles. Although several studies have failed to observe isolated centrioles in ciliated cells (Lenhossek, 1898; Anderson and Brenner, 1971; Lemullois et al., 1988), one study has observed a centriole deep in the cytoplasm of a ciliated cell (Kalnins et al., 1972). Final resolution of these important questions will require tracking of individual centrioles in live cells during ciliogenesis.

Is cell-cycle-dependent duplication or centriole multiplication the default pathway in cells? Given the deleterious consequences of uncontrolled centriole proliferation, it could be argued that cell-cycle-dependent centriole duplication represents the default pathway. On the other hand, whereas most cells lacking centrioles undergo cell cycle arrest (Hinchcliffe et al., 2001), HeLa cells in which the centrosome has been surgically removed can produce multiple centrioles throughout the cytoplasm (La Terra et al., 2005). This implies that an existing centriole prevents production of further centrioles, and that newly synthesised centriole precursors destined for the existing centrosome will, in its absence, form multiple foci throughout the cytoplasm

that produce centrioles independently of each other. This suggests that increased centriole production might be the default pathway for cells and that this is suppressed by an existing centriole. However, it is apparent that centriole production in HeLa cells must be uncoupled from the cell cycle and thus these cells do not necessarily represent the in vivo state.

1.5 Centriole migration and acquisition of accessory structures

How centrioles migrate during primary cilium formation remains unresolved, although the cytoskeleton is likely to be involved. Microtubules position the interphase centrosome (Burakov et al., 2003). The Rho-associated protein kinase p160ROCK maintains the position of the mature centriole (Chevrier et al., 2002), however, the upstream and downstream events remain unknown. In multi-ciliated cells, duplicated centrioles migrate towards the apical surface, where they dock to become basal bodies. Actin and myosin are associated with centrioles or centriolar material (Klotz et al., 1986; Lemullois et al., 1987; Lemullois et al., 1988), and treatment of ciliogenic oviducts with agents that inhibit actin polymerisation (Boisvieux-Ulrich et al., 1990) or myosin function (Boisvieux-Ulrich et al., 1987) prevents centriole migration, while drugs that target the microtubule network do not directly stop migration (Boisvieux-Ulrich et al., 1989).

After migration, centrioles attach to the membrane and serve as basal bodies for ciliary elongation. Ultrastructural analysis has uncovered a plethora of accessory structures that are associated with centrioles and basal bodies (Fig. 1.1 C), including centriolar satellites, transitional fibres, striated rootlets and basal feet, that are associated with both primary cilia and multi-ciliated epithelia. The timing of

acquisition of these structures is unclear: transitional fibres and/or basal feet are found associated with migrating centrioles in some studies (Anderson and Brenner, 1971; Lemullois et al., 1988) but not in others (Frisch and Farbman, 1968; Hagiwara et al., 1992). However, when centriole migration is perturbed (Boisvieux-Ulrich et al., 1990), the centrioles that remain cytoplasmic acquire accessories. Therefore, subcellular location is not the determining factor.

1.6 Diseases associated with dysfunctional ciliogenesis

An increasing number of genetic diseases are associated with defects in ciliogenesis or ciliary function (reviewed by (Afzelius, 2004; Badano et al., 2005; Badano et al., 2006). These comprise a diverse group of pathologies including cystic kidney disease, infertility, retinal degeneration, hydrocephalus, laterality defects, and chronic respiratory problems. More recent work has identified cilia and basal body dysfunction as the underlying cause of various systemic diseases, including Bardet-Biedl, Alstrom, Orofaciodigital and Meckel syndromes (Andersen et al., 2003; Ansley et al., 2003; Romio et al., 2004; Kyttala et al., 2006), and these have expanded the range of ciliopathy phenotypes to include obesity, diabetes, hypertension and cardiac abnormalities (Badano et al., 2006). The affected tissues vary between diseases but all have motile or immotile cilia.

The gene products implicated in the ciliopathies can affect ciliary function for example motility or signalling, or affect ciliogenesis itself. Mice lacking the transcription factor FoxJ1 have laterality defects and a loss of cilia (Chen et al., 1998) due to a failure in centriole migration (Brody et al., 2000; Gomperts et al., 2004). A second protein, Seahorse, is implicated in polycystic kidney disease (Sun

et al., 2004) and is required to regulate basal body duplication in the parasitic protozoan *Trypanosoma brucei* (Morgan et al., 2005). Seahorse (also known as TbLRTP) localises to the distal part of the trypanosome basal body. While overexpression of the protein suppresses flagellum assembly, RNA-interference experiments result in excess basal bodies, suggesting that Seahorse is a negative regulator of basal body duplication. Polycystic kidney disease and Bardet-Biedl syndrome can be caused by a failure in IFT (Pazour et al., 2000; Blacque et al., 2004; Li et al., 2004; Ou et al., 2005), the final stage of ciliogenesis. To date, eleven genes are known to cause Bardet-Biedl Syndrome; it is now known that of one of these, BBS4 functions as an adaptor protein to the p150glued protein to help recruit PCM1 to the centriole (Kim et al., 2004). Finally, mice lacking the Orofaciodigital syndrome gene *OFD1* show defective cilium formation (Ferrante et al., 2001). Based on the phenotypic overlap with Bardet-Biedl syndrome, a role for OFD1 in IFT has been proposed (Ferrante et al., 2001), however, as OFD1 is a centrosomal/basal body protein (Romio et al., 2004), it could also function in earlier stages of ciliogenesis.

Much work on elucidating the biology of cilia disease genes has been carried out in model organisms (e.g. Pazour et al., 2000; Blacque et al., 2004; Sun et al., 2004; Dawe et al., 2005). However, the question of why gene malfunction leads to some tissues being affected and not others in mammalian systems is difficult to address in single-celled models. It is likely that tissue-specific transcriptional control plays a part. Mice lacking the polycystic kidney disease gene product polycystin 1 have polycystic kidneys but no laterality defects, correlating with polycystin 1 absence in nodal cilia (Karcher et al., 2005). Turnover is also likely to be important. Ciliary

tubulin continually turns over (Stephens and Lemieux, 1999), however the rate varies between tissues. The stability of the cilium and/or the cell is also likely to vary from tissue to tissue. Comparison of published flagellar proteomes (Ostrowski et al., 2002; Pazour et al., 2005; Smith et al., 2005; Broadhead et al., 2006) from a number of model organisms reveals a surprising diversity despite overall structural conservation (Broadhead, 2006 #2), suggesting the canonical axonemal structure is dependent on a central cohort of conserved proteins with organism-, cell- and tissue-type elaborations. This diversity could contribute to tissue-specific functional specialisation.

1.7 Trypanosomes as a model organism for study of flagella

1.7.1 Trypanosomiasis

The protozoan parasite *Trypanosoma brucei* is the causative agent of disease in both humans and livestock in a large area of subsaharan Africa covering some 36 countries. There are three subspecies: *T. brucei rhodiense* which is prevalent in eastern and southern Africa, *T. b. gambiense* which is prevalent in western and central Africa and *T. b. brucei* which is responsible for Nagana in cattle. The parasites are transmitted between mammalian hosts by the bite of the Tsetse fly, and once in the bloodstream replicate and may cross the blood–brain barrier, leading to central nervous system symptoms and finally coma – giving rise to the name sleeping sickness – and death if untreated. Bloodstream form trypanosomes evade the host immune system by the mechanism of antigenic variation (Taylor and Rudenko, 2006).

The area at risk of trypanosomiasis is huge with over 60 million people at risk of contracting the disease. However, with much of this area being rural surveillance levels for the disease are very low, making it difficult to estimate the number of cases. Estimates suggest that the number of cases is between 300 – 500,000 annually, with 66,000 deaths. There is an urgent need for improved treatment for sleeping sickness as current drug regimes require repeated trips to hospital and are therefore not completed.

1.7.2 Life cycle of *T. brucei*

Short stumpy trypomastigotes are taken up with blood by the Tsetse fly during a blood meal on an infected host. These then differentiate to become procyclic trypomastigotes which reproduce in the anterior region of the midgut of the fly. Differentiation to mesocyclic trypomastigotes then takes place and these long, very thin forms migrate to the salivary glands. Mesocyclic epimastigotes then undergo an asymetric division to produced epimastigotes which are able to attach to the wall of the salivary glands by their flagella. Metacyclic trypomastigotes are produced here and during a blood meal are transferred into a mammalian host. They rapidly differentiate into long slender trypomastigotes, which are spread throughout the host tissues by the blood and may cross the blood-brain barrier into the central nervous system. As the parasites reach peak parasitaemia, some slender trypomastigotes differentiate to produce stumpy trypomastigotes, which are adapted for the environment of the fly vector.

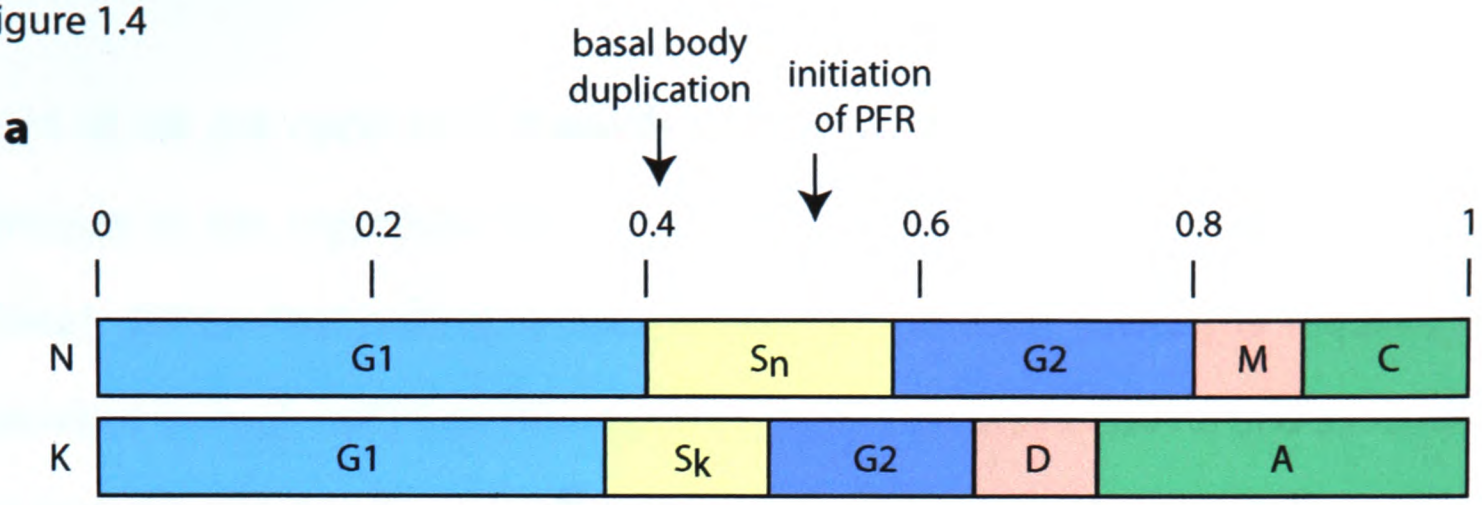
Unlike the other trypanosomatids *T. cruzi* and *L. major*, *T. brucei* remains extracellular throughout its lifecycle in the mammalian host. While the role of the

flagellum is understood in the fly for migration from midgut to salivary glands and also for attachment once there, in the mammalian bloodstream the requirement for motility is less clear as the parasites are carried in the circulation of the mammalian host.

1.7.3 Cell cycle

Figure 1.4 shows the morphogenesis of a procyclic *T. brucei* cell during five stages of the cell cycle, as well as the timings of the different stages with regard to the kinetoplast and nucleus (Fig 1.4 a). During cell division, all cytoskeletal components and single copy organelles must be replicated and precisely positioned within the cell such that each daughter cell inherits a complete complement of organelles and cytoskeleton. The first of these morphogenetic changes is the maturation of the probasal body and production of two new probasal bodies (Fig 1.4 c). The newly matured basal body elongates to subtend a new flagellum, which is attached to the lateral aspect of the old flagellum by the flagella connector (Fig 1.4 d). As the new flagellum elongates, the kinetoplast segregates. Studies have found that the flagella connector reaches a fixed point along the length of the old flagellum beyond which it will not travel. At this point, pressure is exerted by the continued growth of the new flagellum that pushes the basal bodies and kinetoplasts of the new and old flagella apart (Fig 1.4 e). The nucleus undergoes mitosis and the two nuclei move apart, with one nucleus moving towards the posterior of the cell toward the new flagellum. The cleavage furrow initiates at the anterior of the cell between the two FAZ (arrow, Fig 1.4 f).

Figure 1.4



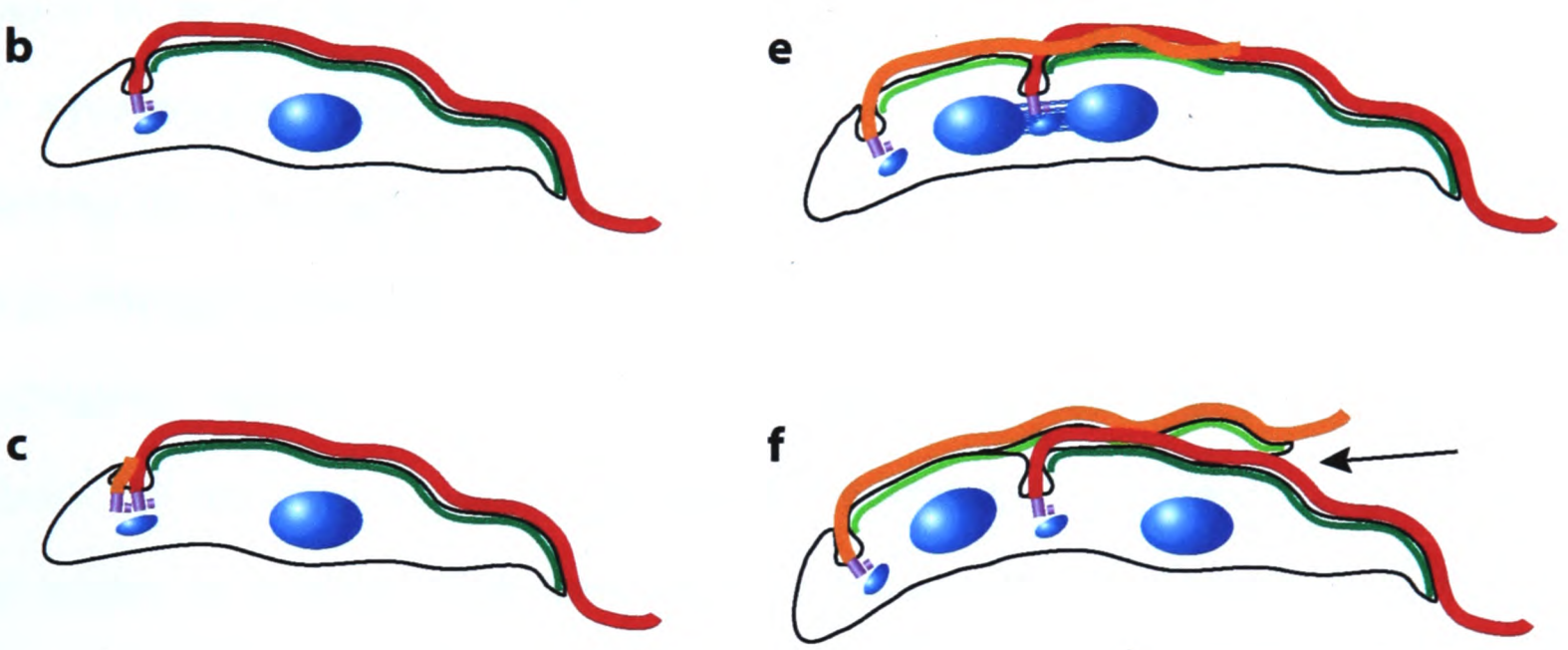


Figure 1.4 Cell cycle of a procyclic *T. brucei*
(a) Schematic representation of the duration of the cell cycle with respect to the nucleus (N) and kinetoplast (K) as a proportion of the cell cycle. Adapted from Woods et al, 1989. (b - f) Cartoons showing five stages of cytoskeletal morphogenesis in the cell cycle of a procyclic *T. brucei.* (b) Cell in G1-phase with 1 flagellum, 1 kinetoplast and 1 nucleus. (c) Duplication of the basal body and extension of a new flagellum posterior to the old flagellum. (d) Elongation of the new flagellum and segregation of the mitochondrial genome. (e) Mitosis; as the new flagellum continues to elongate, it exerts pressure on the kinetoplasts via the basal body, helping to drive the separation of the kinetoplasts. (f) Cytokinesis: the cleavage furrow begins at the anterior end of the new FAZ and progresses posteriorly through the cell as indicated by arrow.

Control of the cell cycle in *T. brucei* is complex, and it is indicated that there are differences in the regulation of the cell cycle between different life cycle stages (McKean, 2003). The activity of cyclin-dependent kinases (CDKs) is required for progression thorugh cell cycle checkpoints, and to date eleven CDKs and ten cyclins have been identified in *T. brucei* (Parsons et al., 2005; Hammarton, 2007), however at present little is known about the pairings between these cyclins and CDKs. CYC6 is known to be required for the G2/M transition in both procyclic and bloodstream form trypanosomes (Hammarton et al., 2003). In the absence of CYC6, an interesting life cycle stage-specific effect occurs – procyclic form trypanosomes were able to undergo cytokinesis despite the failure of mitosis, producing a division where one daughter cell was 1K1N with the nucleus being in the 4C state and the other daughter cell lacking a nucleus (1K0N, a zoid). In contrast, bloodstream form cells were unable to undergo cytokinesis and maintained only one nucleus while the kinetoplast continued to duplicate and segregate. The nucleus in bloodstream form cell was often seen to be bilobed, a phenomenon not seen in procyclic cells, prompting the authors to suggest that CYC6 acts later in mitosis in bloodstream form cells. CYC6 is known to interact with CRK3, the Cdc2/CDK1 homologue in Kinetoplastids (Hassan et al., 2001; Hammarton et al., 2003).

1.8 Cell morphogenesis

1.8.1 Subpellicular microtubules

The elongated shape of the trypanosome cell body is maintained by a highly ordered array of microtubules that underlies the plasma membrane. These are associated with numerous microtubule associated proteins (MAPs), which interconnect the

microtubules in order to maintain their position and uniform spacing. The polarity of the microtubules is such that the plus ends are positioned at the posterior end of the cell (Robinson et al., 1995). During the cell division cycle, the subpellicular corset remains and new microtubules are nucleated between existing microtubules to provide the expansion of the cell body.

1.8.2 Flagellum attachment zone

The flagellum of *T. brucei* is physically attached to the cell body via the flagellum attachment zone, or FAZ. The FAZ consists of a cytoplasmic filament cross-linked to the flagellum through the cell and flagellar membranes and a set of four specialised subpellicular microtubules (Fig 1.5 a) which are associated with the smooth endoplasmic reticulum. The filament is located in a gap in the subpellicular corset, with the four specialised microtubules positioned on the left of the filament when the cell is viewed from the posterior end. The four microtubules are nucleated at the basal body and are therefore antiparallel to the microtubules of the corset, being situated with their plus ends at the anterior of the cell.

At present there is relatively little in the published literature of the composition of the FAZ. Several antibodies recognise constituents of the FAZ by immunofluorescence and high molecular weight proteins by immunoblotting (Woods et al., 1989a; Woodward et al., 1995; Kohl and Gull, 1998). The antigen to one such monoclonal antibody was recently identified as a large repeat-containing protein named FAZ1 (Vaughan et al., in press). By immunogold electron microscopy, FAZ1 was located to the FAZ filament on the cell body side (Kohl and Gull, 1998). Knockdown of FAZ1 by

Figure 1.5

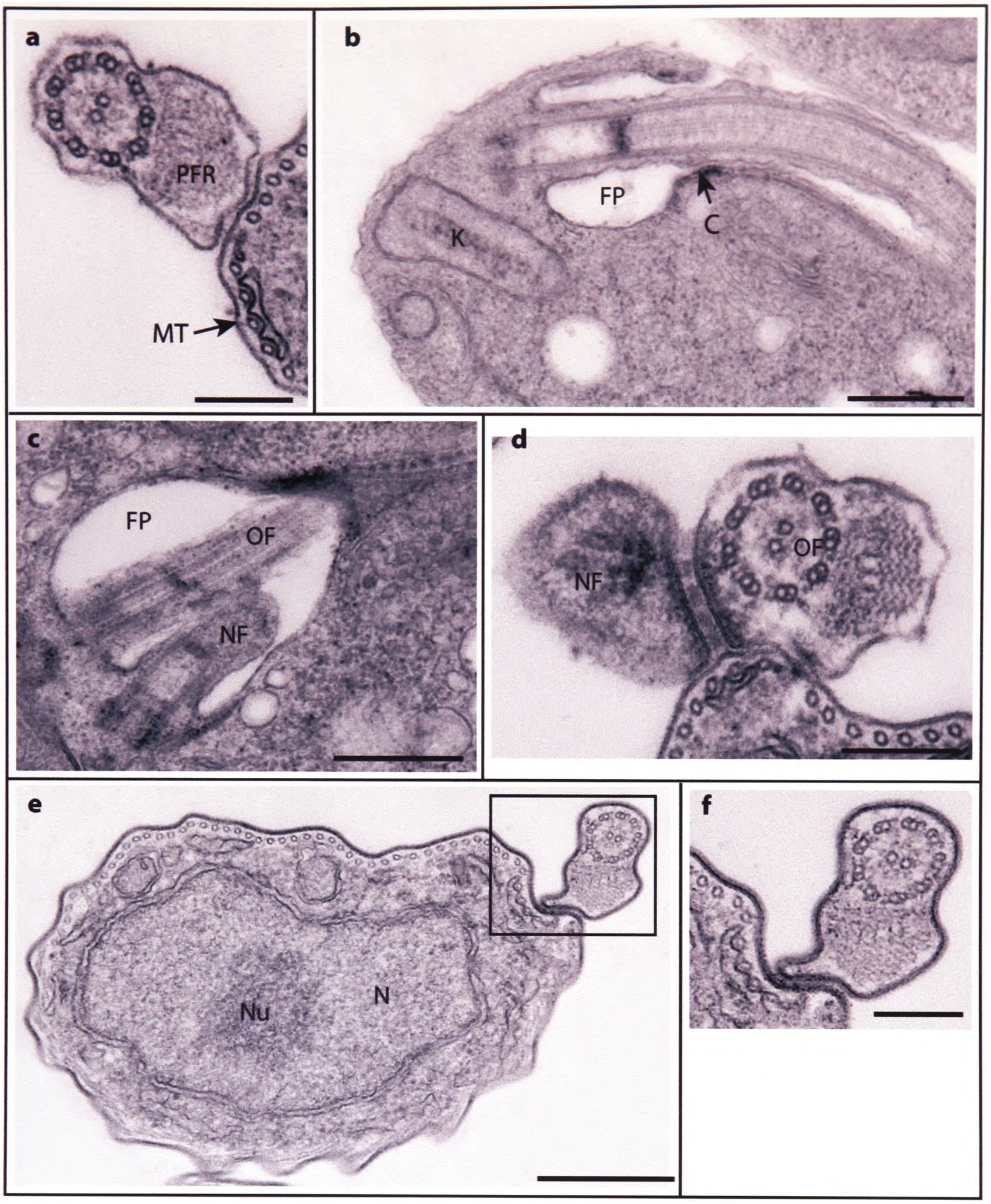


Figure 1.5 Morphogenesis of *T. brucei* by TEM
(a) Trasverse section through the flagellum of procyclic form *T. brucei* cell, showing the axoneme, PFR and the four microtubules of the FAZ (MT). (b) Longitudinal section through the flagellum as it travels through the flagellar pocket (FP), with the kinetoplast also seen (K). At the neck of the flagellar pocket is the collar (C). (c) The extension of the new flagellum (NF) initially into the same flagellar pocket as the old flagellum (OF). (e) Transverse section through the cell body and flagellum of a bloodstream form *T. brucei* cell, showing the nucleus (N) and nucleolus (Nu). The boxed region is enlarged in (f). Scale bars (a, d and f) = 200 nm, (b, c and e) = 500 nm.

RNAi leads to detachment of the flagellum, and additionally to cytokinesis defects (Vaughan et al., in press).

1.8.3 Flagellar pocket

One of the functions of the flagellum in *T. brucei* is in defining the process of cell morphogenesis. Where the flagellum exits the cell body it defines a special region of the cell surface, a invagination into the cell body called the flagellar pocket. The subpellicular microtubules prevent endocytosis from occuring elsewhere on the cell body so it is in this region that all endocytic functions of the cell must occur. At the neck of the pocket the cell membrane is tightly gathered around the flagellar membrane with an electron dense collar visible on the inside of the cell membrane by TEM (Fig 1.5 b).

1.8.4 Flagella connector

As the new flagellum is elongated it remains in contact with the lateral aspect of the old flagellum (Fig 1.5 c, d), which thus acts as a template for the formation of the new flagellum as it follows the path of the old flagellum around the cell body. The mechanism for this attachment was discovered by EM studies of procyclic form trypanosomes (Moreira-Leite et al., 2001) which revealed that there was a physical attachment linking the tip of the new flagellum to the old flagellum. Significantly, the junction is not fixed: it was found to migrate along the old flagellum as the new flagellum elongates. Further EM studies examined the flagella connector in detergent-extracted whole mount cytoskeletons by negative-staining TEM revealed further detail on the structure (Briggs et al., 2004b). By this method the flagella

connector consists of three layers with an overall width of approximately 90 nm; this trilaminar structure is around 400 nm in length running parallel to the microtubules of the old flagellum. The layer closest to the new flagellum is connected to the tip of the axoneme by a set of filaments. Thin section EMs revealed that the three plates of the flagellar connector link the membrane of each flagellum to the microtubules of that flagellum by filaments. The authors propose that the membranes of the two flagella are linked by interstitial central material (Briggs et al., 2004b). Intriguingly, no flagella connector structure has been described in bloodstream form trypanosomes, though the new flagellum still appears to follow the path of the old flagellum.

During growth of the new flagellum, a correlation exists between the length of the new flagellum and inter-basal body distance (Robinson et al., 1995; Davidge et al., 2006). This occurs in two phases: the initial phase of flagellum growth during which time the flagella connector travels along the old flagellum until it reaches a fixed point at about 0.5 of the length of the old flagellum. At this point the flagella connector ceases to travel along the old flagellum, while the new flagellum continues to elongate pushing the two basal bodies apart (Davidge et al., 2006). This suggests that there is a defined 'stop' point for the flagella connector although no structural buffer has been found. A correctly made FAZ structure is thought to be important in order for the pressure to be exerted on the basal bodies and hence on the kinetoplasts: in the FAZ1 mutant (Vaughan et al., in press) an incomplete FAZ structure is made resulting in flagellar detachment, and also in cytokinesis defects.

An interesting insight into the motor of the flagella connector came from the examination of trypanosome IFT mutants which are unable to build a new flagellum

(Davidge et al., 2006). In these cells, in the absence of a flagellum being built, a flagella connector was constructed within the flagellar pocket and could be seen by SEM and TEM imaging to migrate along the old flagellum pulling with it a 'sleeve' of flagellar membrane lacking the axoneme and PFR. This strongly suggests that at least a part of the motor for the flagella connector is contained within the old flagellum, however the growth of the new flagellum may also act to push the flagella connector along.

1.9 The Eukaryotic Flagellum

1.9.1 Intraflagellar Transport (IFT)

For most eukaryotic cilia and flagella, intraflagellar transport or IFT is the process that carries the proteins from the cytoplasm to the growing distal tip of the axoneme. There are exceptions to this however: in the apicomplexan *P. falciparum* the flagella of the male gametes are extended within the cytoplasm by a mechanism other than IFT, and several other Apicomplexa lack many of the IFT signature proteins (Briggs et al., 2004a). IFT also moves proteins destined for the ciliary membrane, and in this capacity is important for the many signalling pathways affected by ciliary membrane receptor proteins.

During IFT large protein complexes are moved along the microtubules of the axoneme by the action of the IFT motors. Anterograde movement, from the basal body to the distal tip, is brought about by kinesin-2, while retrograde transport occurs by the action of cytoplasmic dynein 2 (although in *Chlamydomonas* this is called cytoplasmic dynein 1b). The anterograde motor in *C. reinhardtii* consists of

heterotrimeric kinesin-2 made up of two motor subunits called FLA10 and FLA8, and a non-motor subunit called Kinesin Associated Protein (KAP). Interestingly, in *C. elegans* anterograde IFT appears to be more complex as there is a second motor, a homodimeric kinesin-2 called OSM-3. It has recently been suggested that different mechanisms of IFT may play a role in ciliary diversity in *C. elegans* (Evans et al., 2006; Mukhopadhyay et al., 2007). The IFT particle itself has been purified from *Chlamydomonas* and shown to consist of at least 17 polypeptides (Piperno and Mead, 1997; Cole et al., 1998), and two complexes A and B. The proteins that form the two complexes in *Chlamydomonas* are known, however less is understood about the functions of individual components. Complex A contains IFT144, IFT140, IFT139, IFT122A, IFT122B and IFT43. Complex B contains a 500 kDa core consisting of IFT88, IFT81, IFT74/72, IFT 52, IFT46 and IFT27 (Lucker et al., 2005), with IFT172 as a peripheral component (Cole et al., 1998). IFT proteins are known to be rich in domains involved in protein-protein interactions such as WD repeats, TPR domains and coiled-coil domains (Cole, 2003).

The first step in the IFT mechanism occurs at the basal body where IFT complexes A and B and the motor complexes gather. The transitional fibres that radiate from the mature basal body act as the docking site for IFT particles. There appears to be a quality control mechanism at this point, whereby tubulin cofactor C embedded at the transitional fibres may act to assess tubulin heterodimers prior to IFT loading (Stephan et al., 2007). The next step is the transport of IFT particles along the B tubule of one of the outer doublet microtubules by the kinesin-2 motor. Active kinesin-2 is attached to IFT complex A, bound in turn to complex B which binds inactive cyotoplasmic dynein 2. Kinesin-2 transports the particle also containing

axonemal precursor proteins to the plus end of the microtubule, where it is suggested that IFT particles are released into the tip compartment. At this point, it is proposed that inactive cytoplasmic dynein is released from complex B, and that active cytoplasmic dynein is bound by complex A (Pedersen et al., 2006). Cytoplasmic dynein 2 then transports the particle back towards the base of flagellum.

Several ciliary diseases are caused by failure to produce cilia, adding to the interest in IFT proteins. Several recent studies have hinted at a dual function for particular IFT proteins. IFT27 was recently shown to function in the cell cycle, as *Chlamydomonas* depleted of IFT27 did not build flagella, as with other IFT mutants, but uniquely were also defective in cytokinesis (Qin et al., 2007). While the molecular mechanism of this is not yet known, the authors suggest that IFT27 may act to delay cell cycle progression until the cilium is reabsorbed.

1.9.2 Dynein arms

Dyneins are large motor proteins which are divided on the basis of their size into three groups. The largest, the dynein heavy chains, contain a very large motor region of around 3000 residues, which forms a heptamer ring containing the site of the ATPase activity (Gibbons et al., 1987; Kon et al., 2004). Structural studies using purified dynein suggest that it is rotational movement of the motor head relative to the N-terminal tail that results in the action of dynein (Burgess and Knight, 2004; Koonce and Samso, 2004). The tail region of dynein heavy chains (DHC) interacts with various intermediate (IC) or light chains (LC) to form the dynein arms. Within the axoneme there are two sets of dynein arms, the outer and inner dynein arms, which

are attached to the A tubule of the outer doublets with the motor domains close to the B tubule of the adjacent doublet. Action of the dynein arms drives microtubule sliding, the mechanism by which axonemal bending is generated. This requires the coordinated activation and de-activation of a large number of dyneins to produce bending. The generally accepted hypothesis for this is the Geometric Clutch hypothesis (Lindemann, 1994), which proposes that the principal regulator of dynein activity is the distorting force across the axoneme that develops on each doublet during bending.

Outer Dynein Arms

The outer dynein arms are localised, as the name suggests, towards the outside of the axoneme on the outer doublet microtubules, arranged with a perioidicity of 24 nm. The outer arms all possess the same dyneins, consisting of three DHCs (α, β and γ), two ICs (IC69 and IC78) and a number of LCs. Outer arms are clearly visible in electron micrographs of the axoneme and have been well characterised. The advances made by electron tomography have improved the understanding of the position and shape of the outer arm dyneins. One such study (Nicastro et al., 2006) looked at the outer dynein arms from sea urchin and *Chlamydomonas* and found that the heptameric rings of the two (sea urchin) or three (*Chlamydomonas*) motor domains formed parallel rings. This study was also able to resolve links between the dynein arms that the authors propose may act to coordinate dynein activity (Nicastro et al., 2006), termed the outer-outer dynein (OOD) linkers.

Inner Dynein Arms

In comparison to the outer dynein arms, the inner dynein arms are more diverse, with 11 inner arm DHCs identified by sequence homology and expression studies . However, to date only eight inner arm DHCs have been identified biochemically from extracted flagella. Seven distinct isoforms of inner arm have been identified and are named *a* - *g*, made up of these eight DHCs in combination with various ICs and LCs. These seven inner dynein arms are arranged in a 96 nm repeat along the length of the axoneme (shown in Fig 1.6). At the proximal end of the repeat is the two-headed inner arm isoform I1 (this is dynein subspecies *f*), composed of two DHCs (1α and 1β), three ICs (97, 138, and 140 kDa) and three LCs (8, 11, 14 kDa). Distal to this there are six single-headed isoforms, each containing a different DHC, whose arrangement is less well characterised. Of these six, all the DHCs are associated with an actin IC, but three DHCs (dynein *a*, *c* and *d*) are associated with a conserved 28 kDa LC called p28, while the other three DHCs are associated with centrin, a 19 kDa LC.

A variety of *Chlamydomonas* dynein arm mutants have made it possible to assess the function of individual dynein arms. Outer dynein arm mutants lacking either a DHC or an IC retain a degree of flagellar motility although at slower wave frequencies (Kamiya, 1988). Analysis of flagellar motility showed that although frequency was reduced the waveform was little altered. Several inner dynein arm mutant have been characterised. Loss of the two-headed dynein *f* subspecies in the ida1 mutant results in slow swimming cells, as does the mutant ida4 which lacks dyneins *a*, *c* and *d* (Kamiya et al., 1991). However, a double mutant with one of these mutations in combination with missing outer arms is paralysed (Kamiya,

Figure 1.6

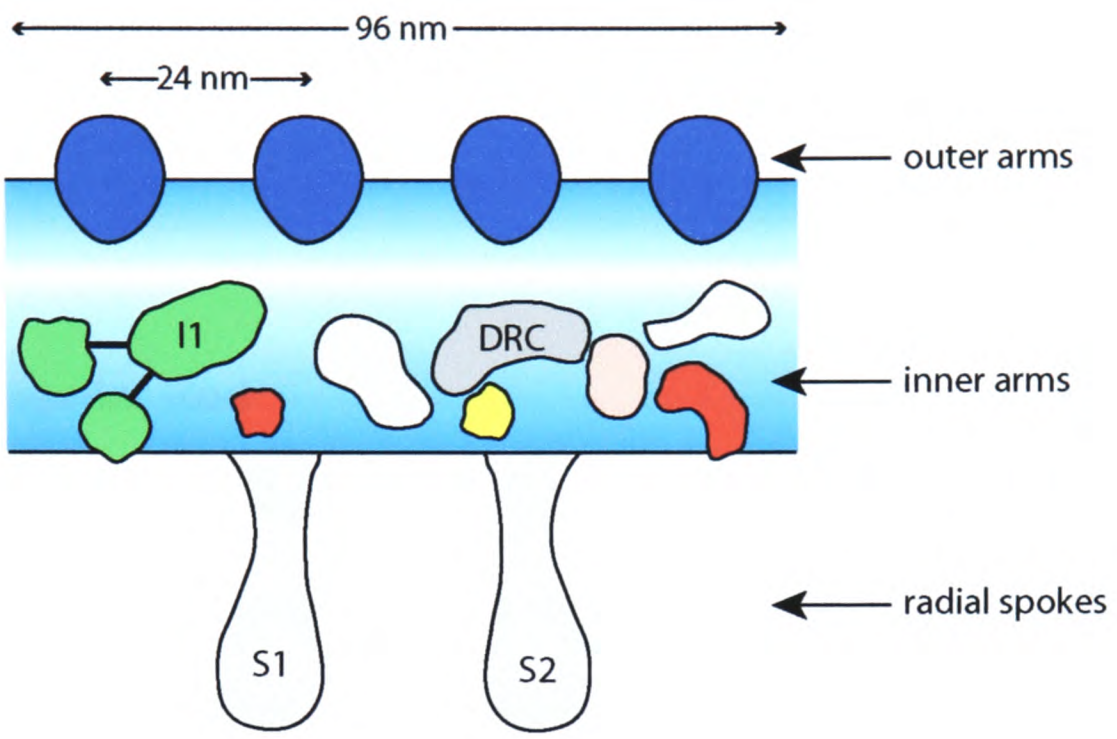


Figure 1. 6. Diagram showing the arrangement of the inner dynein arms and other structures on the A-tubule of the outer doublet. The structures are repeated with a 96 nm periodicity, and are viewed here as from the B-tubule of the adjacent outer doublet. The dynein subspecies are shown where known, the position of dynein a and d is at present interchangeable as there are no mutants lacking only one of these two. The three inner arms associated with p28 are a, d (red) and c (yellow).

1995). The loss of inner arm dynein *f* in combination with *a*, *c*, and *d* results in paralysed flagella, while *a*, *c*, *d* and *e* does not. Thus, it appears that while there is functional redundancy between the DHCs, different DHCs do play different functions with a degree of overlap and all of these functions are important for axonemal motility.

1.9.3 Paraflagellar Rod

The paraflagellar rod (PFR) is an extra-axonemal structure unique to the Kinetoplastida. This distinctive lattice-like structure runs alonside the axoneme within the flagellar membrane. The PFR is composed of two major proteins PFR1 and 2 (previously known as PFR C and PFR A, respectively (Gadelha et al., 2004)) and a number of minor proteins. In *T. brucei* the PFR is present from just distal to the point of flagellar exit from the cell to close to the distal tip. Until quite recently, the endosymbiont-containing group of trypanosomatids including *Crithidia deanei* and *Crithidia oncopelti*, were described as lacking a PFR. A study examined this group to determine the presence or absence of genes for PFR1; a homologue found to be present within the *C. deanei* genome and under examination by TEM a reduced PFR structure was observed (Gadelha et al., 2005). Furthermore, complementation studies using a *Leishmania mexicana* PFR1 knockout demonstrated that *C. deanei* PFR1 was able to localise correctly to the flagellum in complemented cell lines (Gadelha et al., 2005).

The PFR appears to be required for a number of functions of the trypanosome flagellum. Firstly, motility: ablation of PFR2 in procyclic form *T. brucei* by RNAi results in a very reduced PFR structure and cell paralysis (Bastin et al., 1998).

Secondly, within the PFR are contained many enzymes important for metabolism, such as the adenylate kinases (Ginger et al., 2005), a fact that may contribute to the motility phenotypes of cells lacking the PFR. Thirdly, it appears that the PFR may play a role in the attachment of parasitic trypanosomes to the invertebrate host: the electron dense plaques contain filaments similar to those of the PFR and originate from it (Vickerman, 1994).

1.10 Investigating the flagellum

1.10.1 Genomic methods

The completion of the genomes for a variety of eukaryotic organisms provided a valuable resource for the identification of flagellar genes. Many known flagellar components display a high degree of conservation between organisms. Comparison between the genomes of flagellate eukaryotes with those of organisms which do not build an axoneme can reveal novel flagellar proteins; several large scale studies have employed similar methodologies. One such study used *Drosophila* as the anchor for genomic comparison (Avidor-Reiss et al., 2004), which builds axonemes both by IFT and additionally, in the case of sperm cells, within the cytosol. Comparison between the genomes of ciliated and non-ciliated organisms identified 187 genes conserved in ciliated organisms. This was categorised further by comparisons within the set of ciliated organisms: 18 of the 187 were present only in organisms with motile cilia and absent from *C. elegans*; while 103 were present in were shared between organisms with compartmentalised cilia biogenesis, meaning that they were absent from *P. falciparum*. A second study (Li et al., 2004) used a similar approach with *C. reinhardtii* as the anchor: the proteomes of *C. reinhardtii*

and *H. sapiens* were compared, and the resulting shared proteome compared against the proteome of *A. thaliana*. A proteome was built of the proteins shared between the two organisms with flagella and absent from *A. thaliana*, termed the flagellar apparatus-basal body proteome (FABB) and consisting of some 688 proteins (Li et al., 2004). Validation for this approach was determined by examining known flagellar and basal body components: of 64 genes examined, 56 were found to be contained within the FABB (Li et al., 2004).

A third study adopted a functional genomics approach, using serial analysis of gene expression (SAGE) to compare *C. elegans* ciliated neuronal cells with non-ciliated cells (Blacque et al., 2005). A number of motifs are preferentially associated with ciliary genes, such as the X box often associated with *C. elegans* ciliary proteins. X boxes are conserved regulatory elements bound by DAF-19, a transcription factor that has been shown to regulate ciliary gene expression (Swoboda et al., 2000). This has been exploited as a method to identify ciliary candidate genes by scanning the *C. elegans* genome for X boxes and examining the genes immediately downstream of the X box elements (Blacque et al., 2005). In this study (Blacque et al., 2005), this method was used in conjunction with serial gene expression analysis (SAGE) to compare gene expression between neuronal ciliated cells with non-ciliated cells in *C. elegans*. Each method independently produced a relatively high false positive rate, however when using the two techniques in combination the authors were able to identify 46 genes that were suggested to be ciliary by both methods.

1.10.2 Proteomes

In recent years there have been several proteomic studies of axonemes. Earlier biochemical studies, mostly with *C. reinhardtii*, had suggested a figure of approximately 250 polypeptides in the eukaryotic flagellum (Luck, 1984). One of the first was a proteome of isolated human cilia from trachea (Ostrowski et al., 2002). This study used a combination of 1D and 2D SDS-PAGE, along with direct mass spectrophotometry (MS) of isolated axonemes and identified some 214 proteins, which included 65 known flagellar proteins.

There are also a number of proteomes of the flagella of unicellular eukaryote model organisms. A proteome of isolated axonemes from the ciliate *T. thermophila* was published in 2005 (Smith et al., 2005). Using MS against two replicate axonemal preparations the authors were able to identify 233 proteins (Smith et al., 2005). A much larger number of proteins was identified by a proteome of *C. reinhardtii* isolated flagella (Pazour et al., 2005), which identified 360 proteins with a high degree of confidence based upon the number of peptides identified by MS, and a further 292 proteins with moderate confidence. In *Chlamydomonas*, and also in *T. thermophila*, deflagellation may be induced by low pH or treatment with dibucaine (Witman, 1986), providing a simple method to obtain the flagellum with the membrane and axoneme together. The point of detachment is immediately distal to the transition zone, meaning that the resulting isolated flagella lack basal bodies (Witman, 1986). Pazour et al (2005) used three methods to fractionate the resulting isolated flagella, producing different fractions: membrane and matrix, and axonemes. The axonemes were further treated with KCl, which removes inner and outer dynein arms, one of the two central pair microtubules and some associated structures. This

gives additional information as to localisation within the axoneme for some proteins, by the fraction in which peptides are found. While the overall number of 652 proteins includes those within the membrane and matrix fractions, within the axoneme fraction there were 279 proteins.

In 2006, a proteome of *T. brucei* flagella was published (Broadhead et al., 2006). The *T. brucei* flagellar proteome (TbFP) contained 331 proteins, and these proteins within the TbFP were screened for their presence in the genomes of other organisms including other kinetoplastids, flagellate eukaryotes and non-flagellates. A high degree of conservation was observed within the kinetoplastids, however it was found that a large proportion were not found outside the kinetoplastids. In part this may reflect the presence of the the PFR in these organisms, however such a large number of proteins was an unexpected finding. The TbFP was also compared to the proteomes of the axonemes of *T. thermophila* and *C. reinhardtii*. This comparison found that 49 proteins were shared between the TbFP and the axonemal fraction of the *C. reinhardtii* flagellar proteome (CrFPaxo). While a further 33 proteins found in the TbFP were contained within the genome of *C. reinhardtii* but not within the CrFPaxo, the remaining 249 proteins, were absent from the genome of *C. reinhardtii*. Comparison of the TbFP against the *T. thermophila* ciliome produced similar findings, as did comparison of the CrFPaxo with the *T. thermophila* ciliome. This suggested that a surprisingly small cohort of conserved proteins is responsible for the structural conservation of the axoneme (Broadhead et al., 2006).

1.10.3 Mutants

In *C. reinhardtti* a great range of mutants exist such as the inner and outer dynein arm mutants, and also those lacking central pair proteins or radial spokes. These mutants were either UV-induced mutants, such as the outer dynein arm mutants (Mitchell and Rosenbaum, 1985; Kamiya, 1988; Sakakibara et al., 1991), or insertional mutants, where a vector is inserted randomly into genome. In either case the resulting mutants are screened for a phenotype of interest, such as slow swimming. In one study of insertional mutants, 3000 mutants were screened and 2.5% had motility phenotypes (Tam and Lefebvre, 1993). This kind of forward genetics is commonly utilised in *Chlamydomonas*, although reverse genetics can also be used by searching a library of mutants for one with mutations in a particular gene of interest. RNAi is used rarely in *C. reinhardtii* due to technical difficulties in producing the cell lines, though has been used for studying flagellar genes (Koblenz and Lechtreck, 2005; Iomini et al., 2006).

Following the discovery of the phenomenon of RNA interference in *C. elegans* (Fire et al., 1998), *T. brucei* was among the first species in which the use of RNAi was demonstrated (Bastin et al., 1998; Ngo et al., 1998). Since this dicovery RNAi has become widely used and well established in *T. brucei* for the downregulation of gene expression in both procyclic and bloodstream form cells. In the classical pathway of RNAi, long double stranded RNA (dsRNA) is cleaved by Dicer, an RNAse III-related enzyme, to produce 20-26 nucleotide short interfering RNAs (siRNAs). Dicer then delivers siRNAs to a complex known as the RNAi-induced silencing complex, or RISC. Activation of RISC by siRNAs enables the complex to cleave target mRNAs. Dicer and proteins of the argonaute (AGO) protein family, which are found in RISC,

are universally associated with RNAi. In *T. brucei* the AGO protein family member is TbAGO1, which is required for RNAi in procyclic trypanosomes (Durand-Dubief and Bastin, 2003; Shi et al., 2004). TbAGO1 knockout cell lines have been constructed and are viable, albeit with slower growth (Durand-Dubief and Bastin, 2003; Shi et al., 2004). More recently a Dicer-like protein was found and characterised in *T. brucei* (Shi et al., 2006).

A number of different vector systems for RNAi in *T. brucei* have been developed. These vectors are stably integrated into the genome by homologous recombination. These employ one of two strategies; either the vector contains inverted repeats of the target sequence separated by a short stretch of stuffer sequence to produce RNA that folds into a stem-loop, thereby producing dsRNA; or alternatively, a fragment of the gene is positioned between two opposing promoters to produce complementary RNA molecules that hybridise to produce dsRNA. Both systems are inducible under the control of tetracycline, providing a simple mechanism to control expression. The stem-loop system typically uses the procyclin promoter to drive RNA production, while vectors containing opposing promoters typically utilise T7 promoters. These vectors, which include pZJM (Wang et al., 2000) and p2T7-177 (Wickstead et al., 2002), are associated with a degree of 'leakage', where RNA synthesis occurs in the absence of tetracycline, attributed to the strong T7 promoter (Motyka and Englund, 2004). In addition to characterisations of individual novel flagellar proteins, the ease of the RNAi system allows for wide scale surveys of flagellar components (Baron et al., 2007).

Unlike *Chlamydomonas*, where flagella can be lost and regrown during the cell cycle, *T. brucei* maintains its flagellum at all time and grows a new one prior to cytokinesis, a feature that can be useful to flagellar studies. 'Old' flagella constructed prior to RNAi induction are generally unaffected by the reduction in protein level; thus in cells with two flagella, the effects of RNAi may be observed on the new flagellum but not the old, for example in the characterisation of γ-tubulin (McKean et al., 2003).

The objective of this thesis was to investigate the functions of novel flagellar components, with the additional aim of finding proteins that may play a role in human ciliary diseases. Novel flagellar proteins were identified from various sources including proteomic studies of cilia and flagella, and from bioinformatic analysis of a disease locus for polycystic kidney disease. The experimental aims included using a bioinformatic screen to determine the phylogenetic distribution of putative flagellar proteins and, if a homologue was present in *H. sapiens*, whether the gene was located in a chromosomal region associated with ciliary disease. Using *T. brucei* as a model organism, I aimed to determine the localisation of proteins by expression of GFP fusion proteins; and functionally characterise the role of putative flagellar proteins by RNAi ablation.

CHAPTER 2

MATERIALS & METHODS

2 Materials and Methods

2.1 Cell lines and cell culture

2.1.1 Transformation of Trypanosomes

For stable transfection of procyclic form *T. brucei*, 29-13 cells co-expressing T7 RNAP and TetR , were harvested from a log phase culture (3-8 x 10^6/ml) with a gentle 4°C spin (500*g* in a table top centrifuge), washed once in ice-cold Zimmerman post-fusion medium (ZPFM) and resuspended at 4-6 x 10^7/ml on ice. To these cells was added 10µg of linearised vector prior to electroporation at 1.5kV with 3 x 100us pulses (Electro Square Porator, BTX). Cells were then transferred to 10 ml SDM-79 medium without drugs and incubated overnight. After 24 hours, cells were diluted 1:20 into SDM-79 with phleomycin at 5µg/ml for RNAi constructs, or Hygromycin at 50µg/ml for pGAD9-177 to select for integrated reporters.

2.1.2 Culture of trypanosomes

Procyclic cells were cultured in SDM-79 medium (Brun and Jenni, 1977) supplemented with 10% foetal calf serum (Gibco) and appropriate antibiotics for transfected cells. Procyclic cells were cultured in 25 cm^2 tissue culture flasks in a 28°C incubator, and were maintained by sub-culture from a growing culture at mid-log phase (~5x10^6 cells ml^{-1}). Bloodstream cells were cultured in HMI-9 medium (Hirumi and Hirumi, 1989) supplemented with 15% foetal calf serum. Bloodstream form cells were cultured in 25 cm^2 tissue culture flasks with vented caps in a 37°C incubator with 5% carbon dioxide. For RNAi, cells were induced using 1 µg ml^{-1}

doxycycline. Cell density was determined either by haemocytometer or with a CASY®1 cell counter (Schärfe systems GmbH).

After the induction of RNAi, procyclic form non-induced and induced cells were passaged to 10^6 cells ml^{-1} every 24 hours by addition of cells to (preheated) SDM 79 medium. Cell counts were taken before and after dilution. In order to determine the growth rate the number of cells counted at the end of the growth period was divided by the number of cells at the start of that growth period. A cumulative growth curve was inferred using this growth rate data.

For the analysis of cells where RNAi was induced in cells expressing GFP:TAX-2, doxycycline was added to cells at $2x10^6$ cells ml^{-1}, and cells were counted at each time-point where cells were fixed for GFP analysis. This was then used to calculate the expected frequency of pre-RNAi flagella at a given time-point after induction, by expressing the ratio of number of cells at 0 hours: number of cells at a particular time-point as a percentage.

2.2 Molecular biology

2.2.1 DNA constructs

To make RNAi constructs, fragments of 600-750bp of the gene of interest were amplified from *T. brucei* genomic DNA, with restriction sites added at each end to allow ligation into the p2T7-177 vector (primer sequences are shown in Table 2.1). In this vector the target sequence is flanked by opposing T7 promoters to produce dsRNA of the target.

To epitope tag the endogenous PACRG genes, the pGAD9-177 vector was used. I amplified the 5'-UTR and 5' end of the gene and inserted them into the vector so that when linearised they would act as targeting sequences. The vector also contains the selective drug marker for resistance to Hygromycin.

For other proteins in this thesis, 150 – 200 bp fragments of the 5'-end of the relevant gene and within the 5' untranslated region (UTR) were amplified with specific primers (primer sequences are shown in Table 2.2) incorporating suitable restriction sites and ligated into a vector for GFP expression (Kelly et al., 2007).

2.2.2 Bacterial cell lines and transformation

DNA cloning was carried out using *E. coli* XL1-blue strain (Stratagene). Liquid cultures of bacteria were made by inoculating 2ml of LB (Luria Broth, 25 g l^{-1}) with a single colony from an agar plate. Liquid cultures were grown in a shaking incubator overnight at 37°C and 200rpm. For preparations for plasmid isolation by Midiprep kit, a 1:1000 dilution of the overnight culture was made with 50 ml LB in an autoclaved conical flask. Bacteria were transformed by incubation of 100 µl of competent cells with recombinant plasmids on ice for 30 minutes. The cells were then subjected to heat shock for 30 s at 42°C and then placed back on ice for 2 minutes. The cells were then spread onto LB-agar plates containing 100mg ml^{-1} ampicillin and incubated overnight at 37°C.

2.2.3 Plasmid DNA isolation

Small-scale plasmid DNA isolation was carried out from 2ml overnight bacterial cultures using the QIAprep® spin miniprep kit (Qiagen GmbH). Larger-scale plasmid DNA isolation was carried out using the Qiagen Mdiiprep kit. All kits were used according to manufacturer's instructions. The final pellet was re-suspended in EB (10mM Tris-HCl buffer, pH 8.5).

2.2.4 Genomic DNA isolation

To isolate genomic DNA from trypanosomes, procyclic form cells were grown to mid-log phase, then harvested by centrifugation for 10 minutes at 800g and resuspended in 500µl gDNA extraction buffer (50 mM Tris-HCl, 100mM NaCl, 1mM EDTA, pH 7.8), 50 µl 1% v/w SDS and 2.5 µl Proteinase K (2.5 µg/ml). The cells were incubated overnight at 37°C and subjected to phenol chloroform extraction followed by ethanol precipitation. The isolated DNA was dissolved in TE (10 mM Tris-HCl, 1 mM EDTA, pH 7.5), aliquoted and stored at -20 °C.

2.2.5 Restriction digests, Gel extraction of DNA fragments and DNA ligation

Restriction enzyme digests were performed according to manufacturer's instructions (Roche). The products were resolved by gel electrophoresis. DNA fragments were excised from 1% agarose gels and purified using the Wizard SV Gel and PCR Clean-Up System (Promega) in accordance with the manufacturer's instructions. Prior to ligations, vectors were dephosphorolated using Alkaline Phosphatase

(Roche) to prevent self-ligation prior to incubation with the fragment to be inserted. DNA ligations were carried out using the

2.2.6 Polymerase Chain Reaction (PCR)

A standard reaction mixture using Phusion enzyme (Roche) and reaction conditions as described in the manufacturer's instructions was used to amplify DNA. Amplification was carried out using a Perkin Elmer GeneAmp 2400 PCR machine. The thermal cycling conditions were 10 minutes at 95 °C followed by 30 cycles of 30 s at 92 °C, 30 s at 60 °C and 1 minute at 72 °C. PCR products were purified using the QIAquick PCR Purification Kit (Qiagen) in accordance with the manufacture's instructions.

2.2.7 qRT-PCR

Total RNA samples were collected from the 29-13 parental cell line, non-induced cells, and induced cells at various time-points after induction. RNA samples were purified using silica gel-based purification methods (High Pure RNA Isolation Kit, Roche) and stored at -80°C. Synthesis of cDNA from 1 µg of RNA was carried out using the Omniscript Reverse Transcription Kit (Qiagen), with oligodT primers at a final concentration of 1 µM. Three reverse transcription reactions were carried out from each RNA sample. Single stranded cDNA products were then analysed by Q-PCR using TaqMan probes against the targeted gene and QM, a 60S ribosomal protein used as a reference gene. For each gene, primers were designed using Oligo4 (DNAStar) to amplify a 100 – 130 base pair region. (PACRG A: GATGTCGGCGATTTGGTTAT, TCTCATACGTCGGCACCATA; PACRG B:

AAATACACGACACCCAACTG, GTAGAGATTGAACACCGGAA; QM: GCGTGCCAACAAG-GAAT GT, GCGAAGTACGTGGAACGGA). Products were detected using TaqMan probes (PACRG A: TCATGGTGGCGACGATGCGT; PACRG B: AACTTGTGGA-GAGCGCCGAC; QM: CCACATGCGTATCCGCGCCC) with 6-FAM on the 5' end and BHQ-1 on the 3' end. Concentration of primers, probes and $MgCl_2$ for each primer set were optimized prior to the experiment. Primer concentrations were between 250 nM and 400 nM, probe concentrations were 200 nM in each case and $MgCl_2$ concentration was between 2.0 mM and 3.0 mM. Reactions were carried out in 25 µl reaction mixtures containing 1x buffer (Promega), 0.2 mM (each) deoxynucleoside triphosphates (dNTPs) and 1.25 U Taq DNA polymerase (Promega). Amplification was performed using the Mx3000P Real-time PCRSystem (Stratagene) under the following cycling conditions: 95°C for 10 minutes and then 40 cycles of 95°C for 30 seconds, 57°C for 1 minute and 72°C for 30 seconds. In each cycle the fluorescence was recorded at the end of the annealing phase. The Ct value for each reaction was measured, and the absolute DNA amount calculated. For each sample this was normalized against the reference gene, QM, and then expressed as a percentage of the 29-13 level.

2.3 Light microscopy

2.3.1 Immunofluorescence

Cells were harvested by centrifugation at 500g for 5minutes in a microfuge. The pellet was washed once with PBS, then resuspended to approximately 10^7 cells ml^{-1}. Cells were then allowed to settle and stick to glass slides before fixing with 1% formaldehyde for 10 minutes. After rinsing with PBS, the cells were then permeabilised with a detergent solution for 5 minutes and washed with PBS again.

For cytoskeletons, 1% Nonidet (NP-40) was added to cells settled onto glass slides in the same way and incubated for 30 s. Following detergent extraction cells were fixed in methanol for 30 minutes at -20°C. Whole cells and detergent extracted cytoskeletons were washed in PBS for 10 minutes prior to pre-blocking with PBS containing 0.1% Tween20, 1% BSA for 30 minutes. Cells were incubated in the primary antibody diluted in PBS. The following primary antibodies and dilutions were used: BB2, the anti-TY tag mAb, at 1:20; L8C4, a mAb against PFR2, at 1:50; BBA4, a mAb that recognises the basal and probasal body, at 1:50; and YL1/2, a mAb which recognises tyrosinated α-tubulin, at 1:50. A commercially available anti-GFP pAb (Roche) was also used at a dilution of 1:100. Cells were incubated with the primary Ab for 45 minutes and then washed 4 times with PBS to remove unbound antibody. The secondary antibody was added and the cells incubated for a further 45 minutes before being washed 4 times with PBS. Cells were then mounted with Vectorshield containing the DNA-binding dye DAPI (4,6-diamidino-2-phenylindole) and sealed with nail varnish.

2.3.2 Fluorescence microscopy of cells expressing GFP

For imaging native GFP, trypanosomes were settled onto glass slides and fixed in 2% paraformaldehyde in PBS for 10 minutes, after which they were permeabilised in 0.1% NP-40 in PBS and washed in PBS. Cells were embedded in Vectashield (Vector Laboratories) with 4,6-diamidino-2-phenylindole (DAPI). Slides were examined on a Zeiss Axioplan 2 microscope using a 100x, 1.4N/A oil immersion lens, captured on a CCD camera controlled by Metamorph software (Universal Imaging) and processed in Metamorph and Adobe Photoshop (Adobe).

2.3.3 Videomicroscopy and analysis of motility

Non-induced cells and induced cells after 72 hours were grown to a density of 2 x 10^6 cells ml^{-1}, and allowed to equilibriate at room temperature for one hour prior to imaging. The motility of these cells was analysed as described by (Gadelha et al., 2005). Briefly, sellotape was used to make a well on a microscope slide 1 cm x 2 cm x ~50 µm when a coverslip was in place, such that a 10 µm drop of cells filled it. The coverslip was sealed to the slide with Vaseline to prevent drift. Images were captured every 2 s for 40 s at low magnification (10×) using phase-contrast illumination. For non-induced and induced cells, velocity measurements were made by tracking >50 cells over the 20 frames, using the software ImageJ (NIH). To analyse for statistical significance, the mean velocities of cells were compared by using the Student T-test in Microsoft Excel.

2.4 Electron microscopy

2.4.1 Preparation of samples for thin section Transmission Electron Microscopy (TEM)

Cells were harvested from culture by centrifugation at 800g for 10 minutes, after which the supernatant was removed. The cells were resuspended and fixed in 2.5% glutaraldehyde, 2% paraformaldehyde, 1% picric acid in 100mM phosphate (pH 6.5). Cells were centrifuged at 13000rpm for one minute to pellet the cells. The supernatant was removed and replaced with fresh fix (as before), in which cells were fixed for 2 hours at 4°C. After washing with phosphate buffer (200mM, pH6.5) secondary fix containing 1% osmium in 100mM phosphate buffer was added and incubated for 1 hour at 4°C. The sample was washed thoroughly with distilled water,

stained with 2% uranyl acetate for 2 hours in the dark, then taken through a series of dehydration steps in acetone followed by propylene oxide. After dehydration the cells were gradually infiltrated in Epon resin.

Thin sections of ~70nm were cut from the hardened blocks using a Diatome ® diamond knife on an Ultracut E ultramicrotome (Reichert-Jung). Sections were collected onto copper grids and double stained with 2% uranyl acetate in 70% ethanol and 0.3% lead citrate in 100mM NaOH. Sections were observed Technei 12 Biotwin transmission electron microscope, at an accelerating voltage of 100 kV.

2.4.2 Scanning Electron Microscopy (SEM)

Bloodstream form trypanosomes were fixed by the addition of paraformaldehyde at a final concentration of 2.5% to cells in HMI-9 medium. Cells were then harvested by centrifugation at 800g for 10 minutes, after which the supernatant was removed. After washing cells with 1ml PBS, cells were settled onto 13 mm glass cover slips (Chance Propper Ltd.) in the wells of a 24-well plate for 30 minutes. After washing with ddH_2O, samples were taken though a series of dehydration steps: 30%, 50%, 70% and 90% ethanol in ddH_2O for five minutes each, followed by three 5 minute washes with 100% ethanol. The coverslips were next prepared in a critical point dryer (Tousimis) according to the manufacturer's instructions. Coverslips were then mounted onto 0.5" SEM 6mm length pin stubs (Agar) with silver DAG (Agar). Once dried, the stubs were coated with gold using a sputter coater according to manufacturer's instructions.

2.5 Protein Biochemistry

2.5.1 Preparation of cell extracts

For whole cell extracts, a suitable volume of a mid-log phase trypanosome culture was centrifuged at 500g for 10 minutes. The supernatant was removed and the pellet immediately solubilised in boiling Laemmli sample buffer (2% w/v SDS, 0.002% w/v bromophenol blue, 10% v/v Glycerol, 50mM Tris-HCl (pH 6.8) and 400mM β-Mercaptoethanol) to give a final concentration of $2.5x10^5$ cells.μl^{-1}. The sample was boiled for 5 minutes and then centrifuged at 14000g for 30 seconds to spin down any precipitates. Samples were stored at -80 °C.

To isolate flagella, a suitable volume of trypanosome culture was centrifuged at 500g for 10 minutes. The supernatant was removed; the pellet re-suspended in 10ml PBS and centrifuged again at 500g for 10 minutes. The supernatant was removed and the pellet re-suspended in 2ml per 10^8 cells PEME-NP40 (1% Nonidet P40 (ICN), 1x Focus Protease arrest (Calbiochem), 7.5μM pepstatin A (Sigma)) to solubilise membranes and centrifuged at 1800g. The supernatant was removed and the pellet re-suspended in 1.5ml per 10^8 cells PEME-NaCl (1M NaCl, 1x Focus Protease arrest (Calbiochem), 7.5μM pepstatin A (Sigma), 200μg.ml^{-1} DNaseI and 50μg.ml^{-1} RNaseA). After incubation on ice for 10minutes, this was centrifuged at 14000g for 10 minutes. A second wash with PEME-NaCl was carried out, after which the sample was washed twice with PEME to remove excess salt. After the final centrifugation step the pellet was resuspended in boiling Laemmli buffer and stored at -80 °C.

2.5.2 SDS-polyacrylamide gel electrophoresis

Proteins were separated by 1D SDS-polyacrylamide gels 0.75mm thick, 60mm length mini-gels (Mighty small, Hoefer). These gels contained either a 10% resolving solution (11.9ml dH2O, 10ml 30% acrylamide (Biorad), 7.5ml 1.5M Tris (pH 8.8), 0.3ml 10% w/v SDS, 0.3ml 10% w/v Alkaline phosphatase (APS) and 0.012ml TEMED (Sigma Aldrich)) or a 8% resolving solution (quantities). In both cases the gel also contained a stacking gel (6.8ml H2O, 1.7ml 30% acrylamide (Biorad), 1.25ml 1M Tris (pH 6.8), 0.1ml 10% w/v SDS, 0.1ml 10% w/v Alkaline phosphatase (APS) and 0.01ml TEMED (Sigma Aldrich). Gels were run in running buffer (25mM Tris, 250mM glycine, 0.1% w/v SDS at pH 8.3) at a 20mA per gel under constant current for ~1 hour.

Visualisation of proteins on SDS-PAGE gels was carried out using the Coomassie blue stain. Gels were incubated for 1 hour in Coomassie blue (2.5g Coomasie brilliant blue R250 in 45% methanol and 10% acetic acid), then incubated twice for 15 minutes in a destaining solution (45% methanol and 7% acetic acid).

2.5.3 Western blotting and immunodetection

Proteins (equivalent to $2.5x10^6$ cells) were transferred onto nitrocellulose membranes for 14 hours with a constant current of 120mA, in transfer buffer (50mM Tris-HCL, 380mM glycine, 0.1% w/v SDS and 20% methanol). Prior to western blotting membranes were stained with Ponceau-S stain (0.1% w/v Ponceau S in 5% acetic acid). The membrane was blocked with 5% w/v skimmed milk powder in TBS (10mM Tris-HCl (pH 7.4) and 140mM NaCl) for 1 hour, before incubating with 1:25 dilution of primary antibody BB2 or 1:300 dilution of anti-Rib72 in 1% skimmed milk

in TBS for 1 hour. The membrane was then washed 5 times for 5 minutes in TBST (TBS with 0.3% v/v Tween-20) then incubated for 1 hour with a 1:10000 dilution of goat anti-mouse horseradish peroxidase conjugated secondary antibody (Sigma Aldrich) in 5% skimmed milk in TBS. The membrane was again washed 5 times for 5 minutes in TBST. Final detection was carried out by adding enhanced chemiluminescence reagent (ECL) according to manufacturer's instructions (Perkin Elmer). The membrane was exposed to Kodak biomax MR film (Anachem) for ~30 s and developed in a Kodak M35-M X-OMAT processor.

Table 2.1 Primers used to amplify DNA for RNAi targeting

	Forward primer	Reverse primer	Fragment size (bp)
TbPACRG A	ATGAGTTACGAGATAC	CGTTGCGCAAAT	627
TbPACRG B	ATGGCGTTCTCACGAA	GACGTTAATGAT	672
TAX-1	CTGTTAAGCACCTAACC	TATCTCAAACCAAATAC	536
TAX-2	GTATCAGGGCACTCGGTACG	GAAGCGCGGGAATGTAATAA	521
TbAAT-1	AGGGAAGAGCGAGAACAACA	CTGGTGCAGCAAAAGCATTA	532
TAX-3	GAACGACTTCGGTTTGGTGT	TCTCGTCCACCTCGTAATCC	541
TbCep76	CGCGAATTTCTTCTTTACGC	TTGCATAAAACGATCGGTGA	556
TbCep164	GGGACAGAAGTGCCAACATT	CACAATGCCTCCATCTCCTT	538
TbWDR16	GCAGCGAAGGAGTACGAAAC	CCGTCAATAGTCCACACACG	551
TbWDR67	ATAGTTGGAAGGGCGAGGTT	TCATCGTAAGAACGCTGCAC	553
Tbmeckelin	CTGCTGCCATTTTGCAACTA	TGCAGAGTCGATAGGCACAC	689

Table 2.2 Primers used to amplify DNA for GFP tagging

		Forward primer	Reverse primer
TbPACRG A	ORF	AGTTACGAGATACAACCCATAT	TATACAAGGATGTCGTGGTG
	UTR	GGTGAGGATACCAGATTTCAC	TTTGTGACACTTCTCGTTGAT
TbPACRG B	ORF	GCGTTCTCACGAAAGGAG	TCCGTATCTTGTTTGCCC
	UTR	TTATGTTTCAACTGCTTTGC	TTATGTTTCAACTGCTTTGC
TAX-1	ORF	CAAGGAGCCAATTTAAAA	CGTCAGCAGCTGCTCAAT
	UTR	GGGTAGAATGCGTCTTTAAA	CCAGCACGTGTTAATAAAG
TAX-2	ORF	CCCCGTTATTACACCCCACA	CGGAATCCCGTCTCTGG
	UTR	GCGTGCGGAACTCTTTCT	CAGGTGGTGCTGCTTCCT
TbAAT-1	ORF	TACTACCGAACGCAGCAGAA	AAATCGAGTTTCCGCAAAT
	UTR	ATTCCCCCTTGCCCTTTT	CGACTTTATGGTACGCAGGA
TAX-3	ORF	GACGGGGATGATGGCAT	CAGTTCCGAAGCCTTCCA
	UTR	GTTTGTCGTGCGCTGTTG	CGCTCCACGTTTTTCTTCC
TbCep76	ORF	TCTGGACCGGTTTCCCAG	GTCCGCACGCTTCTCATC
	UTR	TAGCGGATTTGCCGTTTC	CGCGCTGACACAAAACAC
TbCep164	ORF	GGGGAGCCAGGGGTTGTC	ACAAGGGCGCCAGTTTTT
	UTR	CCTCCTGTATCCCGTCATTC	TCAGCCGAGTAACAAAAACG
TbWDR16	ORF	GCAGCGAAGGAGTACGAAA	CACGGCCAGGTAGCTGAT
	UTR	CTTTCGCAAACCCATTCG	AACGGAAGGGTGGCAGTT

CHAPTER 3

RESULTS

Survey of Flagellar Proteins

3 Survey of Flagellar Proteins

3.1 Using flagellar proteomes to identify novel flagellar proteins

While there is much ultrastructural work on eukaryotic flagella in the published literature, until recently there was a relative paucity of information on the molecular components. Estimates of the number of proteins involved in these intricate molecular machines suggested at least 250 proteins (Luck, 1984; Dutcher, 1995). Recently several approaches, both genomic and proteomic, have been employed to identify novel components of eukaryotic cilia and flagella (as discussed in the introduction, section 1.9). This resource of information has now been collected together to form the ciliome (www.ciliome.com) (Inglis et al., 2006) however, even prior to this, information from individual studies allowed me to apply bioinformatic screening to select proteins of particular interest. With these resources to work from, I compiled a survey of flagellar proteins from several proteomes: the human ciliary proteome (Ostrowski et al., 2002), the *T. brucei* flagellar proteome (Broadhead et al., 2006) and two proteomes of centrioles (Andersen et al., 2003; Keller et al., 2005).

One of the earliest proteomes of cilia studied cilia isolated from human trachea (Ostrowski et al., 2002) and produced a list of 80 proteins. The *T. brucei* flagellar proteome (TbFP) identified 331 proteins, a large number of which have not previously been identified as being part of the flagellum (Broadhead et al., 2006). In addition to proteomic studies of the cilia or flagella of several species or cell types, there are also a number of proteomic studies addressing the protein composition of centrioles/ centrosomes or basal bodies from various organisms. I examined proteins identified from two of these, one a study of human centrosomes (Andersen

et al., 2003) and one of *C. reinhardtii* basal bodies (Keller et al., 2005), in order to identify proteins which were conserved in *T. brucei*, and which might be found within the TbFP.

Defects in ciliary structure or function are increasingly being recognised as the cause of human diseases with a wide range of symptoms and affected systems. As more has become known about the phenotypes of ciliary disease, predicting ciliary diseases and therefore identifying the causative gene has been facilitated (Badano et al., 2006). Polycystic kidney disease is known to result from dysfunctional primary cilia in the collecting tubules of the kidneys (Yoder, 2007). I took a known locus of a rat model for polycystic kidney disease, the Wpk rat (Gattone et al., 2004), and used a bioinformatic screening process to determine the phylogenetic distribution of the genes within it.

3.2 Selected gene set

The bioinformatic screen I utilised was essentially the same for all proteins, regardless of where genes of interest had been selected from. The object of this screen was to determine the phylogenetic distribution of a gene of interest. Known flagellar components are well conserved in organisms which build a eukaryotic flagellum, and are usually absent from organisms which never build cilia, or do not possess centrioles. The organisms interrogated included those which build a classical eukaryotic flagellum, *Homo sapiens*, *Chlamydomonas reinhardtii*, *Drosophila melanogaster*; the ciliates *Paramecium tetraurelia* and *Tetrahymena thermophila*; *Caenorhabditis elegans* (which possesses only sensory cilia that lack the central pair); the trypanosomatids *Trypanosoma brucei*, *Trypanosoma cruzi* and

Leishmania major; and non-flagellated organisms *Schizosaccharomyces pombe*, *Arabidopsis thaliana* and *Cyanidioschyzon merolae*. Homologues were identified by reciprocal BLAST. The bioinformatic screen resulted in a set of 11 proteins, whose phylogenetic distribution in flagellate organisms strongly suggested a relationship with the expression of a flagellum (Fig. 3.1).

The proteins identified from the human cilia proteome were the Parkin co-regulated gene (PACRG) (West et al., 2003) which was found to have two paralogues in *T. brucei* (Tb927.3.3210 and Tb09.211.1470) and a conserved hypothetical protein of unknown function which was named Trypanosome Axonemal protein-1 (TAX-1) (Tb09.211.1790).

I selected three proteins from the TbFP whose phylogenetic distribution, conserved in many flagellate organisms but absent from *C. elegans*, suggested a function in motility. One of these, previously named Amy-Associating protein expressed in Testis (AAT-1α) (Tb11.02.0354) was known to play a role in spermatogenesis (Yukitake et al., 2002). Two further conserved hypothetical proteins were contained in this set of motility-type proteins: Tb10.70.7560 and Tb927.7.2970. These were named TAX-2 and TAX-3 respectively.

While researching an additional protein from the TbFP, Tb11.02.3520, I found that the human homologue had been identified in a proteome of human centrosomes and named Cep164. This finding led me to look at the other proteins identified from this study (Andersen et al., 2003), for other proteins with homologues in *T. brucei*. Five proteins from this study (out of 23 proteins identified) possessed homologues in *T.*

Figure 3.1

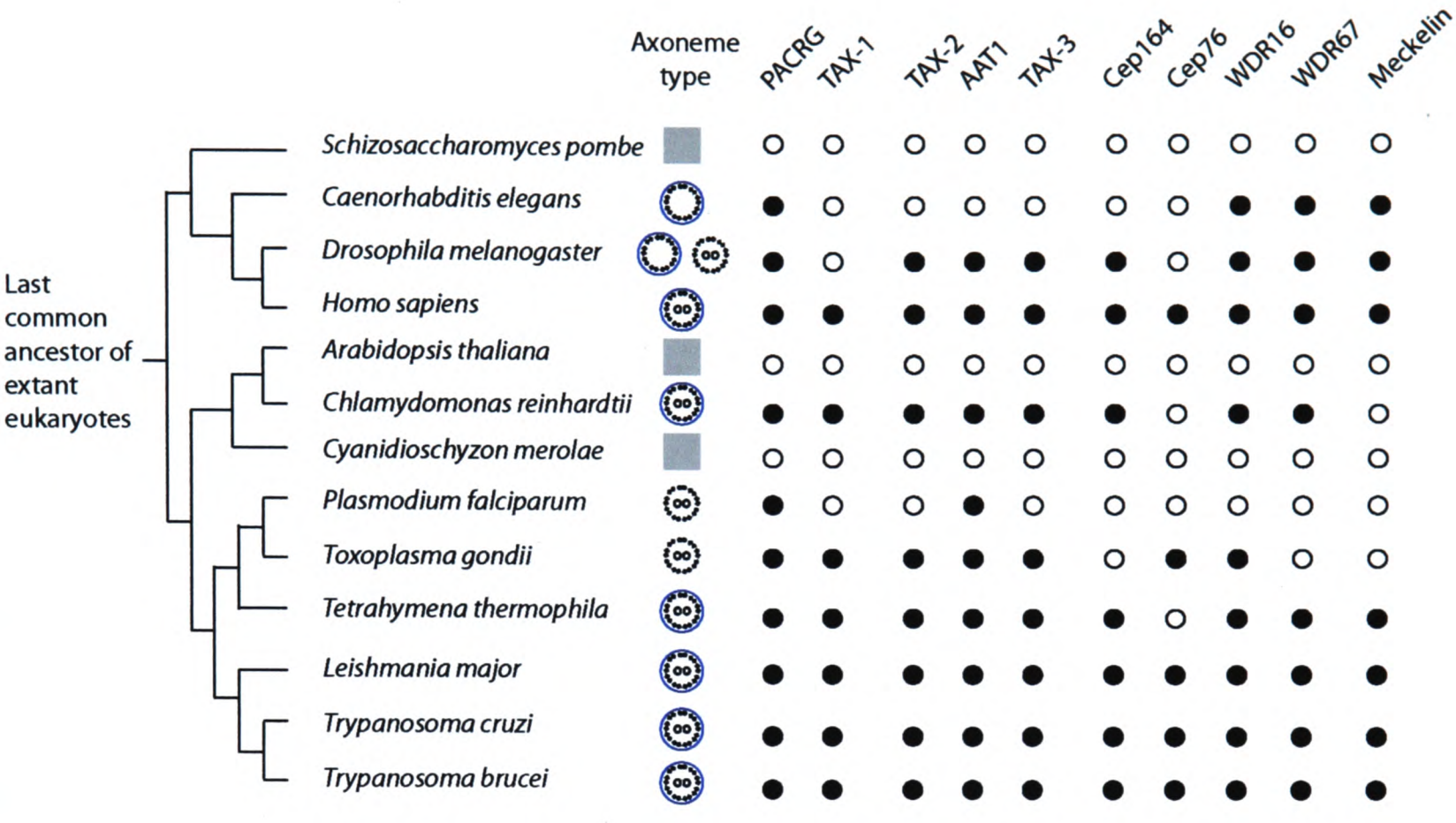


Fig. 3.1 Phylogenetic distribution of flagellar protein survey set reveals conservation among many flagellated eukaryotes. Phylogenetic tree showing distance between the organisms used for bioinformatic screen, with the type of axoneme (motile, non-motile, built in compartment or in cytoplasm) indicated alongside. Columns for each protein indicate whether a homologue is present (black circles) or absent (white circles).

brucei, of which only one was found within the TbFP. This protein, Cep164, and one other Cep76 (Tb11.01.0600) were brought into the gene survey. I also examined the results of a proteome of isolated *C. reinhardtii* basal bodies (Keller et al., 2005). This study identified 18 proteome of centriole (POC) proteins, four of which I found to possess homologues in *T. brucei*. Again, only one of these was found in the TbFP. I took this protein (Tb11.02.5550) and one other from this study (Tb10.6k15.0190) into my gene survey set.

The Wpk rat is a murine model for polycystic kidney disease (PKD), first described in 2000 (Nauta et al., 2000). In addition to cysts forming in the kidney, the Wpk rat develops extrarenal symptoms most obviously in the brain, including reduction in size of the corpus callosum, a phenotypic feature common to many ciliary diseases. The locus for the causative gene was defined by Gattone et al (Gattone et al., 2004) as being on rat chromosome 5, close to the D5Rat73 marker. Using comparative genomics I established the pattern of phylogenetic occurrence of 94 genes in the region of the D5Rat73 marker, as it appears on the NCBI Rat Genome browser, by reciprocal best-hit BLASTp searches. This search yielded a promising candidate gene, named in the rat genome LOC313067. This gene was also brought into the gene survey set, and was subsequently identified as the causative gene responsible for both the wpk rat and a human disease, Meckel-Gruber Syndrome (Smith et al., 2006).

3.3 Applying the RNAi phenotype test

The well established inducible RNAi system in *T. brucei* was then used to assess function of this set of proteins in both procyclic and bloodstream trypanosomes. Our

laboratory discovered that RNAi ablation of many flagellar proteins in bloodstream form trypanosomes rapidly leads to cytokinesis defects and cell death. Growth of both forms of trypanosomes was monitored after RNAi induction. In bloodstream form trypanosomes, defects in growth rate became apparent within 24 hours of induction. In procyclic form trypanosomes, flagellar phenotypes often do not affect growth rate, however motility phenotypes may be visualised, most commonly as non-motile cells sediment on the base of the culture flask. Motility can be assessed by taking time-lapse microscopy images every 2 seconds for a period of 40 seconds and tracking individual cells in all 20 frames to give measurements of velocity.

Of the set of 11 proteins selected by bioinformatic screening, 3 gave a motility phenotype in procyclic form trypanosomes and a phenotype of growth and cytokinesis defects in bloodstream form trypanosomes. These were the two conserved hypothetical proteins TAX-1 and TAX-2 and the known protein TbAAT-1 whose function in the axoneme had not been previously characterised. Two further proteins from the set, PACRG A and PACRG B, share a high degree of sequence conservation. RNAi ablation of each individually produced no phenotype in procyclic forms however, simultaneous ablation led to flagellar paralysis. The data on these five proteins will be presented individually in the following Results Chapters. For the remainder of this chapter I will deal with the data I acquired from the survey on those proteins whose RNAi ablation did not produce a phenotype, but nevertheless remain intriguing putative components of flagella or basal bodies. The data I acquired and present here on their localisation provides more detail on these proteins than is available at the current time in the published literature. The phenotype results from all eleven proteins are summarised in Figure 3.2.

Name	Accession Number	Human chromosome location	Procyclic RNAi phenotype?	BSF RNAi Phenotype?	TEM Defect?	GFP localisation
TbPACRGA	Tb927.3.2310	6q26	No	Growth and cytokinesis	No	axoneme only
TbPACRGB	Tb09.211.1470	-	No	No	No	axoneme only
TbPACRGAB	Tb927.3.2310 & Tb09.211.1470	-	Paralysed	Growth and cytokinesis	missing outer doublets	axoneme only
TAX-1	Tb09.211.1790	1p34.2	Motility	Growth and cytokinesis	No	axoneme only
TAX-2	Tb10.70.7560	17p13.1	Motility	Growth and cytokinesis	various	axoneme only
TbAAT-1	Tb11.02.0354	3q12-q13.3	Motility	Growth and cytokinesis	No	axoneme only
TAX-3	Tb927.7.2790	7q31.32	No	No	ND	axoneme only
TbWDR16	Tb11.02.5550	17p13.1	No	ND	ND	axoneme , BB and proBB
TbCep164	Tb11.01.3520	11q23.3	No	No	ND	"doughnuts"
TbWDR67	Tb10.6k15.0190	8q24.13	No	No	ND	ND
TbCep76	Tb11.01.0600	18p11.21	No	No	ND	BB and proBB
Meckelin	Tb927.5.3540	8q22.1	No	No	ND	ND

Figure 3.2 Summary of the characterisation of novel flagellar proteins.
Table shows protein names, *T. brucei* accession numbers, the chromosomal locus of the human homologue, and summarises the RNAi phenotype in procyclic and bloodstream form cells, the presence or absence of axonemal defects visible by TEM, and the GFPlocalisation. ND stands for not done.

3.3.1 Localisation studies

To localise these proteins in procyclic *T. brucei*, strains were constructed in which one copy of the two endogenous genes in the diploid genome was replaced with a GFP tagged fusion protein, which contained a short TY epitope between the GFP and the protein sequence at the N-terminus, so allowing both live cell imaging and immunological detection. The vector used to construct these strains, pEnT6B-G (Kelly et al., 2007) contains the Aldolase 5' untranslated region (UTR) ahead of the GFP-TY fusion, so the resulting fusion protein will be expressed using the Aldolase 5' UTR, but with the endogenous 3'UTR which is believed to dominate control of expression level (Clayton, 2002).

3.4 Proteins identified from a *T. brucei* Flagellar Proteome (TbFP)

3.4.1 TAX-3

The gene encoding TAX-3 (Tb927.2.2970) encodes a protein of 701 amino acids, with a predicted molecular weight of 79.3 kDa and isoelectric point of pH 4.8. It is conserved in other flagellate eukaryotes, with homologues present in *H. sapiens* (NP_849149), *C. reinhardtii* (C_370121) and *T. thermophila* (XP_001021374) in addition to the kinetoplastids. The *C. reinhardtii* homologue (C_370121) was identified in a proteome of *C. reinhardtii* isolated flagella (Pazour et al., 2005). TAX-3 is predicted to contain an IQ calmodulin-binding motif between residues 430 – 450. This domain and its position are conserved in homologues of TAX-3. Additionally, the human homologue is predicted to contain a ubiquitin domain. The human homologue (NP_849149) is named IQ motif and ubiquitin domain containing, or

IQUB. This is situated on chromosome 7q31.32, in a locus for retinitis pigmentosa, but for which one causative gene is known to be the IMP dehydrogenase-1 gene, IMPHD1 (Bowne et al., 2002). However, TAX-3 may still be a candidate gene as mutations in IMPHD1 do not account for all cases (Sullivan et al., 2006).

RNAi ablation of TAX-3 in procyclic form trypanosomes had no effect on growth or motility of cells (Fig. 3.3), and continued to produce new flagella at each cell division. No significant difference was observed in mean velocity between non-induced and induced cells. Non-induced cells had a mean velocity of 2.1 μm s^{-1} ± 0.03 μm s^{-1}(n = 47), compared with a mean velocity for induced cells of 2.6 μm s^{-1} ± 0.03 μm s^{-1}(n = 63). RNAi ablation of TAX-3 in bloodstream form trypanosomes also produced no growth phenotype over an induction of one week and cells appeared as wild-type.

TAX-3 was localised by replacing one copy of the two endogenous genes in the diploid genome with a GFP:TY:TAX-3 fusion. The native GFP signal was examined in fixed cells, where it was located along the full length of the flagellum but not to the basal body, and appeared punctate (Fig. 3.4A). The signal extended from immediately distal to the basal body, through the flagellar pocket and to the distal tip and was therefore clearly axonemal rather than in the PFR.

Figure 3.3

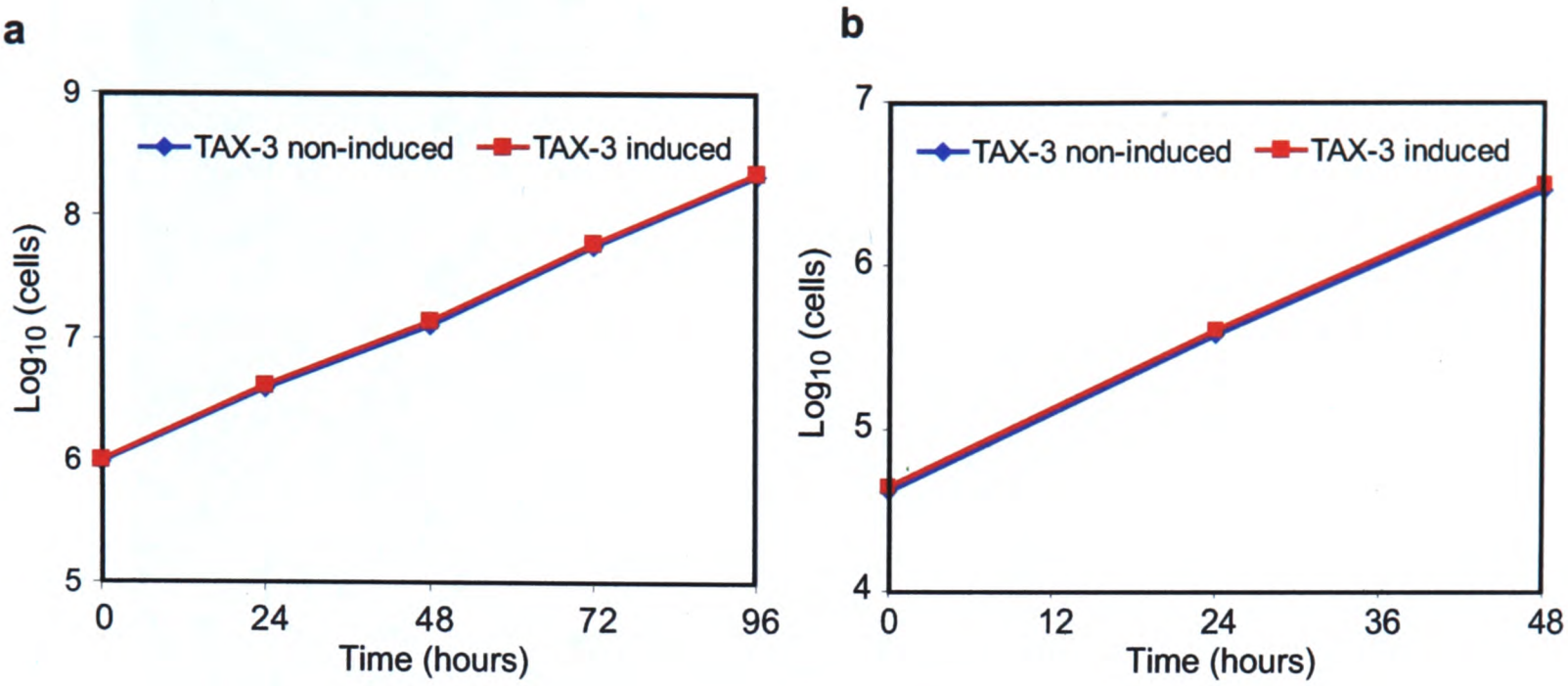


Figure 3.3 Characterisation of RNAi against TAX-3 on growth in procyclic and bloodstream form trypanosomes.

(a) Inferred cumulative growth curve showing no alteration in growth kinetics in procyclic form induced cells (red) compared to non-induced controls (blue).

(b) Inferred cumulative growth curve showing no alteration in growth kinetics in bloodstream form induced cells (red) compared to non-induced controls (blue).

(c) Tracks of non-induced (blue) and induced (red) cells from which mean speeds were calculated. For each, 30 representative tracks are shown. Scale bar = 100 μm

Figure 3.4

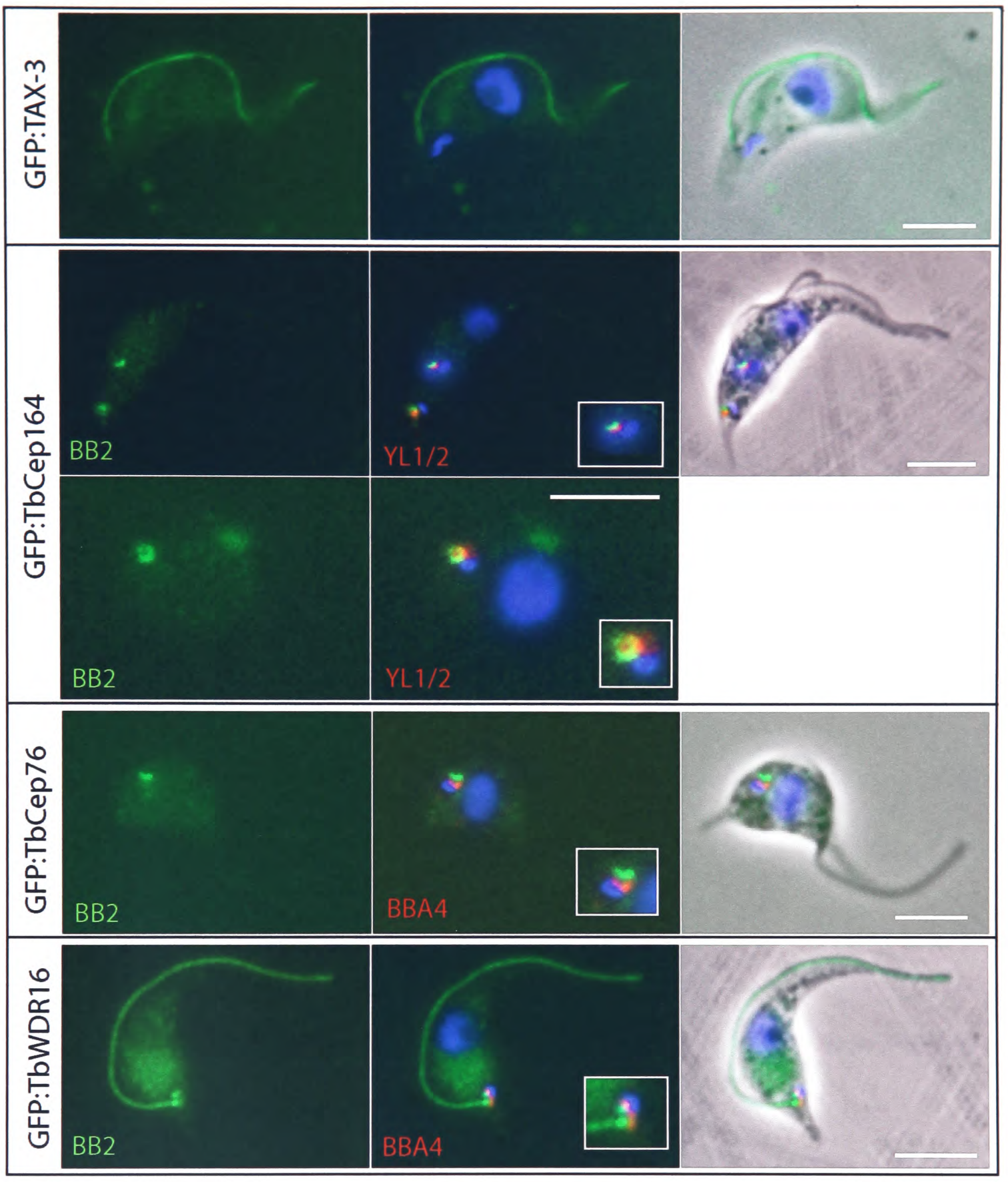


Fig. 3.4 GFP and TY epitope tagging provides localisations to a range of flagellar compartments. Fluorescence and phase microscopy images of procyclic form trypanosomes containing GFP and TY tagged protein of interest. (A) native GFP:TAX-3 in paraformaldehyde-fixed cells localises to the axoneme but not the basal body. (B, C) Dual labelling immunofluorescence with the anti-TY antibody BB2 (green) and anti-alpha-tyrosinated tubulin antibody YL1/2 (red) shows localisation of tagged GFP:TbCep164 to the basal body in a similar pattern to YL1/2 staining. (B) shows the two dots seen when signal is viewed from side. (C) The ring around the basal body can be seen. (D) Dual labelling immunofluorescence with the anti-TY antibody BB2 (green) and BBA4 (red) shows localisation of tagged GFP:TbCep76 to the basal body and probasal body in a pattern similar to, but not co-localising with BBA4. (E) Dual labelling immunofluorescence with the anti-TY antibody BB2 (green) and BBA4 (red) shows localisation of tagged GFP:TbCep76 to the basal body and probasal body, as well as to the length of the axoneme. Scale bars = 5 μm.

3.5 Proteins that are predicted to be associated with the basal body

3.5.1 Cep164

The gene encoding Tb11.01.3520 encodes a protein of 1006 amino acids with a predicted molecular weight of 111 kDa and isoelectric point of pH 8.3, with a predicted WW domain close to the N-terminus. This domain contains two highly conserved tryptophans spaced 20-23 residues apart and has been shown to bind proline-rich peptides in vitro (Chen and Sudol, 1995; Macias et al., 2002). The *H. sapiens* homologue was identified in a proteomic study of centrosomes (Andersen et al., 2003) and named centrosomal protein of 164kDa, or Cep164 (NP_055771). In addition there are homologues in *D. melanogaster*, *C. reinhardtii* (C_150016), and *T. thermophila*, as well as the kinetoplastids.

GFP localisation of GFP:TY:TbCep164 is consistent with the identification of Cep164 in a proteome of human centrosomes: the fusion protein localises to the mature basal body, where it forms a ring around the distal part of the structure (Fig. 3.4 B, C). Immunofluorescence using the mAb BB2 reveals that it co-localises with YL1/2 staining in this region which detects tyrosinated α-tubulin (Stephan et al., 2007).

RNAi ablation of TbCep164 in procyclic form trypanosomes had no observable effect on growth (Fig. 3.5 a), cell morphology or motility, and cells continued to produce new flagella at each cell division. RNAi ablation in bloodstream form trypanosomes did not produce the characteristic flagellar phenotype of growth and cytokinesis defects (Fig. 3.5 b).

Figure 3.5

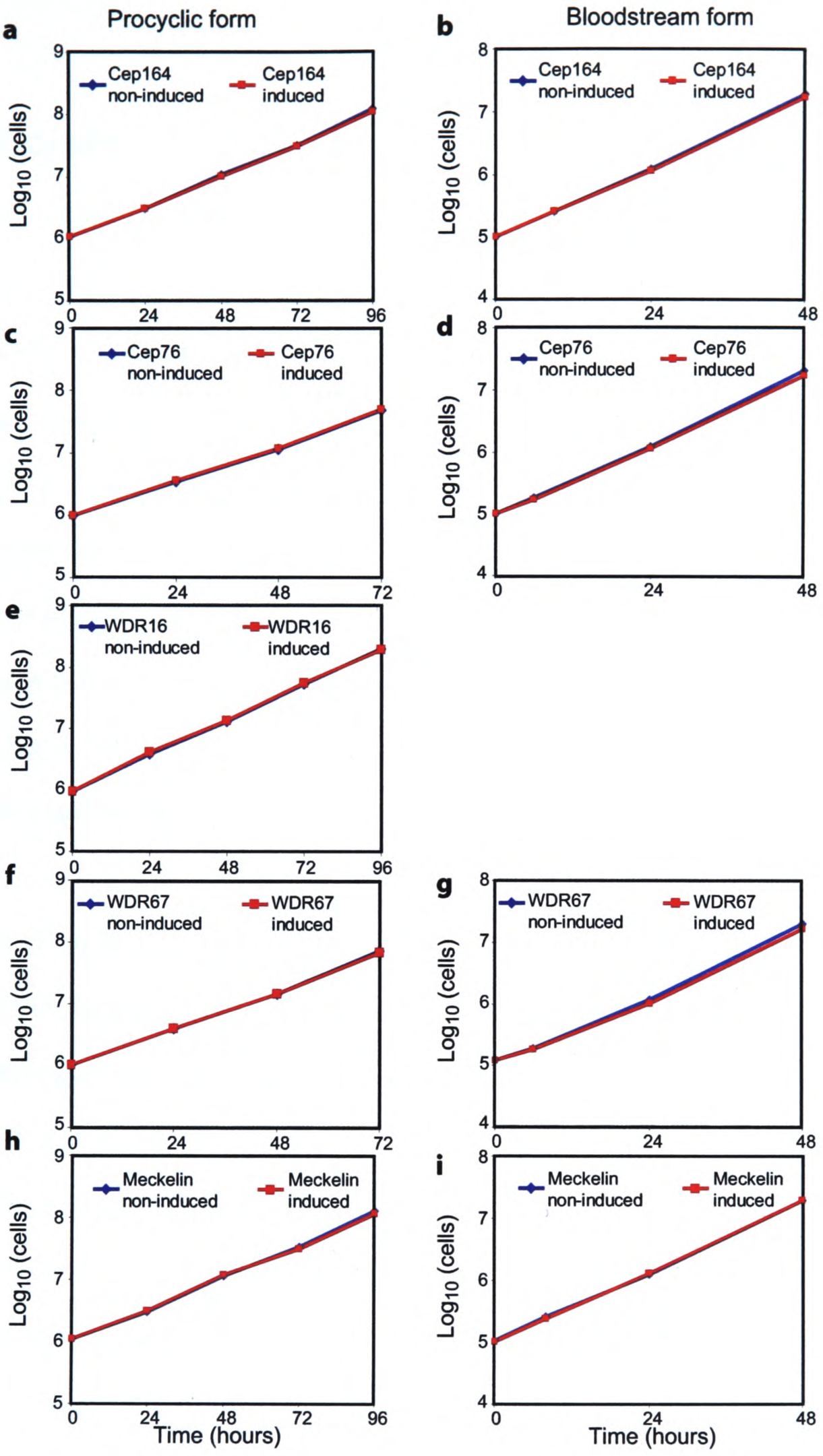


Figure 3.5. Effect of RNAi on growth in procyclic and bloodstream form trypanosomes.

Cumulative growth curves showing no difference in growth kinetics in induced cells (red) and non-induced cells (blue) in procyclic (a, c, e, f and h) and bloodstream form (b, d, g and i) cells. (a, b) TbCep164 RNAi (c, d) TbCep76 RNAi (e) TbWDR16 RNAi (f, g) TbWDR67 RNAi (h, i) Tbmeckelin RNAi

3.5.2 Cep76

Tb11.01.0600 encodes a protein of 632 amino acids with a predicted molecular weight of 70.9 kDa and isoelectric point of pH 6.9. This protein was not present in our TbFP, but the human homologue had been identified from a proteomic study of human centrosomes (Andersen et al., 2003), and named centrosomal protein of 76kDa, or Cep76 (NP_079175). Intriguingly, while this protein is conserved between trypanosomatids and vertebrates, it is apparently absent from the genomes of many other flagellate organisms. There are no homologues in *C. elegans* or *D. melanogaster*, nor in *C. reinhardtii* and *T. thermophila.* However, a well conserved homologue is found in *P. tetraurelia* (XP_001456918), a ciliate which possesses several hundred basal bodies.

The localisation of GFP:TY:TbCep76 was examined both directly in fixed cells and using the BB2 antibody. In cells possessing one flagellum, two dots are visible corresponding to the basal body and probasal body. Once the new flagellum is initiated and extended, four dots are visible, corresponding to the two mature basal bodies and two probasal bodies present at this stage of the cell cycle. Immunofluorescence using the anti-TY antibody BB2 and a monoclonal antibody which detects the proximal end of the basal and probasal bodies, BBA4, reveals that the two do not co-localise (Fig. 3.4 D). The BB2 signal for TbCep76 appears distal to the BBA4 signal.

RNAi ablation of TbCep76 in procyclic form trypanosomes had no observable effect on growth (Fig. 3.5 c), cell morphology or motility, and cells continued to produce

new flagella at each cell division. RNAi ablation in bloodstream form trypanosomes did not produce the characteristic flagellar phenotype of growth and cytokinesis defects (Fig. 3.5 d).

3.5.3 WDR16

Tb11.02.5550 encodes a protein of 629 amino acids, with a predicted molecular weight of 67.6 kDa and isoelectric point of pH 6.5. It is predicted to contain eight WD40 domains, also known as G-beta repeats. These repeats consist of about 40 conserved residues, are found in a wide variety of protein families and have been implicated in many cellular functions including signal transduction, transcriptional control, cell cycle control and apoptosis. Underlying these varying functions is the role of the WD40 domain repeats as a rigid scaffold for protein interactions in the coordination of multi-protein complex assemblies.

The human homologue of Tb11.02.5550 is found at the 17p13.1 locus, and has been named WDR16 for WD40 repeat containing protein 16 (NP_659491). It is also referred to as WDRPUH, for WD-repeat containing protein up-regulated in hepatocellular carcinoma (Silva et al., 2005). Studies on this protein have shown that it is expressed only at very low levels in normal tissues with the exception of testis, suggesting it may be involved in spermatogenesis. The intracellular location of WDRPUH was studied by exogenously expressing a WDRPUH:Myc fusion protein which localised to the cytoplasm in two tumour cell lines, HepG2 hepatoma cells and in Tera-1 testicular cancer cells (Silva et al., 2005). A second study found that in addition to its expression in testis, WDR16 is also expressed in the cilia-bearing ependymal cells of the brain, but not other brain areas (Hirschner et al., 2007). In

this study the authors also assessed localisation within sperm by western blotting and found that following head/tail separation, WDR16 was found within the tail fraction. Interestingly, the authors reported that knockdown of WDR16 in zebrafish caused hydrocephalus, however by videomicroscopy no changes in ciliary motility of the ependymal cells were observed.

Several disease loci for likely ciliary diseases are located in the 17p13.1 chromosome region. These include Leber congenital amaurosis (LCA) (Hameed et al., 2000), retinal cone dystrophy 2 (RCD2) (Greenberg et al., 1994) and central areolar choroidal dystrophy (CACD). LCA is known to be caused by mutations in the retinal guanidine cyclase gene GUCY2D (Perrault et al., 1996), and arylhydrocarbon-interacting receptor protein like 1, AIPL1 (Sohocki et al., 2000). Causative genes for CACD and RCD2 are not known although the region contains a number of candidate genes including GUCY2D, AIPL1, pigment epithelium-derived factor (PEDF) and recoverin. However, these are not diseases affecting either testis or the ependymal cells of the brain, the only tissues that have been shown to express WDR16, so it may be considered an unlikely, though possible, candidate.

The native GFP signal of GFP:TY: TbWDR16 was examined directly in fixed cells, where it was located along the full length of the flagellum. At the basal body and probasal body, two dots are visible in cells possessing one flagellum. Once the new flagellum has initiated and extended, 4 dots are visible, corresponding to the two mature basal bodies and two probasal bodies present at this stage of the cell cycle. Immunofluorescence using the anti-TY antibody BB2 and a monoclonal antibody which detects the proximal end of the basal and probasal bodies, BBA4, reveals that

the two do not co-localise (Fig. 3.4 E). The BB2 signal for TbWDR16 is located distal to the BBA4 signal.

RNAi ablation of TbWDR16 in procyclic form trypanosomes had no effect on growth (Fig. 3.5 e), cell morphology or motility, and cells continued to produce new flagella at each cell division. I was unable to construct a strain of bloodstream form trypanosomes possessing the inducible RNAi cassette and resistance markers.

3.5.4 TbWDR67

The gene encoding TbWDR67 (Tb10.6k15.0190) encodes a protein of 1086 amino acids, with a predicted molecular weight of 121.4 kDa and isoelectric point of pH 8.4. It is predicted to contain several WD40 domains, which span much of the length of the protein.

TbWDR67 is well conserved in the genomes of flagellate organisms with homologues in *H. sapiens* (NP_663622), *C. reinhardtii* (C_50227), *D. melanogaster* (NP_611973) and *T. thermophila* (XP_001017230) in addition to the kinetoplastids. The human homologue (NP_663622) is situated at chromosome locus 8q24.13, in a locus for Juvenile Myoclonic epilepsy. While there is no direct evidence that in this case this is caused by defects in ciliary function, the protofilament ribbon protein Rib72 is also linked to this form of epilepsy (King, 2006), demonstrating the varied disease phenotypes caused by ciliary dysfunction. The human homologue WDR67 is predicted to contain five WD40 domains spanning the following residues: 48-70, 116-153, 159-196, 225-242 and 296-334.

RNAi ablation of TbWDR67 in procyclic form trypanosomes had no observable effect on growth (Fig. 3.5 f), cell morphology or motility, and cells continued to produce new flagella at each cell division. RNAi ablation in bloodstream form trypanosomes did not produce the characteristic flagellar phenotype of growth and cytokinesis defects (Fig. 3.5 g). I was unable to obtain a GFP localisation for TbWDR67.

3.6 A protein identified in searching a locus linked to ciliary disease

3.6.1 Meckelin

Tb927.5.3540 encodes a protein of 1007 amino acids, with a predicted molecular weight of 111.9kDa and isoelectric point of pH6.5. It is predicted to contain a signal peptide at the N-terminus (signal peptide probability 0.987) with a cleavage site probability of 0.725 between residues 19-20 predicted by SignalP3.0 (Bendtsen et al., 2004). There are also 7 probable transmembrane helices toward the C-terminal. The human homologue (NP_714915) of Tb927.5.3540 has recently been identified as causative gene of Meckel-Gruber Syndrome and therefore the protein is named meckelin (Smith et al., 2006). Homologues of meckelin are also found within the genomes of *D. melanogaster* (NP_650900), *C. elegans* (NP_495591) and *T. thermophila* (XP_001030784).

RNAi ablation of meckelin in procyclic form trypanosomes had no observable effect on growth (Fig. 3.5 h), cell morphology or motility, and cells continued to produce new flagella at each cell division. RNAi ablation in bloodstream form trypanosomes

did not produce the characteristic flagellar phenotype of growth and cytokinesis defects (Fig. 3.5 i). I was unable to obtain a GFP localisation for meckelin.

3.7 Conclusions and discussion

This chapter deals with the results of a survey of flagellar proteins, identified from several proteomes of flagella, and one from a ciliary disease locus. The selected proteins were then subjected to bioinformatic screening to establish the phylogenetic distribution. I then used GFP and epitope tagging to localise the proteins, and RNAi to address function. This process is shown in Fig. 3.6. In this chapter I have presented localisation data and bioinformatics for those proteins which did not give a discernable phenotype following RNAi ablation. The pattern of immunofluorescence signal for the basal body proteins TbCep76 and TbCep164 suggests the approximate localisations shown in Fig. 3.7.

Of the set of proteins I examined, surprisingly few RNAi phenotypes were observed following ablation of protein expression. The six proteins that did not produce motility phenotypes following RNAi induction were the 4 predicted basal body proteins TbCep76, TbCep164, TbWDR16 and TbWDR67; one protein which I have shown to be axonemal, TAX-3; and one predicted membrane protein, meckelin. As I have no data on the extent of RNAi knockdown for these, it is possible that the RNAi knockdown was unsuccessful. A second possibility is that these proteins may be expressed at low levels: RNAi may for this reason be less effective at achieving a level of knockdown sufficient to produce a phenotype.

Figure 3.6

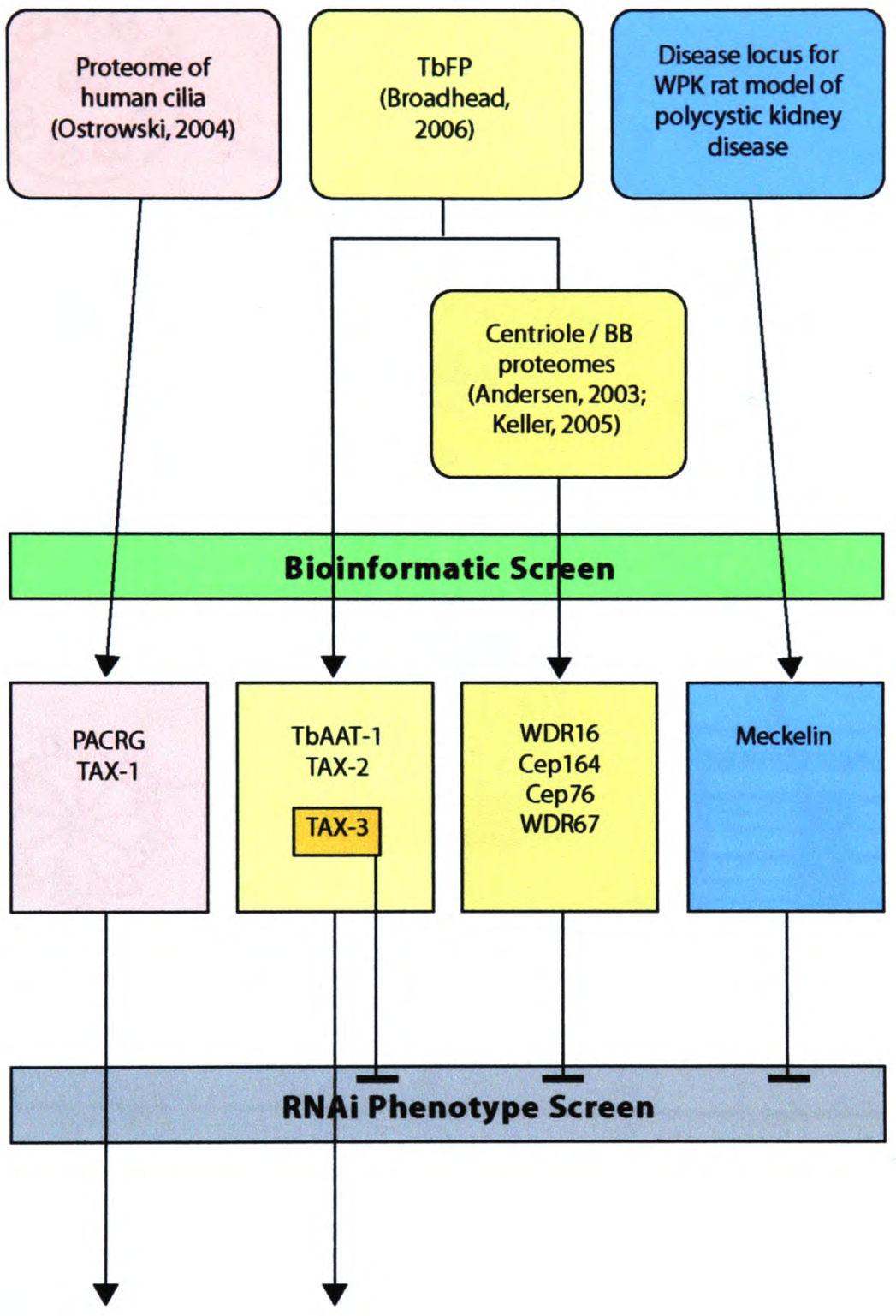


Fig. 3.6 Flagellar protein survey set: several sources resulting in a set of 11 proteins screened bioinformatically and using inducible RNAi. Flow chart showing the process of the survey and proteins involved. Proteins were selected from several proteomes, before being screened using a bioinformatic approach. Function was assessed using the inducible RNAi system in procyclic and bloodstream form trypanosomes. Those which had a detectable phenotype were deemed the "pass" set, as shown by arrows. Those with no detectable RNAi phenotype were not investigated further (arrows stop at RNAi screen).

Figure 3.7

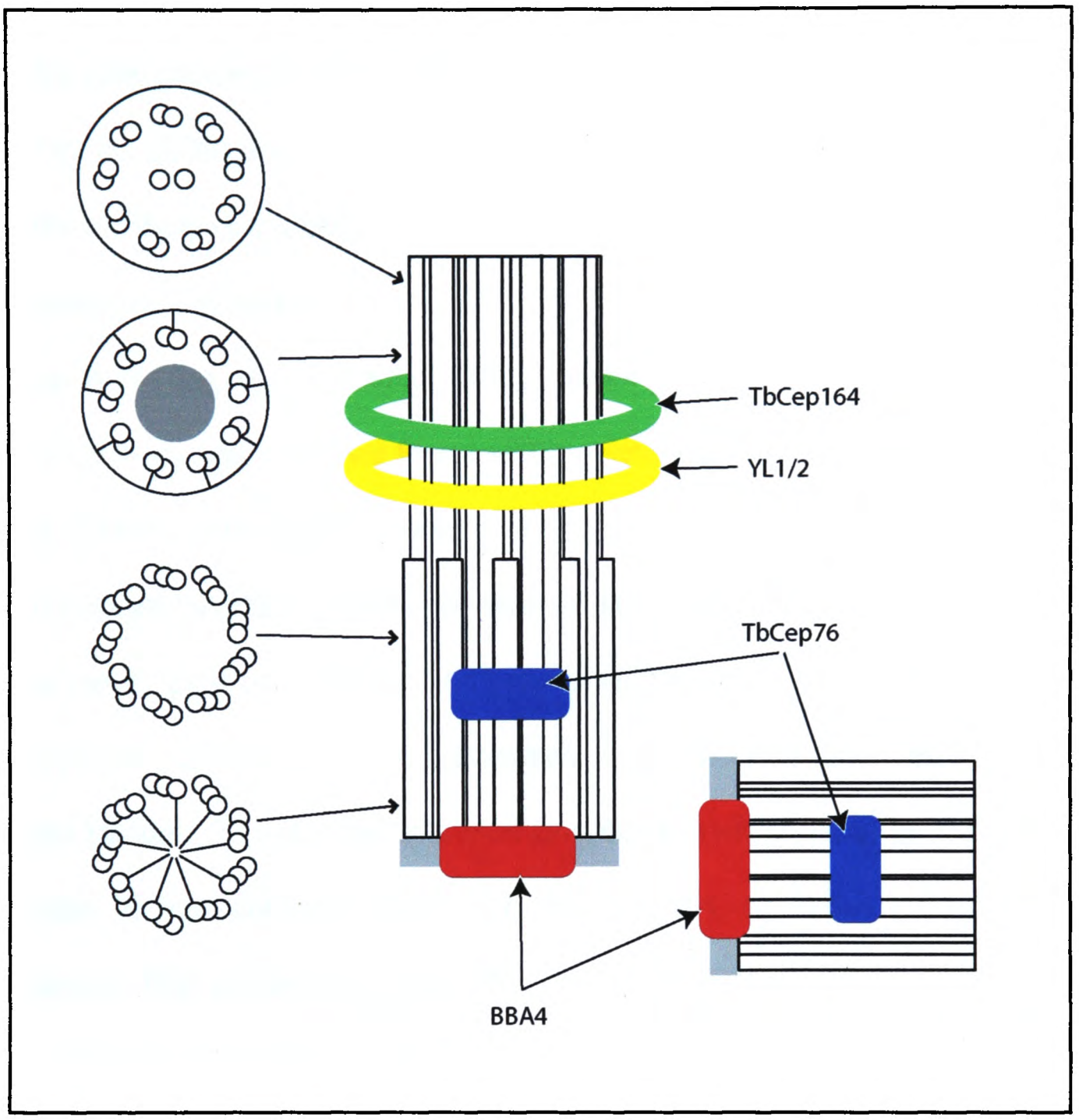


Fig. 3.7 Immunofluorescence of tagged basal body proteins suggests possible localisations within the basal body. The cartoon shows the basal body and probasal body with the locations of the antigens of BBA4 and YL1/2 marked. Immunofluorescence using this antibodies and BB2 to detect tagged TbCep76 and TbCep164 suggests the marked locations for these proteins.

The increasing number of flagellar proteomes available provides a valuable resource for researchers. In addition to the proteomes I used to search for proteins, two further flagellar proteomes of interest are those of isolated flagella from *C. reinhardtii* (Pazour et al., 2005) and *T. thermophila* (Smith et al., 2005). The method of isolation of flagella for these proteomes was deflagellation, a mechanism whereby cells shed their flagella in response to pH change or treatment with dibucaine. The point of breakage in the flagellum is beyond the transition zone, therefore proteins found only at the basal body would not be found within such proteomes. Hence, the basal body proteins Cep76 and Cep164 were not identified by either of these proteomes. Isolated flagella for the *C. reinhardtii* flagellar proteome (CrFP) were extracted in two different ways, producing several different fractions that provide some clue for the ultrastructural localisation. TAX-3 peptides were found mostly within the Tergitol extracted fraction. Tergitol disrupts membranes without destroying them, but allows the matrix to be washed away, so this fraction contains the axoneme and membranes. The extracted axoneme fraction, in which TAX-3 was also detected though with fewer peptides, contains axonemes stripped by KCl extraction of outer and inner dynein arms. That fewer peptides are detected in the fraction lacking outer or inner dynein arms may suggest that TAX-3 is associated with these structures. TbWDR16 was also detected in the CrFP, with multiple peptides detected in several fractions.

A recent large-scale survey of flagellar proteins identified through genomic comparison (which were named components of motile flagella or CMF) includes several proteins from this set (Baron et al., 2007). This study used RNAi to ablate protein expression of some 76 proteins in procyclic form trypanosomes, and

assessed phenotype in terms of cytokinesis defects. The authors attribute this, which they term 'clumping', to defects in cytokinesis caused by reduced motility. TbWDR16 (CMF-15) and TbCep164 (CMF-64) were found to exhibit little or no clumping following RNAi ablation, consistent with my findings. However, TAX-3 (CMF-10) and TbWDR67 (CMF-14) were found to produce clumping following RNAi ablation. While the link between motility and clumping is not fully determined, I observed no phenotype of reduced growth or cytokinesis defects or clumping in either of these cases.

Meckel-Gruber Syndrome, the disease caused by meckelin, is a severe autosomal recessive disorder characterised by renal cysts, developmental defects in the central nervous system and polydactyly. At present 3 loci for this disease are known, and named MKS1-3. MKS3, situated on human chromosome 8q21.13 – q22.1, is the first locus in which a causative gene has been identified. Sequnce prediction of meckelin suggests it is a transmembrane receptor, spanning the membrane 7 times. The function of meckelin remains unknown, and the protein shares little homology to any known proteins. However, there is topological similarity to the Frizzled (FZ) family, a family of receptor proteins that have been shown in *D. melanogaster* to play a role in planar cell polarity, a signal pathway also disrupted in Bardet-Biedl Syndrome.

CHAPTER 4

RESULTS

Characterisation of the Parkin co-regulated gene product, PACRG

4 Characterisation of the Parkin co-regulated gene product, PACRG

Preface
The work presented in this chapter is the result of collaboration within our laboratory. The work encompassed by Figures 4.4, 4.5 and 4.6 were contributed by Helen Dawe and Mike Shaw. The combined work was published as: Dawe, H. R., Farr, H., Portman, N., Shaw, M. K. and Gull, K. (2005) The Parkin co-regulated gene product, PACRG, is an evolutionarily conserved axonemal protein that functions in outer doublet microtubule morphogenesis. *J Cell Sci* **118**, 5421-30

4.1 Introduction

PACRG was originally identified (West et al., 2003) as a gene lying upstream of, and sharing a common promoter with *Parkin*, the gene implicated in juvenile Parkinson's disease. The quaking mouse (Sidman et al., 1964) is a spontaneous mutation with a large deletion in chromosome 17 that results in the loss of expression of both Parkin and PACRG (Lockhart et al., 2004). Mice have tremors characteristic of Parkinson's disease and in addition male homozygotes are sterile. PACRG loss has been identified as the cause of the male sterility component of this phenotype (Lorenzetti et al., 2004).

4.2 Two PACRG family members in *Trypanosoma brucei*

PACRG homologues were found to be widely conserved among flagellate organisms, including *Caenorhabtidis elegans* (Fig. 4.1). Sequences showed most

Figure 4.1

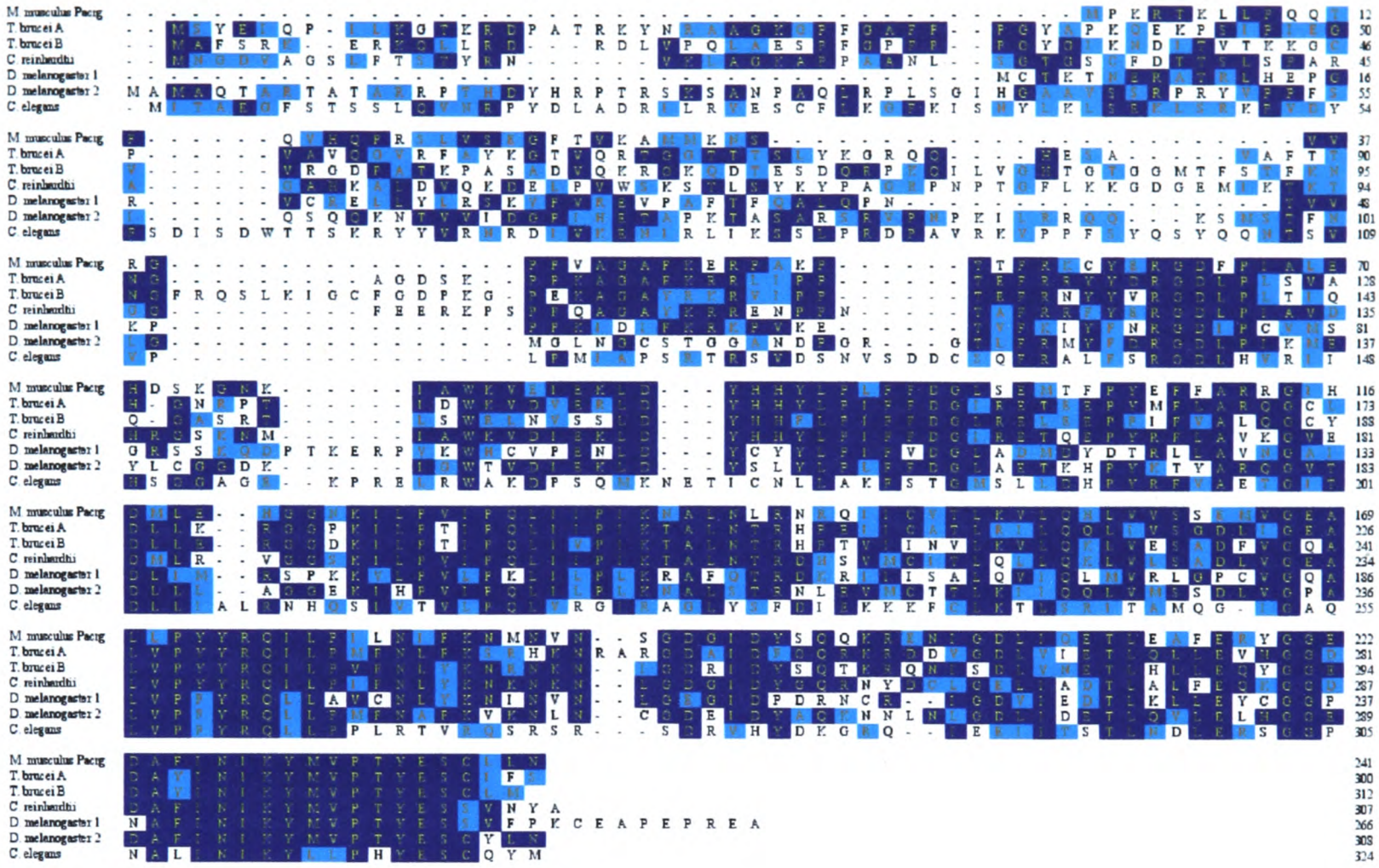


Figure 4.1. Two PACRG paralogues in *T. brucei*
Protein sequence alignment of two *T. brucei* PACRG-like proteins (Tb03.4808.210 and Tb09.210.1470) with gene products from *M. musculus* (XP_128418), *C. reinhardtii* (C_20334), *D. melanogaster* (CG179349 and CG15120) and *C. elegans* (NP_495496). Orthology was determined by examination of candidate sequences including reciprocal BLAST. Identical residues are shown in dark blue; similar residues are shown in light blue.

homology in the C-terminal region as shown by the large blocks of dark blue indicating identical residues in Fig. 4.1. Homologues were not found in the genomes of non-flagellate organisms including *Arabidopsis thaliana, Cyanidioschyzon merolae* and *Schizosaccaromyces pombe*. The protozoan parasite *T. brucei* was found to contain two paralogues with a high degree of conservation. These were named TbPACRG A and TbPACRG B, with TbPACRG A slightly more closely related to mouse and human PACRG homologues. TbPACRG A and B are conserved within the kinetoplastids *Leishmania major* and *Trypanosoma cruzi* in addition to *T. brucei.* PACRG appears to have been subject to multiple gene duplication events in several lineages: mammals possess a PACRG-like protein, *D. melanogaster* possesses two homologues and the ciliates *P. tetraurelia* and *T. thermophila* also have an expanded number of PACRG family members.

4.3 Ablation of both TbPACRG mRNAs produces slow growth and paralysis in procyclic form trypanosomes

To understand the function of PACRG in *T. brucei*, we used RNAi to ablate protein expression of the two PACRG family members both independently and together. Ablation of TbPACRG A or TbPACRG B alone produced no effect on cell growth rate (Fig. 4.2 b and 4.2 d respectively), however qRT-PCR analysis showed that the RNA levels fell to 9% (Fig. 4.2 a) and 8% (Fig. 4.2 c) of the parental (29-13 cell line) level respectively. The control containing sample mRNA that had not been treated with reverse transcriptase demonstrated minimal DNA contamination. Simultaneous ablation of TbPACRG A and B, with a reduction of TbPACRG A to 10% and TbPACRG B to 20% (Fig. 4.2 e), produced a slow growth phenotype first apparent at

Figure 4.2

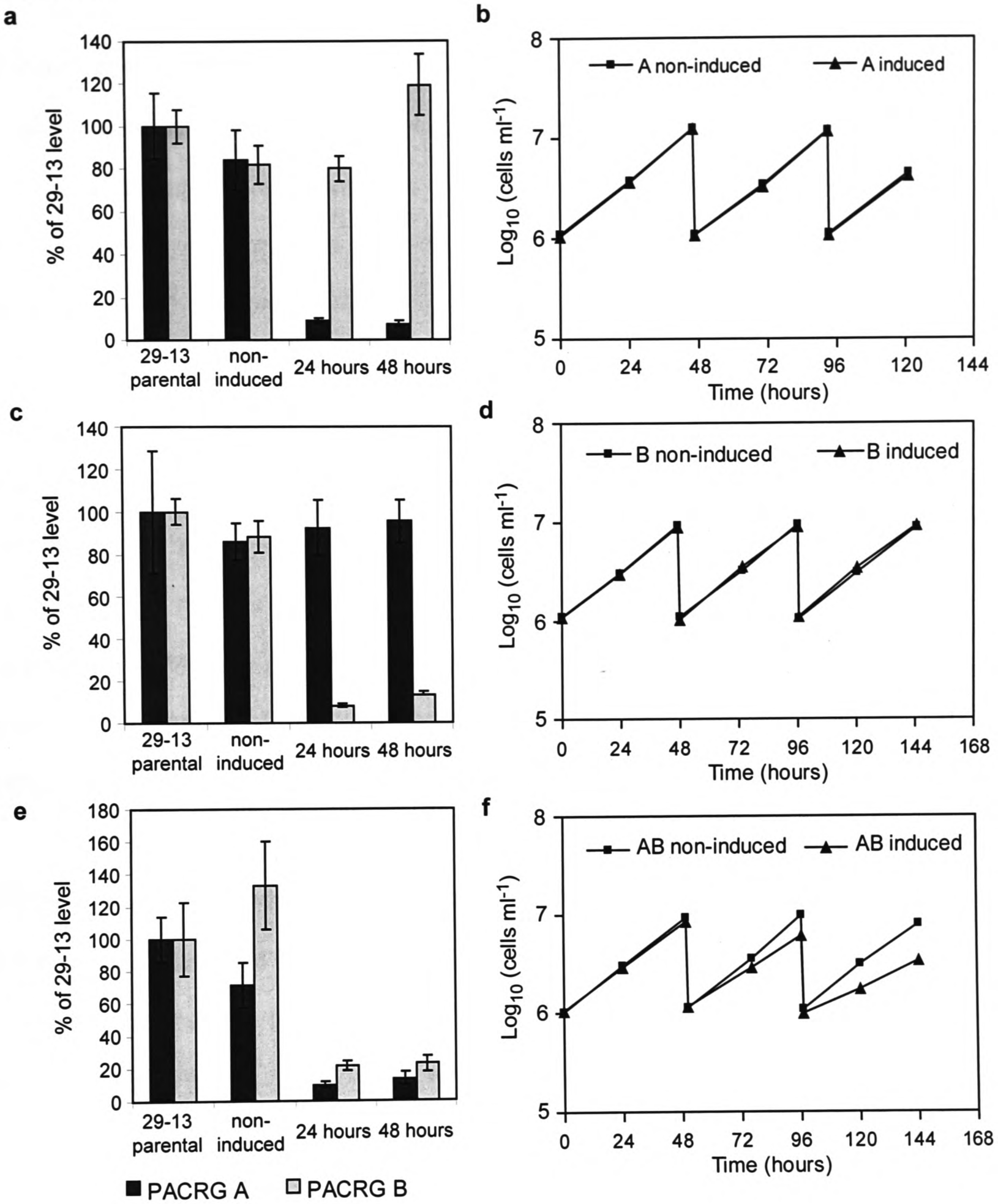


Figure 4.2. Ablation of PACRG AB produces slow growth phenotype
(a and b) RNAi of TbPACRG A. (a) Q-PCR data shows the reduction of mRNA signal of TbPACRG A (dark grey bars) but not TbPACRG B (light grey bars). Graph is expressed as mean +/- SEM. (b) Representative growth curve showing no alteration in growth kinetics in TbPACRG A RNAi-induced cells (black squares) compared to non-induced controls (triangles). (c and d) RNAi of TbPACRG B. (c) Q-PCR data shows the reduction of mRNA signal of TbPACRG B (light grey bars) but not TbPACRG A (dark grey bars). Graph is expressed as mean +/- SEM. (d) Representative growth curve showing no alteration in growth kinetics in TbPACRG B RNAi-induced cells (black squares) compared to non-induced controls (triangles). (e and f) RNAi of TbPACRG AB. (e) Q-PCR data shows the reduction of mRNA signal of TbPACRG A (dark grey bars) and TbPACRG B (light grey bars). Graph is expressed as mean +/- SEM. (f) Representative growth curve shows growth defect starting 72 hours after induction in TbPACRG AB RNAi-induced cells (black squares) compared to non-induced controls (triangles). For the growth curves (b, d, and f), cells were maintained in log phase by diluting the culture every 48 hours.

72 hours post-induction (Fig. 4.2 f). Induced cells appeared morphologically normal by phase contrast microscopy (Fig. 4.3, compare a and b to c and d), however in 27% cells undergoing cytokinesis (n = 200) there was incorrect positioning of the kinetoplast (Fig. 4.3). In some cells the kinetoplast was closer than normal to the nucleus (Fig. 4.3, compare distance between nucleus and kinetoplast in a to that in e), whilst in others it was positioned almost anterior to the most posterior daughter nucleus (Fig. 4.3 f, arrow indicates posterior kinetoplast). In each case of mis-positioning, the kinetoplast that is most affected tends to be that associated with the new flagellum, located at the posterior end of the cell. I also observed a small increase in the number of cells with two nuclei and two kinetoplasts (17% of the population in PACRG AB RNAi-induced cells compared to 12% in non-induced controls), suggestive of the fact that RNAi-induced cells have difficulties in late phases of the cell cycle.

TbPACRG AB RNAi-induced cells possessed flagella of normal length (20.3 μm ± 0.6 in non-induced cells (n = 100) compared with 20.3 μm ± 0.6 in induced cells (n = 100)) and continued to build a new flagellum each cell cycle. However, cell motility was strongly affected. At 24 hours after induction 20% of cells had a paralysed flagellum (n=108 cells) and did not locomote. By 48 hours this had increased to 48% (n=102 cells), and at 72 hours after induction, 73% of flagella (n=48 cells) were paralysed. Highly significant differences were observed between RNAi induced (n = 53) and non-induced cells (n = 38) in terms of minimum, mean and maximum speeds (Table 4.1, $P < 0.001$). Also shown for comparison in this table is the data for TbPACRG A RNAi-induced and non-induced cells, showing no significant difference in these parameters for these cells ($P = 0.28$).

Table 4.1

Population motility parameter		Minimum speed (μm/s)	Mean speed (μm/s)	Maximum speed (μm/s)
TbPACRG AB	Non-induced (n = 38)	1.1 ± 0.2	3.0 ± 0.2	4.8 ± 0.3
	Induced (n=53)	0.1 ± 0.1	0.8 ± 0.1	1.6 ± 0.2
TbPACRG A	Non-induced (n = 41)	1.9 ± 0.3	4.9 ± 0.3	8.1 ± 0.5
	Induced (n=39)	2.6 ± 0.4	5.6 ± 0.5	8.9 ± 0.7

Table 4.1. Induction of TbPACRG AB RNAi causes a severe loss in motility.
Speeds shown are the average minimum, mean and maximum speeds for a population of TbPACRG AB RNAi-induced and non-induced cells, and for a population of TbPACRG A RNAi-induced and non-induced cells.

Figure 4.3

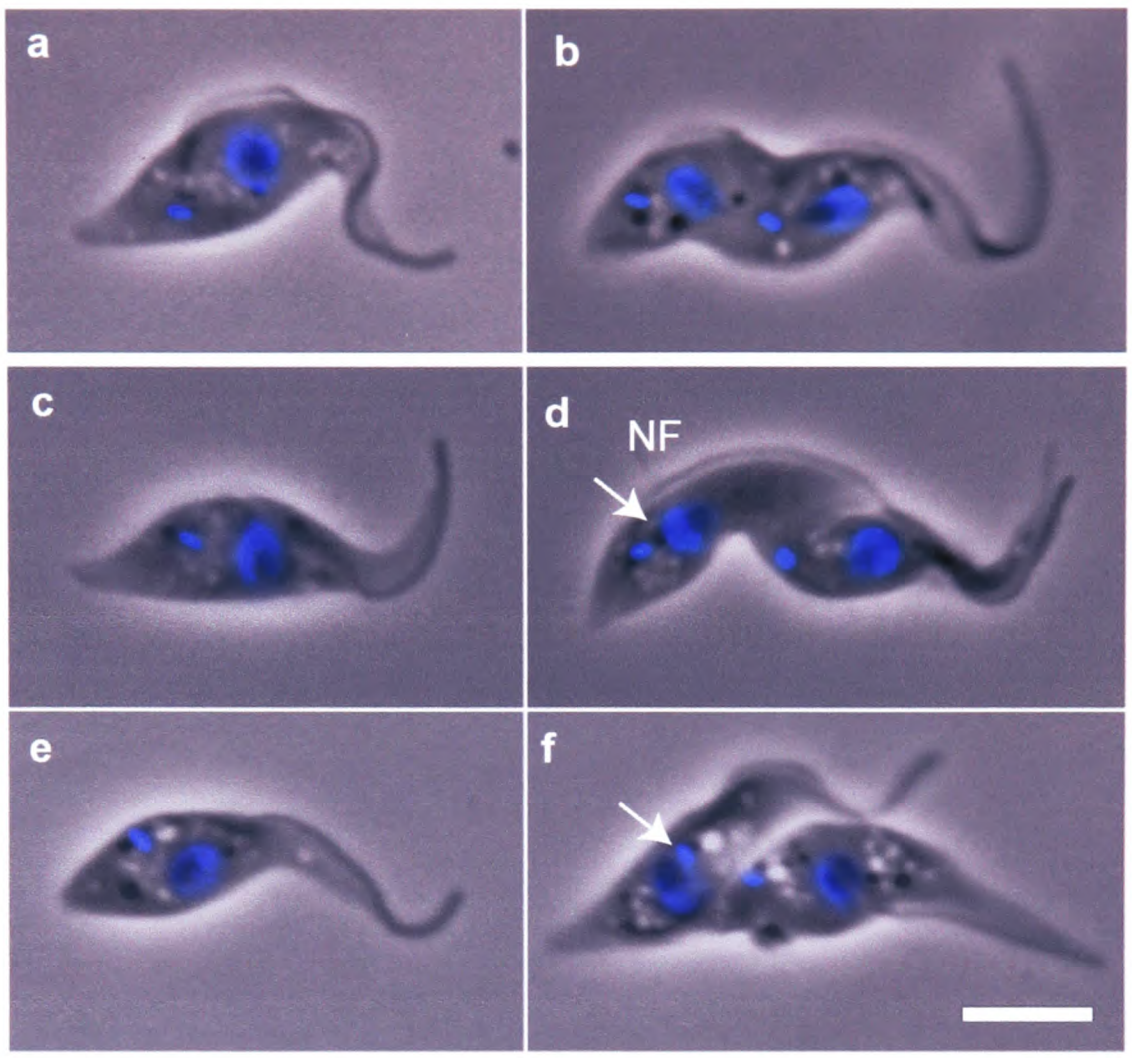


Figure 4.3. Induced cells build a flagellum, however daughter kinetoplast position is impaired.

Phase contrast images of control cells (a, b) and TbPACRG AB RNAi-induced cells at 72 hours (c - f) with nuclear and kinetoplast DNA overlaid in blue. (a) a non-induced cell with one kinetoplast and one nucleus (1K1N). (b) a non-induced cell with duplicated nucleus and kinetoplast (2K2N cell) showing correct positioning of both kinetoplasts. (c) a TbPACRG AB RNAi-induced cell with correct positioning of the kinetoplast. (d) a TbPACRG AB RNAi-induced cell undergoing division where the distance between the daughter kinetoplast (arrow) and the daughter nucleus is reduced compared to that of the parent cell. Note the formation of the new flagellum (NF). (e) a TbPACRG AB RNAi-induced 1K1N cell where the kinetoplast is mislocalised. (f) a TbPACRG AB RNAi-induced cell undergoing cytokinesis where the daughter kinetoplast (arrow) is mispositioned, anterior to the daughter nucleus. Bar = 5 μm.

4.4 TbPACRG AB RNAi induction causes loss of outer doublet microtubules

To understand the paralysis of the flagellum, TbPACRG AB RNAi-induced and non-induced cells were prepared for ultrastructural analysis by thin section transmission electron microscopy. A significant difference in the 9+2 architecture of the trypanosome flagellum was observed. In non-induced control cell profiles, 98% (n=922) possessed a canonical 9+2 axonemal arrangement (Fig. 4.4A a). In contrast, 53% (n=953, $P<0.001$) of axonemal profiles in induced TbPACRG AB RNAi cells exhibited loss of at least one of the nine outer doublet microtubules (Fig. 4.4A b-d). A minority of flagella profiles in TbPACRG AB RNAi-induced cells (4%) contained one or more displaced doublets outwith of the partial axoneme. The number of missing doublets varied; approximately equal numbers of 8+2, 7+2, 6+2 and 5+2 axonemes were observed. The central pair microtubules generally remained present until more than four outer doublet microtubules had been lost (Fig. 4.4A b and c). Axonemes containing four or fewer outer doublet microtubules lacked the central pair in 88% of cases (Fig. 4.4A d). Cells that were in division (n=50) and had two adjacent flagella profiles (the old flagellum and the newly-built flagellum) were examined. At cell division the cell maintains the old flagellum and assembles a new flagellum; it is possible to distinguish between the two as the old flagellum is always on the left when viewed from posterior to anterior (Sherwin and Gull, 1989). 51% of the cell profiles examined had two affected flagella, with at least one outer doublet missing from each. 18% of cell profiles exhibited one unaffected old flagellum and one affected new flagellum. The remainder had two unaffected flagella.

Figure 4.4

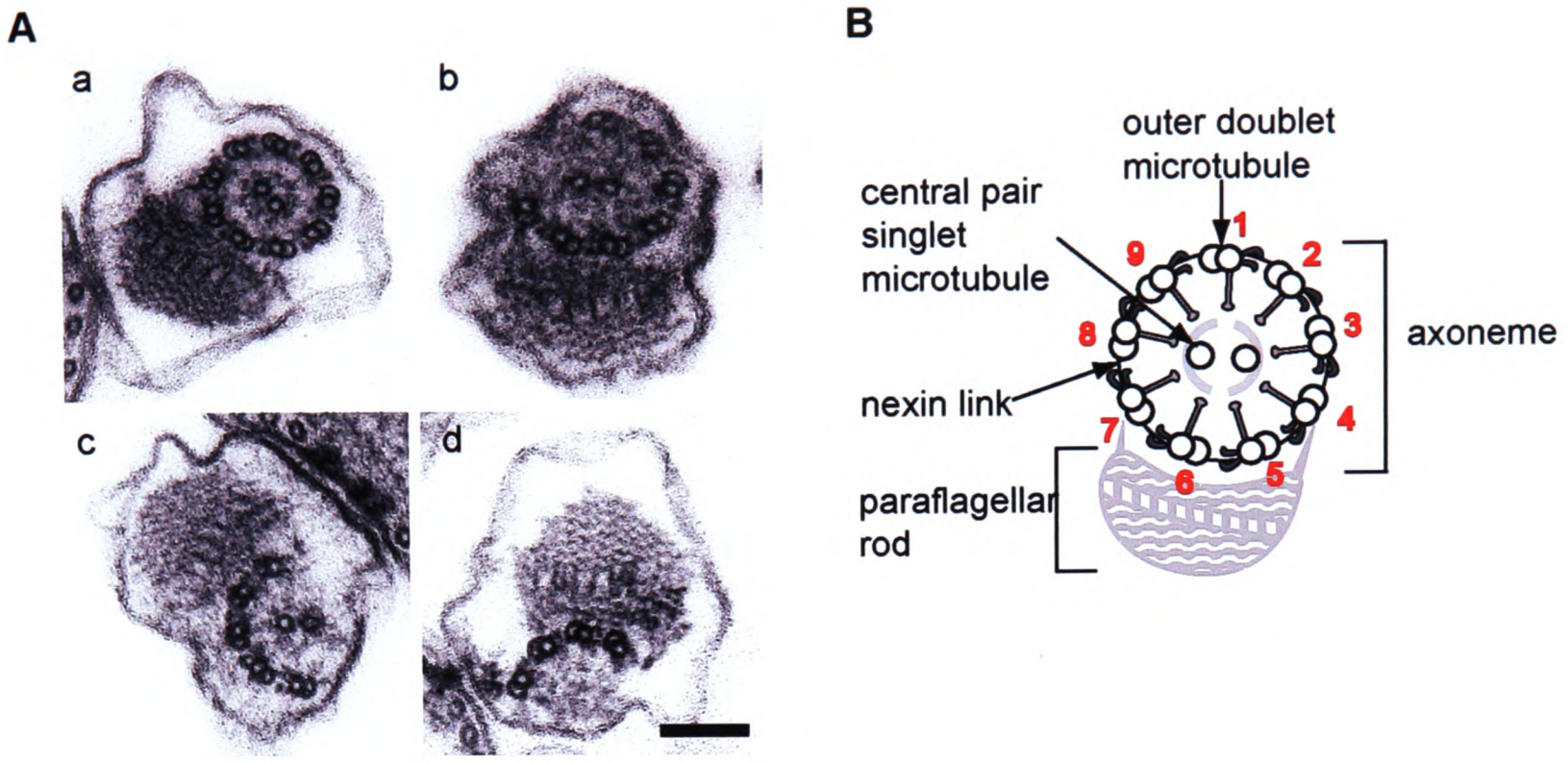


Figure 4.4. PACRG AB RNAi induction causes loss of outer doublet microtubules.

(A) Transmission electron microscopy images of TbPACRG AB non-induced cells (a) and RNAi-induced cells 72 hours after induction (b-d). Note the loss of variable numbers of outer doublet microtubules in b-d). (B) Cartoon showing relevant structures in a T. brucei flagellum. Numbers refer to the convention of numbering outer doublets according to their position relative to the central pair and PFR. (C) Graph to show the frequency of loss of specific outer doublet microtubules. Scale bar = 200 nm.

In *T. brucei*, outer doublets are numbered according to their position relative to the central pair and the PFR (Fig. 4.4B), with the doublet directly opposed to the central pair being numbered as 1 and stable connections to the PFR on doublets 4 and 7. Where multiple doublets had been lost, it was almost invariably those adjacent to each other that were absent (see Fig. 4.4A b for an example). The doublets furthest from the PFR - doublets 9 and 1 – were found to be most likely to be lost, followed by doublets 2 and 8 (Fig. 4.4C). The doublets adjacent to the PFR were rarely missing; doublets 4 and 7, which are most obviously attached to the PFR (Fig. 4.4B) were missing in only 4.7% of axonemes, while doublets 5 and 6 were absent in only 2.6% and 2.1% of axonemes, respectively (Fig. 4.4C).

4.5 Outer doublet microtubule number decreases towards the distal tip of the flagellum

Variability in the number of missing doublets raised the possibility that there could be a variation in the number of missing doublets along the length of an individual axoneme in TbPACRG AB RNAi-induced cells. To determine if fewer outer doublets were present at either the distal end of the flagellum or the proximal end, the number of outer doublets present at various positions along the axoneme was quantifed (Fig. 4.5). As the flagellum of *T. brucei* is attached to the cell body, which has different widths and morphology along its length, it is possible to position an axonemal profile in any given electron micrograph to a particular region of the flagellum. The flagellar profiles were then characterised into five subsets according to the adjacent cellular structures: transition zone, flagellum pocket, exit point of flagellum from cell, mid-cell region and anterior tip of cell. The basal bodies and transition zones (Fig. 4.5A) of

Figure 4.5

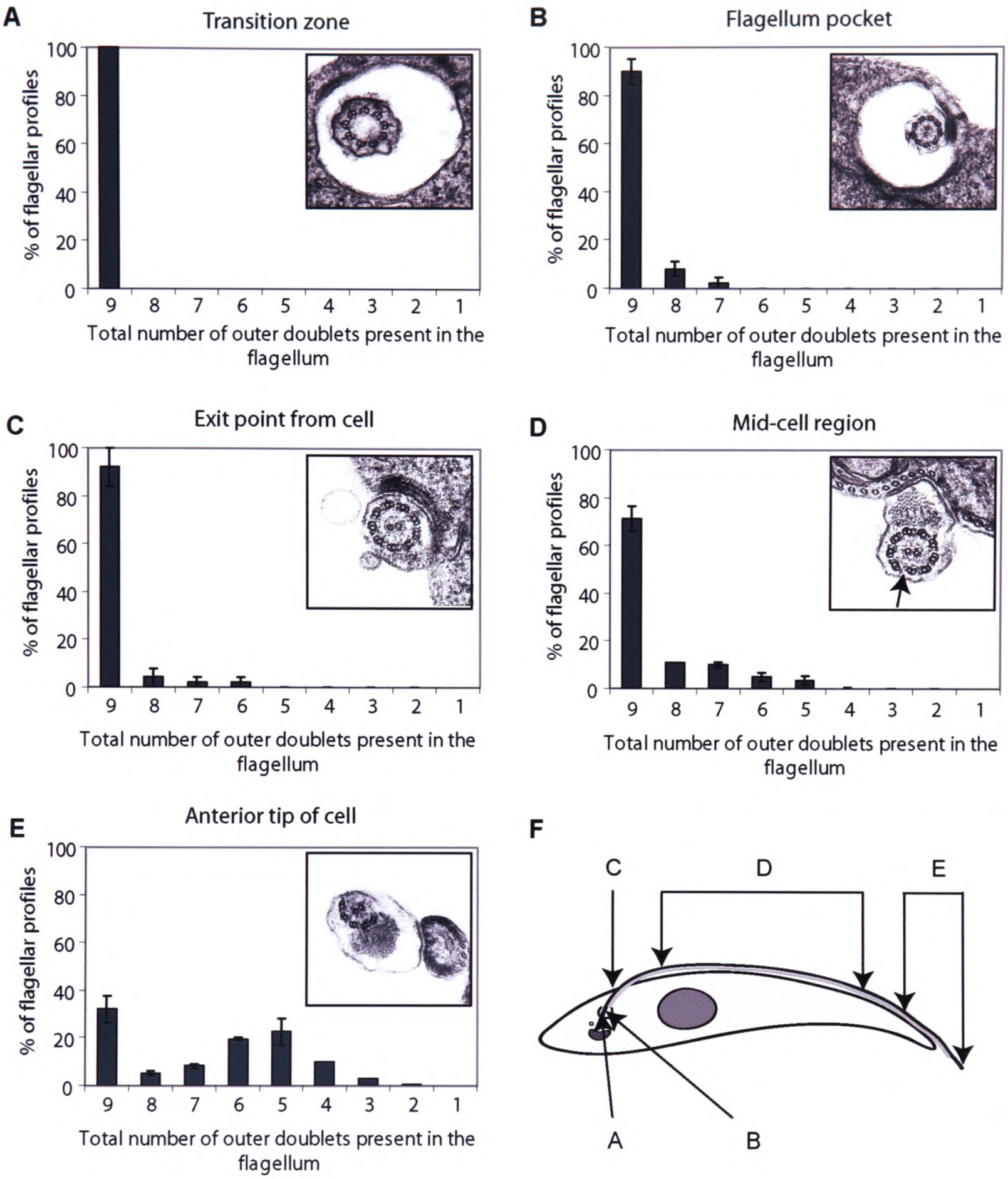


Figure 4.5. Multiple outer doublet loss occurs more frequently at the anterior of the cell.

(A-E) The number of outer doublets was quantified at various positions along the axoneme. Graphs show the number of outer doublets present plotted against the frequency of occurance in flagella profiles observed. Inset images show representative micrographs of flagella profiles at each position. The arrow in (D) indicates the break between two outer doublets that is observed prior to doublet loss. (F) Cartoon of a *T. brucei* cell indicating the positions along the flagellum quantified in A-E. Scale bar = 200 nm.

Figure 4.6

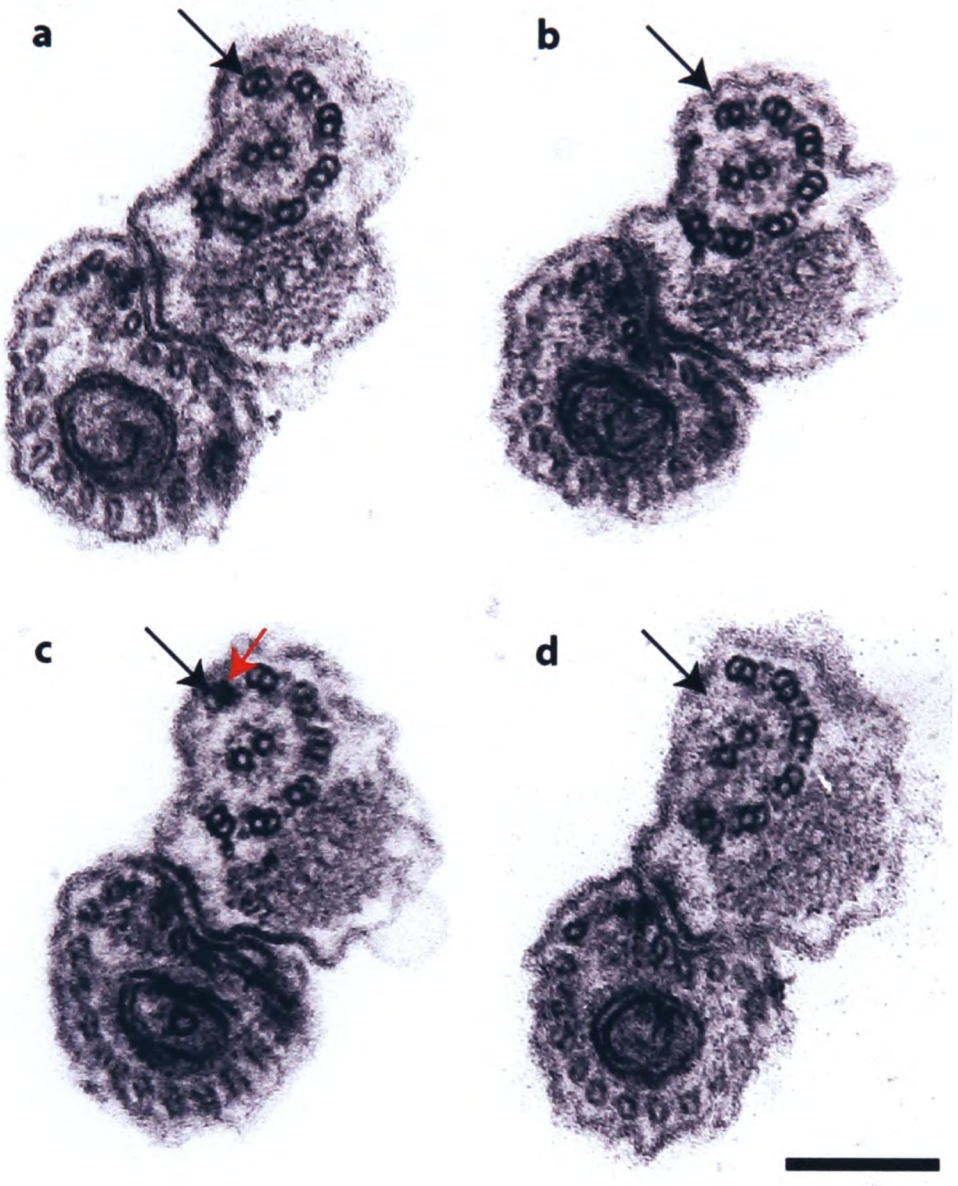


Figure 4.6. The A and B tubules terminate simultaneously.
Serial electron micrographs (from proximal to distal, a - d) showing loss of an outer doublet along a single axoneme. The black arrows indicate the position of the doublet that will be lost. Note the electron dense lumen in the A tubule (red arrow) immediately prior to doublet loss. Scale bar = 200 nm.

RNAi-induced flagella appeared normal. Over 90% of axonemes found within, or just exiting the flagellar pocket had nine outer doublets, with only a minority having up to three doublets missing (Fig. 4.5B and 4.5C, respectively). However, the number of outer doublets decreased significantly from then on along the length of the cell body (Fig. 4.5D), such that at the distal tip of the flagellum only 32% of axonemes exhibited a 9+2 configuration, with 55% composed of six or fewer outer doublets (Fig. 4.5E).

Serial thin section micrographs were prepared and examined in order to establish whether the missing doublets resulted from doublet termination. Serial sectioning through the distal tip region revealed that both the A and B tubules of a doublet terminated simultaneously (Fig. 4.6, black arrows show the doublet that is lost). An electron dense lumen was observed only in the A tubule (Fig. 4.6, red arrow) immediately prior to the loss of that doublet, similar to that observed in capped *Chlamydomonas* flagella (Dentler, 1980), suggesting that the doublet may be capped prior to termination.

4.6 GFP:TbPACRG fusion proteins localise to the axoneme

To localise each of the two TbPACRG proteins within *T. brucei*, one copy of the two endogenous genes was replaced with a GFP:TbPACRG fusion. Cell lines were constructed individually expressing GFP:TbPACRG A or GFP:TbPACRG B. In both instances, live cells exhibited a fluorescent flagellum. I performed immunofluorescence on detergent extracted cytoskeletons using anti-GFP polyclonal antibody (Invitrogen) and antibodies against the paraflagellar rod (L8C4 (Kohl et al., 1999)) or against the distal end of the basal body (BBA4 (Woods et al.,

Figure 4.7

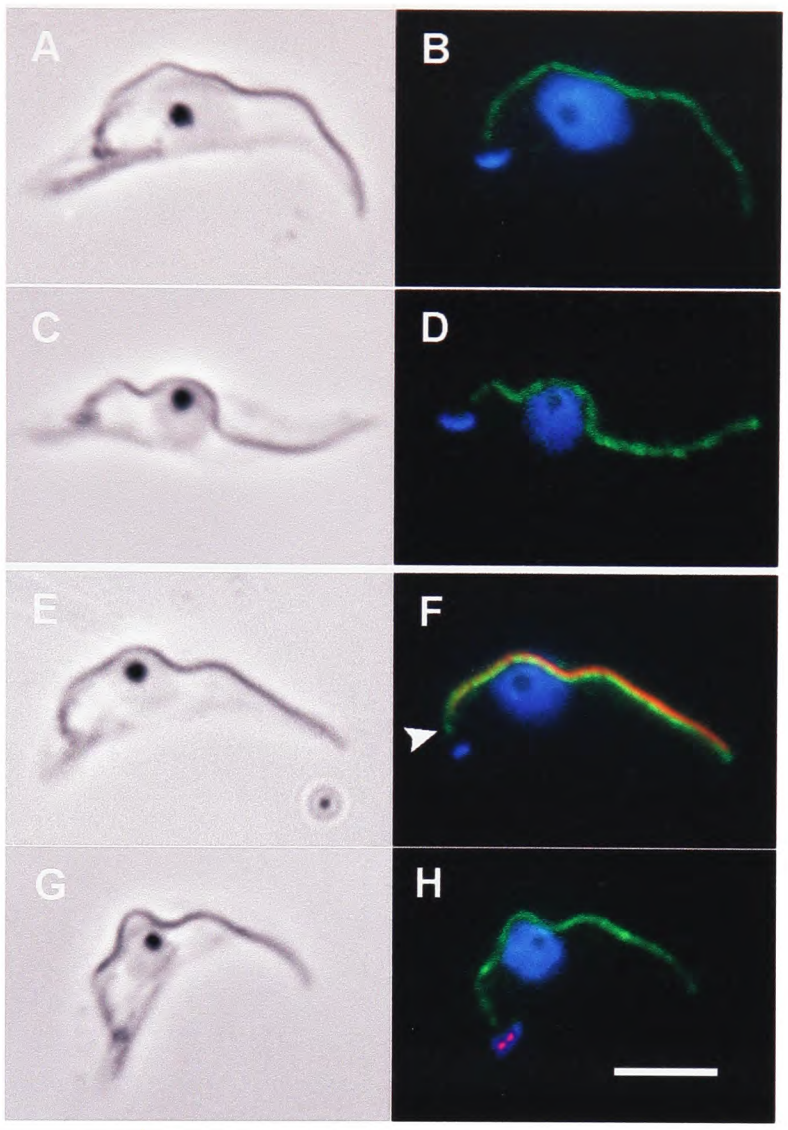


Figure 4.7. GFP-TbPACRG fusion proteins localise to the axoneme.
Phase contrast microscopy (A, C, E and G) and fluorescence (B, D, F and H) images of detergent extracted trypanosome cytoskeletons. DNA is labelled with DAPI (blue), and GFP is identified by anti-GFP polyclonal antibody. (green) (A, B) cells expressing GFP-TbPACRG A. (C, D) cells expressing GFP-TbPACRG B. (E, F) cells expressing GFP-TbPACRG A; the PFR is identified by the L8C4, anti-PFR, monoclonal antibody (red). Note the GFP signal extends proximal to the PFR staining (F, arrow). (G, H) cells expressing GFP-TbPACRG A; the distal end of the basal body is identified by the BBA4 monoclonal antibody (red). Scale bar = 5 μm.

1989b)). The anti-GFP staining ran along the entire length of the flagellum in cells expressing either GFP:TbPACRG A, (Fig. 4.7A, B) or GFP:TbPACRG B (Fig. 4.7C, D). I investigated to which subcompartment of the flagellum TbPACRG A was localised using dual labelling with antibodies to both the basal body and the PFR. The anti-GFP signal (Fig. 4.7F, green, arrow) extended beyond that of the PFR (Fig. 4.7F, red), demonstrating that GFP:TbPACRG is localised to the axoneme and not the PFR. No colocalisation was observed with the basal body (Fig. 4.7H, red staining marks the basal body), suggesting that TbPACRG appears in the flagellum distal to this structure. These localisation experiments were performed independently for both TbPACRG A and TbPACRG B, with identical results.

4.7 RNAi ablation of PACRG A and B in bloodstream form trypanosomes

TbPACRG A and TbPACRG B were ablated by RNAi in bloodstream form trypanosomes independently and together. This was done using the same RNAi constructs as were used in procyclic form trypanosomes. However, the results were unexpectedly different. As can be seen in Fig 4.8, RNAi ablation of TbPACRG A produced a phenotype of slow growth and defects in cytokinesis (Fig. 4.8 a, b), while RNAi ablation of TbPACRG B did not (Fig. 4.8 c, d). Ablation of both proteins simultaneously also produced a phenotype of slow growth and cytokinesis defects (Fig. 4.8 e, f).

Following induction of TbPACRG A or TbPACRG AB RNAi, bloodstream cells ceased dividing but continued to progress through the cell cycle. RNAi-induced cells

Figure 4.8

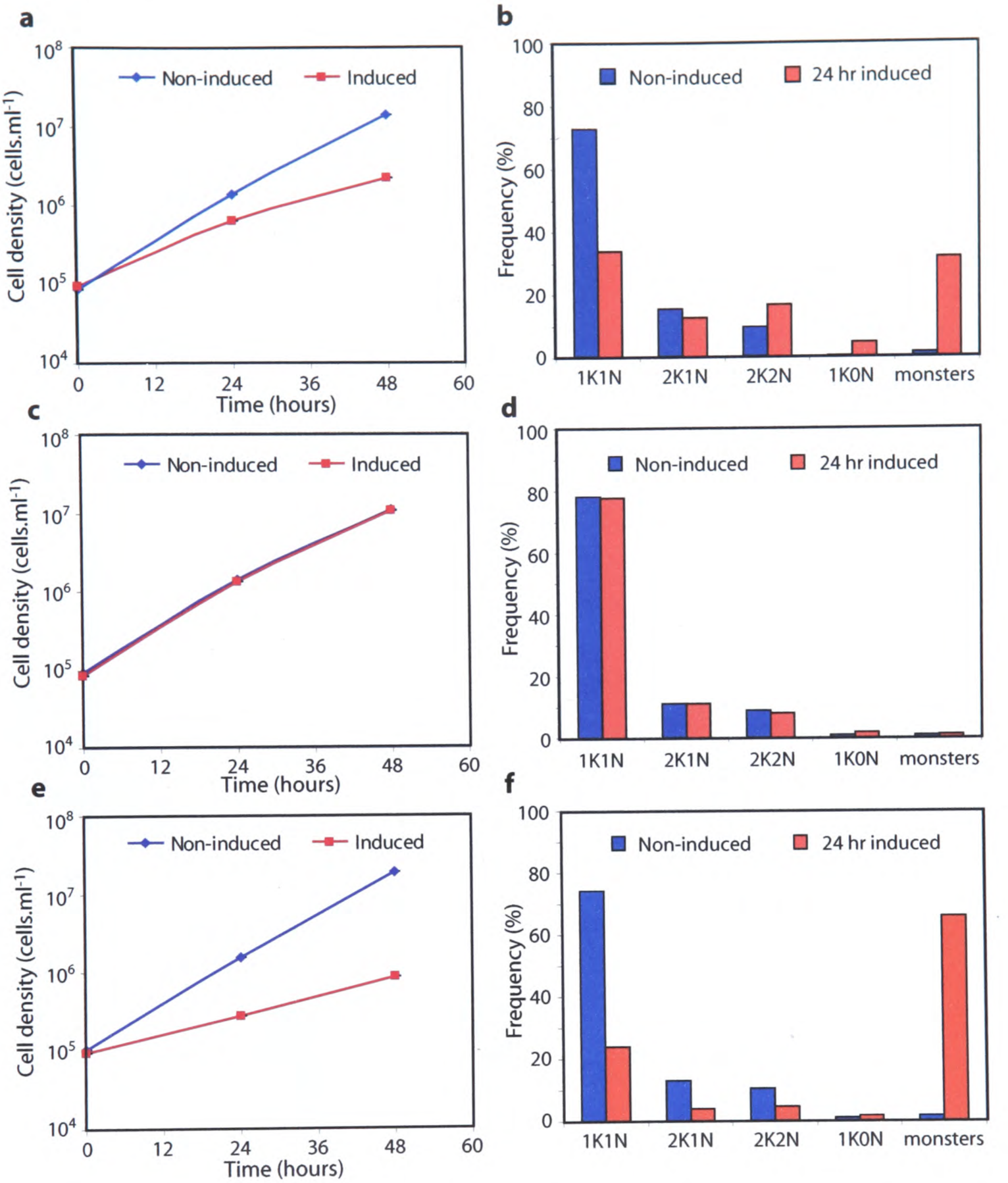


Figure 4.8 RNAi ablation of TbPACRG A and B in bloodstream form trypanosomes. (a, b) RNAi of TbPACRG A (a) Cumulative growth curve showing slow growth of TbPACRG A RNAi-induced cells (red) compared to non-induced controls (blue). (b) Counts of nuclei and kinetoplasts reveals a reduction of 1K1N cells and increase in monsters in TbPACRG A RNAi-induced cells (red) compared to non-induced controls (blue). (c, d) RNAi of TbPACRG B (c) Cumulative growth curve showing no alteration in growth kinetics of TbPACRG B RNAi-induced cells (red) compared to non-induced controls (blue). (b) Counts of nuclei and kinetoplasts reveals no difference in nucleua and kinetoplast number in TbPACRG B RNAi-induced cells (red) compared to non-induced controls (blue). (e, f) RNAi of TbPACRG AB (e) Cumulative growth curve showing slow growth of TbPACRG AB RNAi-induced cells (red) compared to non-induced controls (blue). (f) Counts of nuclei and kinetoplasts reveals a reduction of 1K1N cells and increase in monsters in TbPACRG AB RNAi-induced cells (red) compared to non-induced controls (blue).

Figure 4.9

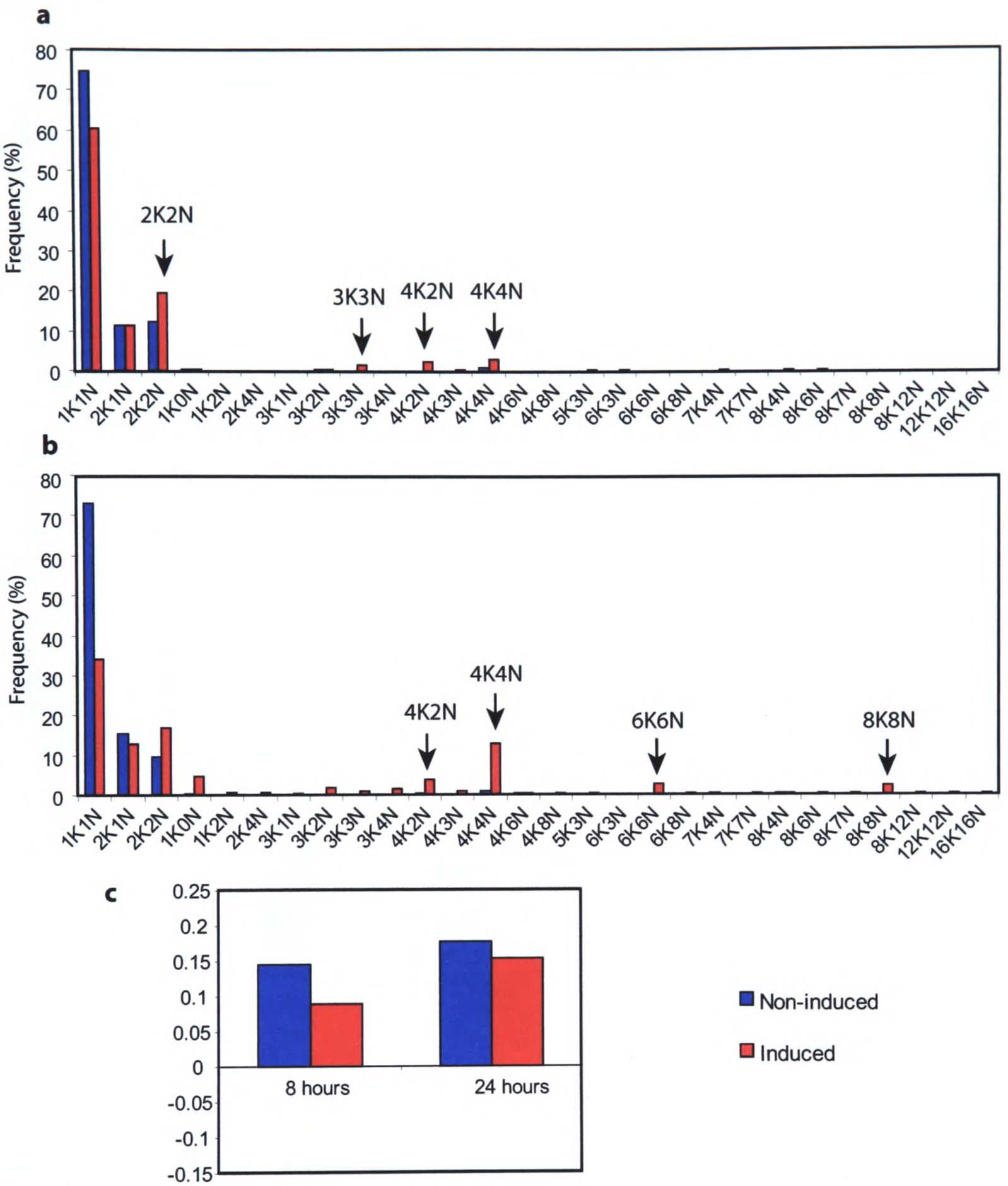
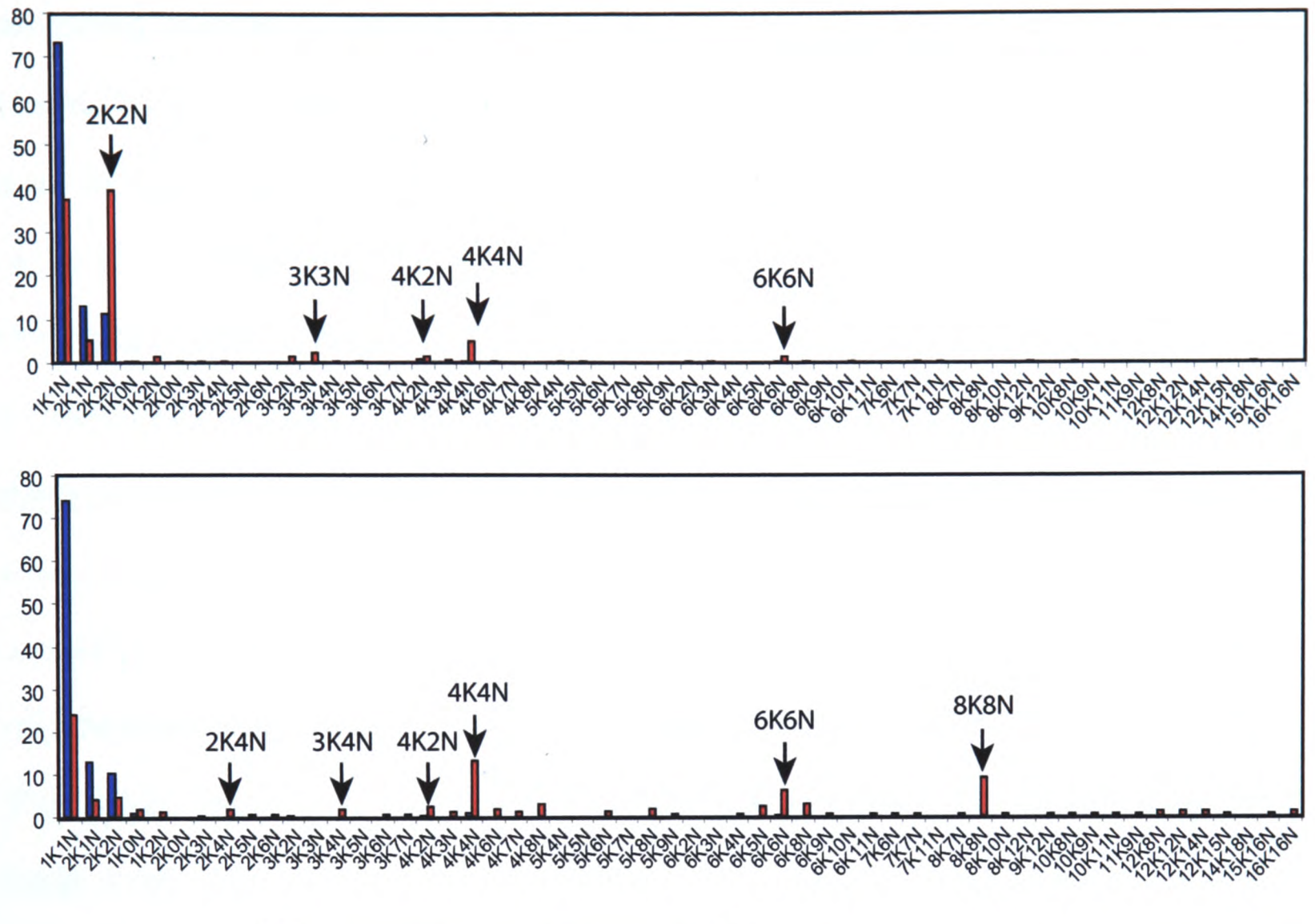


Figure 4.9. Counts of kinteoplast and nucleus number for TbPACRG A RNAi bloodstream form trypanosomes

(a) Counts of kinetoplast and nucleus number of TbPACRG A RNAi-induced cells at 8 hours post-induction (red, n=500) and non-induced controls (blue, n=500), revealing an increase in 2K2N cells and the presence of 3K3N, 4K2N and 4K4N cells in the population. (b) Counts of kinetoplast and nucleus number of TbPACRG A RNAi-induced cells at 24 hours post-induction (red, n=298) and non-induced controls (blue, n=500), revealing an increase in multinucleate cells in the population. (c) graph showing the log ratio of total number of K: total number of N in the population of non-induced cells (blue bars) compared with induced cells (red bars) at 8 and 24 hours post-induction.

Figure 4.10



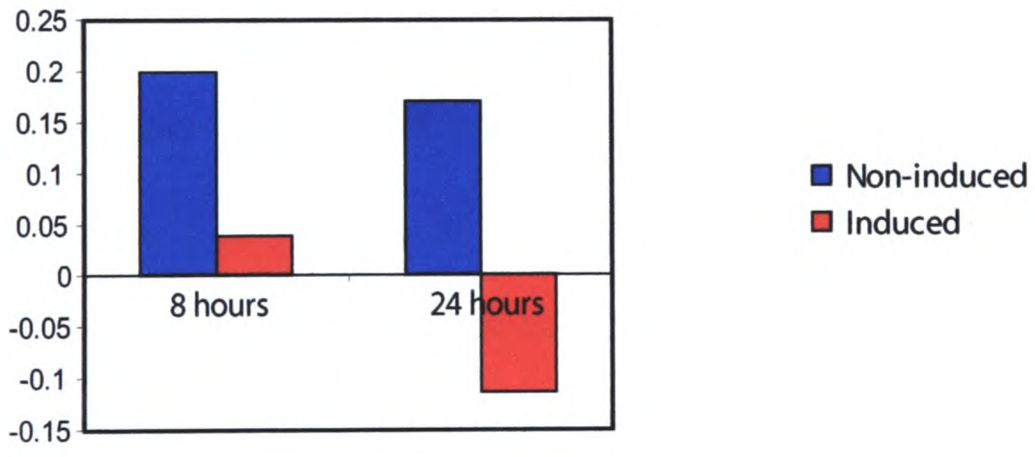


Figure 4.10. Counts of kinteoplast and nucleus number for TbPACRG AB RNAi bloodstream form trypanosomes

(a) Counts of kinetoplast and nucleus number of TbPACRG AB RNAi-induced cells at 8 hours post-induction (red, n=500) and non-induced controls (blue, n=500), revealing an increase in 2K2N cells and the presence of 3K3N, 4K2N, 4K4N and 6K6N cells in the population. (b) Counts of kinetoplast and nucleus number of TbPACRG AB RNAi-induced cells at 24 hours post-induction (red, n=175) and non-induced controls (blue, n=500), revealing an increase in multinucleate cells in the population. (c) graph showing the log ratio of total number of K: total number of N in the population of non-induced cells (blue bars) compared with induced cells (red bars) at 8 and 24 hours post-induction. The log ratio of K:N is decreases in RNAi-induced cells compared to control cells.

initiated new rounds of S phase and mitosis, leading to large contorted cells containing multiple kinetoplasts and nuclei. The phenotype caused by ablation of TbPACRG AB simultaneously is apparently more severe than A alone, as can be seen by comparing growth rate and frequency of cells with abnormal numbers of nuclei and kinetoplasts (Fig. 4.8, compare (a, b) with (e, f)). Counts of number of kinetoplasts and nuclei in cells reveal that at 8 hours post-induction, the population of TbPACRG A RNAi-induced cells exhibit a higher frequency of cells with 2 kinetoplasts and 2 nuclei (2K2N, Fig. 4.9a). Additionally cells are observed that have undergone further rounds of mitosis and kinetoplast segregation with 3K3N, 4K2N and 4K4N configurations (Fig. 4.9a). This is increased by 24 hours post-induction with RNAi-induced cells possessing a variable number of nuclei and kinetoplasts (Fig. 4.9b); from these counts it is possible to calculate the total number of kinetoplasts and nuclei in the population. This is displayed as the log ratio of kinetoplasts to nuclei (Fig. 4.9c). A ratio of 1 kinetoplast:1 nucleus would give a log ratio of zero, so a positive log ratio indicates more kinetoplasts than nuclei in the population. The log ratio of kinetoplasts:nuclei remains similar between non-induced and induced TbPACRG A cells, suggesting that mitosis and segregation of kinetoplasts are occurring synchronously in induced cells. In contrast to this, a feature of the cytokinesis phenotype of TbPACRG AB RNAi-induced cells is the change in log ratio of kinetoplasts: nuclei. At 8 hours post-induction there is a large increase in frequency of 2K2N cells from 11% in non-induced control cells to 40% in RNAi-induced cells (Fig. 4.10a). By 24 hours the frequency of cells possessing abnormal numbers of kinetoplasts and nuclei is 65%. Of these, a large number possess more nuclei than kinetoplasts. As zoids (cells with 1 kinetoplast and no nucleus) are not observed in large numbers (Fig. 4.10b), this suggests failure of

kinetoplast replication or segregation, as indicated by the decrease in log ratio to below -0.1 in TbPACRG AB RNAi-induced cells (Fig. 4.10c).

On RNAi induction, cells produced new flagella but did not complete division. At 8 hours post-induction this is reflected by an increase in the number of cells with 2 flagella (Fig. 4.11 c). This continued through to 24 hours, producing cells that had lost their normal morphogenetic axes, with the multiple flagella twisted around the enlarged cell body (Fig. 4.11 e, f). Thin-section transmission electron microscopy showed that the cell periphery was highly convoluted; this can be seen at the earlier time-point (Fig. 4.12 a, b) in addition to at 24 hours (Fig. 4.12 c). Multiple nuclei were present ('N', Fig. 4.12 c) and some flagella were attached to the outside of the cell, while others were located in a highly enlarged flagellar pocket (Fig. 4.12 f). Missing outer doublets were observed in axonemal profiles; as with the procyclic phenotype it was most frequently the non-PFR associated doublets that were missing (Fig. 4.12 d, e, g).

4.8 Conclusions and discussion

The aim in this work was to characterise the location and function of the evolutionarily conserved protein PACRG. I have shown that TbPACRG A and TbPACRG B localise to the axoneme of the eukaryotic flagellum and that simultaneous ablation of TbPACRG A and B expression produces a dramatic motility phenotype caused by loss of outer doublet microtubules. Taken together these results identify a novel axonemal protein that appears to play a role in outer doublet microtubule stability.

Figure 4.11

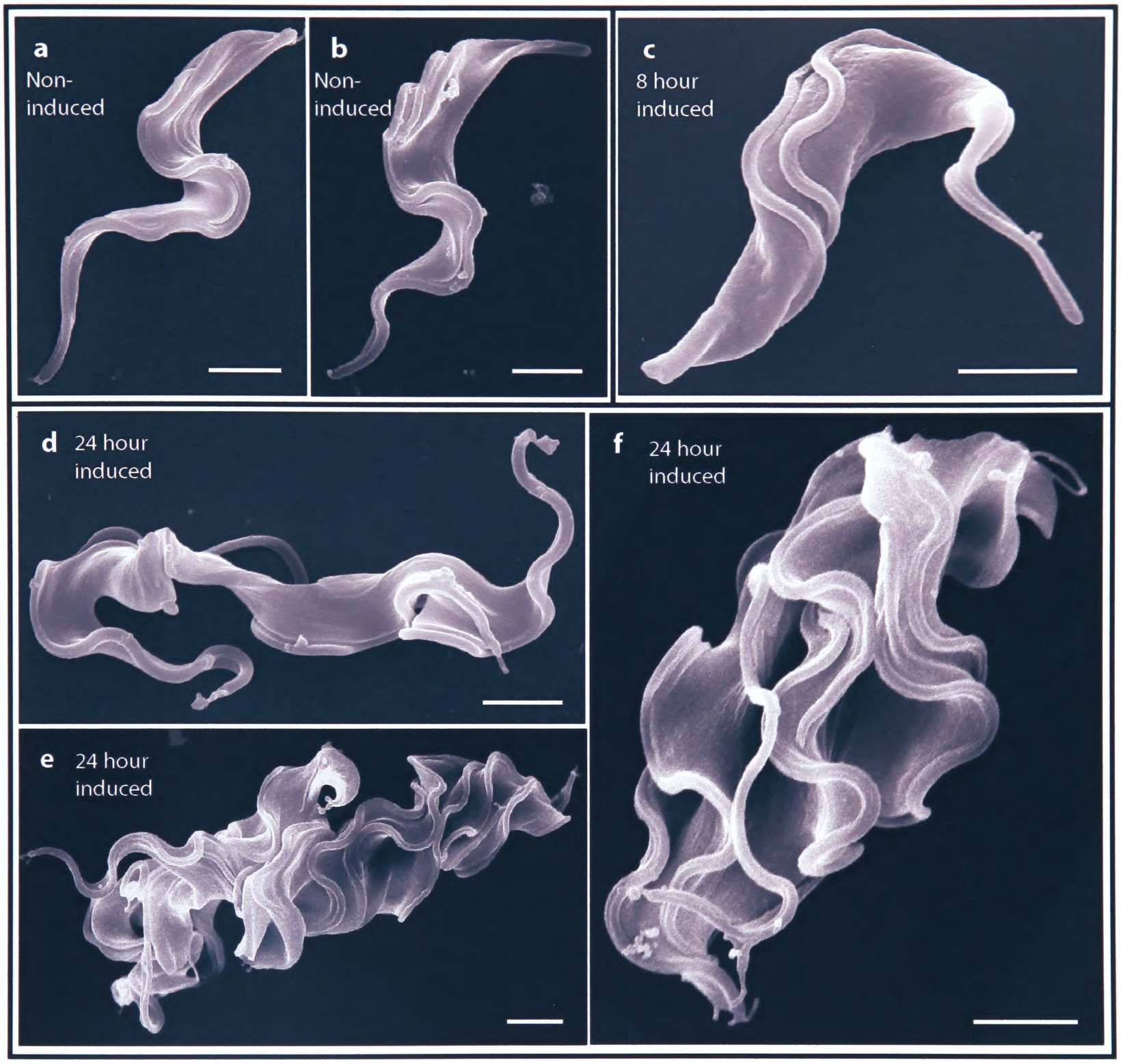


Figure 4.11. Scanning Electron Microscopy reveals enlarged cells with multiple flagella

(a-b) micrographs of non-induced TbPACRG A cells. (c) shows a cell with 2 flagella at 8 hours post-induction. (d-f) show cells at 24 hours post-induction with multiple flagella. Scale bars = 2 um

Figure 4.12

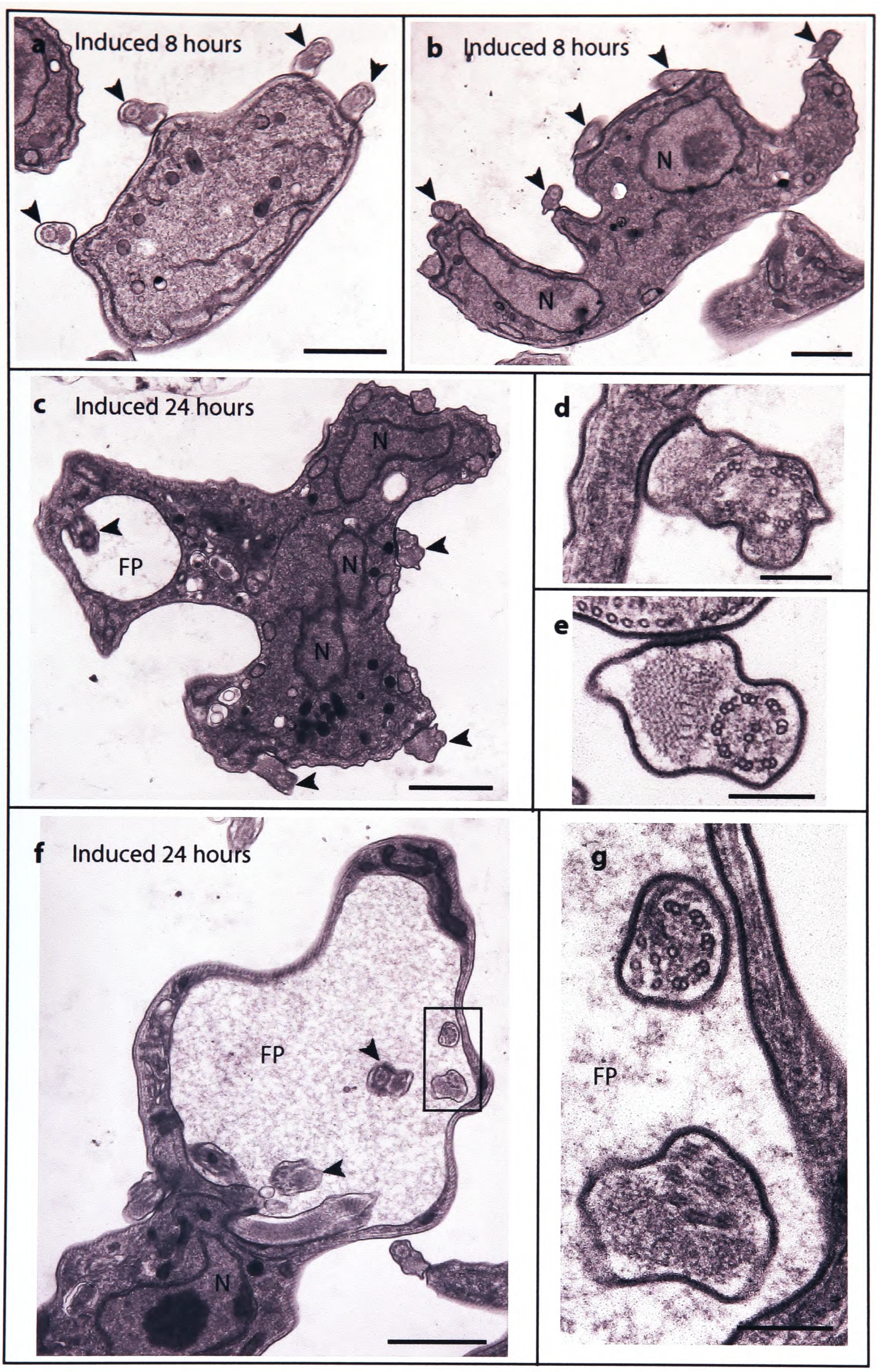


Figure 4.12. Transmission Electron Microscopy reveals cells with multiple nuclei and large flagellar pockets.

(a-b) show TbPACRG AB RNAi-induced cells at 8 hours post-induction. (c) shows a cell with multiple nuclei, several flagella and an enlarged flagellar pocket. (d-e) show axonemal profiles with missing or disrupted outer doublets. (f) shows a cell containing a very large flagellar pocket-like structure with several flagellar profiles within it. The boxed area is enlarged in (g), showing two of the flagellar profiles, both of which have missing doulets. N, nuclei; FP, flagellar pocket; arrowheads mark flagellar profiles. Scale bars in (a-c, f) = 1 um, scale bars in (d, e, g) = 200 nm.

I have shown using bioinformatics that *T. brucei* possesses two closely related PACRG paralogues. Two other kinetoplastid protozoa, *T. cruzi* and *L. major*, also possess two PACRG paralogues, indicating the situation in *T. brucei* is not the result of a recent gene duplication. To date there is no evidence to suggest functional differences between the two proteins. Although very similar at the protein level and therefore likely to share functionality, they are different enough at the nucleic acid level for us to select between them with RNAi.

RNAi of TbPACRG A and B produces a major motility phenotype in procyclic form trypanosomes. Despite the lack of cell locomotion the flagellum is built and at the light microscope level extends to essentially the same length as that observed in non-induced controls. There are, in addition, detectable cellular consequences for cell morphogenesis. First, the adversely affected new flagellum is associated with a mis-positioning and/or mal-segregation of the replicated kinetoplast. The importance of the flagella connector in trypanosome procyclic cell morphogenesis has been shown previously, and it is thought that force applied by the new flagellum via connector attachment to the old is responsible for kinetoplast segregation in procyclic trypanosomes (Moreira-Leite et al., 2001; Briggs et al., 2004b). This present evidence shows that impairment of flagellar structure and flagella connector action produces an ineffective movement of the new basal body / kinetoplast. Ultimately, such defects in cellular morphogenesis appear to accumulate and become compounded such that cell growth is affected.

A previous study has shown that mouse Pacrg was present in the sperm flagellum (Lorenzetti et al., 2004) but its localisation to a flagellar compartment or function was

not elucidated. I used GFP-PACRG fusion proteins to confirm this general localisation in trypanosome flagella, specifically the axoneme. Furthermore, TbPACRG A and B are both present in a preparation of the detergent-insoluble flagellar fraction (Broadhead et al., 2006). I found that it did not localise to the basal body in *T. brucei*, however there is evidence that in other systems PACRG is associated with the basal body. A recent proteome of *T. thermophila* basal bodies identified PACRG as a component (Kilburn et al., 2007), although it is worth noting that in this organism there has been extensive expansion of the PACRG family, perhaps reflecting additional functions that may not occur in *T. brucei*. Furthermore, PACRG was identified from a proteome of centrioles from *Chlamydomonas* (Keller et al., 2005). I have been unsuccessful at localising TbPACRG A or TbPACRG B at the ultrastructural level. Aspects of the phenotype suggested possibilities for its sub-axonemal localisation, leading us to propose the nexin interdoublet links as a likely localisation. The interdoublet or nexin linkages have long been defined (Gibbons, 1965; Stephens, 1970; Stephens and Edds, 1976; Warner, 1976; Olson and Linck, 1977) as an electron dense band connecting the A tubule of one doublet to the B tubule of the adjacent doublet. It is proposed that these are elastic structures (Minoura et al., 1999) that enable the sliding of the doublets, yet to date their molecular identity remains unknown. Weakening of the nexin or other intermicrotubule linkages would be expected to lead to flagellar paralysis as the dynein-mediated interdoublet sliding that results in motility would be compromised. A recent study has localised PACRG in (Keller et al., 2005), where it was found to localise along the outer doublet microtubules in both the axoneme and basla body (Ikeda et al., 2007). The localisation of PACRG suggested that it formed a structural

component of the outer doublet microtubules, possibly involved in the attachment of the interdoublet links to the microtubules.

One other protein is known to cause immotile sperm due to outer doublet loss (Sampson et al., 2001). However, this protein, a voltage dependent anion channel called VDAC3, localises to the outer dense fibres of sperm (Hinsch et al., 2004) rather than the axoneme and loss of only a single outer doublet microtubule has been observed (Sampson et al., 2001). The presence of TbPACRG A and TbPACRG B along the whole length of the axoneme suggests that they are not required for outer doublet initiation. Further evidence for this comes from the absence of TbPACRG A and B from the basal body and transition zone regions, which appear normal by electron microscopy in TbPACRG AB RNAi-induced cells. It is known that flagellar paralysis can result from loss of structures such as the PFR (Bastin et al., 1998), axonemal radial spokes and central pair (Warr et al., 1966; Witman et al., 1978; Smith and Lefebvre, 1997; McKean et al., 2003), however these structures are all present in TbPACRG AB RNAi-induced cells. The central pair remains present until more than four outer doublets have been lost, suggesting that this is a secondary effect of loss of multiple outer doublets. The presence of a *PACRG* homologue in the *C. elegans* genome supports the idea that TbPACRG A and B are involved in the formation of outer doublet microtubules but not the central pair.

In the majority of dividing cells both the old and new flagella exhibited outer doublet loss. This suggests that an affected old axoneme does not immediately stop morphogenesis of new axonemal/cytoskeletal architecture. This finding also

demonstrates that the new axoneme starts to show doublet abnormalities before cytokinesis has occurred – in other words, during its late morphogenesis.

Outer doublet number along was found to be normal at the proximal end of the flagellum and varied at the distal end, suggesting that axoneme formation is initiated normally. One possibility for PACRG function could be a role in outer doublet extension. Depletion of PACRG would therefore lead to premature termination of outer doublet microtubules, an idea supported by the capped A tubule seen in Fig. 4.6 prior to disappearance of that doublet. This explanation would fit with the observed increase in the number of missing microtubules along the flagellum, as observed in Fig. 4.5. The lack of random doublet termination around the axoneme would be explained by the fact that those doublets attached to the PFR would be preferentially stabilised by this connection. Alternatively, the microtubule outer doublets might be extended to their full length and then undergo partial catastrophe. Again, firmer linkages between doublets adjacent to the PFR could lead to their preferential stabilisation. Premature termination of doublets could result from weakened interdoublet linkages. Axonemes were observed which contained nine outer doublet microtubules where there is an apparent break in the connection between two adjacent doublets (e.g. Fig. 4.5D, inset, arrow indicates break), suggesting the integrity of the linkages may be compromised. One feature of the phenotype was the preferential loss of specific outer doublets. Those furthest from the PFR (9, 1 and 2) were most frequently lost, suggesting that the PFR may play a stabilising role. The physical connection between the PFR and doublets 4 and 7 is expected to reduce strain on the ring structure in this region by restricting lateral movement of the associated doublets, and hence stabilise the axoneme at this point.

Further stabilisation here is likely to come from the linkage between doublets 5 and 6, which previous studies in other systems suggest are more stable than other interdoublet linkages, (reviewed by (Lindemann and Kanous, 1997)). Loss of the intact ring structure of the axoneme would be expected to promote further loss of adjacent doublets due to increased strain on the doublets located either side of the gap.

Although PACRG is predominantly expressed in testis (Lorenzetti et al., 2004), EST evidence suggests a wider tissue distribution. Owing to the co-regulation of *PACRG* and *Parkin* in mammals, one study examined the role of PACRG in neurodegenerative disorders (Imai et al., 2003). In neuronal tissue, PACRG is found in neurodegenerative inclusions, where it is thought to form part of a complex that includes members of the chaperonin and heat shock protein (HSP) families including HSP70, HSP90 and various TCP1 members (Imai et al., 2003). It remains to be seen if PACRG has similar binding partners in the axoneme, but it is worth noting that cilia and flagella are known to contain an HSP70 family member (Bloch and Johnson, 1995; Stephens, 1997; Williams and Nelsen, 1997; Stephens and Lemieux, 1999), an HSP90 family member (Williams and Nelsen, 1997; Stephens and Lemieux, 1999) and a chaperonin of the TCP1 family (Soares et al., 1994; Cyrne et al., 1996; Stephens and Lemieux, 1999). In addition, an HSP40 family member has recently been identified as a component of the radial spoke complex (Satouh et al., 2005; Yang et al., 2005).

CHAPTER 5

RESULTS

Characterisation of

Trypanosome Axonemal Protein-1

5 Characterisation of Trypanosome Axonemal Protein-1

TAX-1 was originally identified from a bioinformatic screen of proteins from a proteome of human cilia (Ostrowski et al., 2002), and also found in the *T. brucei* Flagellar Proteome (Broadhead et al., 2006). Since being identified in the TbFP, the homologue of TAX-1 in *Chlamydomonas* (C_30068) has been identified by proteomic methods as a component of inner arm dynein subspecies *d* (Yamamoto et al., 2006). The authors proposed that TAX1, which they call p38, represents the docking site for dynein *d* based on the evidence that p38 remains in axonemes lacking dynein *d*. Dynein *d* consists of the dynein heavy chain DHC2, actin, the light chain p28, a 44kDa protein and TAX-1 (Yamamoto et al., 2006).

5.1 TAX-1 is well conserved in flagellate eukaryotes

The gene encoding TAX-1 (Tb09.211.1790) encodes a protein of 363 amino acids, with a predicted molecular weight of 40.6 kDa and predicted isoelectric point of pH 6.7. I named it TAX-1 for Trypanosome Axonemal protein 1.

TAX-1 is conserved exclusively in flagellate eukaryotes, with homologues in *H. sapiens* (NP_115633), *C. reinhardtii* (C_30068) and the kinetoplastids *T. cruzi* and *L. major*. There is no homologue present in the genomes of *D. melanogaster* and *C. elegans*. The human homologue is named zinc-finger MYND domain containing protein 12, or ZMYND12. The zinc finger MYND domain consists of a conserved series of cysteine residues and is thought to be involved in protein-protein interactions (Gross and McGinnis, 1996; Spadaccini et al., 2006). In addition to the *H. sapiens* homologue, this domain is also found in the TAX-1 homologues in *G.*

Figure 5.1

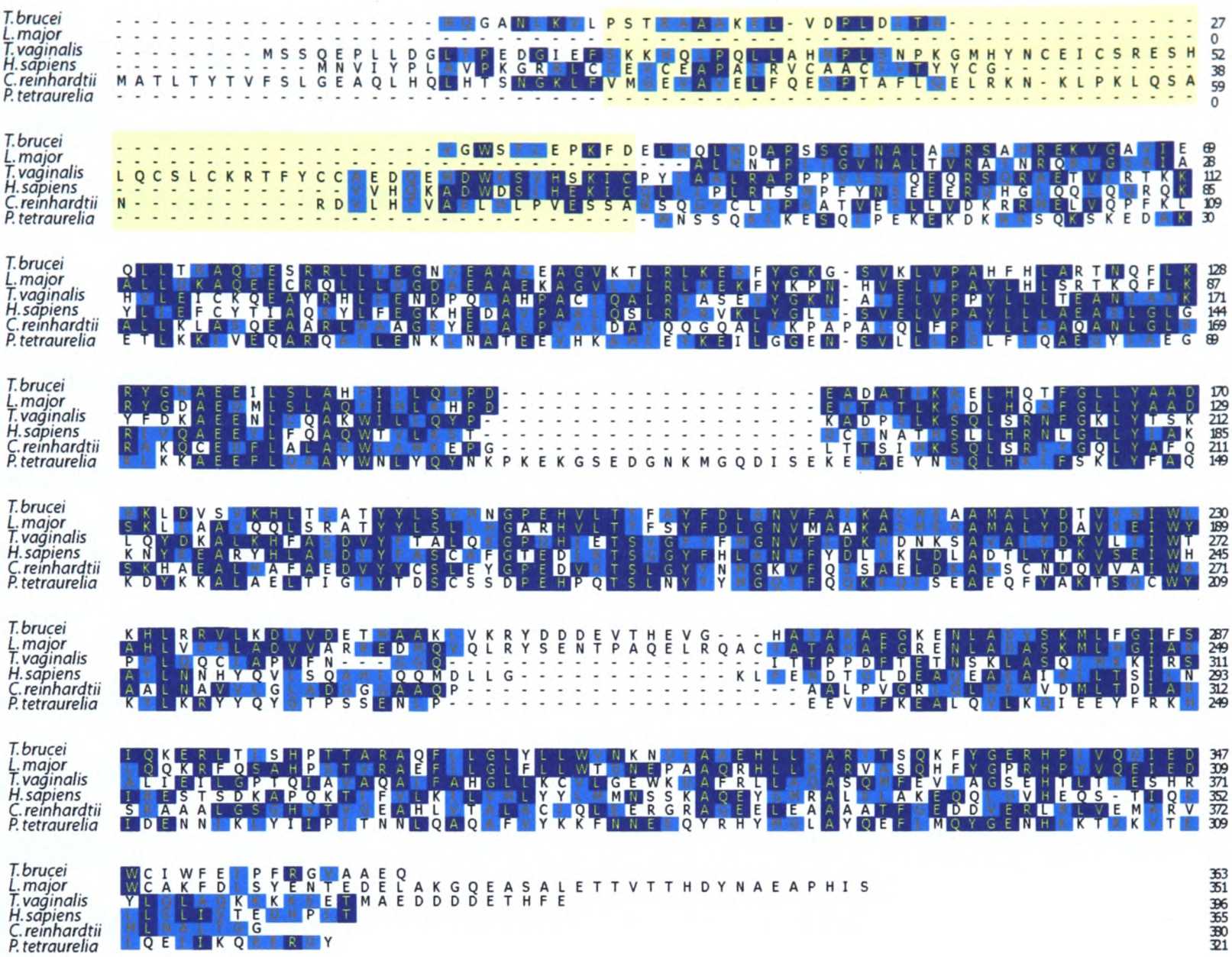


Figure 5.1. Alignment of TAX-1 protein sequences
Protein sequence alignment of TAX-1 proteins from *T. brucei* (Tb09.211.1790), *L. major* (LmjF35.4390), *T. vaginalis* (XP_001325626), *H. sapiens* (NP_115633), *C. reinhardtii* (C_30068) and *P. tetraurelia* (XP_001448418). Orthology was determined by examination of candidate sequences including reciprocal BLAST. Identical residues are shown in dark blue; similar residues are shown in light blue.

lamblia, *T. thermophila*, *T. gondii* and *T. vaginalis*, but is not found in the *C. reinhardtii* homologue or within the kinetoplastids. Figure 5.1 shows the alignment of the proteins sequences of TAX-2 homologues as determined by best hit reciprocal BLASTp searches, showing identical residues in dark blue and similarity in light blue.

5.2 GFP:TY:TAX-1 fusion protein localises to the axoneme

To examine the localisation for TAX-1 in trypanosomes I constructed a strain in which one copy of the two endogenous TAX-1 genes was replaced with a GFP:TY:TAX-1 fusion. Examination of the native GFP signal in paraformaldehyde-fixed whole cells revealed that GFP:TY:TAX-1 localises to the entire length of the flagellum from close to the kinetoplast (Fig. 5.2 a-c). As the PFR is only present in the flagellum from the point where the flagellum exits the cell body, the presence of GFP:TY:TAX-1 signal within the flagellar pocket indicates that TAX-1 is axonemal rather than within the PFR. GFP:TY:TAX-1 can be seen to be built into the growing new flagellum during its extension (Fig. 5.2 d – i).

5.3 RNAi against TAX-1 in procyclic form *T. brucei* cells reduces cell motility

To address the function of TAX-1 I used the inducible RNAi system to ablate protein expression. Ablation of TAX-1 produced no effect on cell growth rate over 144 hours (Fig. 5.3 a). To assess the level of knockdown of the RNAi we performed qRT-PCR on mRNA samples collected from the parental cell line 29-13 cells, non-induced cells and induced cells at various time-points after induction (Fig. 5.3 b). The control containing sample mRNA that had not been treated with reverse transcriptase

Figure 5.2

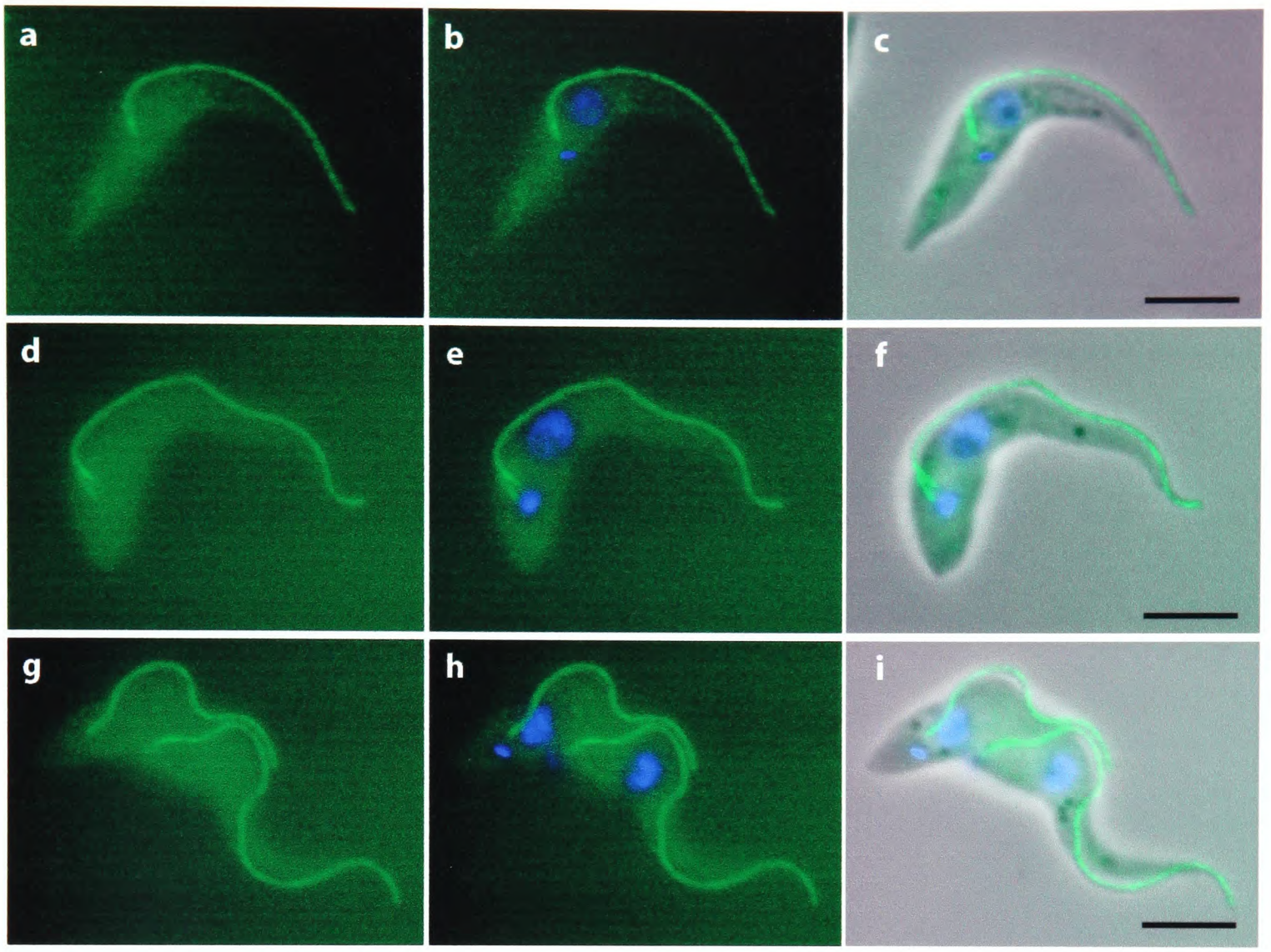
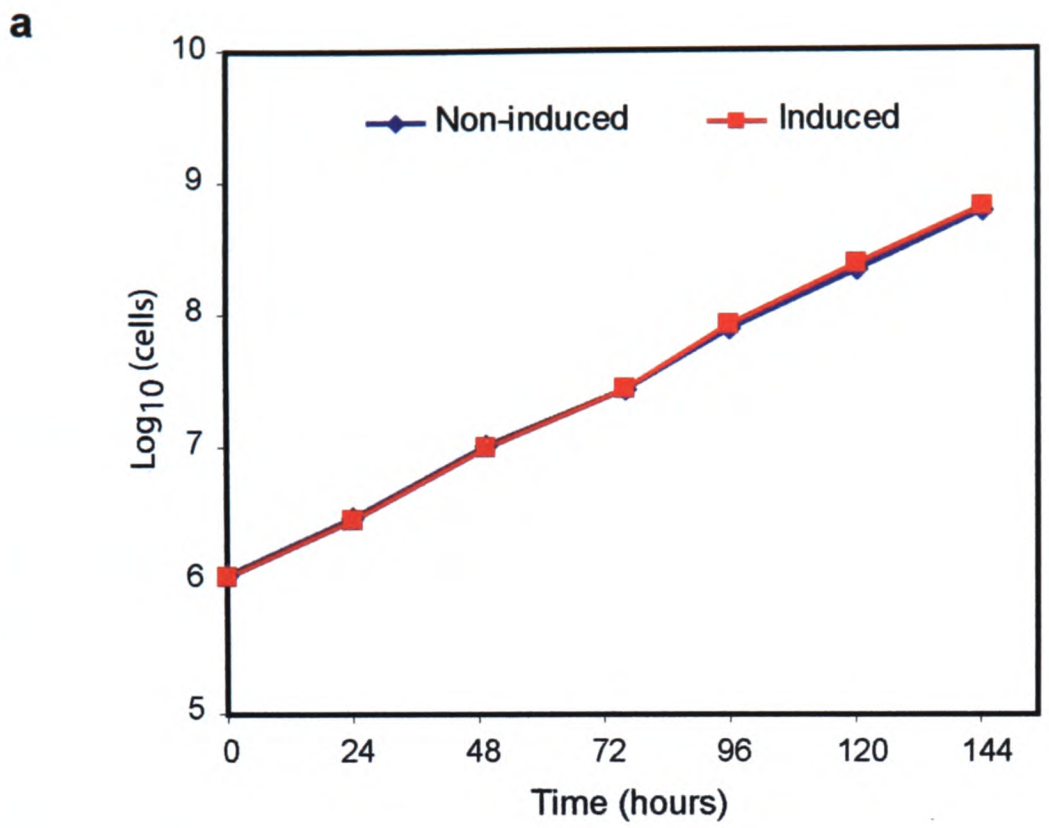


Figure 5.2 GFP:TAX-1 fusion protein localises to the axoneme.
Fluorescence microscopy (a, b, d, e, g and h) and phase contrast microscopy images overlaid (c, f and i) images of paraformaldehyde-fixed whole cells. DNA is labelled with DAPI (blue), and native GFP is shown in green. (a - c) Cell with one flagellum, one kinetoplast and one nucleus expressing GFP:TAX-1 which localises to the length of the axoneme. (d - f) Cell one full length flagellum and extending new flagellum, one kinetoplast and one nucleus expressing GFP:TAX-1 which localises to the axonemes of both the new and old flagella. (g - i) Cell with two flagella, two kinetoplasts and two nuclei expressing GFP:TAX-1 which localises to the axonemes of both the new and old flagella. Scale bar = 5μm.

Figure 5.3



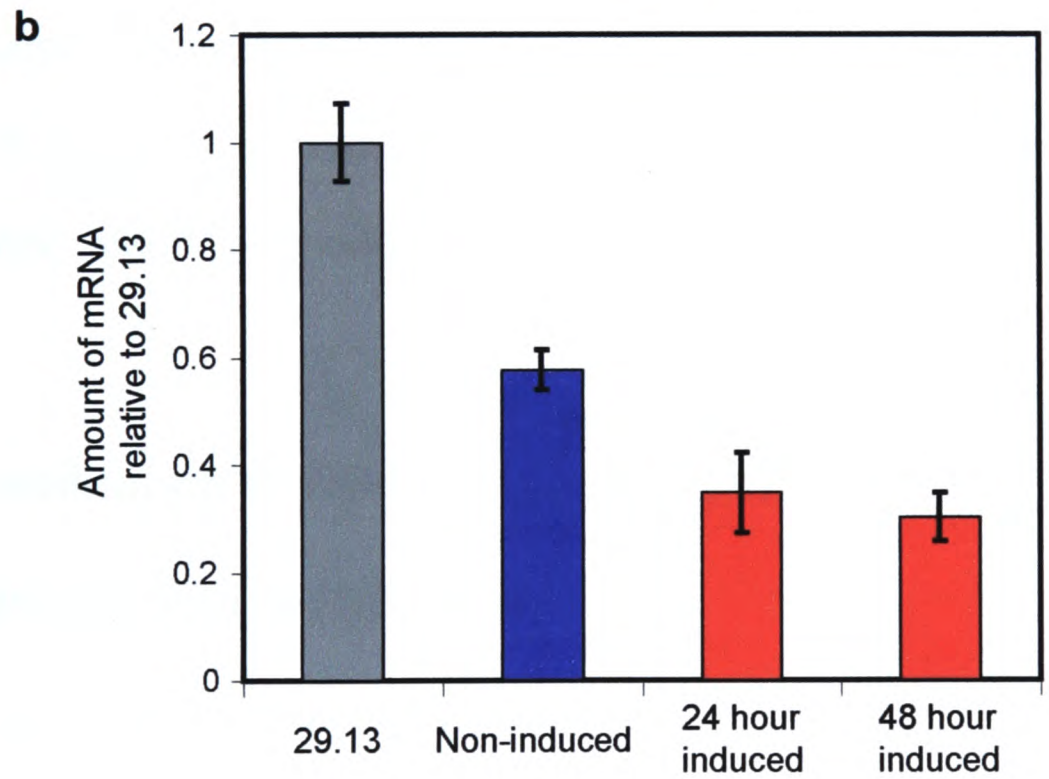


Figure 5.3 RNAI ablation of TAX-1 in procyclic form trypanosomes does not affect growth

(a) Inferred cumulative growth curve showing no alteration in growth kinetics in TAX-1 RNAi-induced cells (red squares) compared to non-induced controls (blue diamonds). (b) Q-PCR data shows the reduction of mRNA signal of TAX-1 in RNAi-induced cells (red bars) compared to non-induced (blue bar), however there appears to be a reduction in the mRNA signal of TAX-1 in non-induced cells compared to the parental cell line 29-13 (grey bar). Graph is expressed as mean +/- SEM.

demonstrated minimal DNA contamination. It appears that there is a level of knockdown in non-induced cells that could be attributable to leakiness of the RNAi construct. In induced cells the level of TAX-1 mRNA is 35% of the level in 29-13 cells at 24 hours post-induction and 30% at 48 hours post-induction.

We observed that TAX-1 RNAi-induced cells continued to build a new flagellum each cell cycle. However, cell motility was affected and induced cells could be observed settling on the base of the culture flask. At 24 hours post-induction a reduction in the motility of induced cells was apparent and motility was further reduced by 72 hours post-induction. Figure 5.4 shows the histogram of mean velocities for non-induced and induced cells, showing the reduction in mean speed in induced cells. A significant difference in mean speed was observed between RNAi 72 hour induced (n = 83) and non-induced cells (n = 85) ($P < 0.001$) at 72 hours.

5.4 Examination of RNAi induced axonemes by Transmission Electron Microscopy (TEM)

Non-induced and induced cells were fixed for thin section transmission electron microscopy 72 hours post-induction. In addition to whole cells, cells were also treated with detergent to produce cytoskeletons, with and without the addition of tannic acid, which stains structures such as the dynein arms more strongly, and also enables visualisation of the protofilaments that form microtubules. Examination of the axoneme profiles of induced cells revealed no obvious differences from those of non-induced controls. Induced axonemes possessed nine outer doublets

Figure 5.4

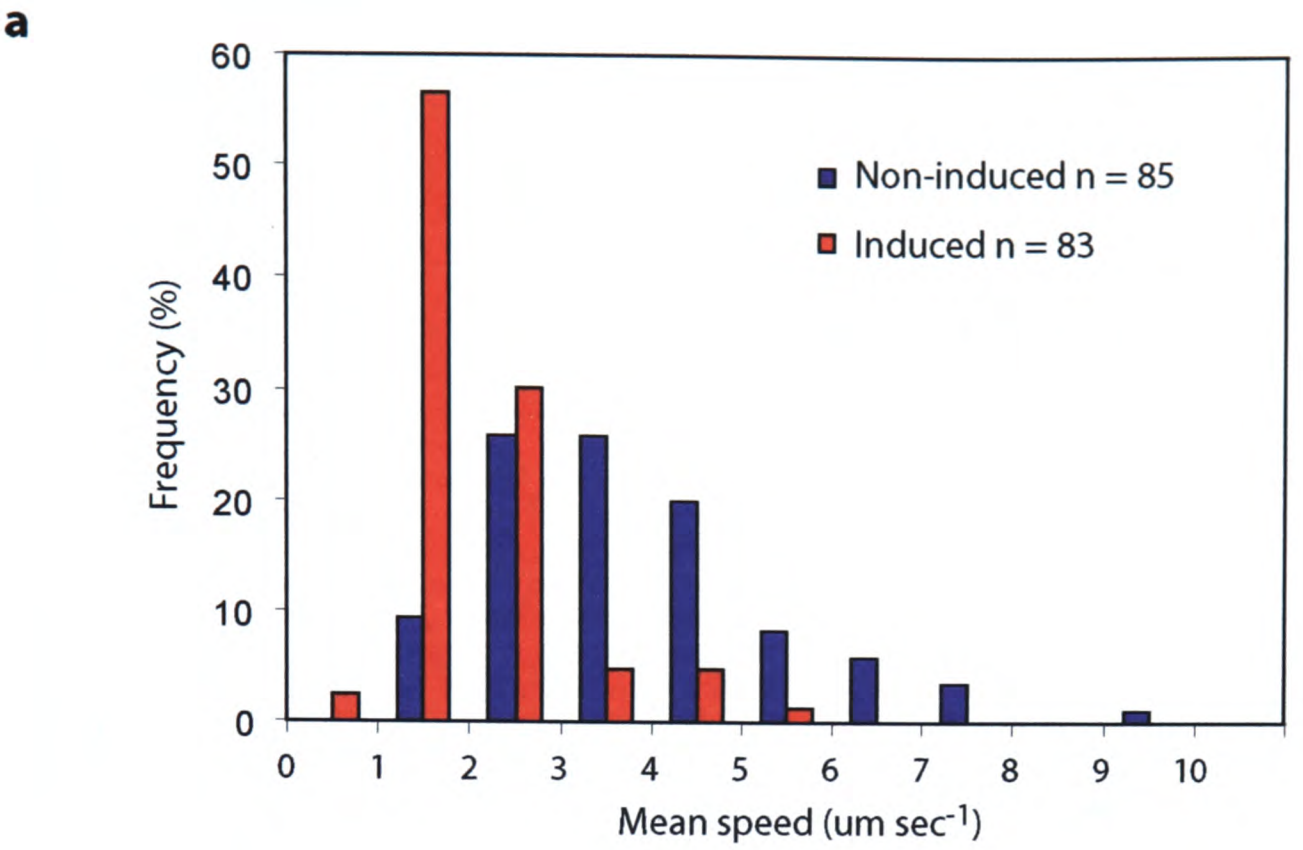


Figure 5.4. Ablation of TAX-2 reduces motility in procyclic form trypanosomes
(a) Histogram showing the frequency distribution of mean speeds of non-induced cells (blue bars) and TAX-2 RNAi induced cells 72 hours post-induction (red bars).
(b) Tracks of non-induced (blue) and induced (red) cells from which mean speeds were calculated. For each, 30 representative tracks are shown. Scale bar = 100 μm

Figure 5.5

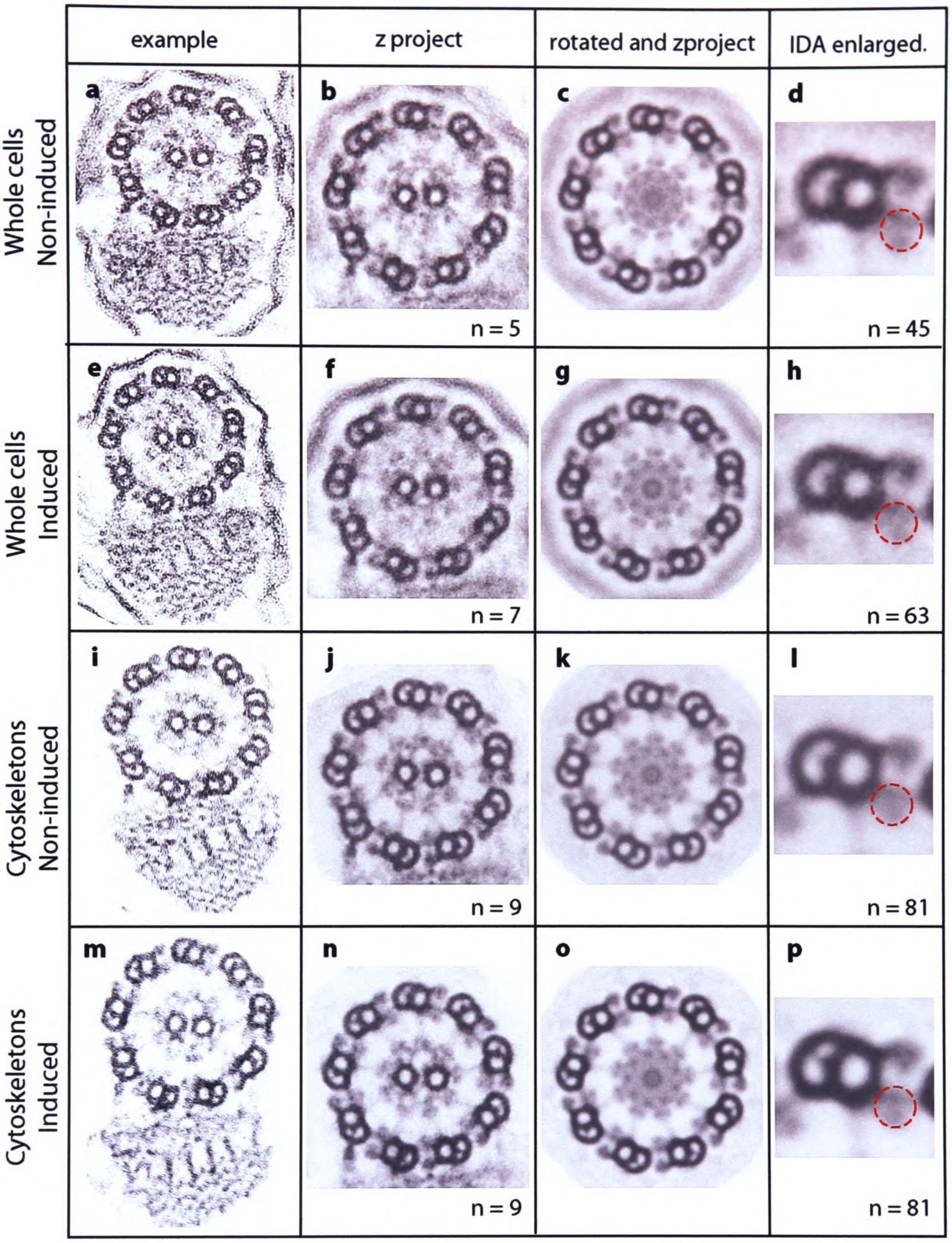
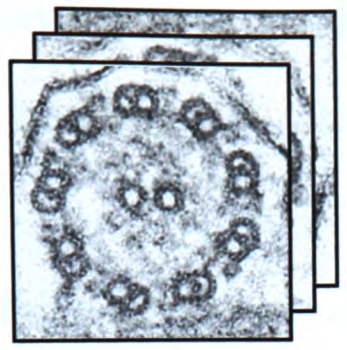


Figure 5.5. TEM examination of TAX-1 RNAi-induced cells

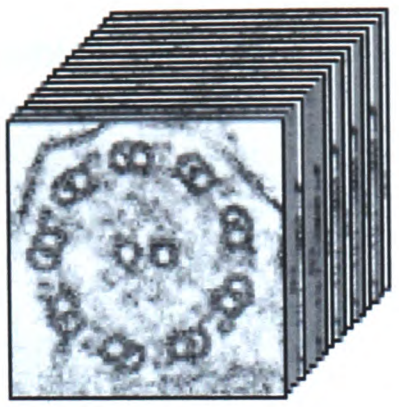
Representative transmission electron micrographs of TAX-1 non-induced and induced whole cells and cytoskeletons (a, e, i, m), averaged overlays of micrographs (b, f, j, n), and nine-fold rotations of the overlays (c, g, k, o), with enlargement of one outer doublet (d, h, l, p). (a - d) Micrograph and overlays of non-induced whole cells. (e - h) Micrograph and overlays of TAX-1 RNAi-induced whole cells. (i - l) Micrograph and overlays of non-induced detergent-extracted cytoskeletons. (m - p) Micrograph and overlays of non-induced detergent-extracted cytoskeletons. The red circle indicates the region of the IDAs compared for differences.

Figure 5.6

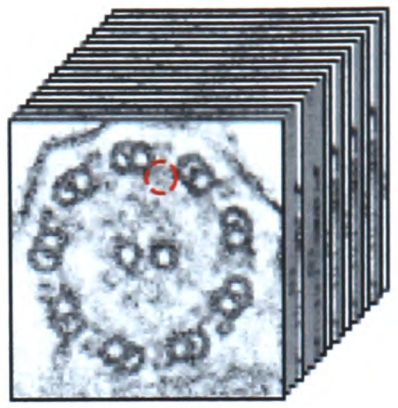


1. Measure mean pixel intensity of each image.

Calculate the mean mean pixel intensity and normalise each image to this.



2. Ninefold rotation of all images in stack so that all inner dynein arms are overlaid in one region.



3. Measure pixel intensity within region of interest (i.e. inner dynein arms) for all images. Compare values for non-induced and induced sets.

non-induced	induced
193.6	175.4
185.1	180.0
183.3	178.4
191.4	190.7
185.6	177.7
173.9	190.3
181.1	161.2
201.8	192.5
197.2	214.7

mean = 186.3

Non-induced		Induced	
167.4	142.1	151	145.3
169.5	133.8	147	152.7
169.7	139.8	150.6	143.4
163.7	150	153	146.9
158.4	158.2	144.5	159.5
160	138.6	145.5	161.7
152.2	146.9	141.7	166.2
164.6	142.8	159.5	156.4
167.9	149.6	158.6	157.8
149.7	139.3	143.9	138.8
158.1	143.6	152.9	151.2
158	131.6	134.6	151.9
161	139.1	155	150.3
147.8	153.2	146.7	144.8
144.7	150.6	130.3	142.9
152.5	164.7	146	152.1
158.9	158.3	155	137.5
155.6	154.8	158.1	125.5
166.2	157.8	128.7	142.1
157.3	159.4	143.3	148.4
161	146	152.9	143.7
155.5	158.9	159.4	147.3
156.9	153.4	138.7	155.4
150.9	146.5	153.6	159.6
158.1	152.6	133.4	148.7
156	163.3	137.1	152.0
162.1	162.5	142.7	142.4
153.3	153.9	163.2	145.1
155.5	158.9	159.7	159.1
154.5	162.4	152	158.2
150.3	156.4	159.7	164.1
156.4	165.4	162.2	166.5
158.8	160.3	146.4	159.0
153.8	160.3	167.4	159.7
148.8	156.8	165.8	165.9
153.3	156	161.5	170.5
162.7	151.8	162	158.9
131.1	157.6	155.6	153.3
141.4	161.7	159.8	163.4
148.2	160.6	162.9	162.6
154.5		155.7	

Figure 5.6 Statistical analysis of TEMs
Figure shows how images were processed for statistical analysis. 1. The mean pixel intensity of each image was measured and the mean (mean intensity) for the set of images was calculated. This was used to normalise each image. The pixel intensity of a region of interest, in this case all the inner dynein arms, was then measured and compared.

surrounding the central pair, which was correctly aligned, with both outer and inner dynein arms clearly visible.

In order to address whether there are less obvious defects in the axonemes of RNAi-induced cells, axoneme profiles of non-induced and induced cells were processed to correct for ellipticalness, then overlaid and averaged (Fig. 5.5). This increases the signal: noise ratio and would reveal if a single structure relating to a particular outer doublet were affected. To further improve the signal: noise ratio in order to assess all inner dynein arms, these overlaid images were first normalised so that they had the same mean pixel intensity and then rotated ninefold to produce an average image of 144 overlaid inner dynein arms for non-induced and for induced axonemes (for full details of the processing, please see Materials and Methods chapter). By drawing a region around the inner dynein arms and measuring the pixel intensity within this region for all inner dynein arms, I could test for statistically significant differences between non-induced and induced axoneme profiles. Despite the sensitivity of this approach, no significant difference was observed in inner dynein arms between non-induced and induced axonemes.

5.5 RNAi against TAX-1 in bloodstream form *T. brucei* cells causes cytokinesis defects

I extended the functional analysis of TAX-1 by carrying out RNAi against TAX-1 in bloodstream form trypanosomes. Ablation of TAX-1 resulted in bloodstream form trypanosomes that did not complete cytokinesis, yielding monstrous cells with an inability to proliferate. Within 12 hours of RNAi induction, growth rate in RNAi-

induced cells was reduced (Fig 5.7 a). Counts of nuclei and kinetoplast number revealed an increase in cells containing multiple nuclei and kinetoplasts at 8 hours post-induction (Fig 5.7 b, c). At 24 hours post-induction, the RNAi-induced population of 'monsters' contained large numbers of 4K4N and 8K8N cells (Fig 5.7 b, d).

A distinct phenotype was observed prior to the death of bloodstream form trypanosomes; on induction of TAX-1 RNAi, bloodstream cells ceased dividing but continued to progress through the cell cycle. Non-induced cells had a normal morphology (Fig 5.8 a, b), producing a new flagellum during the cell cycle before cytokinesis, with the flagellum emerging from the flagellar pocket and extending along the trypanosome. On RNAi induction, cells produced new flagella but did not complete division and lost their normal morphogenetic axes, with the multiple flagella twisted around the enlarged cell body in a left-handed helix (Fig. 5.8 c, d).

Thin-section electron microscopy showed that the cell periphery was highly convoluted; multiple nuclei were present and some flagella were attached to the outside of the cell, while others were located in a highly enlarged flagellar pocket (Fig. 5.8 e - g). The phenomenon of two axonemes being contained within one flagellar membrane, seen for example in PFR2 RNAi-induced cells (Broadhead et al., 2006), is not observed in TAX-1 RNAi induced cells. Examination of the flagellar pockets indicated that although large they still showed clathrin-coated pits, suggesting that endocytotic processes were operating to some extent in some cells (Fig. 5.8 i, arrows).

Figure 5.7

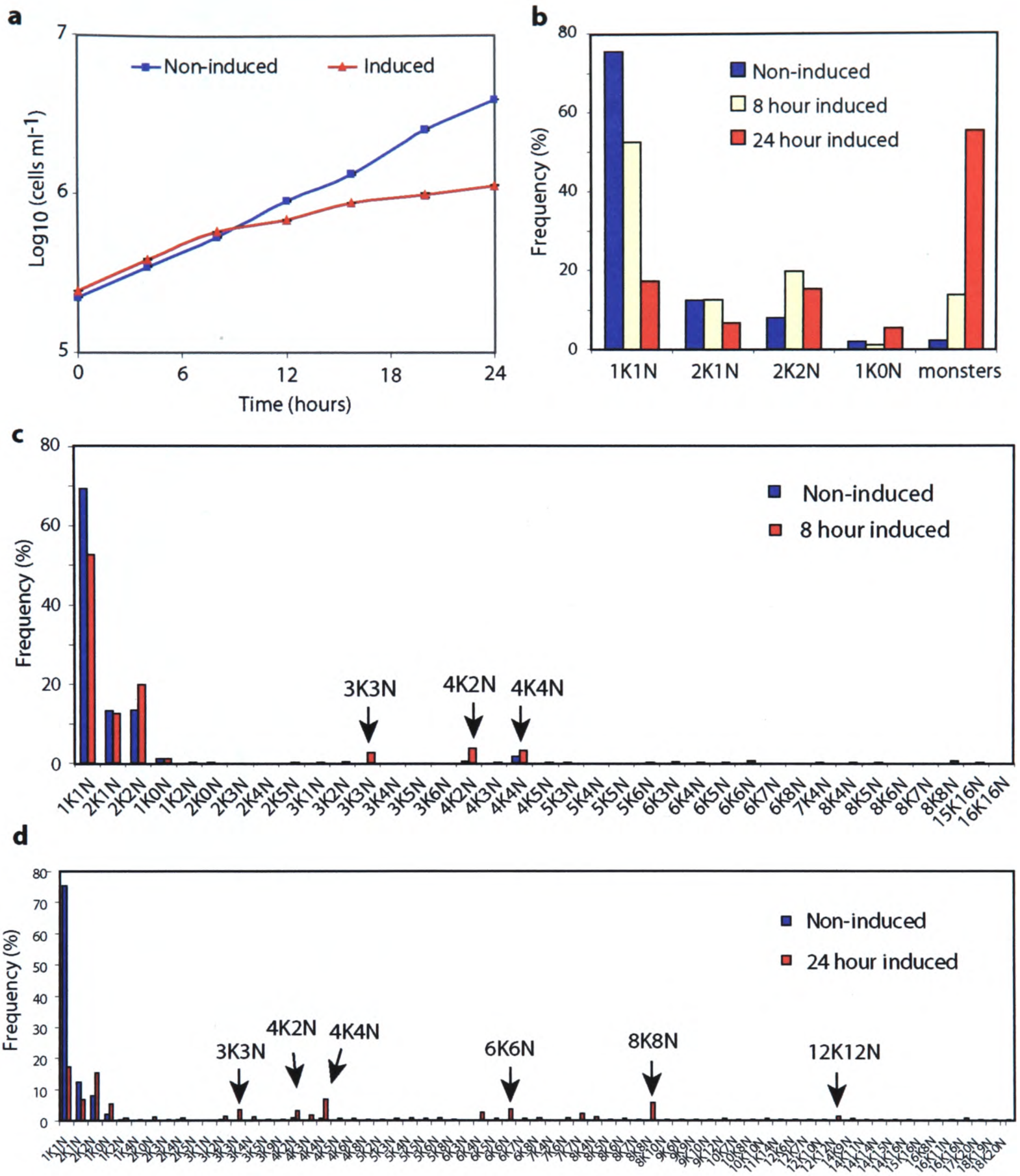


Figure 5.7. TAX-1 RNAi in bloodstream form trypanosomes affects growth and cytokinesis.
(a) Representative growth curve showing alteration in growth kinetics in induced cells (blue line) compared to non-induced controls (red line). (b) Counts of nuclei (N) and kinetoplasts (K) in non-induced (blue) and induced cells after 8 hours (yellow) and 24 hours (red), showing a reduction in 1K1N cells and increase in cells with more than 2 nuclei and 2 kinetoplasts. (c) Counts of kinetoplast and nucleus number of TAX-1 RNAi-induced cells at 8 hours post-induction (red, n=500) and non-induced controls (blue, n=500), revealing an increase in cells undergoing a second round of S phase. (d) Counts of kinetoplast and nucleus number of TAX-1 RNAi-induced cells at 24 hours post-induction (red, n=500) and non-induced controls (blue, n=500), revealing an increase in multinucleate cells in the population.

Figure 5.8

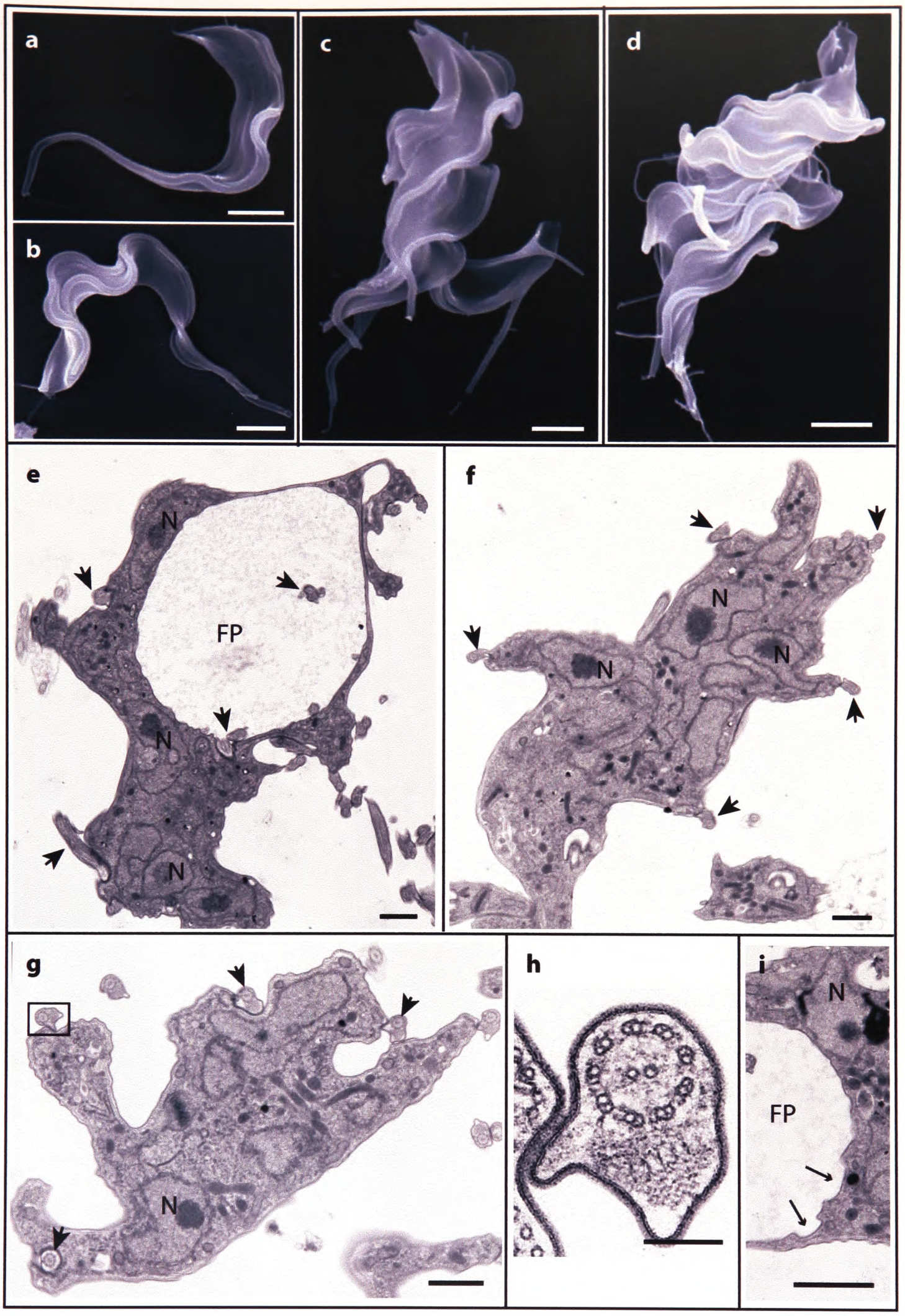


Figure 5.8 RNAi ablation of TAX-1 in bloodstream form trypanosomes produces large, monstrous cells

(a - b) Scanning electron micrographs of TAX-1 non-induced cells. (c - d) Scanning elctron micrographs of TAX-1 RNAi-induced cells at 24 hours post-induction, showing multiple flagella. (e - g) Thin section transmision electron micrographs of TAX-1 RNAi-induced cells at 24 hours post-induction, showing multiple nuclei (N), flagellar profiles (arrowheads) and enlarged flagellar pocket-like structures (FP). (h) shows the flagellar profile boxed in (g). (i) shows one of the enlarged flagellar pokets contining clathrin-coated pits (arrows). Scale bars in (a - d) = 2 um, scale bars in (e - g, i) = 1 um, scale bar in (h) = 200 nm.

We then assayed the motility of a population of TAX-1 non-induced and induced RNAi bloodstream cells (Fig. 5.9), as we did for procyclic form cells. Cells were captured at 7 hours post-induction; at this early stage of RNAi-induction there should be only a small effect on the frequency of 2K2N and multinuclear cells in the population, to minimise the effect that these might have on mean velocity. Non-induced and RNAi induced cells were also fixed for nuclear and kinetoplast counts at the same time-point. These revealed very little difference in the frequency of different cell types between non-induced and RNAi induced cells: the frequency of 1K1N cells in the non-induced population was 76%, compared to 74% for induced cells while the frequency of 2K2N cells increased from 8% in the non-induced population to 12% after 7 hours of induction.

Bloodstream form cells in HMI-9 medium exhibit a particular tumbling motility; to increase productive motility a final concentration of 0.5% methylcellulose was added to both cultures prior to the assay. Timelapse microscopy images were captured every 2 s for 40 s, and individual cells were tracked over all 21 frames, enabling velocity measurements to be recorded, as for procyclic form cells. The mean velocity of the population of non-induced cells (n = 41) was 2.9 μm s^{-1} ± 0.03 μm s^{-1} compared to a mean velocity for the population of induced cells (n = 50) of 1.6 μm s^{-1} ± 0.01 μm s^{-1}.

5.6 Conclusions and discussion

Previously, the *C. reinhardtii* homologue of TAX-1 (p38) has been identified as a component of a subset of inner dynein arms, as it was shown to associate with dynein subspecies *d* (Yamamoto et al., 2006). Immunoprecipitation experiments

Figure 5.9

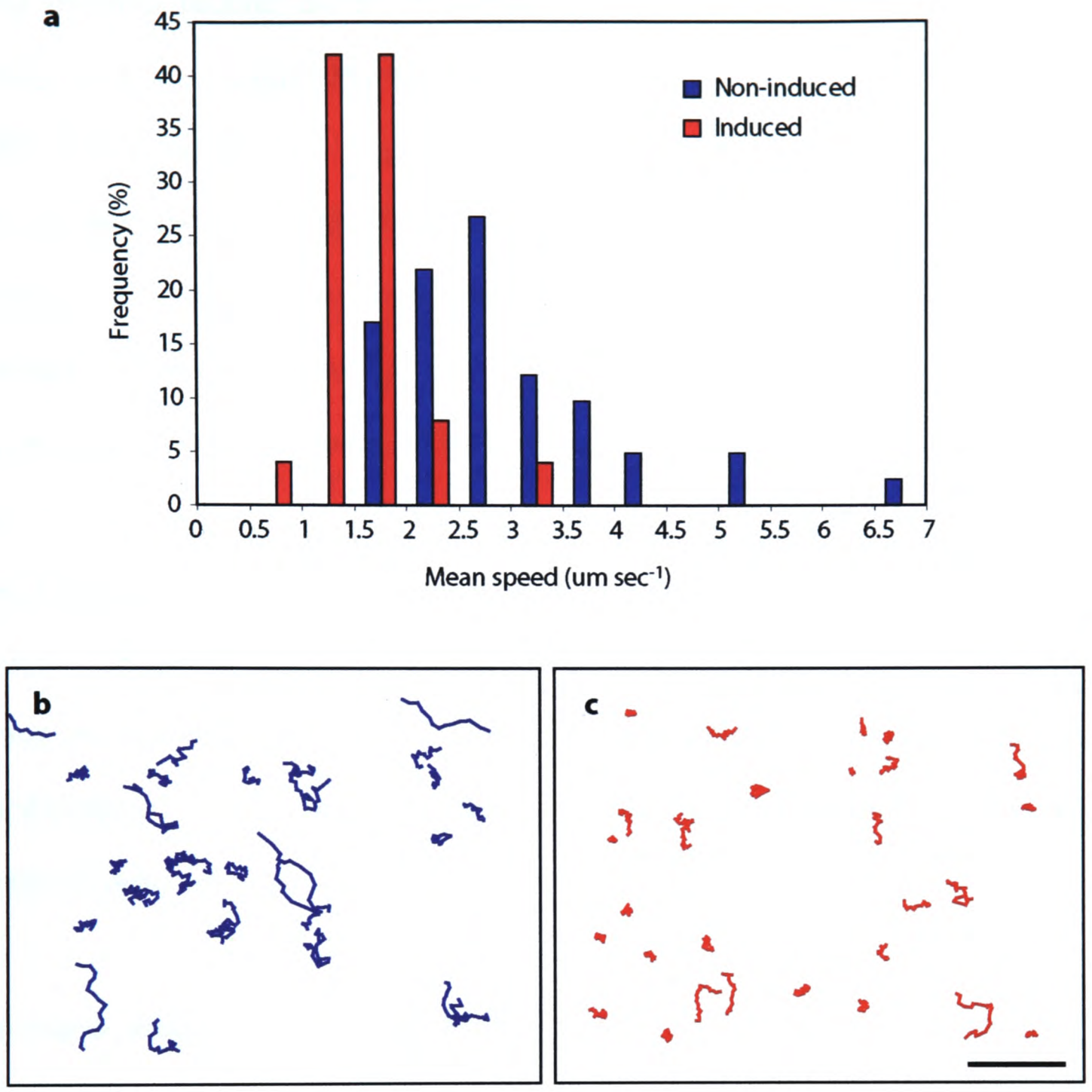


Figure 5.9 RNAi ablation of TAX-1 in bloodstream form trypanosomes leads to reduced motility.
(a) Histogram showing the frequency distribution of mean speeds of non-induced cells (blue bars) and TAX-2 RNAi induced cells 72 hours post-induction (red bars). (b - c) Tracks of non-induced (blue) and induced (red) cells from which mean speeds were calculated. Scale bar = 100 μm

using mutants lacking dynein *d* revealed that TAX-1 was present in axonemes lacking dynein *d*, suggesting that it may form the docking site (Yamamoto et al., 2006). Based on this, we might expect to observe loss of particular inner dynein arms in the axonemes of TAX-1 RNAi-induced cells. However, examining non-induced and induced axonemes in transverse sections revealed no difference in the structure of the inner dynein arms. One possible reason for this is that within the thickness of a 70nm section for TEM there would be several inner dynein arms, only one of which we might expect to be absent in induced axonemes. This same study used a polyclonal antibody raised against TAX-1 to localise TAX-1 in *C. reinhardtii* by immunofluorescence. The authors found TAX-1 to localise to the axoneme, in agreement with my localisation of TAX-1 in *T. brucei*, however there was also non-specific signal in the basal body area and nucleus where inner dynein arms are not present (Yamamoto et al., 2006).

The model system *C. reinhardtii* has been extensively used in studying the inner dynein arms and there are a number of mutants lacking one or more inner dynein arms. Two mutants exist which lack dynein subspecies *d*, for which TAX-1 is proposed to act as the docking site. However, both mutants lack further dynein subspecies in addition to dynein *d*: ida4 lacks dynein subspecies *a*, *c* and *d*, while ida5 lacks *a*, *c*, *d* and *e*. The flagellar motility of these mutants has been analysed; in both mutants the flagellar waveform has the same frequency but reduced amplitude, leading to a decrease in swimming velocity. Inner dynein arms are thought to play a role in producing the waveform, while the outer arms are responsible for beating at high frequency. A *C. reinhardtii* mutant which lacks just one dynein subspecies is *ida9*, lacking dynein *c*. The mutant *ida9* was able to swim with only a slight reduction

in normal medium but in more viscous medium swam with greatly reduced motility compared to normal cells (Yagi et al., 2005).

In the *C. reinhardtii* model of inner dynein arms, there are two possible positions for dynein *d*, and by inference TAX-1, within the 96 nm repeat along the longitudinal axis of the axoneme. As there does not exist a mutant lacking only dynein *a* or dynein *d*, the localisations of these two subspecies are at present interchangeable; either close to the radial spoke S1, or at the most distal part of the repeat unit (Yagi et al., 2005).

The zinc finger MYND domain found within the human homologue of TAX-1 is often found in proteins with programmed cell death / developmental functions. These include Nervy, a Drosophila protein involved in neural tube development; DEAF-1, which is required for embryonic development in both *Drosophila* and mammals where it is expressed in the central nervous system; and Programmed cell death 2 (PDCD2, or RP8). Although it is a zinc finger motif consisting of a series of conserved cysteines, often associated with DNA binding functions, the MYND domain is thought to instead function in protein-protein interactions (Spadaccini et al., 2006). Evidence for this comes from the functional characterisation of DEAF-1 protein, which does bind to DNA. Mutating the cysteine residues within the MYND domain was found not to affect the DNA binding ability of DEAF-1 (Gross and McGinnis, 1996). The MYND domain is present in some homologues of TAX-1 but not all; in addition to the kinetoplastids, the *C. reinhardtii* homologue lacks this domain.

CHAPTER 6

RESULTS

Characterisation of

Trypanosome Axonemal Protein-2

6 Characterisation of Trypanosome Axonemal Protein-2

Amongst the proteins identified from the *T. brucei* flagellar proteome (TbFP) I was interested by a previously uncharacterised protein widely and exclusively conserved in flagellate organisms. I chose this for further analysis and named it Trypanosome Axonemal protein-2, or TAX-2. In addition to its identification from our TbFP, the *Chlamydomonas reinhardtii* TAX-2 homologue (C_220104) is also present in the proteome of isolated *C. reinhardtii* flagella (Pazour et al., 2005), and has been shown to be upregulated following deflagellation of this alga (Pazour et al., 2005; Stolc et al., 2005). The CrFP analysis of peptides derived from differently extracted flagella preparations revealed that TAX-2 remains with the axoneme fraction after KCl extraction (Pazour et al., 2005).

6.1 TAX-2 is evolutionarily conserved in many flagellates

The gene encoding TAX-2 (Tb10.70.7560) encodes a protein of 220 amino acids, predicted molecular weight of 25.5 kDa and predicted isoelectric point of pH 4.7. It is widely and exclusively conserved in flagellate eukaryotes, with homologues in the other kinetoplastids *Trypanosoma cruzi* and *Leishmania major*, in addition to *Homo sapiens*, *Drosophila melanogaster*, *Chlamydomonas reinhardtii*, *Giardia lamblia* and *Tetrahymena thermophila.* Notably absent from this list is the nematode *Caenorhabditis elegans* which builds only immotile sensory cilia lacking the central pair and inner and outer dynein arms. Searching the Apicomplexa *Plasmodium falciparum*, *Toxoplasma gondii*, *Theileria annulata* and *Cryptosporidium parvum* genomes with this sequence reveals that a homologue is present only in *T. gondii*.

Figure 6.1

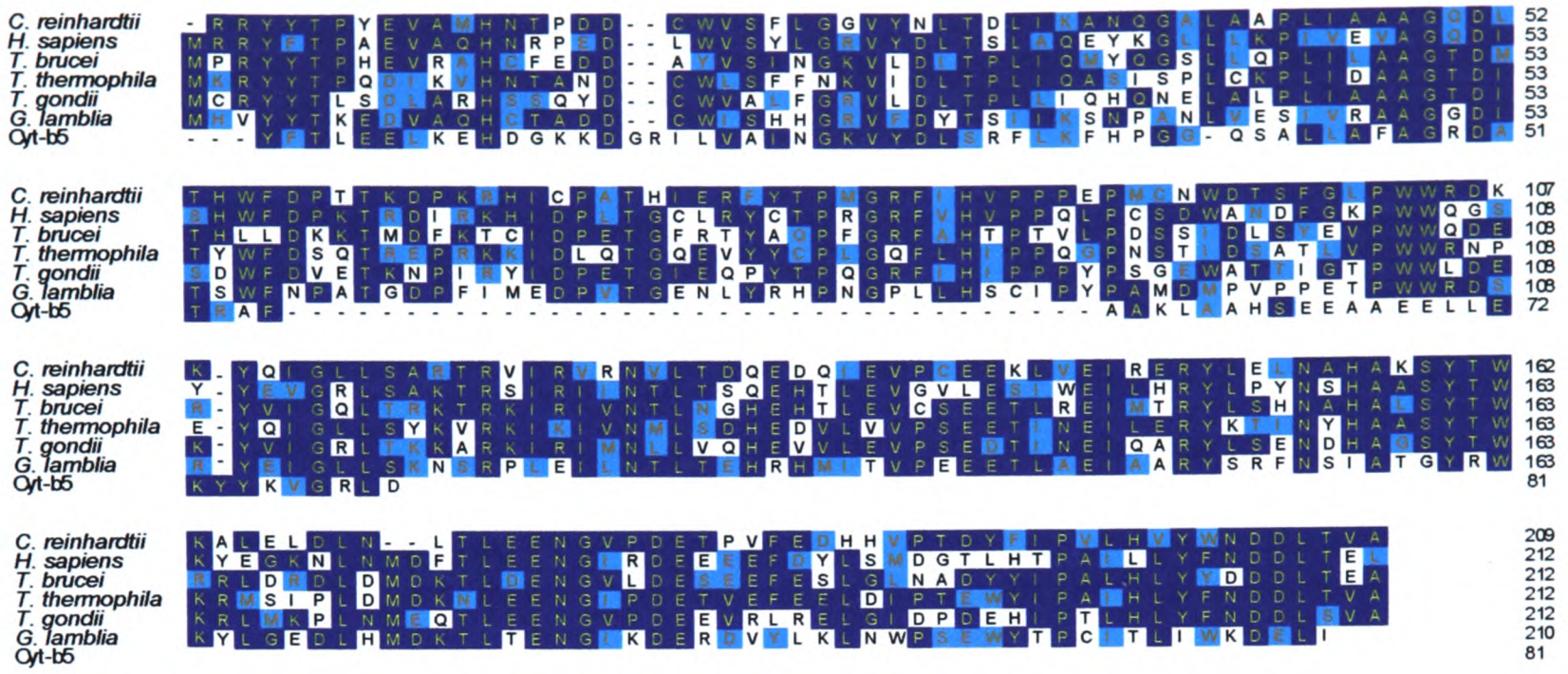


Figure 6.1. TAX-2 is widely conserved in flagellates

Figure shows the protein sequence alignment of *T. brucei* TAX-2 (Tb10.70.7560) with gene products from *H. sapiens*, *C. reinhardtii* (C_220104), *T. thermophila*, *T. gondii* and *G. lamblia* with the sequence of the cytochrome b5 domain (Cyt-b5), which spans residues 4-120. Orthology was determined by examination of candidate sequences including reciprocal BLAST. Identical residues are shown in dark blue boxes; similar residues are shown in light blue.

TAX-2 is predicted to contain a Cytochrome b5-like Heme/Steroid binding domain spanning approximately the N-terminal half of the protein (Fig. 6.1). This domain and its position are conserved in TAX-2 homologues in other organisms, with the exception of the *D. melanogaster* protein in which no such domain was detected. BLASTp searches using the human TAX-2 homologue against the human genome reveals that there is no similarity to any other proteins outside the Cytochrome b5 domain. The structure of the Cytochrome b5 domain is known to consist of a series of β-sheets and short α-helices (Argos and Mathews, 1975), which provide a frame surrounding the central heme group. This domain is found in eukaryotes where it functions as an electron transporter (Schenkman and Jansson, 2003). Additionally, the family of Cytochrome b5 domain-containing proteins includes progesterone binding receptors (Gerdes et al., 1998). In this large family of proteins, the Cytochrome b5 domain is found in conjunction with many other domains, and often with a transmembrane helix. The transmembrane domain is not present in TAX-2, and no other domains were found.

6.2 TAX-2 localises to the axoneme of *T. brucei*

To localise TAX-2 in *T. brucei*, a strain was constructed in which one copy of the two endogenous genes in the diploid genome was replaced with a GFP:TY:TAX-2 fusion, containing a short TY epitope between the GFP and TAX-2 so allowing immunological detection with the anti-TY tag mAb BB2. The native GFP signal was examined directly in fixed cells, where it was located along the full length of the flagellum but not in the basal body, and appeared punctate. The signal extended from the level of the transition zone, through the flagellar pocket and to the distal tip and was therefore clearly axonemal rather than in the PFR. The PFR is an extra

axonemal structure present in the trypanosome flagellum only from the point of exit from the cell. To understand the function of TAX-2 in *T. brucei*, I used RNAi to ablate protein expression in the strain expressing GFP:TY:TAX-2 fusion protein. The RNAi construct was targeted against TAX-2 mRNA and is be capable of ablating both the GFP:TY:TAX-2 fusion and wild-type TAX-2 RNA. Expression levels of the GFP:TY:TAX-2 could then be used for assessing the level of TAX-2 reduction. Ablation of GFP:TY:TAX-2 could be visualised directly by the loss of GFP signal from the axoneme, and by western blotting using the mAb BB2.

6.3 Ablation of TAX-2 affects motility in procyclic form trypanosomes

Ablation of TAX-2 in procyclic cells produced no effect on cell growth rate (Fig. 6.2a). Western blotting against the TY tag attached to GFP:TY:TAX-2 reveals that the level of TAX-2 is much reduced by 24 hours post-induction, with no band visible by 48 hours post-induction. We observed that TAX-2 RNAi-induced cells continued to build a new flagellum each cell cycle. However, cell motility was affected with a small but statistically significant difference in mean speed observed between RNAi induced and non-induced cells ($P < 0.001$).

6.4 Loss of GFP:TY:TAX-2 from the axoneme after RNAi induction

In order to assess the kinetics of the loss of TAX-2, the flagella of non-induced cells and induced cells at 4, 8, 16, 24, and 48 hours after induction were counted and classified by their GFP signal. Examples of the four categories are shown in the fluorescence microscopy images in Fig. 3a-h. GFP signal was categorised as 'full

Figure 6.2

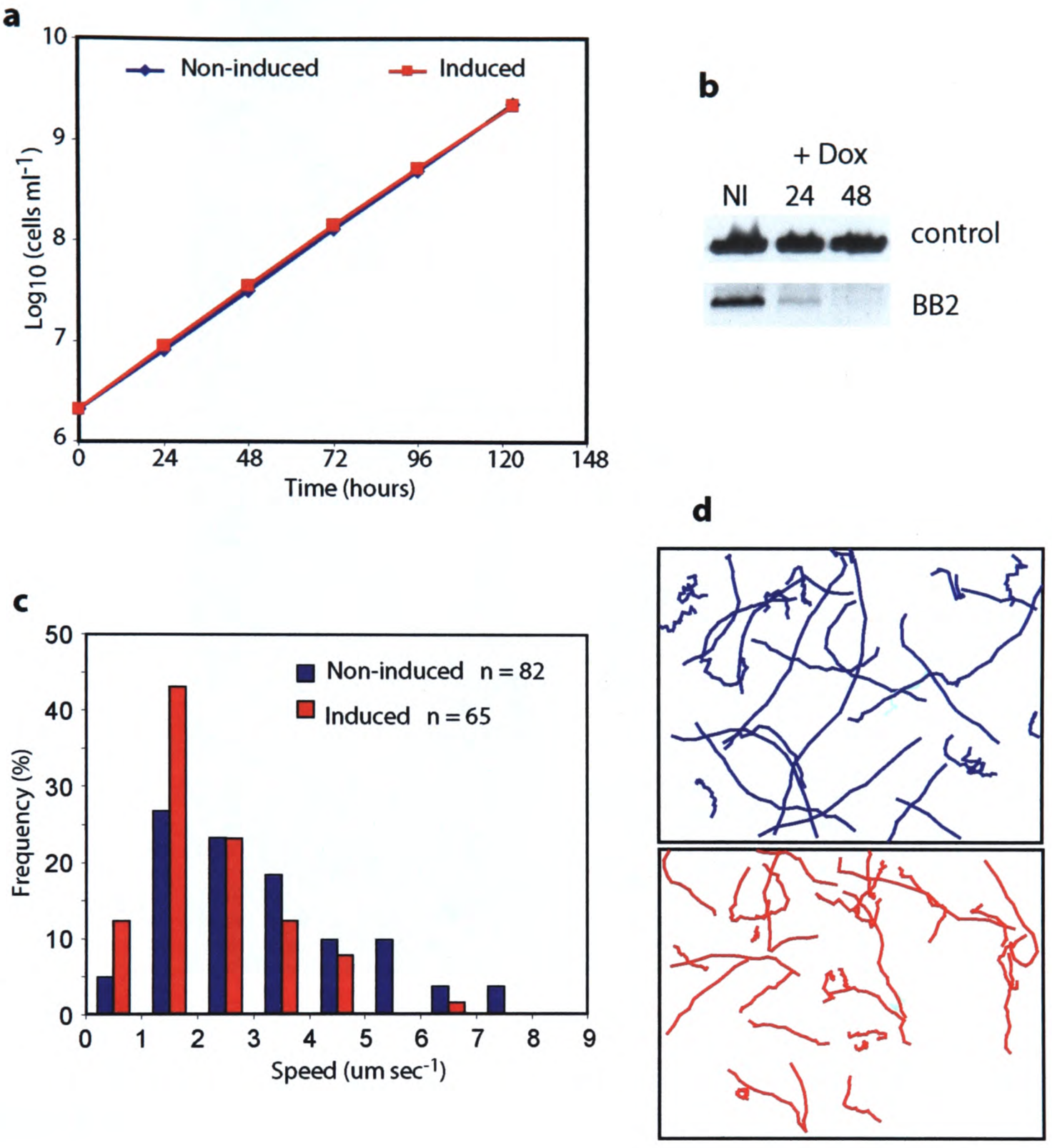


Figure 6.2. Ablation of TAX-2 reduces motility in procyclic form trypanosomes
(a) Representative growth curve showing no alteration in growth kinetics in induced cells (blue line) compared to non-induced controls (red line). (b) Western blot with BB2 antibody showing reduction in GFP:TAX-2 protein level after RNAi induction. Loading control with Rib72 shows no reduction in Rib72 protein level. (c) Histogram showing the frequency distribution of mean speeds of non-induced cells (blue bars) and TAX-2 RNAi induced cells 72 hours post-induction (red bars). (d) Tracks of non-induced (blue) and induced (red) cells from which mean speeds were calculated. For each, 30 representative tracks are shown.

Figure 6.3

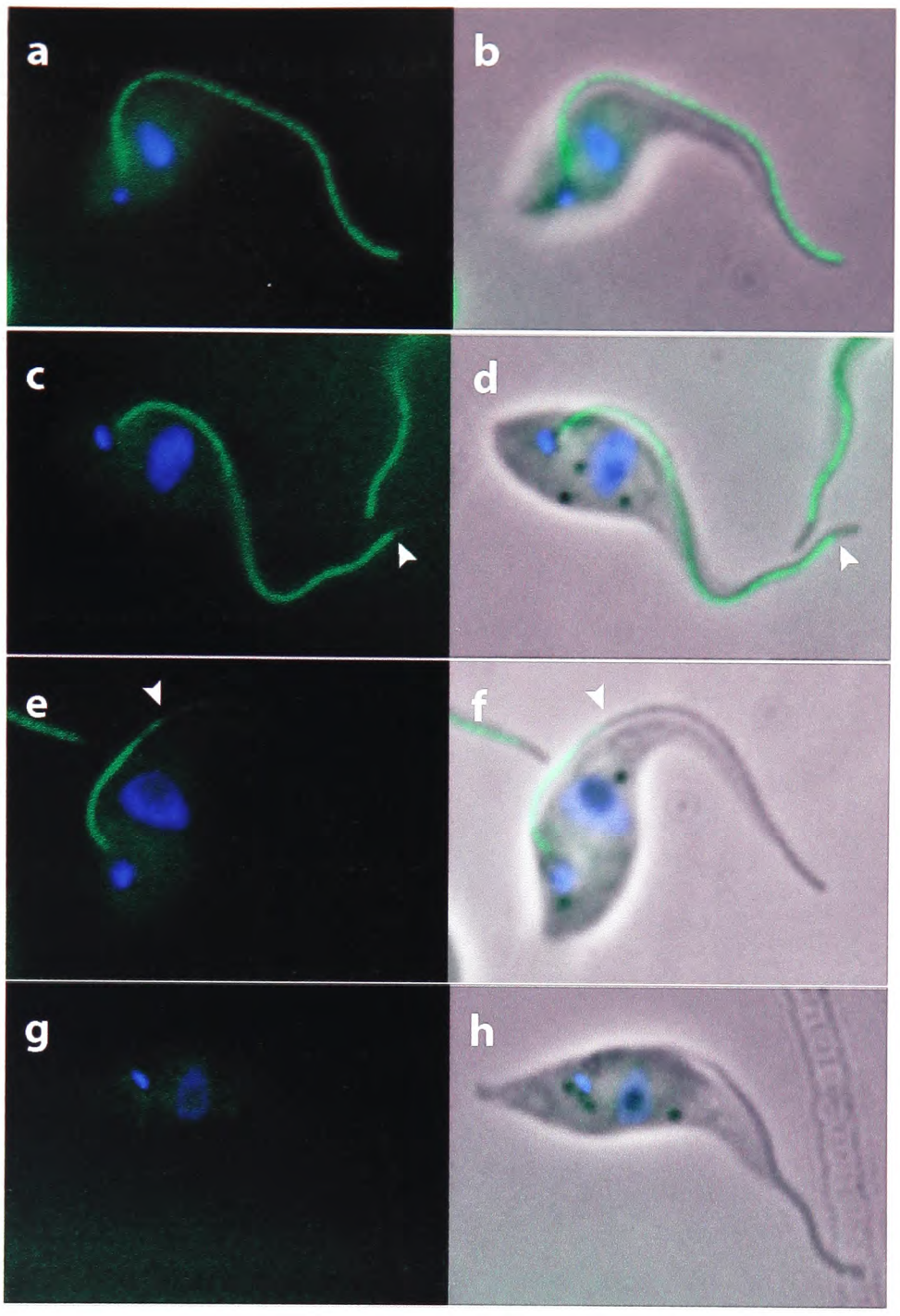


Figure 6.3. Loss of GFP:TAX-2 from the axonemes of induced cells
Fluorescence (a, c, e and g) and phase contrast microscopy (b, d, f and h) images of induced TAX-2 RNAi cells, with DNA labeled with DAPI (blue), and native GFP (green): (a, b) cell with full length GFP flagellum; (c, d) cell with missing distal tip GFP flagellum; (e, f) cell with partial GFP flagellum; (g, h) cell with GFP negative flagellum.

length' (Fig 6.3a, b), 'absent' (Fig. 6.3g, h), 'proximal partial' (Fig. 6.3e, f), or 'negative distal tip' (Fig 6.3c, d). In 'negative distal tip' flagella the GFP signal was present from the proximal end near the basal body, along the length of the flagellum, stopping abruptly ~1μm before the distal tip. In flagella defined as 'proximal partial' the GFP signal decreased in intensity from proximal to distal end, becoming undetectable at some point along the length of the flagellum. In non-induced cells, 95% of flagella had GFP signal along the full length of the flagellum (n = 151). The remaining flagella were GFP negative. After induction, the frequency of 'full length GFP' flagella decreased (Fig. 6.4a). Between 4 and 8 hours post-induction there was a rapid increase in the number of 'proximal partial' flagella produced which we interpret as the new flagella produced as cells became depleted of TAX-2. The frequency of 'GFP absent' flagella increased throughout the time course, reaching 92% by 48 hours post-induction. Between 4 and 16 hours post-induction, 'negative distal tip GFP' flagella were produced. These could also represent new flagella produced as cells become depleted of TAX-2, but this fails to account for the clear difference in the appearance of the GFP signal between 'negative distal tip GFP' flagella and 'proximal partial' flagella.

6.4.1 GFP:TY:TAX-2 is lost from the distal tip of the axoneme

As stated above, 95% of non-induced flagella are 'full length GFP'. If these flagella, made before RNAi induction (pre-RNAi flagella), retain their GFP:TY:TAX-2 in the flagellum after RNAi induction then the frequency of 'full length GFP' flagella should equal the frequency of pre-RNAi flagella, as calculated from the measured growth rate of the population. However, the frequency of 'full length GFP' flagella detected drops more rapidly that can be accounted for by the assembly of axonemes after

Figure 6.4

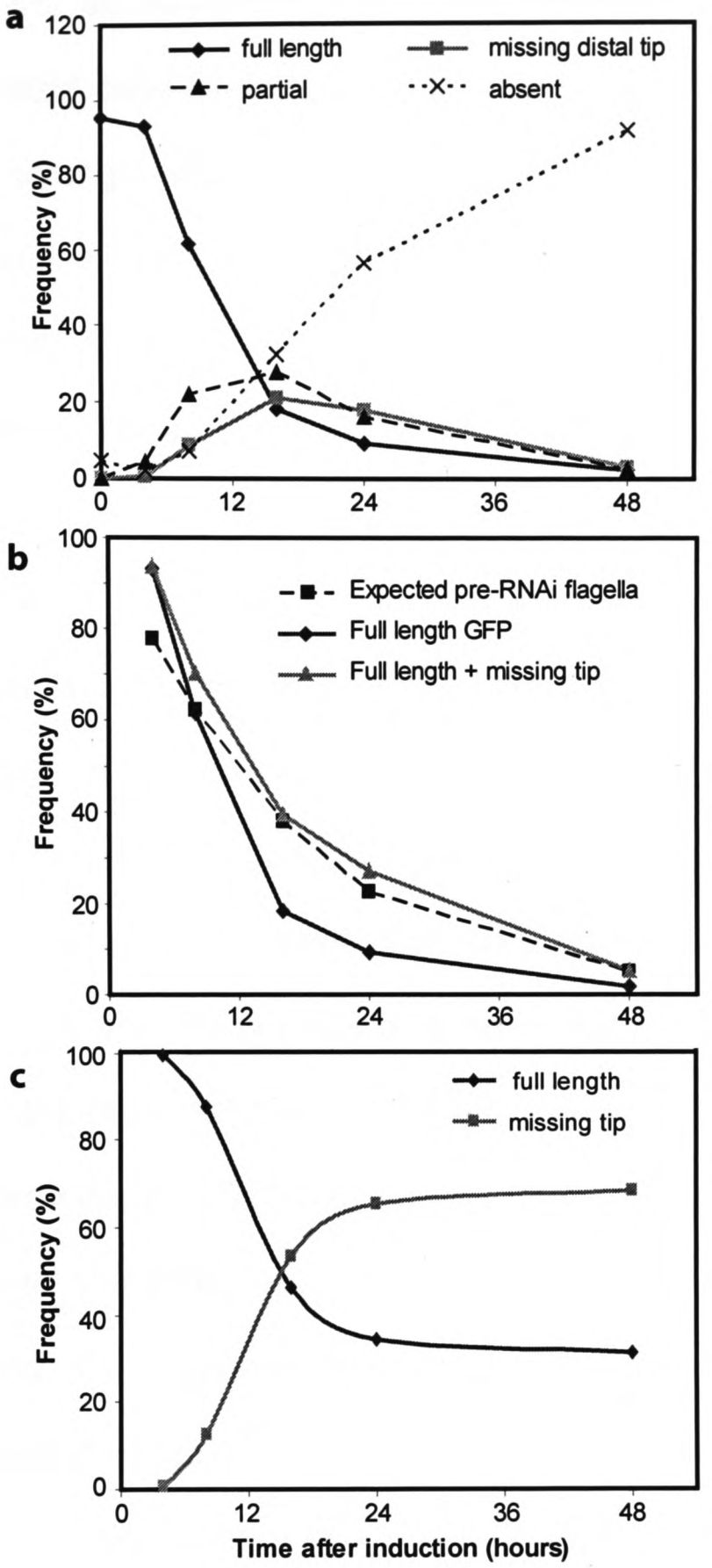


Figure 6.4. Loss of GFP:TY:TAX-2 from the axonemes of induced cells
(a) After induction the frequency of full length GFP flagella (solid black line) decreases; there is a temporary increase in the frequencies of partial GFP (dashed line, triangles) and missing distal tip GFP (solid grey line) flagella and a steady increase in GFP absent flagella (dashed line, crosses). (b) The frequency of flagella made before RNAi induction was calculated from the growth rate (dashed black line, squares); the frequency of full length GFP flagella (solid black line) is less than this, suggesting that GFP is being lost from pre-RNAi flagella; the combined frequency of full length GFP flagella and missing distal tip GFP flagella (grey line, triangles) is equal to the frequency of pre-RNAi flagella. (c) The ratio of full length GFP flagella to missing distal tip GFP flagella initially changes but reaches a plateau at 24 hours.

RNAi induction: just 18% at 16 hours post-induction, compared with 40%, the frequency of the calculated pre-RNAi flagella that should be present at this time-point (Fig. 6.4b). This strongly suggests that GFP:TY:TAX-2 protein is lost from flagella after RNAi induction. However, the frequency of flagella with either 'full length GFP' or 'negative distal tip' closely matches that of pre-RNAi flagella. Therefore these 'negative distal tip GFP' flagella are likely to represent flagella made before RNAi induction.

There are several possible explanations for this 'negative distal tip' phenomenon: first, that there is turnover of the axoneme and this is restricted to a region at the distal tip of the flagellum; second, that flagellar growth is not complete at cytokinesis and the new flagellum continues to grow after cytokinesis; and thirdly that the flagellum can vary in length and the distal tip is in flux. If this third theory of distal tip flux is true, it should be the case that 'full length GFP' flagella should be shorter than flagella with 'missing distal tip GFP' because flagella that are 'full length GFP' should be at their shortest length. We addressed this by comparing flagellar length between 'full length GFP' flagella and 'negative distal tip GFP' flagella. All measurements were taken from the cells which had one flagellum, or the old flagellum of cells with two flagella. We found no significant difference in the mean length of 'full length GFP' flagella (19.8 μm ±1.8 μm (n = 105)) compared to 'negative tip GFP' flagella (19.3 μm ±1.6 μm (n = 105)). This suggests that the third possibility, constant change of flagellar length due to growth and catastrophe of the distal tip region, is not the explanation for the appearance of 'negative distal tip GFP' flagella. A fourth possibility, that the axoneme continues to extend indefinitely in the absence of TAX-

2, is also excluded by the finding that 'negative distal tip GFP' flagella are the same length as 'full length GFP' flagella.

6.4.2 Analysis of GFP:TY:TAX-2 loss indicates a post-cytokinesis flagellum growth phenomenon

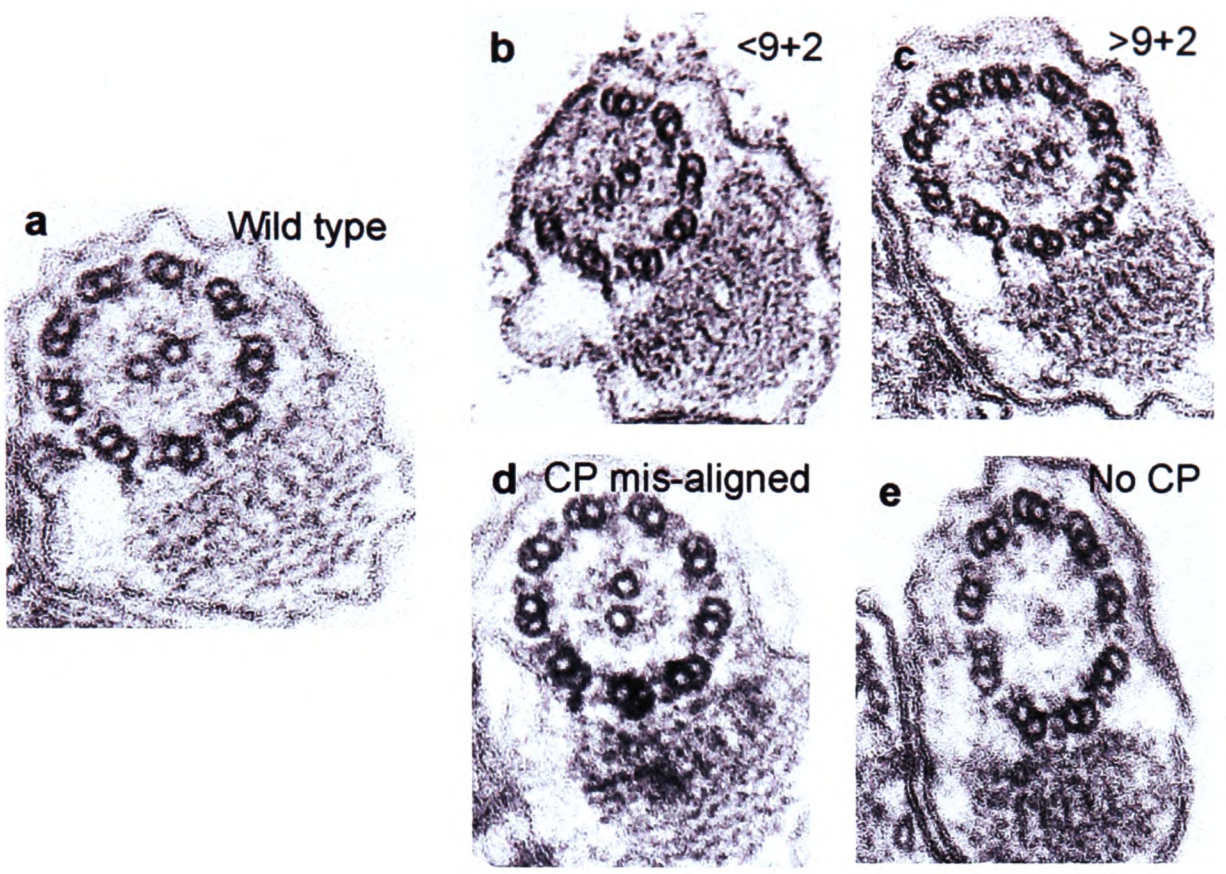
To differentiate between growth and turnover, we examined the ratio of 'full length GFP' flagella to 'negative distal tip GFP' flagella at 4, 8, 16, 24 and 48 hours after induction (Fig. 6.4c). The expectation is that, if turnover is responsible, all 'full length GFP' flagella should eventually lose the GFP signal from the tip region. Continuation of growth of new flagella made in the previous cell cycle, should however affect only these cells, so if this explanation is correct we should observe an initial decrease in the frequency of 'full length GFP' flagella which should then plateau at a non-zero frequency. The plateau would occur after all the 'new' flagella have elongated in the absence of GFP:TY:TAX-2, while flagella that had grown to their full length before RNAi induction would remain 'full length GFP' flagella. As shown in Fig. 6.4c, there is an initial change in the ratio, with a decrease in the frequency of 'full length GFP' flagella and an increase in the frequency of 'negative distal tip GFP' flagella, mostly occurring between 8 and 16 hours post-induction. Between 24 and 48 hours however there is no further change to the ratio, which remains at 1:2. This suggests that growth rather than turnover may account for the appearance of 'negative tip GFP' flagella. The emergence of these cells between 8 and 16 hours post-induction suggests that extra growth of the flagellum after cytokinesis may continue through the early stages of at least one cell cycle, possibly more.

6.5 TAX-2 RNAi causes a range of axonemal defects

RNAi-induced and non-induced cells were prepared for transmission electron microscopy and axonemal profiles examined for any defects. In non-induced cells, all axonemal profiles examined (n = 123) appeared as wild-type, possessing a 9+2 axoneme and PFR. Outer and inner dynein arms were visible and the central pair was positioned at the invariant position, parallel to the PFR, as is seen in wild-type *T. brucei* axonemes (Branche et al., 2006; Gadelha et al., 2006). At 72 hours post-induction, we observed that 86% of axonemes (n = 98) in RNAi-induced cells appeared indistinguishable from wild-type (Fig. 6.5). Of the remainder, a variety of axonemal defects were observed, most frequently missing outer doublets (11%). Other defects that were observed included extra outer doublets, either incorporated into the circular profile of the axoneme or outside of it (2%); mis-alignment of the central pair (1%); or absence of the central pair (2%). The outer doublet microtubules of the trypanosome axoneme can be numbered using the PFR as an external reference, whereby doublet 1 is opposite the central pair and the furthest from the PFR. Where outer doublet microtubules were missing from an axoneme, it was most frequently the non-PFR associated doublets (8, 9, 1, 2, and 3) that were missing, as was observed in PACRG AB RNAi-induced cells.

The analysis by TEM was carried out on cells which had also been examined and quantified in terms of GFP signal in the flagellum, in order to confirm successful knockdown of GFP:TY:TAX-2. At 72 hours post-induction 93% of flagella were entirely absent of GFP (n = 140), therefore the fact that the majority of axoneme profiles are normal in appearance by TEM is not due to lack of penetrance of the RNAi. An advantage of *T. brucei* is that it is possible to estimate the position of a

Figure 6.5



f

	Induced	Non-induced
Wild-type	84%	100%
<9+2	11%	0%
>9+2	2%	0%
CP mis-aligned	1%	0%
No CP	2%	0%

Figure 6.5. TAX-2 RNAi induction causes axonemal defects.
Transmission electron microscopy images of TAX-2 non-induced (a) and induced (b-e) cells. (f) table showing frequencies of particular defects in induced and non-induced cells.

Figure 6.6

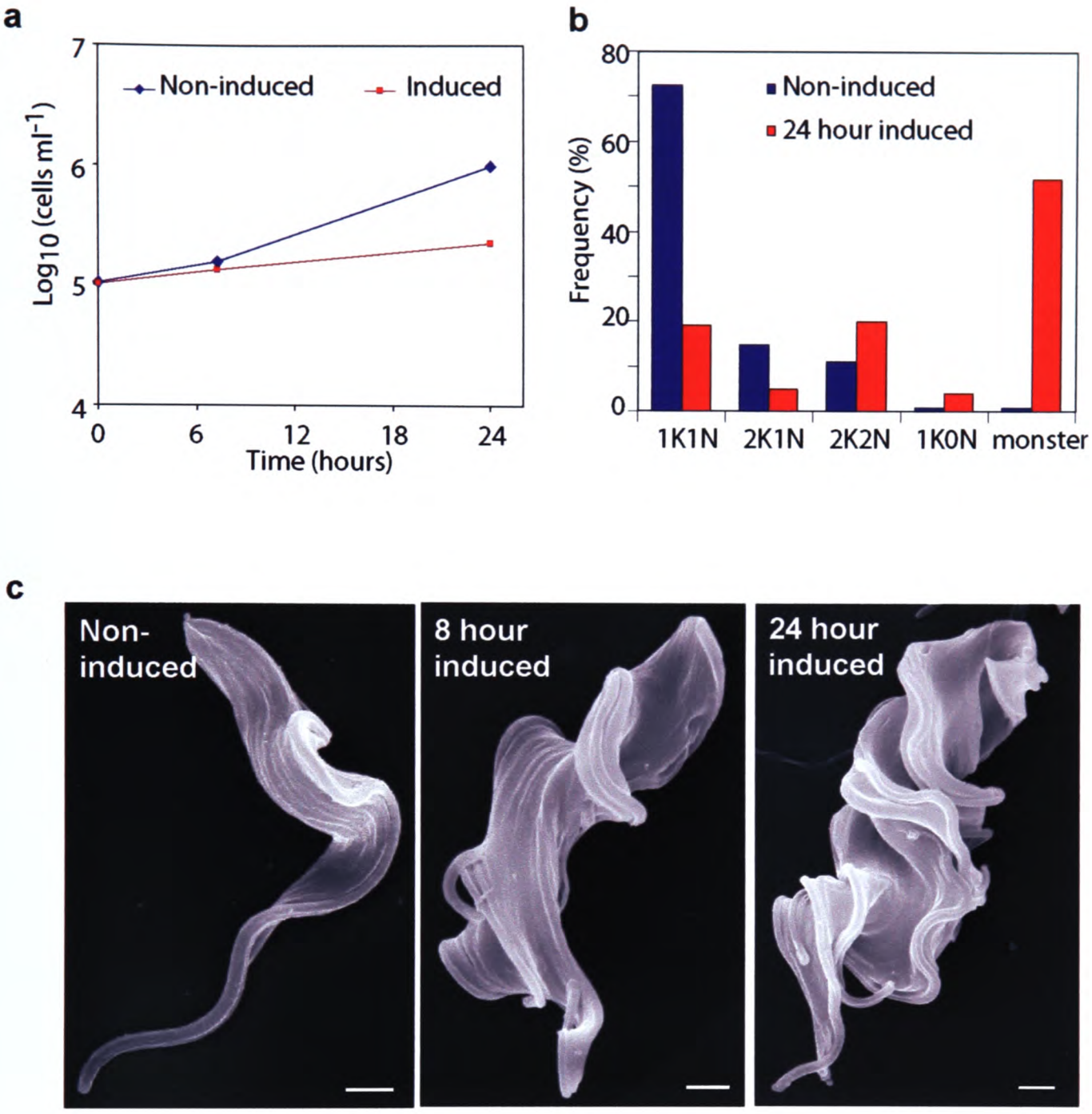


Figure 6.6. TAX-2 RNAi in bloodstream form trypanosomes affects growth and cytokinesis.

(a) Representative growth curve showing alteration in growth kinetics in induced cells (black line) compared to non-induced controls (dashed grey line). (b) Counts of nuclei (N) and kinetoplasts (K) in non-induced (black) and induced cells after 24 hours (grey), showing a reduction in 1K1N cells and increase in cells with more than 2 nuclei and 2 kinetoplasts. (c) Scanning electron micrographs of a non-induced cell with 1 flagellum, a cell with 2 flagella at 8 hours post-induction and a cell with at least 4 flagella at 24 hours post-induction. Scale bars = 1 μm.

cross-section along the flagellum (Dawe et al., 2005) using markers in the cell body. By this means we observed that defects in axoneme structure were not restricted to the distal region but could also be found in the flagellum alongside the cell body and within the flagellar pocket, i.e. throughout the length. All basal bodies examined (n=23) appeared normal in structure, however it is possible that defects were not observed due to the small number and low frequency of defects.

6.6 TAX-2 RNAi induction in bloodstream form cells causes defects in growth and cytokinesis

The same construct for RNAi was then used to transform bloodstream form *T. brucei* cells. Upon induction, RNAi-induced cells rapidly exhibited defects in cytokinesis and were unable to proliferate (Fig. 6.6a). Examination of the DAPI staining of RNAi-induced cells revealed that nuclei and kinetoplasts were able to divide and segregate, but cells did not undergo cytokinesis. A reduction in the frequency of 1K1N cells was observed, along with an increase in 2K2N cells (Fig. 6.6b). Successive rounds of kinetoplast segregation and mitosis produced a large number of cells with the phenotype 4K4N and 8K8N. Cells also continued to produce new flagella, which are wrapped around the enlarged cell body in a left-handed helix (Fig. 6.6c).

6.7 Conclusions and discussion

TAX-2 is widely conserved with a high degree of similarity within the flagellated eukaryotes, with a high degree of similarity. Homologues were not found in all organisms that exhibit cilia / flagella however, as it appears to be absent in *C.*

elegans, which produces only non-motile sensory cilia lacking the central pair. This suggests that the function of TAX-2 may be in motility or in the morphogenesis of the central pair. Furthermore, a TAX-2 homologue was not found in the apicomplexan *Plasmodium falciparum* which does possess an axoneme with a central pair. We know that variation in occurrence of axonemal proteins amongst Apicomplexa (TAX-2 is present in *Toxoplasma*) likely represents genuine differences in axonemal components rather than being due to incompleteness of genomes or gene models. Several bioinformatic analyses show that there are distinct variations in the components of axonemes within Plasmodium which displays an ephemeral axoneme only in the male gamete (Briggs et al., 2004a).

TAX-2 and its homologues are predicted to contain a Cytochrome b5 heme/steroid binding domain, spanning approximately the N-terminal half of the protein. A large number of proteins contain this domain, frequently in combination with signal peptides or transmembrane domains as many are membrane-associated. To date, no other Cytochrome b5 domain-containing proteins have been identified from flagellar or ciliary proteomes. The lack of similarity to any other protein families outside of the domain region makes elucidating function by comparison difficult. It remains an intriguing domain but with no obvious candidate for a ligand.

The results of this study show that in procyclic form *T. brucei*, RNAi ablation of TAX-2 leads to a small decrease in motility. A recent general survey of flagellar components (Baron et al., 2007) found that TAX-2 did not exhibit the phenotype of 'clumping' which the authors attribute to defects in cytokinesis owing to reduced motility. No data are presented for the motility of these cells, but we found no effect

on growth or cytokinesis following RNAi against TAX-2 in procyclic form trypanosomes despite the specific reduction in motility. Structural defects were present in a minority of axonemal profiles. Similar defects have been previously observed in other RNAi cell lines: missing outer doublets are observed in the RNAi phenotype of PACRG (Dawe et al., 2005) and δ-tubulin (Gadelha et al., 2006); absence of the central pair microtubules is produced by ablation of γ-tubulin (McKean et al., 2003). In such mutants however, these defects lead to more extreme forms of flagellar impairment. It is possible therefore that the decrease in motility observed in the population of RNAi-induced cells comes from a minority of cells that are severely affected structurally; however this appears to be unlikely since completely paralysed cells are not observed and the majority of cells show only a slight reduction in motility. A second possibility is that these defects in axonemal structure such as are seen in Fig. 6.5 affect only a small region of the flagellum. TEM examination of RNAi induced cells revealed defects along the length of the flagellum, perhaps suggesting that there may be intermittent defects in axoneme structure. The defects, either loss of central pair or loss of outer doublet microtubules, seen in the axonemes of RNAi-induced cells by TEM might suggest that TAX-2 may be involved in linking outer doublet microtubules to the central pair apparatus; unfortunately, I have been unable to confirm this with an ultrastructural localisation for TAX-2. Missing doublets could be caused as outer doublets are broken due to a loss of the connection with the central pair under the constraint of TAX-2 depletion. A break in an outer doublet could allow movement of that doublet caused by the motility of the axoneme and microtubule sliding, such that the broken doublet 'walked' along adjacent doublets and resulting in a region with a missing doublet and further along the axoneme, a region containing an additional doublet. Of

course, such a defect could also be caused by the loss of connections between the outer doublets. The presence of axonemes in which the central pair is mis-aligned or absent also suggests defects in the connections between the central pair and outer doublets. Loss of connections between the central pair and outer doublets could allow the central pair to become mis-aligned, or to break in the absence of the stability afforded by the connections to the outer doublet microtubules. Finally, the presence of a large proportion of GFP-negative flagella coupled with the finding that the majority of axonemes appear as wild-type by TEM demonstrates that axonemes can be built in the absence of TAX-2.

There are several further lines of evidence that support a function for TAX-2 in or around the central pair. Firstly, TAX-2 remained in the proteome of isolated *Chlamydomonas* axonemes following biochemical extraction with KCl (Pazour et al., 2005). This preparation was obtained from a mutant cell line whose flagella lacked outer dynein arms and the resulting KCl extracted preparation was shown to consist of the outer doublets, lacking outer and inner dynein arms and also the C2 microtubule plus accessory proteins. This suggests that TAX-2 is not part of the outer or inner dynein arms, but may be bound to outer doublets or be a component of the central pair accessory structures or radial spokes. A function and localisation around the central pair would be in agreement with its longitudinal localisation to axoneme but not the basal body and transition zone where there are no central pair microtubules or radial spokes. Furthermore, there is no TAX-2 homologue in *C. elegans* which builds cilia with a 9+0 structure. The absence of a TAX-2 homologue in *P. falciparum* (which possesses a central pair) may be explained by the apparently 'stripped-down' and transient axoneme of this organism.

The human homologue of TAX-2, CYB5D1 is located at locus 17p13.1, a region linked to a number of retinal cone diseases. These include Leber congenital amaurosis (LCA) (Hameed et al., 2000), retinal cone dystrophy 2 (RCD2) (Greenberg et al., 1994) and central areolar choroidal dystrophy (CACD). LCA is known to be caused by mutations in the retinal guanidine cyclase gene GUCY2D (Perrault et al., 1996), and arylhydrocarbon-interacting receptor protein like 1, AIPL1 (Sohocki et al., 2000). Causative genes for CACD and RCD2 are not known although the region contains a number of candidate genes including GUCY2D, AIPL1, pigment epithelium-derived factor (PEDF) and recoverin. These diseases, however, if ciliary, are likely to be attributable to primary cilia which possess a non-motile 9+0 axoneme; if our suggested localisation for TAX-2 is correct it would be unlikely to be a candidate gene for these diseases.

The use of GFP tagging in the same cell line as RNAi ablation of both the tagged and untagged protein provides the opportunity for studying the kinetics of protein loss directly. The novel finding that not all pre-RNAi flagella contained GFP:TY:TAX-2 signal to the distal tip demonstrated that there may be either turnover at the distal tip region or additional growth after cytokinesis. The kinetics of the change of pre-RNAi flagella from 'full length GFP' to 'negative distal tip GFP' indicates that the more likely explanation is additional growth of the new flagellum for some time after cytokinesis has occurred. This has been implied previously in studies where the length of the new flagellum had been compared to that of the old flagellum (Sherwin and Gull, 1989; Davidge et al., 2006; Absalon et al., 2007). If this is a general feature of the flagellum of *T. brucei*, it should be observable in RNAi experiments with other

axonemal proteins using our new vector system to perform GFP tagging and inducible RNAi in the same cell (Kelly et al., 2007). Furthermore, in inducible GFP or TY tag expression studies one might see the addition of tagged proteins to the distal tip of the old flagellum. This experiment has only been carried out to my knowledge with inducible TY tagged PFR2 and cells were examined in the hours following induction of expression (Bastin et al., 1999). While cells were observed in which the distal part of the flagellum contained the TY epitope, in this case it would be difficult to differentiate in 1K1N cells between a flagellum that had continued to grow after cytokinesis and the newly produced flagellum that was still the daughter flagellum of a 2K2N cell when expression was induced.

The results of this study provide a further example of a flagellar protein that affects cytokinesis and growth in the bloodstream form but not the procyclic form of *T. brucei*. Furthermore, protein knockdown in procyclic form trypanosomes causes only a slight defect in motility, with the majority of axonemes structurally unaffected. Despite this, in bloodstream forms the phenotype is as rapid and dramatic as the knockdown of flagellar proteins that have stronger procyclic motility phenotypes (Broadhead et al., 2006; Ralston and Hill, 2006). Finally the novel use in *T. brucei* of an inducible RNAi system that targets both the endogenous and epitope tagged protein in the same cell provides a useful method of observing the loss and consequences of ablating a protein of interest.

CHAPTER 7

RESULTS

Characterisation of TbAAT-1

7 Characterisation of TbAAT-1

Amongst the proteins identified from the *T. brucei* flagellar proteome (TbFP) I was interested by a protein widely and exclusively conserved in flagellated organisms, which I chose for further analysis. This protein had originally been identified as a binding partner of AMY-1, a c-Myc binding protein, therefore was named AMY-1-associating protein expressed in testis-1 or AAT-1 (Yukitake et al., 2002). In addition to its identification from our TbFP, the *Chlamydomonas reinhardtii* TbAAT-1 homologue is also present in the proteome of isolated *C. reinhardtii* flagella (Pazour et al., 2005), and has been shown to be slightly upregulated following deflagellation of this alga (Pazour et al., 2005; Stolc et al., 2005). The CrFP analysis of peptides derived from differently extracted preparations revealed that TbAAT-1 remains with the axoneme fraction after KCl extraction (Pazour et al., 2005).

7.1 TbAAT-1 is evolutionarily conserved in many flagellates

The gene encoding TbAAT-1 (Tb11.02.0354) encodes a protein of 709 amino acids, predicted molecular weight of 80.0 kDa and predicted isoelectric point of pH 6.1. It is widely and exclusively conserved in flagellate eukaryotes, with homologues in the other kinetoplastids *T. cruzi* and *L. major*, in addition to *H. sapiens* (NP_203528), *D. melanogaster* (NP_609849), *C. reinhardtii* (C_450119) and *T. thermophila* (XP_001022857). Notably absent from this list is the nematode *Caenorhabditis elegans* which builds only immotile sensory cilia lacking the central pair and inner and outer dynein arms. Searching the Apicomplexa *Plasmodium falciparum* and *Toxoplasma gondii* genomes with this sequence reveals that both contain a homologue; this is noteworthy as many other widely conserved flagellar proteins do

Figure 7.1

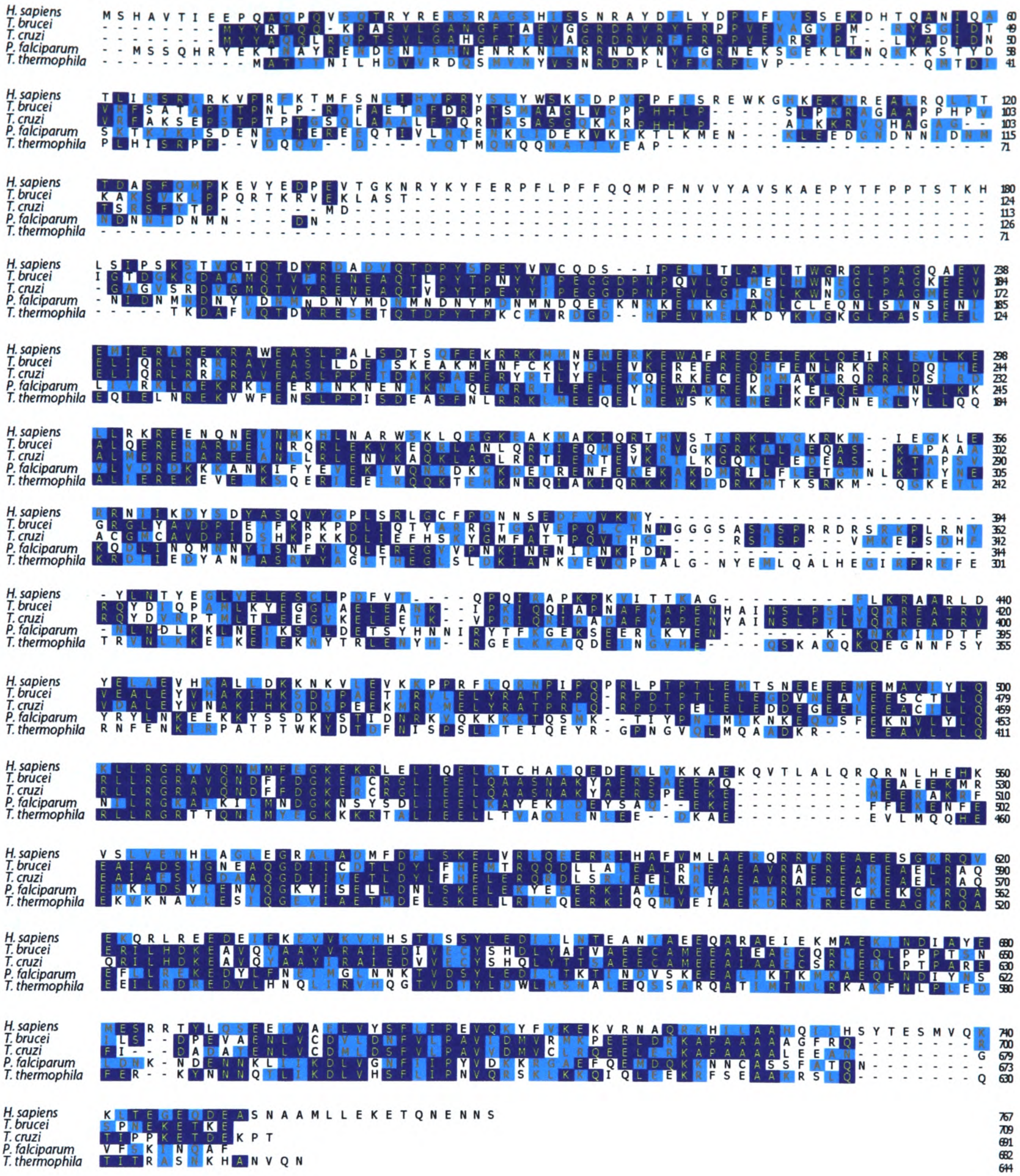


Figure 7.1 TbAAT-1 is widely conserved in flagellates
Protein sequence alignment of *T. brucei* TbAAT-1 (Tb11.02.0354) with gene products from *H. sapiens* (NP_203528), *T. cruzi* (XP_818207), *T. thermophila* (XP_001022857) and *P. falciparum* (XP_001349047). Orthology was determined by examination of candidate sequences including reciprocal BLAST. Identical residues are shown in dark blue boxes; similar residues are shown in light blue.

not have homologues in *P. falciparum* (for example TAX-1 and TAX-2). TbAAT-1 is not predicted to contain any known domains.

7.2 GFP:TY:TbAAT-1 fusion protein localises to the axoneme in *T. brucei*

To localise TbAAT-1 in *T. brucei*, a strain was constructed in which one copy of the two endogenous genes in the diploid genome was replaced with a GFP:TY:TbAAT-1 fusion, which contained a short TY epitope between the GFP and TbAAT-1 so allowing immunological detection. The GFP signal was examined in fixed cells (Fig. 7.2), where it was located along the full length of the flagellum but not at the basal body, and appeared punctate. The signal extended from the basal body, through the flagellar pocket and to the distal tip and was therefore clearly axonemal rather than in the PFR.

7.3 RNAi ablation of TbAAT-1 in procyclic form trypanosomes

To understand the function of TbAAT-1 in *T. brucei*, we used RNAi to ablate protein expression in both the 29-13 strain and the strain expressing the GFP:TY:TbAAT-1 fusion protein. The RNAi construct was targeted against TbAAT-1 mRNA and so would be capable of ablating both the GFP:TY:TbAAT-1 fusion and wild-type TbAAT-1 RNA. Expression levels of the GFP:TY:TbAAT-1 could then be used for assessing the level of TbAAT-1 reduction. Ablation of GFP:TY:TbAAT-1 could be visualised directly by western blotting using the monoclonal antibody BB2.

Figure 7.2

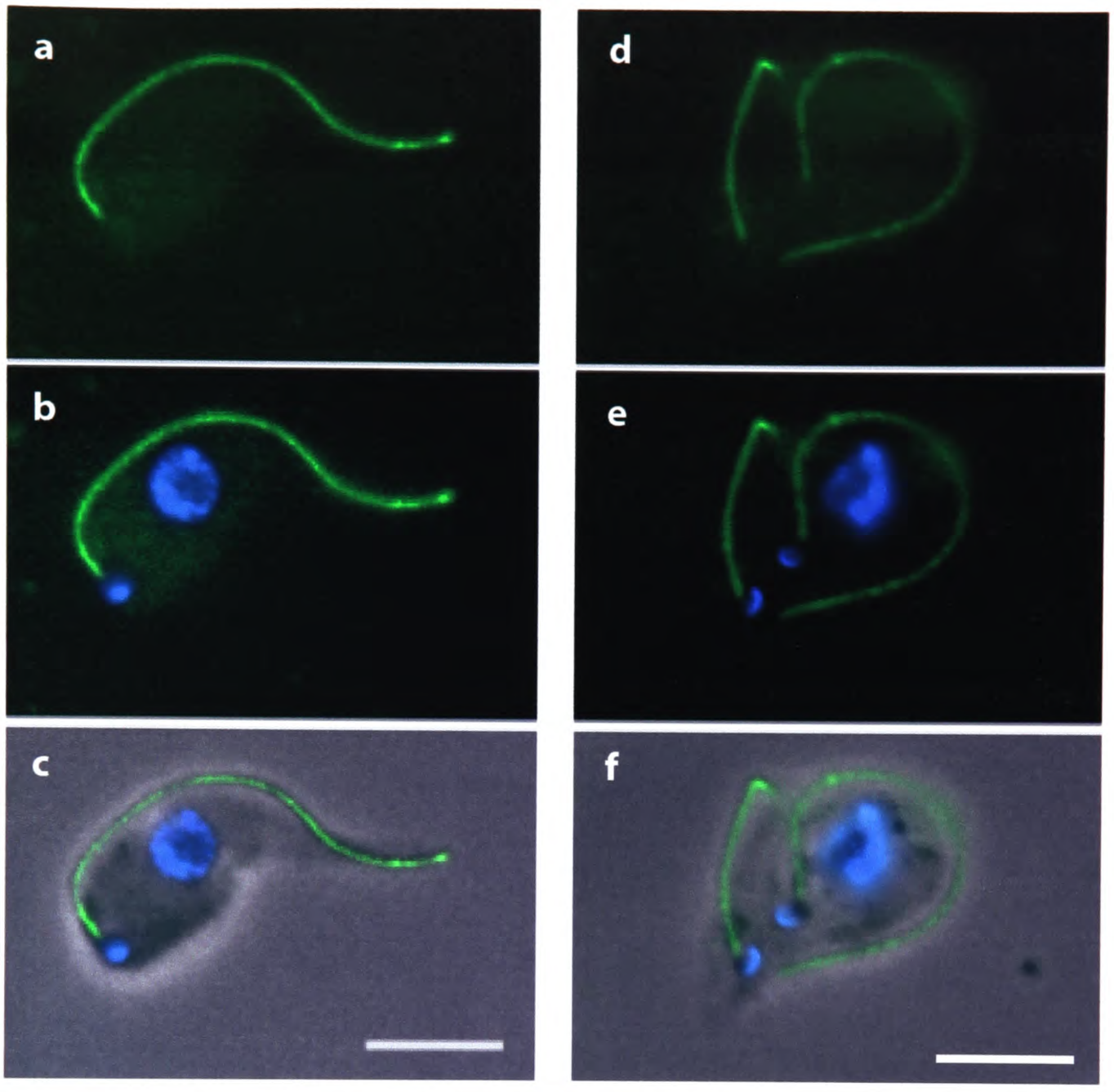
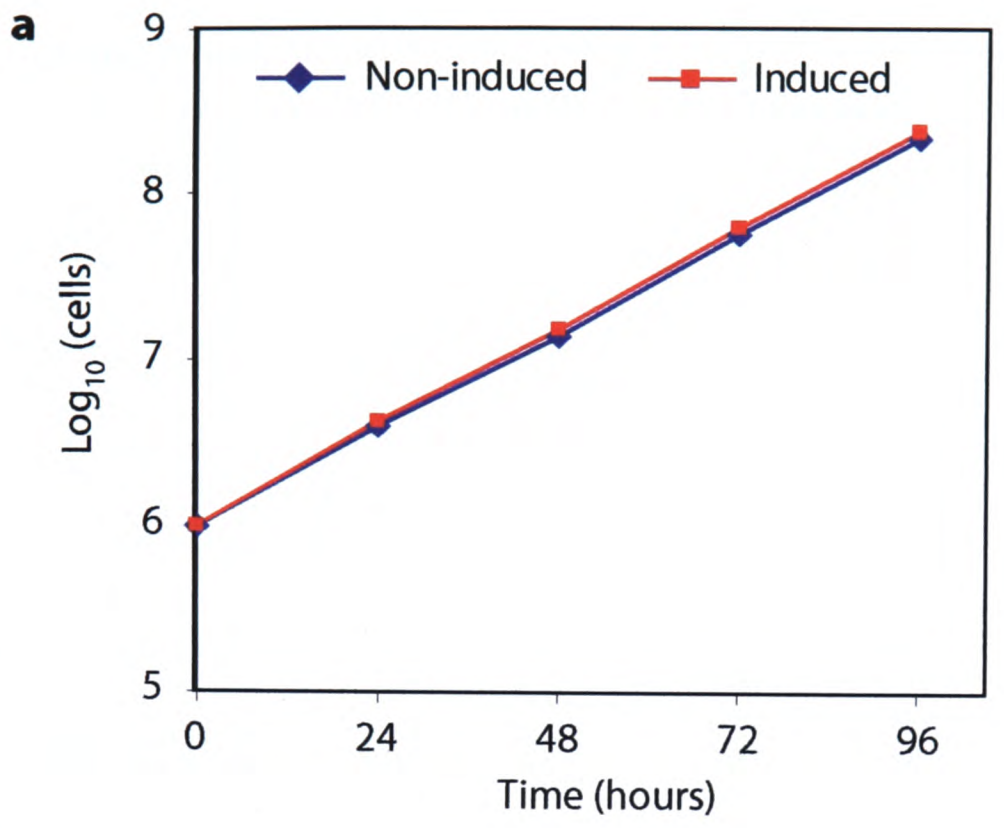


Figure 7.2. GFP:TbAAT-1 fusion protein localises to the axoneme.
Fluorescence microscopy (a, b, d and e) and phase contrast microscopy images overlaid (c and f) images of detergent extracted trypanosome cytoskeletons. DNA is labelled with DAPI (blue), and native GFP is shown in green. (a - c) Cell with one flagellum, one kinetoplast and one nucleus expressing GFP:TbAAT-1 which localises to the length of the axoneme. (d - f) Cell with two flagella, two kinetoplasts and one nucleus expressing GFP:TbAAT-1 which localises to the axonemes of both the new and old flagella. Scale bar = 5μm.

Figure 7.3



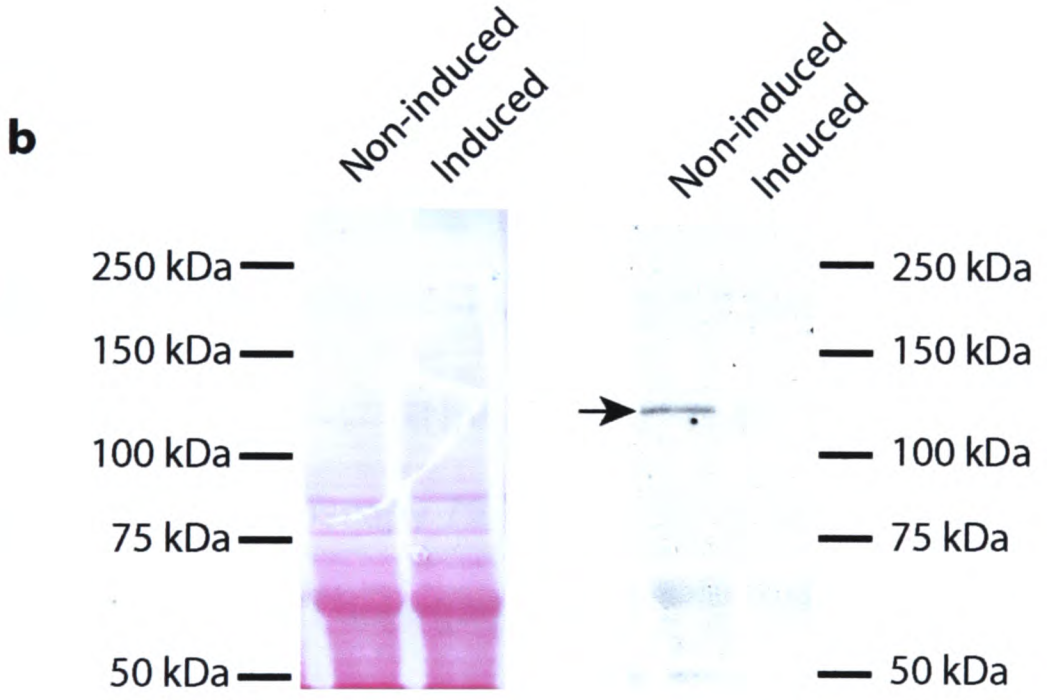


Figure 7.3 RNAi ablation of TbAAT-1 in procyclic form trypanosomes
(a) Inferred cumulative growth curve showing no alteration in growth kinetics in TbAAT-1 RNAi-induced cells (red squares) compared to non-induced controls (blue diamonds).
(b) Western blot with BB2 antibody showing reduction in GFP:TbAAT-1 protein level 72 hours after RNAi induction. Arrow indicates the band at ~115 kDa, the size of tagged TbAAT-1. Ponceau staining of membrane shows even gel loading between the two lanes.

Ablation of TbAAT-1in procyclic cells produced no effect on cell growth rate (Fig. 7.3a). Western blotting against the TY tag attached to GFP:TY:TbAAT-1 reveals that the level of TbAAT-1 is much reduced in RNAi- induced cells by 72 hours post-induction, such that no band is detected in the western blot (Fig. 7.3b). However, the loss of GFP:TY:TbAAT-1 was not examined in fixed cells as I did with TAX-2. TbAAT-1 RNAi-induced cells continued to build a new flagellum each cell cycle, however cell motility was affected. A significant difference in mean speed was observed between RNAi induced and non-induced cells ($P < 0.001$). As shown by the histogram of mean speeds in Fig 7.4 (a), the majority of RNAi-induced cells have a mean speed of less than 2 μm s^{-1}. The tracks of individual cells reveal that induced cells demonstrate reduced productive motility over the 40 sec period than non-induced controls (Fig 7.4 b - c).

7.4 TbAAT-1 RNAi induction does not affect axoneme structure

Non-induced and TbAAT-1 RNAi-induced cells were fixed for thin section transmission electron microscopy 72 hours post-induction. In addition to whole cells, cells were also treated with detergent to produce cytoskeletons. Examination of the axoneme profiles of induced cells revealed no obvious differences from those of non-induced controls. Induced axonemes possessed nine outer doublets with both outer and inner dynein arms clearly visible, surrounding the correctly aligned central pair.

In order to address whether there are less obvious defects in the axonemes of RNAi-induced cells, a number of axoneme profiles each of non-induced and induced whole cells and cytoskeletons (example images shown in Fig 7.5 a, d, g, j) were

Figure 7.4

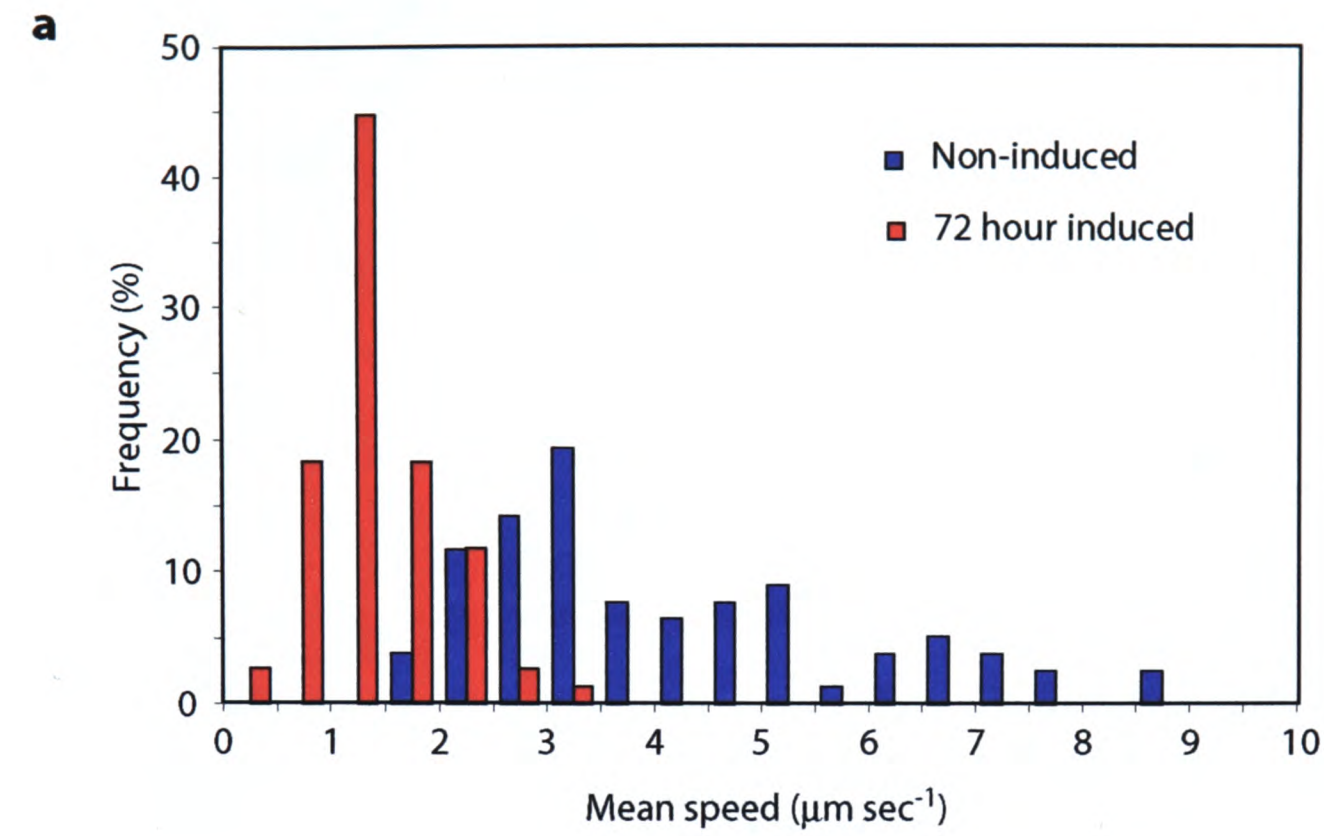


Figure 7.4. Ablation of TbAAT-1 reduces motility in procyclic form trypanosomes

(a) Histogram showing the frequency distribution of mean speeds of non-induced cells (blue bars) and TbAAT-1 RNAi induced cells 72 hours post-induction (red bars). (b - c) Tracks of non-induced (blue) and induced (red) cells from which mean speeds were calculated. For each, 30 representative tracks are shown. Scale bar = 100 µm

Figure 7.5

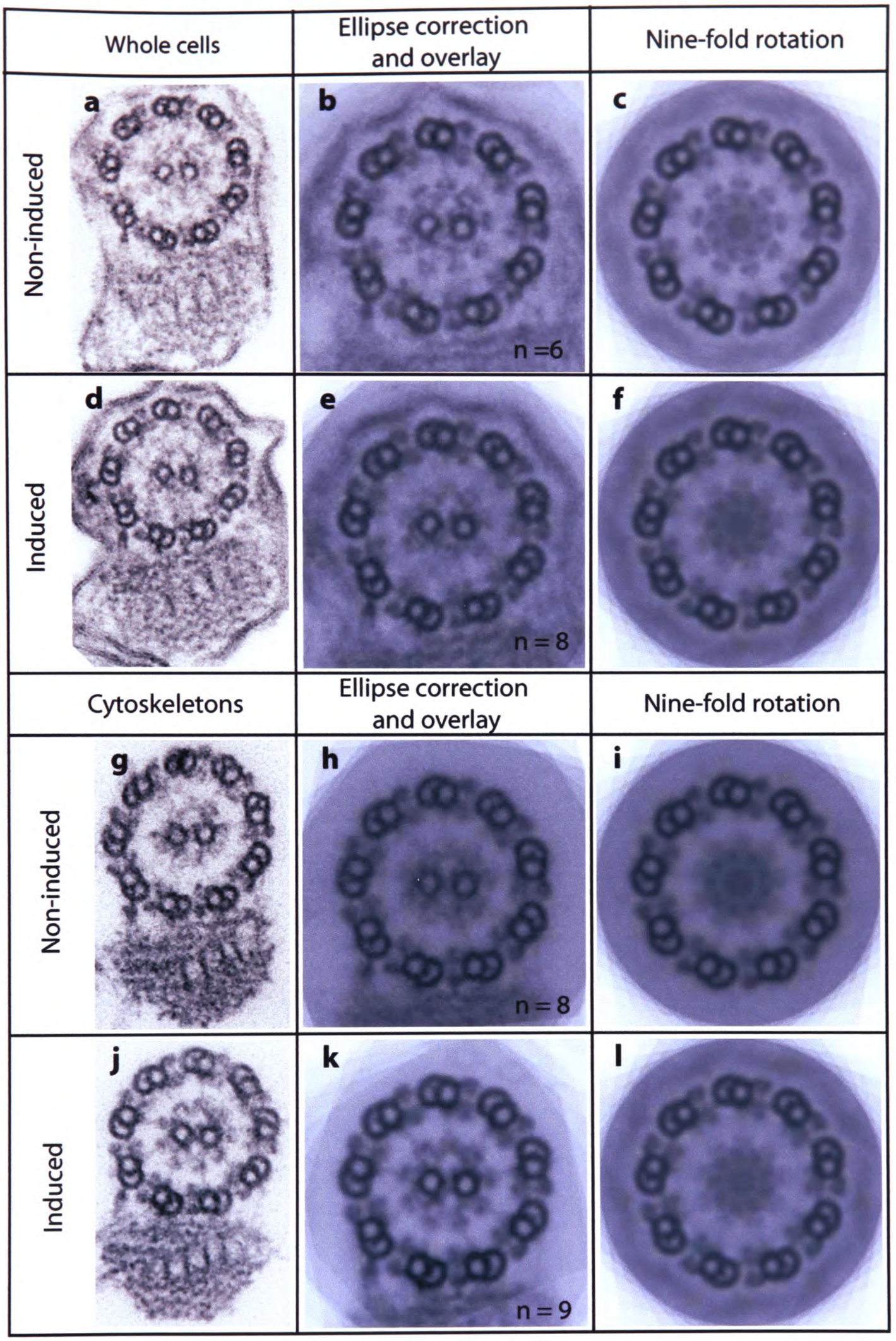


Figure 7.5. TEM examination of TbAAT-1 RNAi-induced cells
Representative transmission electron micrographs of TbAAT-1 non-induced and induced whole cells and cytoskeletons (a, d, g, j), averaged overlays of micrographs (b, e, h, k), and nine-fold rotations of the overlays (c, f, j, l). (a - c) Micrograph and overlays of non-induced whole cells. (d - f) Micrograph and overlays of TbAAT-1 RNAi-induced whole cells. (g - i) Micrograph and overlays of non-induced detergent-extracted cytoskeletons. (j - l) Micrograph and overlays of non-induced detergent-extracted cytoskeletons.

processed to correct for ellipticalness, then overlaid and averaged (Fig. 7.5 b, e, h, k). This increases the signal: noise ratio and would reveal if structure relating to a particular outer doublet were affected. To further improve the signal: noise ratio, these overlaid images were then rotated nine-fold to produce an average image for non-induced and for induced axonemes (Fig. 5.7 c, f, i, l). Despite the sensitivity of this approach, no differences were observed in axoneme structure between non-induced and induced axonemes.

7.5 RNAi ablation of TbAAT-1 in bloodstream form trypanosomes

When the RNAi analysis was extended to the bloodstream form, I found that RNAi-induced cells quickly ceased to undergo cytokinesis leading to death of the population within 24 hours of induction (Fig. 7.6a). Mitosis continued, as did the production of new flagella, producing many large multi-nucleate cells with many flagella (Fig. 7.6b). The kinetoplast also divided, however with less frequency than the nucleus. While there were many cells in the population with the karyotypes 4K4N, 6K6N and 8K8N, others were found which contained fewer kinetoplasts than nuclei e.g. 1K2N, 2K4N and 3K4N (Fig. 7.6c). From the counts of kinetoplasts and nuclei it is possible to calculate the total number of kinetoplasts and nuclei in the population and therefore the ratio of kinetoplasts to nuclei. This is displayed as the log ratio of kinetoplasts to nuclei (Fig. 7.6d). A ratio of 1 kinetoplast/ 1 nucleus would give a log ratio of zero, so a positive log ratio indicates more kinetoplasts than nuclei in the population. However, a feature of the cytokinesis phenotype specific to TbAAT-1 RNAi-induced cells is the change in log ratio of kinetoplasts/ nuclei. A small increase in the frequency of zoids is observed (3 %, Fig. 7.6c), however this is not enough to balance the number of nuclei in the population. This suggests failure

Figure 7.6

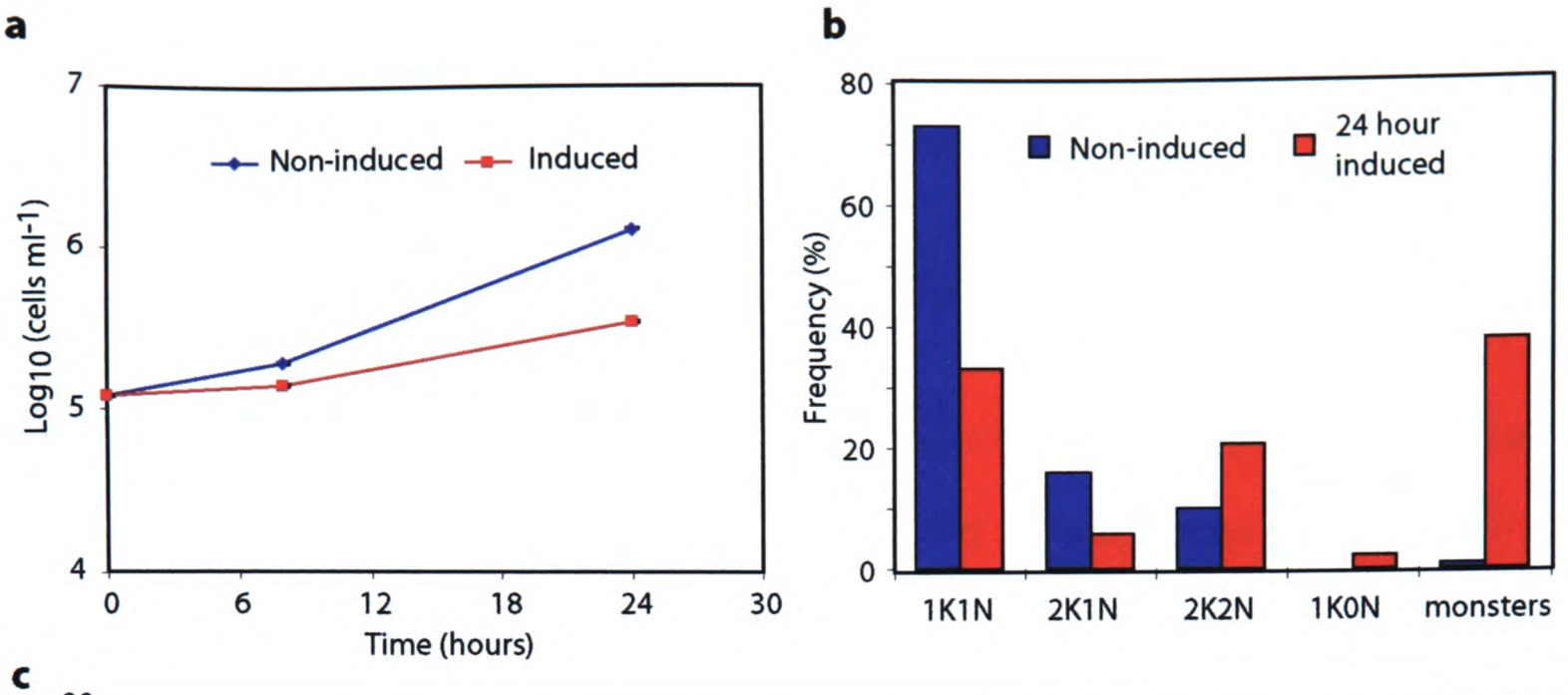


Figure 7.6 RNAi ablation of TbAAT-1 in bloodstream form trypanosomes causes defects in growth and cytokinesis

(a) Representative growth curve showing slow growth of TbAAT-1 RNAi-induced cells (red) compared to non-induced controls (blue).

(b) Counts of nuclei and kinetoplasts reveal a reduction of 1K1N cells and increase in 2K2N cells and monsters in TbAAT-1 RNAi-induced cells (red) compared to non-induced controls (blue).

(c) Counts of kinetoplast and nucleus number of TbAAT-1 RNAi-induced cells at 24 hours post-induction (red, n=400) and non-induced controls (blue, n=500), revealing an increase in multinucleate cells in the population.

(d) Graph showing the log ratio of total number of K: total number of N in the population of non-induced cells (blue bars) compared with induced cells (red bars) at 8 and 24 hours post-induction.

of kinetoplast replication or segregation, as indicated by the decrease in log ratio to -0.08 in TbAAT-1 RNAi-induced cells (Fig. 7.6d).

7.6 Conclusions and discussion

Yukitake et al (Yukitake et al., 2002) found 3 splice variants of AAT-1 (named AAT-1α, β and γ) of which AAT-1α is the longest with β and γ sharing the C-terminal 31 amino acids (Matsuda et al., 2005). However, there is only one homologue in *T. brucei*, where the huge majority of genes do not have exons and are not cis-spliced. Several proteins associating with AAT-1 have been identified from previous studies. AMY-1, a c-Myc binding protein, was used to identify AAT-1 in yeast-two-hybrid screening. AMY-1 has also been shown to interact with a protein kinase A anchor protein, S-AKAP84/149. Of these likely binding partners for AAT-1, in trypanosomes only a homologue for AMY-1 is found (accession number: Tb09.211.0775). This was not identified as being present in the trypanosome flagellum by the TbFP. AMY-1 has been shown to be strongly expressed exclusively in testis (Furusawa et al., 2001) where it localises to the mitochondria of sperm, as does S-AKAP84 (Furusawa et al., 2001). AAT-1α has also been shown to be expressed strongly in testis, where it was found to co-localise with AMY-1 in the mitochondria at the neck region of sperm (Yukitake et al., 2002). The finding of this study that AAT-1α localises to mitochondria clearly disagrees with my own finding that it localises to the axoneme of *T. brucei*.

However, evidence that supports the localisation of TbAAT-1 to the axoneme comes not only from my work on trypanosomes but also from the proteomes of flagella from *C. reinhardtii* (Pazour et al., 2005) and *T. thermophila* (Smith et al., 2005).

Furthermore, the *Chlamydomonas* homologue of AMY-1 was found within the CrFP (Pazour et al., 2005). Both AAT-1 and AMY-1 remained in the proteome of isolated *Chlamydomonas* axonemes following biochemical extraction with KCl; for TbAAT-1 no peptides were found in the KCl-soluble fraction (Pazour et al., 2005). The preparation of extracted axonemes was obtained from a mutant cell line lacking outer dynein arms and the resulting preparation was shown to consist of the outer doublets and one of the central pair microtubules with some of the associated proteins, but lacking outer and inner dynein arms and also the C2 microtubule. This suggests that TbAAT-1 is not part of the outer or inner dynein arms, but may be bound to outer doublets or be a component of the central pair accessory structures. A function and localisation around the central pair would be in agreement with its longitudinal localisation to axoneme but not the basal body and transition zone where there is no central pair and no radial spokes. Furthermore, there is no TbAAT-1 homologue in *C. elegans* which builds cilia with a 9+0 structure.

The human homologue of TbAAT-1 is located on human chromosome 3q12-q13.3. This region contains disease loci for diverse diseases, however none that fit a ciliary disease phenotype profile.

The phenotype of TbAAT-1 in trypanosomes provides the first RNAi characterisation of this protein. There is a strong motility phenotype in procyclic form trypanosomes despite the lack of defects in axoneme structure. This translates to the growth and cytokinesis phenotype seen in bloodstream form trypanosomes, again without structural defects in the axoneme, and additionally featuring failure to replicate or segregate the kinetoplasts.

CHAPTER 8

DISCUSSION

8 Discussion

The increase in research into cilia and flagella over the course of my D.Phil research has been dramatic, and has been accompanied by an increase in our knowledge on these well-conserved yet enigmatic organelles. I have addressed discussion points pertaining to individual proteins in the relevant chapters; therefore in this section I hope it will be useful to analyse how and why this great advance in our knowledge has come about. The recent research can be broadly defined within two themes: firstly, the identification of components of eukaryotic cilia and flagella and secondly to understand the function of these components, particularly in relation to health and disease. In this discussion I will examine these two themes, using examples of my own work.

8.1 Identifying the components of cilia and flagella

While the iconic structure of the 9+2 axoneme has been known since early electron microscopy studies, until quite recently the number of known components in the public domain was woefully small. The range of human disease that is now known to be attributable to dysfunctional cilia has grown in recent years, driving interest in elucidating the protein constituents involved. Biochemistry had previously estimated a figure of 250 proteins found within the flagellum, based on spots on 2D SDS-PAGE gels of isolated flagella (Dutcher, 1995), however known flagellar genes counted for only a small minority of these. The increase in knowledge of the protein constituents of eukaryotic flagella in the last four years has been of exponential proportions. The major factor that has enabled this increase in the number of known flagellar genes has been the completion of genomes from various species.

Prior to the genomic era, a number of types of studies contributed to our knowledge of the components of flagella thereby providing interesting clues but not an overall picture. Forward genetics and mutant analysis using the model organism *Chlamydomonas* provided much functional data on the functions of axonemal components for example the radial spokes (Witman et al., 1978). Biochemistry studies provided some information and were particularly effective at examining the molecular motors within the flagellum, such as the studies on isolated dyneins or kinesins from *Chlamydomonas*. Studies of human disease also provided a few of the components, by identifying the genes responsible for disease phenotypes.

The completion of genomes from a number of species enabled a rapid increase in identified components of flagella by the use of comparative genomics and proteomics. Comparative genomics identified sets of putative flagellar genes by finding genes shared between flagellate organisms and absent in non-flagellates. Several studies used similar approaches in 2004 (Avidor-Reiss et al., 2004; Li et al., 2004). Using the genomes of organisms with known flagellar characteristics, such as *C. elegans* which produces only sensory cilia, enabled one such study to link particular sets of genes and their probable function within the flagellum (Avidor-Reiss et al., 2004).

The existence of genomes also enabled the use of proteomics for identification of large numbers of flagellar proteins, as predicted protein sequences allowed for the identification of proteins from isolated flagella by mass spectrophotometry. There is a collected ciliome resulting from these proteomes and comparative genomic studies

containing many as yet uncharacterised proteins (Inglis et al., 2006). The proteomes of cilia and flagella from model organisms such as *C. reinhardtii*, *T. thermophila* and *T. brucei* have brought together model systems with human diseases, for example one study that used the known proteins of *Chlamydomonas* to predict candidate genes for Primary Ciliary Dyskinesia (Pazour et al., 2006). A number of disease genes found among proteomes and characterised in model organisms. One such example is the hydrocephalus-causing gene Hydin, characterised in both *Chlamydomonas* and *T. brucei* (Broadhead et al., 2006; Dawe et al., 2007; Lechtreck and Witman, 2007). Defects in PACRG, though not linked directly as the cause of human ciliary disease, are known to cause male sterility in mice.

While there are now a number of flagellar (Ostrowski et al., 2002; Pazour et al., 2005; Smith et al., 2005; Broadhead et al., 2006) and centrosomal / centriolar (Andersen et al., 2003; Keller et al., 2005) proteomes from evolutionarily diverse organisms, primary cilia as they exist on most cells within human tissues, have not yet been subjected to proteomic analysis. In recent months, a proteome of the modified connecting cilium of the photoreceptor has been published. The composition of the primary cilium is therefore unknown, although likely to contain several hundred proteins including core components shared with motile cilia. A surprising result from the collective set of proteomes is the degree of diversity in protein components between species given the observed structural conservation.

The availability of genomes has further enabled the linking of known flagellar genes with disease loci. One example of this is the now well known association of IFT proteins with polycystic kidney disease. When the candidate gene for a mouse

model of polycystic kidney disease was first identified asTg737 in 1994, its function was unknown (Moyer et al., 1994) and it was not until 2000 that this gene was found to be a homologue of IFT88, a gene for which an insertional mutant existed. The IFT88 mutant did not build flagella (Pazour et al., 2000). Furthermore, improved mapping of the human genome has resulted in more candidate genes being linked to ciliary disease. Meckelin is now known to be the causative gene product of both Meckel-Gruber Syndrome and the phenotype of the wpk rat (Smith et al., 2006).

Each of these techniques is flawed when taken individually: Comparative genomics is unlikely to find organism-specific flagellar genes, while proteomes are unlikely to find regulatory proteins (i.e. DAF-19) as these are not commonly found in the end flagellum itself, but within the cell body. Comparative genomics, however, has proved effective at identifying regulatory proteins (Blacque et al., 2005; Laurencon et al., 2007), however, this technique will not identify proteins with cytosolic functions in addition to roles in ciliogenesis, such as tubulin. Much valuable research has come from studies using model organisms; however work with single-celled model organisms cannot distinguish the mechanisms underlying primary cilium formation from those that organise a multiciliated epithelium. This highlights the value of combining data from several methodologies in building a more complete view of the ciliome.

8.2 From components to function in morphogenesis and disease

The paucity of information on the protein constituents of cilia and basal bodies has in the past hampered research. Following the identification of flagellar proteins, the next major challenge is to determine their function within the flagellum. With the

resources now available, including databases of flagellar proteins, much research is now being generated in this area. In terms of human disease, it will be essential to understand why loss of ciliary function leads to disease – and why it should produce such a range of symptoms affecting different tissues. Primary ciliary dyskinesia, caused by single gene mutations, affects the motility of cilia in various locations: the ciliated trachea of the airways, the nodal cilia in the embryo and male fertility. While these symptoms may be readily ascribed to the loss of ciliary motility, in the case of Bardet-Biedl Syndrome (BBS), in which symptoms in addition to retinitis pigmentosa and renal anomalies include obesity and polydactyly, the way in which cilia affect such systems is a question that remains to be answered.

Improved imaging techniques, such as confocal microscopy, have contributed to determining precise localisations for proteins and structures of the flagellum. The increased resolution of electron tomography has provided a level of detail in the structures of the flagellum not previously available. In my research I was able to use a system of GFP-tagging and RNAi in the same cell line, which provided a very interesting method of studying the loss of protein from the axoneme following RNAi induction, and furthermore gave rise to the observation that axoneme growth in *T. brucei* continues after cytokinesis.

Cilia and flagella also have functions in morphogenesis at both the cell and at the tissue level. Loss of motility in the nodal cilia in the embryo affects asymmetry leading to situs inversus. Furthermore, ciliary proteins are required to set up the polarity of epithelia. In trypanosomes the flagellum is an important determinant for correct cell morphogenesis: if the flagellum is not made, as in IFT mutants, or is

detached, as in FAZ mutants, there are consequences on cytokinesis. In the absence of an attached flagellum cells lose their elongated shape and polarity, and become round and are unable to undergo correct cytokinesis. In my research I found that missing outer doublets in the PACRG mutant were associated with effects on kinetoplast positioning and cytokinesis, demonstrating the importance of an intact flagellum structure to cytokinesis. In procyclic form *T. brucei*, motility defects where the structure of the flagellum is intact do not commonly lead to cytokinesis defects, seen in the TAX-1 and TbAAT-1 RNAi mutants. Interestingly, in bloodstream form trypanosomes there appears to be a requirement for flagellar motility for cytokinesis both in vitro (Broadhead et al., 2006) and in vivo (Griffiths et al., 2007). Defects in flagellar motility occurring prior to cytokinesis defects have been measured in my work using the TAX-1 RNAi mutant, and published for the PFR2 mutant (Griffiths et al., 2007). While the reasons for the requirement for motility are unclear, there are several known differences in the biology of the two forms that may be contributing factors or provide clues to the mechanisms responsible. The mechanism of cell division is different between the two forms; during cell division, segregation of the organelles occurs differently, with the kinetoplasts remaining closer together in bloodstream form trypanosomes until the cleavage furrow divides them. The absence of a defined flagella connector, which in procyclic forms is important for kinetoplast segregation, in bloodstream form trypanosomes may place additional pressure on the requirement for an intact and functioning flagellum. The discovery that motility is required for cytokinesis in bloodstream form *T. brucei*, and subsequent validation in vivo, raises the profile of flagellar proteins as possible drug targets.

In this thesis I have described the functional characterisation of five proteins, identified from proteomic or genomic sources. Two of these, the PACRG homologues in *T. brucei*, required simultaneous ablation in procyclic form trypanosomes in order to produce a phenotype of flagellar paralysis. This was caused by missing outer doublet microtubules from the structure of the axoneme, suggesting a role for PACRG in maintaining the outer doublets of the axoneme. Ablation of a second protein, TAX-2, was also associated with loss of outer doublets and other structural defects and is also indicated in a role in the stability of the outer doublets. TAX-1, recently identified as a component of a subset of inner dynein arms, is required for normal motility however, in this case no structural differences were detected. Nor were structural differences detected in the axonemes of TbAAT-1 RNAi induced flagella.

The title of my thesis 'The eukaryotic flagellum in health and disease', originally referred to the role played by cilia and flagella in human disease, with the aim of examining the function of possible ciliary disease genes, such as PACRG. While I started by using *T. brucei* as a model organism in which to study these genes, the discovery that there is a requirement for flagellar motility in this pathogen raises many new possibilities. The challenge for the future will be to consolidate the advances of the last few years, by establishing what the protein networks are that regulate motility and assembly in eukaryotic flagella.

CHAPTER 9

REFERENCES

References

Absalon, S., Kohl, L., Branche, C., Blisnick, T., Toutirais, G., Rusconi, F., Cosson, J., Bonhivers, M., Robinson, D. and Bastin, P. (2007). Basal Body Positioning Is Controlled by Flagellum Formation in *Trypanosoma brucei*. *PLoS ONE* **2**, e437.

Abughrien, B. M. and Dore, M. A. (2000). Ciliogenesis in the uterine tube of control and superovulated heifers. *Cells Tissues Organs* **166**, 338-48.

Afzelius, B. A. (2004). Cilia-related diseases. *J Pathol* **204**, 470-7.

Alieva, I. B. and Vorobjev, I. A. (2004). Vertebrate primary cilia: a sensory part of centrosomal complex in tissue cells, but a "sleeping beauty" in cultured cells? *Cell Biol Int* **28**, 139-50.

Andersen, J. S., Wilkinson, C. J., Mayor, T., Mortensen, P., Nigg, E. A. and Mann, M. (2003). Proteomic characterization of the human centrosome by protein correlation profiling. *Nature* **426**, 570-4.

Anderson, R. G. and Brenner, R. M. (1971). The formation of basal bodies (centrioles) in the Rhesus monkey oviduct. *J Cell Biol* **50**, 10-34.

Andre, J. and Bernhard, W. (1964). The centriole and the centriolar region. *Excerpta Med Int Cong Ser* **77**, 9.

Ansley, S. J., Badano, J. L., Blacque, O. E., Hill, J., Hoskins, B. E., Leitch, C. C., Kim, J. C., Ross, A. J., Eichers, E. R., Teslovich, T. M., Mah, A. K., Johnsen, R. C., Cavender, J. C., Lewis, R. A., Leroux, M. R., Beales, P. L. and Katsanis, N. (2003). Basal body dysfunction is a likely cause of pleiotropic Bardet-Biedl syndrome. *Nature* **425**, 628-33.

Argos, P. and Mathews, F. S. (1975). The structure of ferrocytochrome b5 at 2.8 A resolution. *J Biol Chem* **250**, 747-51.

Avidor-Reiss, T., Maer, A. M., Koundakjian, E., Polyanovsky, A., Keil, T., Subramaniam, S. and Zuker, C. S. (2004). Decoding cilia function: defining specialized genes required for compartmentalized cilia biogenesis. *Cell* **117**, 527-39.

Badano, J. L., Mitsuma, N., Beales, P. L. and Katsanis, N. (2006). The Ciliopathies: An Emerging Class of Human Genetic Disorders. *Annu Rev Genomics Hum Genet.*

Badano, J. L., Teslovich, T. M. and Katsanis, N. (2005). The centrosome in human genetic disease. *Nat Rev Genet* **6**, 194-205.

Balczon, R., Bao, L., Zimmer, W. E., Brown, K., Zinkowski, R. P. and Brinkley, B. R. (1995). Dissociation of centrosome replication events from cycles of DNA

synthesis and mitotic division in hydroxyurea-arrested Chinese hamster ovary cells. *J Cell Biol* **130**, 105-15.

Baron, D. M., Ralston, K. S., Kabututu, Z. P. and Hill, K. L. (2007). Functional genomics in *Trypanosoma brucei* identifies evolutionarily conserved components of motile flagella. *J Cell Sci* **120**, 478-91.

Bastin, P., MacRae, T. H., Francis, S. B., Matthews, K. R. and Gull, K. (1999). Flagellar morphogenesis: protein targeting and assembly in the paraflagellar rod of trypanosomes. *Mol Cell Biol* **19**, 8191-200.

Bastin, P., Sherwin, T. and Gull, K. (1998). Paraflagellar rod is vital for trypanosome motility. *Nature* **391**, 548.

Beisson, J. and Wright, M. (2003). Basal body/centriole assembly and continuity. *Curr Opin Cell Biol* **15**, 96-104.

Bendtsen, J. D., Nielsen, H., von Heijne, G. and Brunak, S. (2004). Improved prediction of signal peptides: SignalP 3.0. *J Mol Biol* **340**, 783-95.

Berdnik, D. and Knoblich, J. A. (2002). Drosophila Aurora-A is required for centrosome maturation and actin-dependent asymmetric protein localization during mitosis. *Curr Biol* **12**, 640-7.

Blacque, O. E., Perens, E. A., Boroevich, K. A., Inglis, P. N., Li, C., Warner, A., Khattra, J., Holt, R. A., Ou, G., Mah, A. K., McKay, S. J., Huang, P., Swoboda, P., Jones, S. J., Marra, M. A., Baillie, D. L., Moerman, D. G., Shaham, S. and Leroux, M. R. (2005). Functional genomics of the cilium, a sensory organelle. *Curr Biol* **15**, 935-41.

Blacque, O. E., Reardon, M. J., Li, C., McCarthy, J., Mahjoub, M. R., Ansley, S. J., Badano, J. L., Mah, A. K., Beales, P. L., Davidson, W. S., Johnsen, R. C., Audeh, M., Plasterk, R. H., Baillie, D. L., Katsanis, N., Quarmby, L. M., Wicks, S. R. and Leroux, M. R. (2004). Loss of *C. elegans* BBS-7 and BBS-8 protein function results in cilia defects and compromised intraflagellar transport. *Genes Dev* **18**, 1630-42.

Bloch, M. A. and Johnson, K. A. (1995). Identification of a molecular chaperone in the eukaryotic flagellum and its localization to the site of microtubule assembly. *J Cell Sci* **108 (Pt 11)**, 3541-5.

Boisvieux-Ulrich, E., Laine, M. C. and Sandoz, D. (1987). In vitro effects of benzodiazepines on ciliogenesis in the quail oviduct. *Cell Motil Cytoskeleton* **8**, 333-44.

Boisvieux-Ulrich, E., Laine, M. C. and Sandoz, D. (1989). In vitro effects of colchicine and nocodazole on ciliogenesis in quail oviduct. *Biol Cell* **67**, 67-79.

Boisvieux-Ulrich, E., Laine, M. C. and Sandoz, D. (1990). Cytochalasin D inhibits basal body migration and ciliary elongation in quail oviduct epithelium. *Cell Tissue Res* **259**, 443-54.

Bowne, S. J., Sullivan, L. S., Blanton, S. H., Cepko, C. L., Blackshaw, S., Birch, D. G., Hughbanks-Wheaton, D., Heckenlively, J. R. and Daiger, S. P. (2002). Mutations in the inosine monophosphate dehydrogenase 1 gene (IMPDH1) cause the RP10 form of autosomal dominant retinitis pigmentosa. *Hum Mol Genet* **11**, 559-68.

Branche, C., Kohl, L., Toutirais, G., Buisson, J., Cosson, J. and Bastin, P. (2006). Conserved and specific functions of axoneme components in trypanosome motility. *J Cell Sci* **119**, 3443-55.

Briggs, L. J., Davidge, J. A., Wickstead, B., Ginger, M. L. and Gull, K. (2004a). More than one way to build a flagellum: comparative genomics of parasitic protozoa. *Curr Biol* **14**, R611-2.

Briggs, L. J., McKean, P. G., Baines, A., Moreira-Leite, F., Davidge, J., Vaughan, S. and Gull, K. (2004b). The flagella connector of *Trypanosoma brucei*: an unusual mobile transmembrane junction. *J Cell Sci* **117**, 1641-51.

Broadhead, R., Dawe, H. R., Farr, H., Griffiths, S., Hart, S. R., Portman, N., Shaw, M. K., Ginger, M. L., Gaskell, S. J., McKean, P. G. and Gull, K. (2006). Flagellar motility is required for the viability of the bloodstream trypanosome. *Nature* **440**, 224-7.

Brody, S. L., Yan, X. H., Wuerffel, M. K., Song, S. K. and Shapiro, S. D. (2000). Ciliogenesis and left-right axis defects in forkhead factor HFH-4-null mice. *Am J Respir Cell Mol Biol* **23**, 45-51.

Brun, R. and Jenni, L. (1977). A new semi-defined medium for *Trypanosoma brucei* sspp. *Acta Trop* **34**, 21-33.

Burakov, A., Nadezhdina, E., Slepchenko, B. and Rodionov, V. (2003). Centrosome positioning in interphase cells. *J Cell Biol* **162**, 963-9.

Burgess, S. A. and Knight, P. J. (2004). Is the dynein motor a winch? *Curr Opin Struct Biol* **14**, 138-46.

Chang, J. P., Mayahara, H., Yoloyama, M., Ubukata, A. and Moller, P. C. (1979). An ultrastructural study of morphogenesis of fibrogranular complex and centriole in ductuli efferentes of Chinese hamster. *Tissue Cell* **11**, 401-12.

Chang, P., Giddings, T. H., Jr., Winey, M. and Stearns, T. (2003). Epsilon-tubulin is required for centriole duplication and microtubule organization. *Nat Cell Biol* **5**, 71-6.

Chen, H. I. and Sudol, M. (1995). The WW domain of Yes-associated protein binds a proline-rich ligand that differs from the consensus established for Src homology 3-binding modules. *Proc Natl Acad Sci U S A* **92**, 7819-23.

Chevrier, V., Piel, M., Collomb, N., Saoudi, Y., Frank, R., Paintrand, M., Narumiya, S., Bornens, M. and Job, D. (2002). The Rho-associated protein kinase p160ROCK is required for centrosome positioning. *J Cell Biol* **157**, 807-17.

Clayton, C. E. (2002). Life without transcriptional control? From fly to man and back again. *Embo J* **21**, 1881-8.

Cole, D. G. (2003). The intraflagellar transport machinery of *Chlamydomonas reinhardtii*. *Traffic* **4**, 435-42.

Cole, D. G., Diener, D. R., Himelblau, A. L., Beech, P. L., Fuster, J. C. and Rosenbaum, J. L. (1998). *Chlamydomonas* kinesin-II-dependent intraflagellar transport (IFT): IFT particles contain proteins required for ciliary assembly in *Caenorhabditis elegans* sensory neurons. *J Cell Biol* **141**, 993-1008.

Cyrne, L., Guerreiro, P., Cardoso, A. C., Rodrigues-Pousada, C. and Soares, H. (1996). The Tetrahymena chaperonin subunit CCT eta gene is coexpressed with CCT gamma gene during cilia biogenesis and cell sexual reproduction. *FEBS Lett* **383**, 277-83.

D'Assoro, A. B., Busby, R., Suino, K., Delva, E., Almodovar-Mercado, G. J., Johnson, H., Folk, C., Farrugia, D. J., Vasile, V., Stivala, F. and Salisbury, J. L. (2004). Genotoxic stress leads to centrosome amplification in breast cancer cell lines that have an inactive G1/S cell cycle checkpoint. *Oncogene* **23**, 4068-75.

Davenport, J. R. and Yoder, B. K. (2005). An incredible decade for the primary cilium: a look at a once-forgotten organelle. *Am J Physiol Renal Physiol* **289**, F1159-69.

Davidge, J. A., Chambers, E., Dickinson, H. A., Towers, K., Ginger, M. L., McKean, P. G. and Gull, K. (2006). Trypanosome IFT mutants provide insight into the motor location for mobility of the flagella connector and flagellar membrane formation. *J Cell Sci.*

Dawe, H. R., Farr, H., Portman, N., Shaw, M. K. and Gull, K. (2005). The Parkin co-regulated gene product, PACRG, is an evolutionarily conserved axonemal protein that functions in outer-doublet microtubule morphogenesis. *J Cell Sci* **118**, 5421-30.

Dawe, H. R., Shaw, M. K., Farr, H. and Gull, K. (2007). The hydrocephalus inducing gene product, Hydin, positions axonemal central pair microtubules. *BMC Biol* **5**, 33.

Dentler, W. L. (1980). Structures linking the tips of ciliary and flagellar microtubules to the membrane. *J Cell Sci* **42**, 207-20.

Dirksen, E. R. (1971). Centriole morphogenesis in developing ciliated epithelium of the mouse oviduct. *J Cell Biol* **51**, 286-302.

Dirksen, E. R. (1991). Centriole and basal body formation during ciliogenesis revisited. *Biol Cell* **72**, 31-8.

Dirksen, E. R. and Crocker, T. T. (1966). Centriole replication in differentiating ciliated cells of mammalian respiratory epithelium. An electron microscope study. *J Micr* **5**, 639-644.

Durand-Dubief, M. and Bastin, P. (2003). TbAGO1, an argonaute protein required for RNA interference, is involved in mitosis and chromosome segregation in *Trypanosoma brucei*. *BMC Biol* **1**, 2.

Dutcher, S. K. (1995). Flagellar assembly in two hundred and fifty easy-to-follow steps. *Trends Genet* **11**, 398-404.

Efimenko, E., Bubb, K., Mak, H. Y., Holzman, T., Leroux, M. R., Ruvkun, G., Thomas, J. H. and Swoboda, P. (2005). Analysis of xbx genes in *C. elegans*. *Development* **132**, 1923-34.

Evans, J. E., Snow, J. J., Gunnarson, A. L., Ou, G., Stahlberg, H., McDonald, K. L. and Scholey, J. M. (2006). Functional modulation of IFT kinesins extends the sensory repertoire of ciliated neurons in *Caenorhabditis elegans*. *J Cell Biol* **172**, 663-9.

Ferrante, M. I., Giorgio, G., Feather, S. A., Bulfone, A., Wright, V., Ghiani, M., Selicorni, A., Gammaro, L., Scolari, F., Woolf, A. S., Sylvie, O., Bernard, L., Malcolm, S., Winter, R., Ballabio, A. and Franco, B. (2001). Identification of the gene for oral-facial-digital type I syndrome. *Am J Hum Genet* **68**, 569-76.

Fire, A., Xu, S., Montgomery, M. K., Kostas, S. A., Driver, S. E. and Mello, C. C. (1998). Potent and specific genetic interference by double-stranded RNA in *Caenorhabditis elegans*. *Nature* **391**, 806-11.

Flock, A. and Duvall, A. J., 3rd. (1965). The Ultrastructure Of The Kinocilium Of The Sensory Cells In The Inner Ear And Lateral Line Organs. *J Cell Biol* **25**, 1-8.

Frisch, D. and Farbman, A. I. (1968). Development of order during ciliogenesis. *Anat Rec* **162**, 221-32.

Furusawa, M., Ohnishi, T., Taira, T., Iguchi-Ariga, S. M. and Ariga, H. (2001). AMY-1, a c-Myc-binding protein, is localized in the mitochondria of sperm by association with S-AKAP84, an anchor protein of cAMP-dependent protein kinase. *J Biol Chem* **276**, 36647-51.

Gadelha, C., LeBowitz, J. H., Manning, J., Seebeck, T. and Gull, K. (2004). Relationships between the major kinetoplastid paraflagellar rod proteins: a consolidating nomenclature. *Mol Biochem Parasitol* **136**, 113-5.

Gadelha, C., Wickstead, B., de Souza, W., Gull, K. and Cunha-e-Silva, N. (2005). Cryptic paraflagellar rod in endosymbiont-containing kinetoplastid protozoa. *Eukaryot Cell* **4**, 516-25.

Gadelha, C., Wickstead, B. and Gull, K. (2007). Flagellar and ciliary beating in trypanosome motility. *Cell Motil Cytoskeleton* **64**, 629-43.

Gadelha, C., Wickstead, B., McKean, P. G. and Gull, K. (2006). Basal body and flagellum mutants reveal a rotational constraint of the central pair microtubules in the axonemes of trypanosomes. *J Cell Sci* **119**, 2405-13.

Gall, J. G. (1961). Centriole replication. A study of spermatogenesis in the snail *Viviparus*. *J Biophys Biochem Cytol* **10**, 163-93.

Gattone, V. H., 2nd, Tourkow, B. A., Trambaugh, C. M., Yu, A. C., Whelan, S., Phillips, C. L., Harris, P. C. and Peterson, R. G. (2004). Development of multiorgan pathology in the wpk rat model of polycystic kidney disease. *Anat Rec A Discov Mol Cell Evol Biol* **277**, 384-95.

Gerdes, D., Wehling, M., Leube, B. and Falkenstein, E. (1998). Cloning and tissue expression of two putative steroid membrane receptors. *Biol Chem* **379**, 907-11.

Gherman, A., Davis, E. E. and Katsanis, N. (2006). The ciliary proteome database: an integrated community resource for the genetic and functional dissection of cilia. *Nat Genet* **38**, 961-2.

Gibbons, B. H. and Gibbons, I. R. (1973). The effect of partial extraction of dynein arms on the movement of reactivated sea-urchin sperm. *J Cell Sci* **13**, 337-57.

Gibbons, I. R. (1965). Chemical dissection of cilia. *Arch Biol (Liege)* **76**, 317-52.

Gibbons, I. R., Lee-Eiford, A., Mocz, G., Phillipson, C. A., Tang, W. J. and Gibbons, B. H. (1987). Photosensitized cleavage of dynein heavy chains. Cleavage at the "V1 site" by irradiation at 365 nm in the presence of ATP and vanadate. *J Biol Chem* **262**, 2780-6.

Ginger, M. L., Ngazoa, E. S., Pereira, C. A., Pullen, T. J., Kabiri, M., Becker, K., Gull, K. and Steverding, D. (2005). Intracellular positioning of isoforms explains an unusually large adenylate kinase gene family in the parasite *Trypanosoma brucei*. *J Biol Chem* **280**, 11781-9.

Gomperts, B. N., Gong-Cooper, X. and Hackett, B. P. (2004). Foxj1 regulates basal body anchoring to the cytoskeleton of ciliated pulmonary epithelial cells. *J Cell Sci* **117**, 1329-37.

Greenberg, J., Goliath, R., Beighton, P. and Ramesar, R. (1994). A new locus for autosomal dominant retinitis pigmentosa on the short arm of chromosome 17. *Hum Mol Genet* **3**, 915-8.

Griffiths, S., Portman, N., Taylor, P. R., Gordon, S., Ginger, M. L. and Gull, K. (2007). RNA interference mutant induction in vivo demonstrates the essential nature of trypanosome flagellar function during mammalian infection. *Eukaryot Cell* **6**, 1248-50.

Gromley, A., Jurczyk, A., Sillibourne, J., Halilovic, E., Mogensen, M., Groisman, I., Blomberg, M. and Doxsey, S. (2003). A novel human protein of the maternal centriole is required for the final stages of cytokinesis and entry into S phase. *J Cell Biol* **161**, 535-45.

Gross, C. T. and McGinnis, W. (1996). DEAF-1, a novel protein that binds an essential region in a Deformed response element. *Embo J* **15**, 1961-70.

Hagiwara, H., Harada, S., Maeda, S., Aoki, T., Ohwada, N. and Takata, K. (2002). Ultrastructural and immunohistochemical study of the basal apparatus of solitary cilia in the human oviduct epithelium. *J Anat* **200**, 89-96.

Hagiwara, H., Ohwada, N., Aoki, T. and Takata, K. (2000). Ciliogenesis and ciliary abnormalities. *Med Electron Microsc* **33**, 109-14.

Hagiwara, H., Shibasaki, S. and Ohwada, N. (1992). Ciliogenesis in the human oviduct epithelium during the normal menstrual cycle. *J Electron Microsc (Tokyo)* **41**, 321-9.

Hameed, A., Khaliq, S., Ismail, M., Anwar, K., Ebenezer, N. D., Jordan, T., Mehdi, S. Q., Payne, A. M. and Bhattacharya, S. S. (2000). A novel locus for Leber congenital amaurosis (LCA4) with anterior keratoconus mapping to chromosome 17p13. *Invest Ophthalmol Vis Sci* **41**, 629-33.

Hammarton, T. C. (2007). Cell cycle regulation in *Trypanosoma brucei*. *Mol Biochem Parasitol* **153**, 1-8.

Hammarton, T. C., Clark, J., Douglas, F., Boshart, M. and Mottram, J. C. (2003). Stage-specific differences in cell cycle control in *Trypanosoma brucei* revealed by RNA interference of a mitotic cyclin. *J Biol Chem* **278**, 22877-86.

Hannak, E., Kirkham, M., Hyman, A. A. and Oegema, K. (2001). Aurora-A kinase is required for centrosome maturation in *Caenorhabditis elegans*. *J Cell Biol* **155**, 1109-16.

Hassan, P., Fergusson, D., Grant, K. M. and Mottram, J. C. (2001). The CRK3 protein kinase is essential for cell cycle progression of *Leishmania mexicana*. *Mol Biochem Parasitol* **113**, 189-98.

Henneguy, L. F. (1898). Sur les rapports des cils vibratiles avec les centrosomes. *Archives d'Anatomie Microscopique* **Tome 1**, 481-496.

Hinchcliffe, E. H., Cassels, G. O., Rieder, C. L. and Sluder, G. (1998). The coordination of centrosome reproduction with nuclear events of the cell cycle in the sea urchin zygote. *J Cell Biol* **140**, 1417-26.

Hinchcliffe, E. H., Li, C., Thompson, E. A., Maller, J. L. and Sluder, G. (1999). Requirement of Cdk2-cyclin E activity for repeated centrosome reproduction in Xenopus egg extracts. *Science* **283**, 851-4.

Hinchcliffe, E. H., Miller, F. J., Cham, M., Khodjakov, A. and Sluder, G. (2001). Requirement of a centrosomal activity for cell cycle progression through G1 into S phase. *Science* **291**, 1547-50.

Hinsch, K. D., De Pinto, V., Aires, V. A., Schneider, X., Messina, A. and Hinsch, E. (2004). Voltage-dependent anion-selective channels VDAC2 and VDAC3 are abundant proteins in bovine outer dense fibers, a cytoskeletal component of the sperm flagellum. *J Biol Chem* **279**, 15281-8.

Hirschner, W., Pogoda, H. M., Kramer, C., Thiess, U., Hamprecht, B., Wiesmuller, K. H., Lautner, M. and Verleysdonk, S. (2007). Biosynthesis of Wdr16, a marker protein for kinocilia-bearing cells, starts at the time of kinocilia formation in rat, and wdr16 gene knockdown causes hydrocephalus in zebrafish. *J Neurochem* **101**, 274-88.

Hirumi, H. and Hirumi, K. (1989). Continuous cultivation of *Trypanosoma brucei* blood stream forms in a medium containing a low concentration of serum protein without feeder cell layers. *J Parasitol* **75**, 985-9.

Ikeda, K., Ikeda, T., Morikawa, K. and Kamiya, R. (2007). Axonemal localization of *Chlamydomonas* PACRG, a homologue of the human Parkin-coregulated gene product. *Cell Motil Cytoskeleton.*

Imai, Y., Soda, M., Murakami, T., Shoji, M., Abe, K. and Takahashi, R. (2003). A product of the human gene adjacent to parkin is a component of Lewy bodies and suppresses Pael receptor-induced cell death. *J Biol Chem* **278**, 51901-10.

Inglis, P. N., Boroevich, K. A. and Leroux, M. R. (2006). Piecing together a ciliome. *Trends Genet* **22**, 491-500.

Iomini, C., Li, L., Mo, W., Dutcher, S. K. and Piperno, G. (2006). Two flagellar genes, AGG2 and AGG3, mediate orientation to light in *Chlamydomonas*. *Curr Biol* **16**, 1147-53.

Ishikawa, H., Kubo, A., Tsukita, S. and Tsukita, S. (2005). Odf2-deficient mother centrioles lack distal/subdistal appendages and the ability to generate primary cilia. *Nat Cell Biol* **7**, 517-24.

Jensen, C. G., Poole, C. A., McGlashan, S. R., Marko, M., Issa, Z. I., Vujcich, K. V. and Bowser, S. S. (2004). Ultrastructural, tomographic and confocal imaging of the chondrocyte primary cilium in situ. *Cell Biol Int* **28**, 101-10.

Kalnins, V. I., Chung, C. K. and Turnbull, C. (1972). Procentrioles in ciliating and ciliated cells of chick trachea. *Z Zellforsch Mikrosk Anat* **135**, 461-71.

Kamiya, R. (1988). Mutations at twelve independent loci result in absence of outer dynein arms in *Chylamydomonas reinhardtii*. *J Cell Biol* **107**, 2253-8.

Kamiya, R. (1995). Exploring the function of inner and outer dynein arms with *Chlamydomonas* mutants. *Cell Motil Cytoskeleton* **32**, 98-102.

Kamiya, R., Kurimoto, E. and Muto, E. (1991). Two types of *Chlamydomonas* flagellar mutants missing different components of inner-arm dynein. *J Cell Biol* **112**, 441-7.

Karcher, C., Fischer, A., Schweickert, A., Bitzer, E., Horie, S., Witzgall, R. and Blum, M. (2005). Lack of a laterality phenotype in Pkd1 knock-out embryos correlates with absence of polycystin-1 in nodal cilia. *Differentiation* **73**, 425-32.

Karsenti, E. (1999). Centrioles reveal their secrets. *Nat Cell Biol* **1**, E62-4.

Keller, L. C., Romijn, E. P., Zamora, I., Yates, J. R., 3rd and Marshall, W. F. (2005). Proteomic analysis of isolated *chlamydomonas* centrioles reveals orthologs of ciliary-disease genes. *Curr Biol* **15**, 1090-8.

Kelly, S., Reed, J., Kramer, S., Ellis, L., Webb, H., Sunter, J., Salje, J., Marinsek, N., Gull, K., Wickstead, B. and Carrington, M. (2007). Functional genomics in *Trypanosoma brucei*: A collection of vectors for the expression of tagged proteins from endogenous and ectopic gene loci. *Mol Biochem Parasitol* **154**, 103-9.

Kilburn, C. L., Pearson, C. G., Romijn, E. P., Meehl, J. B., Giddings, T. H., Jr., Culver, B. P., Yates, J. R., 3rd and Winey, M. (2007). New *Tetrahymena* basal body protein components identify basal body domain structure. *J Cell Biol* **178**, 905-12.

Kim, J. C., Badano, J. L., Sibold, S., Esmail, M. A., Hill, J., Hoskins, B. E., Leitch, C. C., Venner, K., Ansley, S. J., Ross, A. J., Leroux, M. R., Katsanis, N. and Beales, P. L. (2004). The Bardet-Biedl protein BBS4 targets cargo to the pericentriolar region and is required for microtubule anchoring and cell cycle progression. *Nat Genet* **36**, 462-70.

King, S. M. (2006). Axonemal protofilament ribbons, DM10 domains, and the link to juvenile myoclonic epilepsy. *Cell Motil Cytoskeleton* **63**, 245-53.

Klotz, C., Bordes, N., Laine, M. C., Sandoz, D. and Bornens, M. (1986). Myosin at the apical pole of ciliated epithelial cells as revealed by a monoclonal antibody. *J Cell Biol* **103**, 613-9.

Koblenz, B. and Lechtreck, K. F. (2005). The NIT1 promoter allows inducible and reversible silencing of centrin in *Chlamydomonas reinhardtii*. *Eukaryot Cell* **4**, 1959-62.

Kochanski, R. S. and Borisy, G. G. (1990). Mode of centriole duplication and distribution. *J Cell Biol* **110**, 1599-605.

Kohl, L. and Gull, K. (1998). Molecular architecture of the trypanosome cytoskeleton. *Mol Biochem Parasitol* **93**, 1-9.

Kohl, L., Sherwin, T. and Gull, K. (1999). Assembly of the paraflagellar rod and the flagellum attachment zone complex during the *Trypanosoma brucei* cell cycle. *J Eukaryot Microbiol* **46**, 105-9.

Kon, T., Nishiura, M., Ohkura, R., Toyoshima, Y. Y. and Sutoh, K. (2004). Distinct functions of nucleotide-binding/hydrolysis sites in the four AAA modules of cytoplasmic dynein. *Biochemistry* **43**, 11266-74.

Koonce, M. P. and Samso, M. (2004). Of rings and levers: the dynein motor comes of age. *Trends Cell Biol* **14**, 612-9.

Kubo, A., Sasaki, H., Yuba-Kubo, A., Tsukita, S. and Shiina, N. (1999). Centriolar satellites: molecular characterization, ATP-dependent movement toward centrioles and possible involvement in ciliogenesis. *J Cell Biol* **147**, 969-80.

Kyttala, M., Tallila, J., Salonen, R., Kopra, O., Kohlschmidt, N., Paavola-Sakki, P., Peltonen, L. and Kestila, M. (2006). MKS1, encoding a component of the flagellar apparatus basal body proteome, is mutated in Meckel syndrome. *Nat Genet* **38**, 155-7.

La Terra, S., English, C. N., Hergert, P., McEwen, B. F., Sluder, G. and Khodjakov, A. (2005). The de novo centriole assembly pathway in HeLa cells: cell cycle progression and centriole assembly/maturation. *J Cell Biol* **168**, 713-22.

Lane, H. A. and Nigg, E. A. (1996). Antibody microinjection reveals an essential role for human polo-like kinase 1 (Plk1) in the functional maturation of mitotic centrosomes. *J Cell Biol* **135**, 1701-13.

Lange, B. M. and Gull, K. (1995). A molecular marker for centriole maturation in the mammalian cell cycle. *J Cell Biol* **130**, 919-27.

Lange, B. M. and Gull, K. (1996). Structure and function of the centriole in animal cells: progress and questions. *Trends Cell Biol* **6**, 348-52.

Laoukili, J., Perret, E., Middendorp, S., Houcine, O., Guennou, C., Marano, F., Bornens, M. and Tournier, F. (2000). Differential expression and cellular distribution of centrin isoforms during human ciliated cell differentiation in vitro. *J Cell Sci* **113 (Pt 8)**, 1355-64.

Laurencon, A. C., Dubruille, R., Efimenko, E., Grenier, G., Bissett, R. E., Cortier, E., Rolland, V., Swoboda, P. and Durand, B. (2007). Identification of novel Regulatory Factor X (RFX) target genes by comparative genomics in *Drosophila* species. *Genome Biol* **8**, R195.

Lechtreck, K. F. and Witman, G. B. (2007). *Chlamydomonas reinhardtii* hydin is a central pair protein required for flagellar motility. *J Cell Biol* **176**, 473-82.

Lemullois, M., Boisvieux-Ulrich, E., Laine, M. C., Chailley, B. and Sandoz, D. (1988). Development and functions of the cytoskeleton during ciliogenesis in metazoa. *Biol Cell* **63**, 195-208.

Lemullois, M., Klotz, C. and Sandoz, D. (1987). Immunocytochemical localization of myosin during ciliogenesis of quail oviduct. *Eur J Cell Biol* **43**, 429-37.

Lenhossek, M. (1898). Ueber Flimmerzellen. *Verhandl. der Anat. Gesel* **12**, 106-128.

Li, J. B., Gerdes, J. M., Haycraft, C. J., Fan, Y., Teslovich, T. M., May-Simera, H., Li, H., Blacque, O. E., Li, L., Leitch, C. C., Lewis, R. A., Green, J. S., Parfrey, P. S., Leroux, M. R., Davidson, W. S., Beales, P. L., Guay-Woodford, L. M., Yoder, B. K., Stormo, G. D., Katsanis, N. and Dutcher, S. K. (2004). Comparative genomics identifies a flagellar and basal body proteome that includes the BBS5 human disease gene. *Cell* **117**, 541-52.

Lindemann, C. B. (1994). A model of flagellar and ciliary functioning which uses the forces transverse to the axoneme as the regulator of dynein activation. *Cell Motil Cytoskeleton* **29**, 141-54.

Lindemann, C. B. and Kanous, K. S. (1997). A model for flagellar motility. *Int Rev Cytol* **173**, 1-72.

Lockhart, P. J., O'Farrell, C. A. and Farrer, M. J. (2004). It's a double knock-out! The quaking mouse is a spontaneous deletion of parkin and parkin co-regulated gene (PACRG). *Mov Disord* **19**, 101-4.

Lorenzetti, D., Bishop, C. E. and Justice, M. J. (2004). Deletion of the Parkin coregulated gene causes male sterility in the quaking(viable) mouse mutant. *Proc Natl Acad Sci U S A* **101**, 8402-7.

Luck, D. J. (1984). Genetic and biochemical dissection of the eucaryotic flagellum. *J Cell Biol* **98**, 789-94.

Lucker, B. F., Behal, R. H., Qin, H., Siron, L. C., Taggart, W. D., Rosenbaum, J. L. and Cole, D. G. (2005). Characterization of the intraflagellar transport complex B core: direct interaction of the IFT81 and IFT74/72 subunits. *J Biol Chem* **280**, 27688-96.

Macias, M. J., Wiesner, S. and Sudol, M. (2002). WW and SH3 domains, two different scaffolds to recognize proline-rich ligands. *FEBS Lett* **513**, 30-7.

Matsuda, E., Ishizaki, R., Taira, T., Iguchi-Ariga, S. M. and Ariga, H. (2005). Structure and characterization of AAT-1 isoforms. *Biol Pharm Bull* **28**, 898-901.

McKean, P. G. (2003). Coordination of cell cycle and cytokinesis in *Trypanosoma brucei*. *Curr Opin Microbiol* **6**, 600-7.

McKean, P. G., Baines, A., Vaughan, S. and Gull, K. (2003). Gamma-tubulin functions in the nucleation of a discrete subset of microtubules in the eukaryotic flagellum. *Curr Biol* **13**, 598-602.

Meraldi, P., Lukas, J., Fry, A. M., Bartek, J. and Nigg, E. A. (1999). Centrosome duplication in mammalian somatic cells requires E2F and Cdk2-cyclin A. *Nat Cell Biol* **1**, 88-93.

Minoura, I., Yagi, T. and Kamiya, R. (1999). Direct measurement of inter-doublet elasticity in flagellar axonemes. *Cell Struct Funct* **24**, 27-33.

Mitchell, D. R. (2003). Orientation of the central pair complex during flagellar bend formation in *Chlamydomonas*. *Cell Motil Cytoskeleton* **56**, 120-9.

Mitchell, D. R. and Rosenbaum, J. L. (1985). A motile *Chlamydomonas* flagellar mutant that lacks outer dynein arms. *J Cell Biol* **100**, 1228-34.

Mizukami, I. and Gall, J. (1966). Centriole replication. II. Sperm formation in the fern, Marsilea, and the cycad, Zamia. *J Cell Biol* **29**, 97-111.

Mogensen, M. M., Malik, A., Piel, M., Bouckson-Castaing, V. and Bornens, M. (2000). Microtubule minus-end anchorage at centrosomal and non-centrosomal sites: the role of ninein. *J Cell Sci* **113 (Pt 17)**, 3013-23.

Moreira-Leite, F. F., Sherwin, T., Kohl, L. and Gull, K. (2001). A trypanosome structure involved in transmitting cytoplasmic information during cell division. *Science* **294**, 610-2.

Morgan, G. W., Denny, P. W., Vaughan, S., Goulding, D., Jeffries, T. R., Smith, D. F., Gull, K. and Field, M. C. (2005). An evolutionarily conserved coiled-coil protein implicated in polycystic kidney disease is involved in basal body duplication and flagellar biogenesis in *Trypanosoma brucei*. *Mol Cell Biol* **25**, 3774-83.

Motyka, S. A. and Englund, P. T. (2004). RNA interference for analysis of gene function in trypanosomatids. *Curr Opin Microbiol* **7**, 362-8.

Moyer, J. H., Lee-Tischler, M. J., Kwon, H. Y., Schrick, J. J., Avner, E. D., Sweeney, W. E., Godfrey, V. L., Cacheiro, N. L., Wilkinson, J. E. and Woychik, R. P. (1994). Candidate gene associated with a mutation causing recessive polycystic kidney disease in mice. *Science* **264**, 1329-33.

Mukhopadhyay, S., Lu, Y., Qin, H., Lanjuin, A., Shaham, S. and Sengupta, P. (2007). Distinct IFT mechanisms contribute to the generation of ciliary structural diversity in *C. elegans*. *Embo J* **26**, 2966-80.

Myles, D. G. (1975). An ultrastructural study of the spermatozoid of the fern, *Marsilea vestita*. *J Cell Sci* **17**, 633-45.

Nauta, J., Goedbloed, M. A., Herck, H. V., Hesselink, D. A., Visser, P., Willemsen, R., Dokkum, R. P., Wright, C. J. and Guay-Woodford, L. M. (2000).

New rat model that phenotypically resembles autosomal recessive polycystic kidney disease. *J Am Soc Nephrol* **11**, 2272-84.

Ngo, H., Tschudi, C., Gull, K. and Ullu, E. (1998). Double-stranded RNA induces mRNA degradation in *Trypanosoma brucei*. *Proc Natl Acad Sci U S A* **95**, 14687-92.

Nicastro, D., Schwartz, C., Pierson, J., Gaudette, R., Porter, M. E. and McIntosh, J. R. (2006). The molecular architecture of axonemes revealed by cryoelectron tomography. *Science* **313**, 944-8.

Olson, G. E. and Linck, R. W. (1977). Observations of the structural components of flagellar axonemes and central pair microtubules from rat sperm. *J Ultrastruct Res* **61**, 21-43.

Omoto, C. K. and Kung, C. (1979). The pair of central tubules rotates during ciliary beat in Paramecium. *Nature* **279**, 532-4.

Omoto, C. K. and Kung, C. (1980). Rotation and twist of the central-pair microtubules in the cilia of *Paramecium*. *J Cell Biol* **87**, 33-46.

Ostrowski, L. E., Blackburn, K., Radde, K. M., Moyer, M. B., Schlatzer, D. M., Moseley, A. and Boucher, R. C. (2002). A proteomic analysis of human cilia: identification of novel components. *Mol Cell Proteomics* **1**, 451-65.

Ou, G., Blacque, O. E., Snow, J. J., Leroux, M. R. and Scholey, J. M. (2005). Functional coordination of intraflagellar transport motors. *Nature* **436**, 583-7.

Ou, Y. Y., Mack, G. J., Zhang, M. and Rattner, J. B. (2002). CEP110 and ninein are located in a specific domain of the centrosome associated with centrosome maturation. *J Cell Sci* **115**, 1825-35.

Paintrand, M., Moudjou, M., Delacroix, H. and Bornens, M. (1992). Centrosome organization and centriole architecture: their sensitivity to divalent cations. *J Struct Biol* **108**, 107-28.

Parsons, M., Worthey, E. A., Ward, P. N. and Mottram, J. C. (2005). Comparative analysis of the kinomes of three pathogenic trypanosomatids: *Leishmania major*, *Trypanosoma brucei* and *Trypanosoma cruzi*. *BMC Genomics* **6**, 127.

Pazour, G. J., Agrin, N., Leszyk, J. and Witman, G. B. (2005). Proteomic analysis of a eukaryotic cilium. *J Cell Biol* **170**, 103-13.

Pazour, G. J., Agrin, N., Walker, B. L. and Witman, G. B. (2006). Identification of predicted human outer dynein arm genes: candidates for primary ciliary dyskinesia genes. *J Med Genet* **43**, 62-73.

Pazour, G. J., Dickert, B. L., Vucica, Y., Seeley, E. S., Rosenbaum, J. L., Witman, G. B. and Cole, D. G. (2000). *Chlamydomonas* IFT88 and its mouse homologue, polycystic kidney disease gene tg737, are required for assembly of cilia and flagella. *J Cell Biol* **151**, 709-18.

Pedersen, L. B., Geimer, S. and Rosenbaum, J. L. (2006). Dissecting the molecular mechanisms of intraflagellar transport in *chlamydomonas*. *Curr Biol* **16**, 450-9.

Perrault, I., Rozet, J. M., Calvas, P., Gerber, S., Camuzat, A., Dollfus, H., Chatelin, S., Souied, E., Ghazi, I., Leowski, C., Bonnemaison, M., Le Paslier, D., Frezal, J., Dufier, J. L., Pittler, S., Munnich, A. and Kaplan, J. (1996). Retinal-specific guanylate cyclase gene mutations in Leber's congenital amaurosis. *Nat Genet* **14**, 461-4.

Piperno, G. and Mead, K. (1997). Transport of a novel complex in the cytoplasmic matrix of *Chlamydomonas* flagella. *Proc Natl Acad Sci U S A* **94**, 4457-62.

Qin, H., Wang, Z., Diener, D. and Rosenbaum, J. (2007). Intraflagellar transport protein 27 is a small G protein involved in cell-cycle control. *Curr Biol* **17**, 193-202.

Ralston, K. S. and Hill, K. L. (2006). Trypanin, a component of the flagellar Dynein regulatory complex, is essential in bloodstream form African trypanosomes. *PLoS Pathog* **2**, e101.

Renaud, F. L. and Swift, H. (1964). The Development Of Basal Bodies And Flagella In *Allomyces Arbusculus*. *J Cell Biol* **23**, 339-54.

Robinson, D. R., Sherwin, T., Ploubidou, A., Byard, E. H. and Gull, K. (1995). Microtubule polarity and dynamics in the control of organelle positioning, segregation, and cytokinesis in the trypanosome cell cycle. *J Cell Biol* **128**, 1163-72.

Romio, L., Fry, A. M., Winyard, P. J., Malcolm, S., Woolf, A. S. and Feather, S. A. (2004). OFD1 is a centrosomal/basal body protein expressed during mesenchymal-epithelial transition in human nephrogenesis. *J Am Soc Nephrol* **15**, 2556-68.

Rosenbaum, J. L. and Witman, G. B. (2002). Intraflagellar transport. *Nat Rev Mol Cell Biol* **3**, 813-25.

Sakakibara, H., Mitchell, D. R. and Kamiya, R. (1991). A *Chlamydomonas* outer arm dynein mutant missing the alpha heavy chain. *J Cell Biol* **113**, 615-22.

Sale, W. S. (1986). The axonemal axis and Ca2+-induced asymmetry of active microtubule sliding in sea urchin sperm tails. *J Cell Biol* **102**, 2042-52.

Sampson, M. J., Decker, W. K., Beaudet, A. L., Ruitenbeek, W., Armstrong, D., Hicks, M. J. and Craigen, W. J. (2001). Immotile sperm and infertility in mice lacking mitochondrial voltage-dependent anion channel type 3. *J Biol Chem* **276**, 39206-12.

Satouh, Y., Padma, P., Toda, T., Satoh, N., Ide, H. and Inaba, K. (2005). Molecular characterization of radial spoke subcomplex containing radial spoke

protein 3 and heat shock protein 40 in sperm flagella of the ascidian *Ciona intestinalis*. *Mol Biol Cell* **16**, 626-36.

Schenkman, J. B. and Jansson, I. (2003). The many roles of cytochrome b5. *Pharmacol Ther* **97**, 139-52.

Scholey, J. M. (2003). Intraflagellar transport. *Annu Rev Cell Dev Biol* **19**, 423-43.

Scholey, J. M. and Anderson, K. V. (2006). Intraflagellar transport and cilium-based signaling. *Cell* **125**, 439-42.

Sherwin, T. and Gull, K. (1989). The cell division cycle of *Trypanosoma brucei* brucei: timing of event markers and cytoskeletal modulations. *Philos Trans R Soc Lond B Biol Sci* **323**, 573-88.

Shi, H., Djikeng, A., Tschudi, C. and Ullu, E. (2004). Argonaute protein in the early divergent eukaryote *Trypanosoma brucei*: control of small interfering RNA accumulation and retroposon transcript abundance. *Mol Cell Biol* **24**, 420-7.

Shi, H., Tschudi, C. and Ullu, E. (2006). An unusual Dicer-like1 protein fuels the RNA interference pathway in *Trypanosoma brucei*. *Rna* **12**, 2063-72.

Sidman, R. L., Dickie, M. M. and Appel, S. H. (1964). Mutant Mice (Quaking And Jimpy) With Deficient Myelination In The Central Nervous System. *Science* **144**, 309-11.

Silflow, C. D. and Lefebvre, P. A. (2001). Assembly and motility of eukaryotic cilia and flagella. Lessons from *Chlamydomonas reinhardtii*. *Plant Physiol* **127**, 1500-7.

Silva, F. P., Hamamoto, R., Nakamura, Y. and Furukawa, Y. (2005). WDRPUH, a novel WD-repeat-containing protein, is highly expressed in human hepatocellular carcinoma and involved in cell proliferation. *Neoplasia* **7**, 348-55.

Sluder, G. and Hinchcliffe, E. H. (1998). The apparent linkage between centriole replication and the S phase of the cell cycle. *Cell Biol Int* **22**, 3-5.

Smith, E. F. and Lefebvre, P. A. (1997). The role of central apparatus components in flagellar motility and microtubule assembly. *Cell Motil Cytoskeleton* **38**, 1-8.

Smith, J. C., Northey, J. G., Garg, J., Pearlman, R. E. and Siu, K. W. (2005). Robust method for proteome analysis by MS/MS using an entire translated genome: demonstration on the ciliome of *Tetrahymena thermophila*. *J Proteome Res* **4**, 909-19.

Smith, U. M., Consugar, M., Tee, L. J., McKee, B. M., Maina, E. N., Whelan, S., Morgan, N. V., Goranson, E., Gissen, P., Lilliquist, S., Aligianis, I. A., Ward, C. J., Pasha, S., Punyashthiti, R., Malik Sharif, S., Batman, P. A., Bennett, C. P., Woods, C. G., McKeown, C., Bucourt, M., Miller, C. A., Cox, P., Algazali, L., Trembath, R. C., Torres, V. E., Attie-Bitach, T., Kelly, D. A., Maher, E. R., Gattone, V. H., 2nd, Harris, P. C. and Johnson, C. A. (2006). The transmembrane

protein meckelin (MKS3) is mutated in Meckel-Gruber syndrome and the wpk rat. *Nat Genet* **38**, 191-6.

Soares, H., Penque, D., Mouta, C. and Rodrigues-Pousada, C. (1994). A *Tetrahymena* orthologue of the mouse chaperonin subunit CCT gamma and its coexpression with tubulin during cilia recovery. *J Biol Chem* **269**, 29299-307.

Sobkowicz, H. M., Slapnick, S. M. and August, B. K. (1995). The kinocilium of auditory hair cells and evidence for its morphogenetic role during the regeneration of stereocilia and cuticular plates. *J Neurocytol* **24**, 633-53.

Sohocki, M. M., Bowne, S. J., Sullivan, L. S., Blackshaw, S., Cepko, C. L., Payne, A. M., Bhattacharya, S. S., Khaliq, S., Qasim Mehdi, S., Birch, D. G., Harrison, W. R., Elder, F. F., Heckenlively, J. R. and Daiger, S. P. (2000). Mutations in a new photoreceptor-pineal gene on 17p cause Leber congenital amaurosis. *Nat Genet* **24**, 79-83.

Sorokin, S. P. (1968). Reconstructions of centriole formation and ciliogenesis in mammalian lungs. *J Cell Sci* **3**, 207-30.

Spadaccini, R., Perrin, H., Bottomley, M. J., Ansieau, S. and Sattler, M. (2006). Structure and functional analysis of the MYND domain. *J Mol Biol* **358**, 498-508.

Steinman, R. M. (1968). An electron microscopic study of ciliogenesis in developing epidermis and trachea in the embryo of *Xenopus laevis*. *Am J Anat* **122**, 19-55.

Stephan, A., Vaughan, S., Shaw, M. K., Gull, K. and McKean, P. G. (2007). An Essential Quality Control Mechanism at the Eukaryotic Basal Body Prior to Intraflagellar Transport. *Traffic*.

Stephens, R. E. (1970). Isolation of Nexin - The linkage protein responsible for the maintenance of the nine-fold configuration of flagellar axonemes. *Biol. Bull.* **139**, 438.

Stephens, R. E. (1997). Synthesis and turnover of embryonic sea urchin ciliary proteins during selective inhibition of tubulin synthesis and assembly. *Mol Biol Cell* **8**, 2187-98.

Stephens, R. E. and Edds, K. T. (1976). Microtubules: structure, chemistry, and function. *Physiol Rev* **56**, 709-77.

Stephens, R. E. and Lemieux, N. A. (1999). Molecular chaperones in cilia and flagella: implications for protein turnover. *Cell Motil Cytoskeleton* **44**, 274-83.

Stolc, V., Samanta, M. P., Tongprasit, W. and Marshall, W. F. (2005). Genome-wide transcriptional analysis of flagellar regeneration in *Chlamydomonas reinhardtii* identifies orthologs of ciliary disease genes. *Proc Natl Acad Sci U S A* **102**, 3703-7.

Sullivan, L. S., Bowne, S. J., Birch, D. G., Hughbanks-Wheaton, D., Heckenlively, J. R., Lewis, R. A., Garcia, C. A., Ruiz, R. S., Blanton, S. H.,

Northrup, H., Gire, A. I., Seaman, R., Duzkale, H., Spellicy, C. J., Zhu, J., Shankar, S. P. and Daiger, S. P. (2006). Prevalence of disease-causing mutations in families with autosomal dominant retinitis pigmentosa: a screen of known genes in 200 families. *Invest Ophthalmol Vis Sci* **47**, 3052-64.

Sun, Z., Amsterdam, A., Pazour, G. J., Cole, D. G., Miller, M. S. and Hopkins, N. (2004). A genetic screen in zebrafish identifies cilia genes as a principal cause of cystic kidney. *Development* **131**, 4085-93.

Swoboda, P., Adler, H. T. and Thomas, J. H. (2000). The RFX-type transcription factor DAF-19 regulates sensory neuron cilium formation in *C. elegans*. *Mol Cell* **5**, 411-21.

Tam, L. W. and Lefebvre, P. A. (1993). Cloning of flagellar genes in Chlamydomonas reinhardtii by DNA insertional mutagenesis. *Genetics* **135**, 375-84.

Tamm, S. L. and Tamm, S. (1981). Ciliary reversal without rotation of axonemal structures in ctenophore comb plates. *J Cell Biol* **89**, 495-509.

Taylor, J. E. and Rudenko, G. (2006). Switching trypanosome coats: what's in the wardrobe? *Trends Genet* **22**, 614-20.

Tsou, M. F. and Stearns, T. (2006). Mechanism limiting centrosome duplication to once per cell cycle. *Nature* **442**, 947-51.

Vaughan, S., Kohl, L., Ngai, I., Wheeler, R. J. and Gull, K. (in press). A repetitive protein essential for the flagellum attachment zone filament structure and function in *Trypanosoma brucei*.

Vaughn, K. C. and Renzaglia, K. S. (2006). Structural and immunocytochemical characterization of the Ginkgo biloba L. sperm motility apparatus. *Protoplasma* **227**, 165-73.

Vickerman, K. (1994). The evolutionary expansion of the trypanosomatid flagellates. *Int J Parasitol* **24**, 1317-31.

Vorobjev, I. A. and Chentsov Yu, S. (1982). Centrioles in the cell cycle. I. Epithelial cells. *J Cell Biol* **93**, 938-49.

Vorobjev, I. A. and Nadezhdina, E. S. (1987). The centrosome and its role in the organization of microtubules. *Int Rev Cytol* **106**, 227-93.

Wang, Z., Morris, J. C., Drew, M. E. and Englund, P. T. (2000). Inhibition of *Trypanosoma brucei* gene expression by RNA interference using an integratable vector with opposing T7 promoters. *J Biol Chem* **275**, 40174-9.

Warner, F. D. (1976). Ciliary inter-microtubule bridges. *J Cell Sci* **20**, 101-14.

Warr, J. R., McVitte, A., Randall, J. and Hopkins, J. M. (1966). Genetic control of flagellar structure in *Chlamydomonas reinhardtii*. *Genet Res* **7**, 335 - 351.

West, A. B., Lockhart, P. J., O'Farell, C. and Farrer, M. J. (2003). Identification of a novel gene linked to parkin via a bi-directional promoter. *J Mol Biol* **326**, 11-9.

Wheatley, D. N., Wang, A. M. and Strugnell, G. E. (1996). Expression of primary cilia in mammalian cells. *Cell Biol Int* **20**, 73-81.

Wickstead, B., Ersfeld, K. and Gull, K. (2002). Targeting of a tetracycline-inducible expression system to the transcriptionally silent minichromosomes of *Trypanosoma brucei*. *Mol Biochem Parasitol* **125**, 211-6.

Williams, N. E. and Nelsen, E. M. (1997). HSP70 and HSP90 homologs are associated with tubulin in hetero-oligomeric complexes, cilia and the cortex of *Tetrahymena*. *J Cell Sci* **110 (Pt 14)**, 1665-72.

Witman, G. B. (1986). Isolation of Chlamydomonas flagella and flagellar axonemes. *Methods Enzymol* **134**, 280-90.

Witman, G. B., Plummer, J. and Sander, G. (1978). *Chlamydomonas* flagellar mutants lacking radial spokes and central tubules. Structure, composition, and function of specific axonemal components. *J Cell Biol* **76**, 729-47.

Wong, C. and Stearns, T. (2003). Centrosome number is controlled by a centrosome-intrinsic block to reduplication. *Nat Cell Biol* **5**, 539-44.

Woods, A., Baines, A. J. and Gull, K. (1989a). Evidence for a Mr 88,000 glycoprotein with a transmembrane association to a unique flagellum attachment region in *Trypanosoma brucei*. *J Cell Sci* **93 (Pt 3)**, 501-8.

Woods, A., Sherwin, T., Sasse, R., MacRae, T. H., Baines, A. J. and Gull, K. (1989b). Definition of individual components within the cytoskeleton of *Trypanosoma brucei* by a library of monoclonal antibodies. *J Cell Sci* **93 (Pt 3)**, 491-500.

Woodward, R., Carden, M. J. and Gull, K. (1995). Immunological characterization of cytoskeletal proteins associated with the basal body, axoneme and flagellum attachment zone of *Trypanosoma brucei*. *Parasitology* **111 (Pt 1)**, 77-85.

Yagi, T., Minoura, I., Fujiwara, A., Saito, R., Yasunaga, T., Hirono, M. and Kamiya, R. (2005). An axonemal dynein particularly important for flagellar movement at high viscosity. Implications from a new *Chlamydomonas* mutant deficient in the dynein heavy chain gene DHC9. *J Biol Chem* **280**, 41412-20.

Yamamoto, R., Yanagisawa, H. A., Yagi, T. and Kamiya, R. (2006). A novel subunit of axonemal dynein conserved among lower and higher eukaryotes. *FEBS Lett* **580**, 6357-60.

Yang, C., Compton, M. M. and Yang, P. (2005). Dimeric novel HSP40 is incorporated into the radial spoke complex during the assembly process in flagella. *Mol Biol Cell* **16**, 637-48.

Yoder, B. K. (2007). Role of primary cilia in the pathogenesis of polycystic kidney disease. *J Am Soc Nephrol* **18**, 1381-8.

Yukitake, H., Furusawa, M., Taira, T., Iguchi-Ariga, S. M. and Ariga, H. (2002). AAT-1, a novel testis-specific AMY-1-binding protein, forms a quaternary complex with AMY-1, A-kinase anchor protein 84, and a regulatory subunit of cAMP-dependent protein kinase and is phosphorylated by its kinase. *J Biol Chem* **277**, 45480-92.

Zou, C., Li, J., Bai, Y., Gunning, W. T., Wazer, D. E., Band, V. and Gao, Q. (2005). Centrobin: a novel daughter centriole-associated protein that is required for centriole duplication. *J Cell Biol* **171**, 437-45.

Appendix

The Parkin co-regulated gene product, PACRG, is an evolutionarily conserved axonemal protein that functions in outer-doublet microtubule morphogenesis

Helen R. Dawe*, Helen Farr*, Neil Portman, Michael K. Shaw and Keith Gull‡

Sir William Dunn School of Pathology, University of Oxford, South Parks Road, Oxford, OX1 3RE, UK

*These authors contributed equally to this work

‡Author for correspondence (e-mail: keith.gull@path.ox.ac.uk)

Accepted 23 August 2005
Journal of Cell Science 118, 5421-5430 Published by The Company of Biologists 2005
doi:10.1242/jcs.02659

Summary

Eukaryotic cilia and flagella are highly conserved structures composed of a canonical 9+2 microtubule axoneme. Comparative genomics of flagellated and non-flagellated eukaryotes provides one way to identify new putative flagellar proteins. We identified the Parkin co-regulated gene, or *PACRG*, from such a screen. Male mice deficient in PACRG are sterile, but its function has been little explored. The flagellated protozoan parasite *Trypanosoma brucei* possesses two homologues of *PACRG*. We performed RNA interference knockdown experiments of the two genes independently and both together. Simultaneous ablation of both proteins produced slow growth and paralysis of the flagellum with consequent effects on organelle segregation. Moreover, using transmission electron microscopy, structural defects were seen in the axoneme, with microtubule doublets missing from the canonical 9+2 formation. The occurrence of missing doublets increased toward the distal end of the flagellum and sequential loss of doublets was observed along individual axonemes. GFP fusion proteins of both PACRG homologues localised along the full length of the axoneme. Our results provide the first evidence for PACRG function within the axoneme, where we suggest that PACRG acts to maintain functional stability of the axonemal outer doublets of both motile and sensory cilia and flagella.

Supplementary material available online at
http://jcs.biologists.org/cgi/content/full/118/23/5421/DC1

Key words: Pacrg, Axoneme, Outer-doublet microtubule, Outer-doublet linkages

Introduction

Cilia and flagella are highly conserved structures that are found on a wide range of cell types and expressed in many different organisms. Cilia and flagella are adapted to perform a large number of functions (El Zein et al., 2003) from motility to mechanosensation. They are typically composed of a microtubule axoneme made up of nine outer-doublet microtubules. In addition to this, motile cilia and flagella usually contain inner- and outer-dynein arms on these doublet microtubules and a central pair of two singlet microtubules.

Comparative bioinformatics demonstrates conservation between known flagellar proteins. Comparison of the genomes of flagellated organisms with those of non-flagellated organisms such as plants, red algae and yeast (e.g. *Arabidopsis thaliana*, *Cyanidioschyzon merolae* and *Schizosaccharomyces pombe*) allows for the identification of novel putative flagellar proteins. We analysed the published human ciliary proteome (Ostrowski et al., 2002) for evolutionarily conserved proteins of unknown function. One of these, annotated only as a hypothetical in the original publication, was revealed by our bioinformatics analyses to be PACRG, a protein that was identified subsequent to the proteomic investigation.

PACRG was originally identified (West et al., 2003) as a gene lying upstream of, and sharing a common promoter with *Parkin*, the gene implicated in juvenile Parkinson's disease. The quaking mouse (Sidman et al., 1964) is a spontaneous mutation with a large deletion in chromosome 17 that results in the loss of expression of both Parkin and PACRG (Lockhart et al., 2004). Mice have tremors characteristic of Parkinson's disease and in addition, male homozygotes are sterile. PACRG loss has been recently identified as the cause of the male sterility component of this phenotype (Lorenzetti et al., 2004). However, its function remains unknown. We hypothesised that PACRG might play a role in the flagellum. This idea is supported by two further analyses using a comparative bioinformatics approach to search for putative flagellar proteins (Avidor-Reiss et al., 2004; Li et al., 2004), in which PACRG is found.

The protozoan parasite *Trypanosoma brucei* is an excellent model organism in which to study cilia and flagella because of its well-characterised cytoskeleton (for a review, see Gull, 1999) and its genetic tractability. It possesses a single flagellum, which exits at the posterior end of the cell from the flagellar pocket and is attached to the cell body along its length,

Journal of Cell Science

proceeding to the anterior tip of the cell. As well as the axoneme, the flagellum contains an additional structure, the paraflagellar rod (PFR). This lattice-like structure runs alongside the axoneme, to which it is attached. At cell division, the cell maintains the old flagellum and assembles a new flagellum.

Here we show that *T. brucei* contains two PACRG paralogues. Using RNA interference (RNAi) in *T. brucei* to address the function of PACRG, we show that simultaneous knockdown of both paralogues produces paralysed flagella. At the ultrastructural level we observe loss of specific outer-doublet microtubules. We show that occurrence of missing outer doublets increases along the length of the flagellum. GFP-PACRG fusion proteins localise along the full length of the axoneme. We propose that PACRG performs a novel function within eukaryotic flagella in maintaining interdoublet linkages and thus preserves axoneme integrity.

Materials and Methods

Bioinformatics

Sequences for TbPACRG A and TbPACRG B were obtained from GeneDB (http://www.genedb.org/) and used to perform BLAST searches (Altschul et al., 1997) on publicly available databases (http://genome.jgi-psf.org/chlre2/chlre2.info.links.html and http://www.ncbi.nlm.nih.gov/BLAST/). Homologues were identified by reciprocal BLAST searches and alignments created using ClustalX (Thompson et al., 1997).

Constructs and trypanosome transfection

For individual TbPACRG A or TbPACRG B RNAi, 600 bp fragments of the relevant gene were amplified by PCR with TbPACRG A or B specific primers (TbPACRG A forward, ATGAGTTACGAGATAC; TbPACRG A reverse, CGTTGCGCAAAT; TbPACRG B forward, ATGGCGTTCTCACGAA; TbPACRG B reverse, GACGTTA-ATGAT) incorporating *Xba*I and *Hin*dIII restriction sites into the forward and reverse primers, respectively. For TbPACRG AB RNAi, the same 600 bp fragment of each gene was amplified using the same primer sequences. For TbPACRG A an *Xba*I site was added to the forward primer and *Eco*RI to the reverse primer; for TbPACRG B, an *Eco*RI site was added to the forward primer and *Hin*dIII to the reverse primer. Fragments were cloned into the p2T7-177-inducible RNAi vector (Wickstead et al., 2002) using the *Xba*I and *Hin*dIII sites. Procyclic *T. brucei* 29-13 cells (Wirtz et al., 1999) were transfected using standard protocols, selected using 5 μg/ml phleomycin, and subsequently cloned by limiting dilution.

To make cell lines expressing endogenously tagged GFP-TbPACRG fusion protein, 150-200 bp fragments of the 5′ end of each TbPACRG gene, and within the 5′ untranslated region (UTR) were amplified with TbPACRG A or B specific primers incorporating suitable restriction sites and ligated into a vector for GFP expression (S. Kelly and K.G., unpublished). Trypanosomes were transfected, and selected using 50 μg/ml hygromycin.

Culture of trypanosomes

Cell lines were cultured in SDM 79 medium supplemented with 10% foetal calf serum and appropriate antibiotics at 28°C. For RNAi, cells were induced using 1 μg/ml doxycycline.

Analysis of motility

Non-induced cells and induced cells after 72 hours were grown to a density of 2×10^6 cells/ml. The motility of these cells was analysed as described by (Gadelha et al., 2005). Cells were tracked for 20 frames, taken over 40 seconds. Movie 1 in supplementary material shows the normal motility of the trypanosome flagellum and the phenotype of cells 72 hours after induction in tissue culture flasks. Cells were examined using a Zeiss Axiovert 35M inverted microscope with a 32× lens and video was captured using a COHU High Performance CCD camera onto a DMR-E85H DVD video recorder (Panasonic).

Immunolocalisation studies and antibodies

For DNA staining, cells were settled onto glass slides, fixed in 3.6% formaldehyde (TAAB) in phosphate-buffered saline (PBS) and embedded in Vectashield (Vector Laboratories) with 4,6-diamidino-2-phenylindole (DAPI). For co-immunofluorescence, trypanosomes were settled onto glass slides, cytoskeletons prepared by extraction with 1% NP-40 in 100 mM PIPES, pH 6.9, 2 mM EGTA, 1 mM $MgSO_4$, 0.1 mM EDTA and fixed in 1.8% formaldehyde in PBS for 10 minutes. Cells were double-labelled with anti-GFP (rabbit polyclonal A11122, Invitrogen) and either anti-PFR (L8C4) (Kohl et al., 1999) or anti-basal body (BBA4) (Woods et al., 1989). Secondary antibodies were Alexa-488-conjugated anti-rabbit (A-11034, Molecular Probes) and Alexa-546-conjugated anti-mouse (A-11030, Molecular Probes). Cells were embedded in Vectashield with DAPI. Slides were examined on a Zeiss Axioplan 2 microscope using a 100×, 1.4 NA oil-immersion lens, captured on a CCD camera controlled by Metamorph software (Universal Imaging) and processed in Metamorph and Adobe Photoshop (Adobe).

Preparation of cells for thin-section TEM

Cells were fixed at 72 hours after induction of RNAi in 2.5% gluteraldehyde, 2% paraformaldehyde and 0.1% picric acid in 100 mM phosphate (pH 6.5) for 2 hours at 4°C followed by post-fixation in 1% osmium tetraoxide in 100 mM phosphate buffer (pH 6.5) for 1 hour at 4°C. The fixed material was stained en bloc with 2% aqueous uranyl acetate for 2 hours at 4°C. Following dehydration through a graded series of acetone and propylene oxide, the material was embedded in epon resin for sectioning and analysis by transmission electron microscopy.

Statistical analysis

Chi-squared and Student's *t*-tests were carried out using Excel (Microsoft).

Real-time quantitative PCR

Total RNA samples were collected from the 29-13 parental cell line, non-induced cells and induced cells 24 hours and 48 hours after induction. RNA samples were purified using silica gel-based purification methods (High Pure RNA Isolation Kit, Roche) and stored at –80°C. Synthesis of cDNA from 1 μg RNA was carried out using the Omniscript Reverse Transcription Kit (Qiagen), with oligo(dT) primers at a final concentration of 1 μM. Three reverse transcription reactions were carried out from each RNA sample. Single stranded cDNA products were then analysed by Q-PCR using TaqMan probes against PACRG A, PACRG B and QM, a 60S ribosomal protein used as a reference gene. A no RT control was used to measure DNA contamination. For each gene, primers were designed using Oligo4 (DNAStar) to amplify a 100-130 bp region. (PACRG A forward, GATGTCGGCGATTTGGTTAT; PACRG A reverse, TCTCATACGTCGGCACCATA; PACRG B forward, AAATACACGACACCCAACTG; PACRG B reverse, GTAGAGATT-GAACACCGGAA; QM forward, GCGTGCCAACAAGGAATGT; QM reverse, GCGAAGTACGTGGAACGGA). Products were detected using TaqMan probes (PACRG A, TCATGGTGGCG-ACGATGCGT; PACRG B, AACTTGTGGAGAGCGCCGAC; QM, CCACATGCGTATCCGCGCCC) with 6-FAM on the 5′ end and BHQ-1 on the 3′ end. Concentrations of primers, probes and $MgCl_2$

for each primer set were optimised prior to the experiment. In each PCR cycle the fluorescence was recorded at the end of the annealing phase. The *Ct* value for each reaction was measured, and the absolute DNA amount calculated. For each sample this was normalised against the reference gene, QM, and then expressed as a percentage of the level in 29-13 cells.

Results

Two PACRG family members in *Trypanosoma brucei*

To determine the genome occurrence pattern of PACRG, we interrogated publicly available databases with the mouse Pacrg protein sequence. PACRG homologues were found to be widely conserved among flagellated organisms, including *Caenorhabditis elegans* (Fig. 1). Sequences showed most homology in the C-terminal region as shown by the large blocks of dark blue indicating identical residues in Fig. 1. Homologues were not found in the genomes of non-flagellated organisms including *Arabidopsis thaliana*, *Cyanidioschyzon merolae* and *Schizosaccharomyces pombe*. In the protozoan parasite *T. brucei*, we found two paralogues with a high degree of conservation. These are equally divergent from mouse Pacrg, and therefore we named them TbPACRG A and TbPACRG B. TbPACRG A and B are conserved within the kinetoplastids *Leishmania major* and *Trypanosoma cruzi* in addition to *T. brucei*.

Ablation of both TbPACRG mRNAs produces slow growth and paralysis

To understand the function of PACRG in *T. brucei*, we used RNAi to ablate protein expression of the two PACRG family members both independently and together. Ablation of TbPACRG A or TbPACRG B alone produced no effect on cell growth rate (Fig. 2B,D respectively) or cell division (data not shown), although the RNA levels fell to 9% (Fig. 2A) and 8% (Fig. 2C) of the parental (29-13 cell line) level respectively. A no-RT control showed minimal DNA contamination. However, simultaneous ablation of TbPACRG A and B, with a reduction of TbPACRG A to 10% and TbPACRG B to 20% (Fig. 2E), produced a slow growth phenotype first apparent at 72 hours post-induction (Fig. 2F). Induced cells appeared morphologically normal by phase-contrast microscopy (Fig. 3, compare A,B to C,D), however in 27% cells undergoing cytokinesis (n=200) we observed incorrect positioning of the kinetoplast (Fig. 3). In some cells the kinetoplast was closer than normal to the nucleus (Fig. 3, compare distance between nucleus and kinetoplast in A to that in E), whereas in others it was positioned almost anterior to the most posterior daughter nucleus (Fig. 3F, arrow indicates posterior kinetoplast). In each case of mispositioning, the kinetoplast that is most affected tends to be that associated with the new flagellum, located at the posterior end of the cell. We also observed a small increase in the number

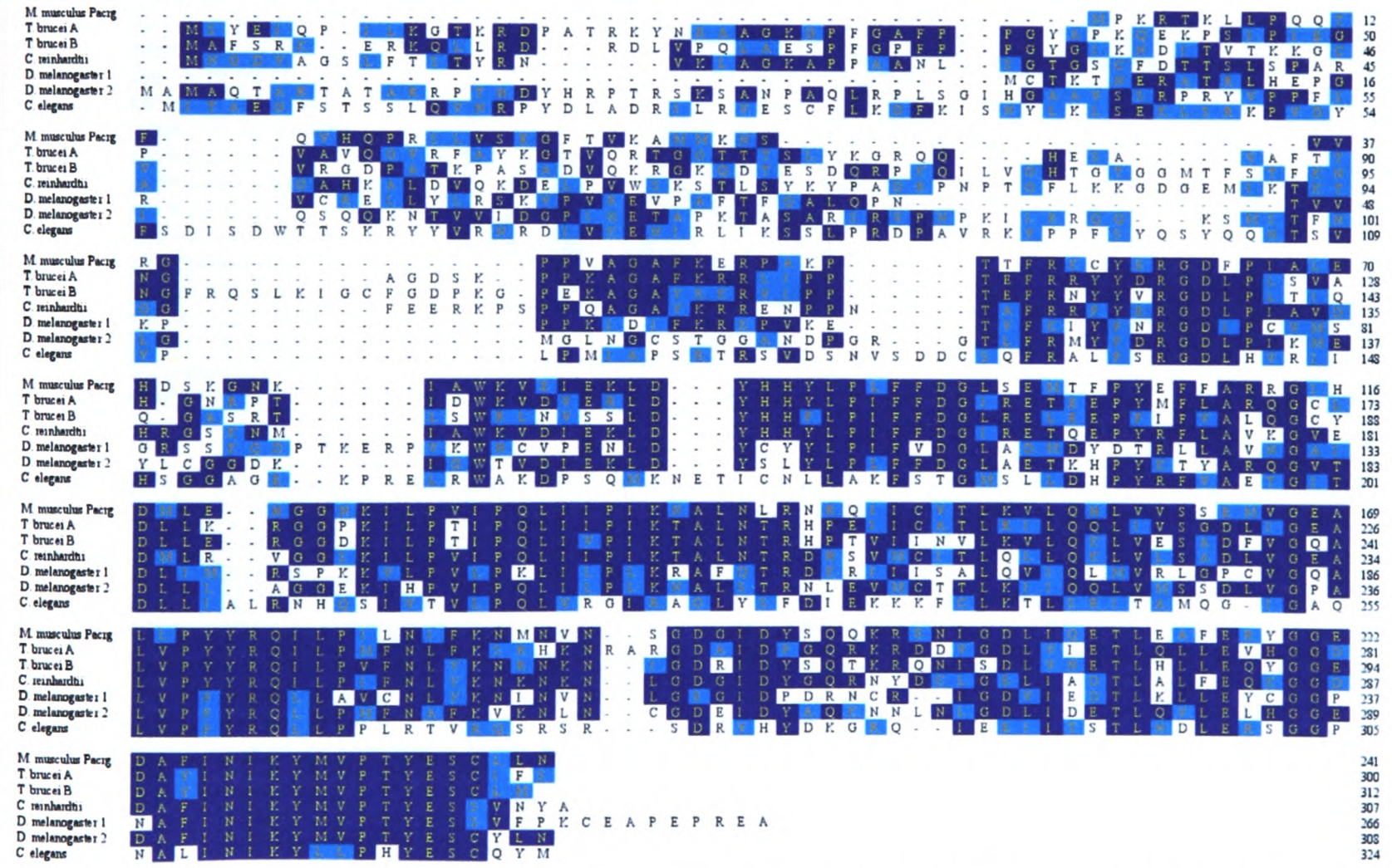


Fig. 1. Two PACRG paralogues in *T. brucei*. Protein sequence alignment of two *T. brucei* PACRG-like proteins (Tb03.4808.210 and Tb09.210.1470) with gene products from *M. musculus* (XP_128418), *C. reinhardtii* (C_20334), *D. melanogaster* (CG179349 and CG15120) and *C. elegans* (NP_495496). Orthology was determined by examination of candidate sequences including reciprocal BLAST. Identical residues are shown in dark blue; similar residues are shown in light blue.

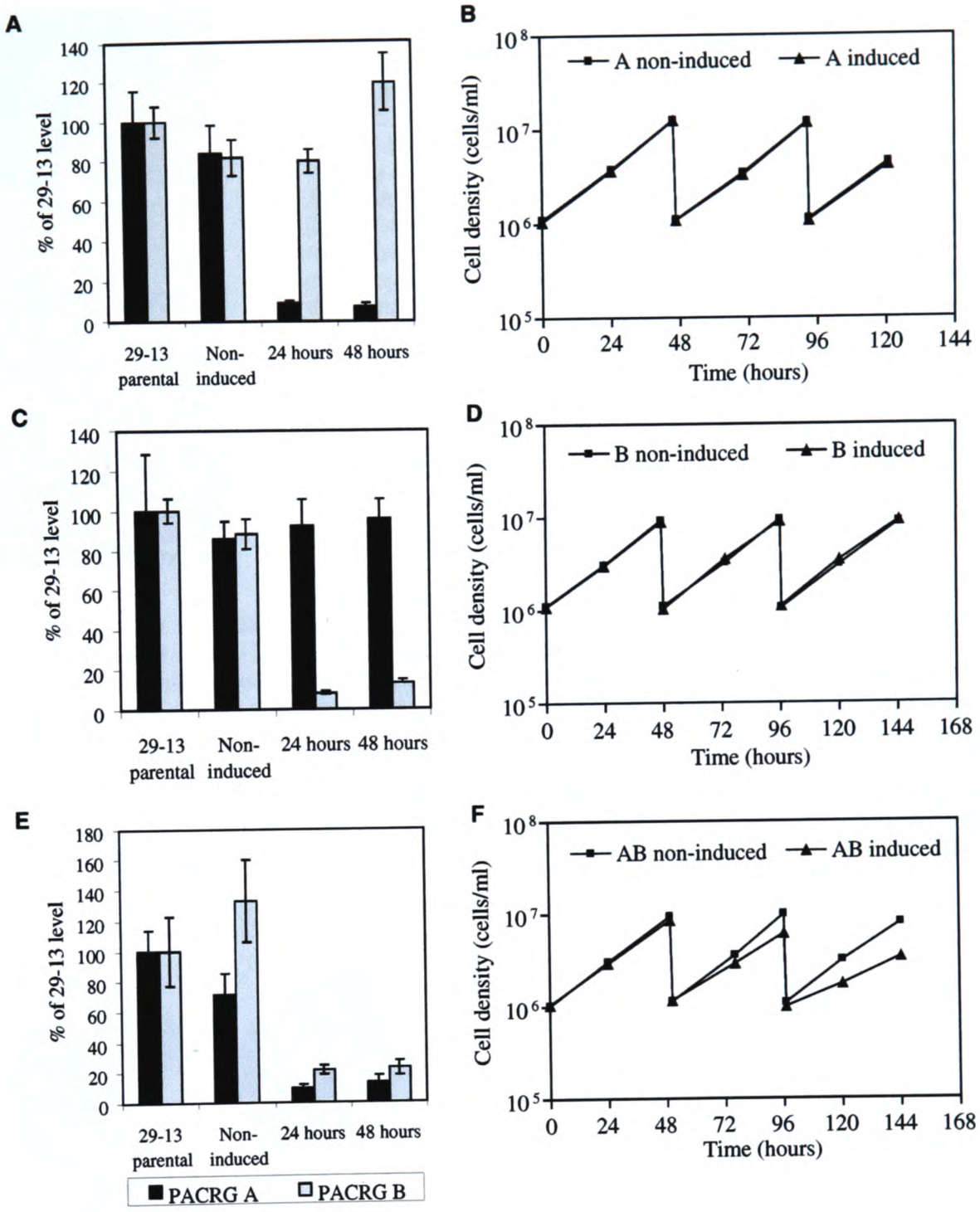


Fig. 2. Ablation of PACRG AB produces a slow-growth phenotype. Q-PCR data (A,C,E) and representative growth curves (B,D,F) of cells undergoing RNAi of TbPACRG A (A,B), TbPACRG B (C,D) or TbPACRG AB (E,F). A reduction of mRNA signal of TbPACRG A (black bars) was seen in RNAi TbPACRG A-treated cells (A). However, there was no alteration in growth kinetics in TbPACRG A RNAi-treated cells (B, triangles) compared to non-induced controls (B, squares). A reduction of mRNA signal of TbPACRG B (grey bars) was observed in RNAi TbPACRG B-induced cells (C), but again, no alteration in growth kinetics was observed compared to the control (D). A reduction of mRNA signal of TbPACRG A (black bars) and TbPACRG B (grey bars) was observed in TbPACRG AB RNAi-treated cells (E) with the representative growth curve (F) showing a growth defect starting 72 hours after induction (triangles) compared to non-induced controls (squares). For the growth curves (B,D,F), cells were maintained in log phase by diluting the culture every 48 hours. Q-PCR values are percentages (mean±s.e.m.) of the control cell signal (A,C,E).

of cells with two nuclei and two kinetoplasts (17% of the population in PACRG AB RNAi-induced cells compared to 12% in non-induced controls), suggesting that RNAi-induced cells have difficulties in late phases of the cell cycle.

We observed that TbPACRG AB RNAi-induced cells possessed flagella of normal length (20.3±0.6 μm in non-induced cells; n=100, compared with 20.3±0.6 μm in induced cells; n=100) and continued to build a new flagellum each cell cycle. However, cell motility was strongly affected. At 24 hours after induction, 20% of cells had a paralysed flagellum (n=108 cells) and did not move. By 48 hours, this had increased to 48% (n=102 cells), and at 72 hours after induction, 73% of flagella (n=48 cells) were paralysed (see also supplementary material Movie 1, compare the induced cells to the non-induced cells). By tracking locomotion of a cohort of individual cells in the population over the course of 40 seconds we were able to measure their speed. Highly significant differences (P<0.001) were observed between RNAi-induced (n=53) and non-induced cells (n=38) in terms of minimum, mean and maximum speeds (Table 1).

TbPACRG AB RNAi induction causes loss of outer-doublet microtubules

To understand the paralysis of the flagellum, we prepared TbPACRG AB RNAi-induced and non-induced cells for

Table 1. Induction of TbPACRG AB RNAi causes a severe loss in motility

Population motility parameter	Non-induced (n=38)	Induced (n=53)
Minimum speed (μm/second)	1.1±0.2	0.1±0.1
Mean speed (μm/second)	3.0±0.2	0.8±0.1
Maximum speed (μm/second)	4.8±0.3	1.6±0.2

Speeds shown are the average minimum, mean and maximum speeds for a population of TbPACRG AB RNAi-induced and non-induced cells.

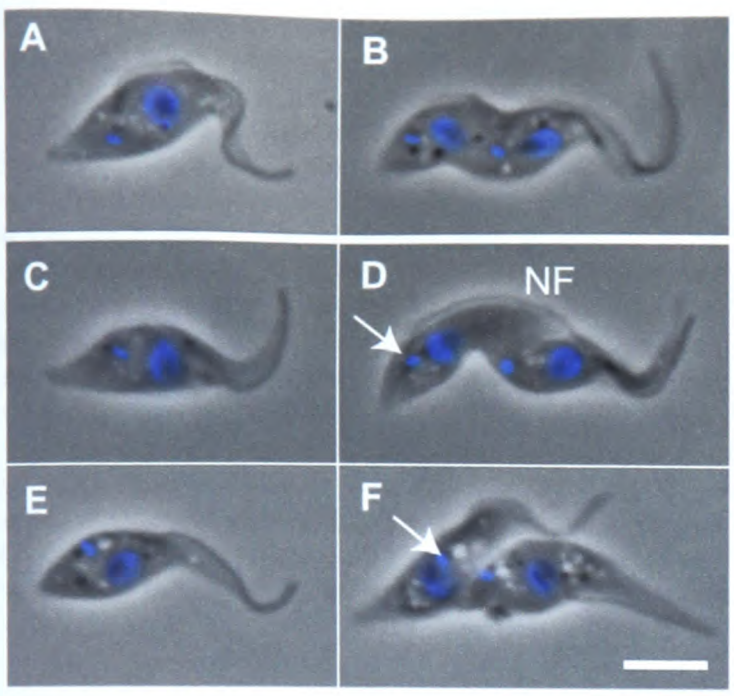


Fig. 3. Induced cells build a flagellum, however daughter kinetoplast position is impaired. Phase-contrast images of control cells (A,B) and TbPACRG AB RNAi-induced cells at 72 hours (C-F) with nuclear and kinetoplast DNA overlaid in blue. (A) A non-induced cell with one kinetoplast and one nucleus (1K1N). (B) A non-induced cell with duplicated nucleus and kinetoplast (2K2N cell) showing correct positioning of both kinetoplasts. (C) A TbPACRG AB RNAi-induced cell with correct positioning of the kinetoplast. (D) A TbPACRG AB RNAi-induced cell undergoing division where the distance between the daughter kinetoplast (arrow) and the daughter nucleus is reduced compared to that of the parent cell. Note the formation of the new flagellum (NF). (E) A TbPACRG AB RNAi-induced 1K1N cell where the kinetoplast is mislocalised. (F) A TbPACRG AB RNAi-induced cell undergoing cytokinesis where the daughter kinetoplast (arrow) is mispositioned, anterior to the daughter nucleus. Bar, 5 μm.

ultrastructural analysis by thin-section transmission electron microscopy. We observed a significant difference in the 9+2 architecture of the trypanosome flagellum. In non-induced control cell profiles, 98% (n=922) possessed a canonical 9+2 axonemal arrangement (Fig. 4A, a). In contrast, 53% (n=953, P<0.001) of axonemal profiles in induced TbPACRG AB RNAi cells exhibited loss of at least one of the nine outer-doublet microtubules (Fig. 4A, b-d). A minority of flagella profiles in TbPACRG AB RNAi-induced cells (4%) contained one or more displaced doublets outside the partial axoneme (data not shown). The number of missing doublets varied; approximately equal numbers of 8+2, 7+2, 6+2 and 5+2 axonemes were observed. The central pair microtubules generally remained present until more than four outer-doublet microtubules had been lost (Fig. 4A, b and c). Axonemes containing four or fewer outer-doublet microtubules lacked the central pair in 88% of cases (Fig. 4Ad). We observed cells that were in division (n=50) and had two adjacent flagella profiles (the old flagellum and the newly built flagellum). At cell division the cell maintains the old flagellum and assembles a new flagellum; late in the cell cycle it is possible to distinguish between the two (Sherwin and Gull, 1989). Of the cell profiles

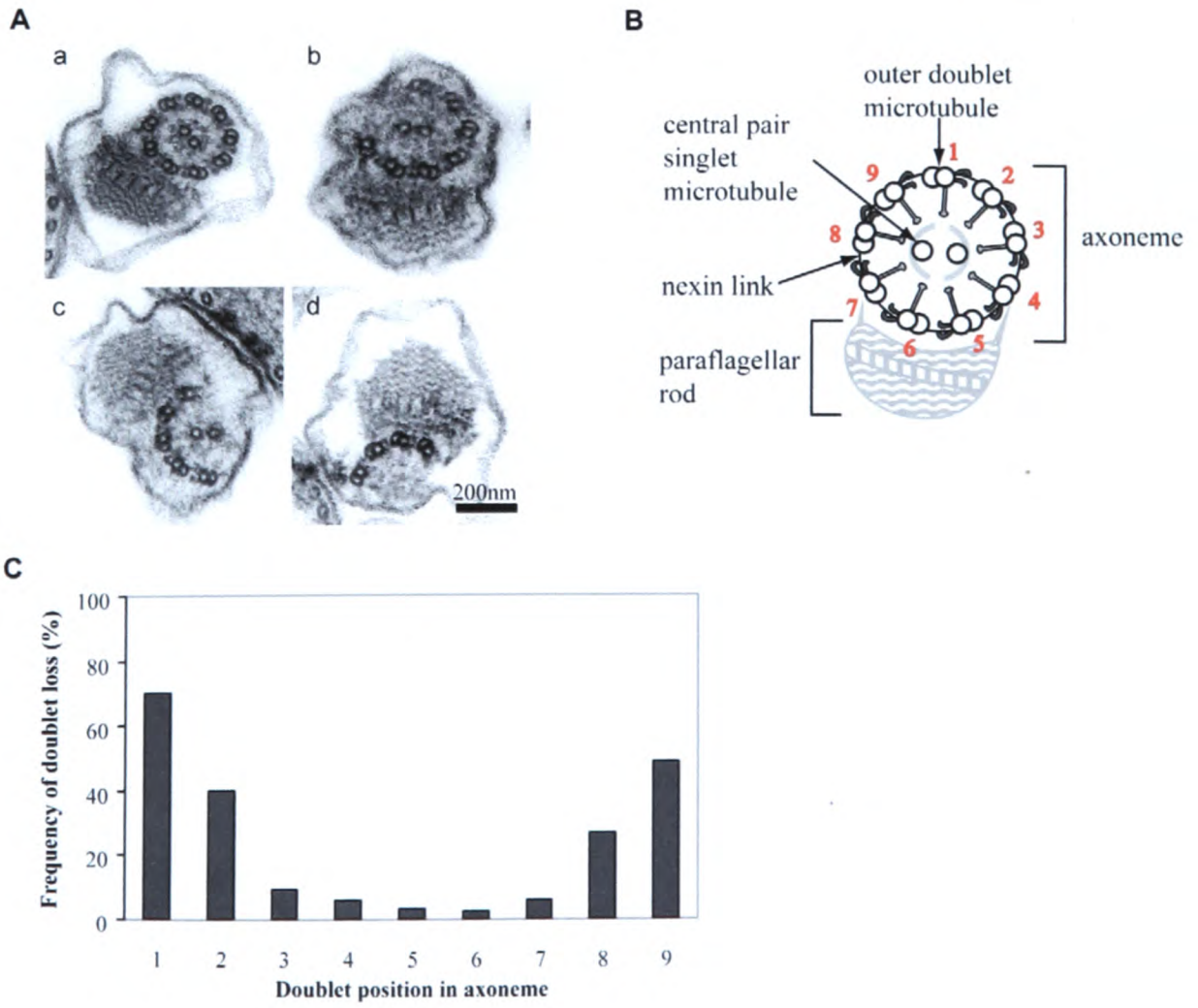


Fig. 4. PACRG AB RNAi induction causes loss of outer-doublet microtubules. (A) Transmission electron microscopy images of TbPACRG AB non-induced cells (a) and RNAi-induced cells 72 hours after induction (b-d). Note the loss of variable numbers of outer-doublet microtubules in b-d. (B) Drawing of relevant structures in a *T. brucei* flagellum. Numbers refer to the convention of numbering outer doublets according to their position relative to the central pair and PFR. (C) Graph of frequency of loss of specific outer-doublet microtubules. Bar, 200 nm.

Journal of Cell Science

examined, 51% had two affected flagella, with at least one outer doublet missing from each; 18% of cell profiles exhibited one unaffected old flagellum and one affected new flagellum; the remainder had two unaffected flagella.

We investigated whether particular outer-doublet microtubules were more susceptible to loss. In *T. brucei*, outer doublets are numbered according to their position relative to the central pair and the PFR (Fig. 4B), with the doublet directly opposed to the central pair being numbered as 1 and stable connections to the PFR on doublets 4 and 7. Where multiple doublets had been lost, it was nearly always adjacent doublets that were absent (see Fig. 4Ab for an example). We found that the doublets furthest from the PFR, doublets 9 and 1, were most likely to be lost, followed by doublets 2 and 8 (Fig. 4C). The doublets adjacent to the PFR were rarely missing; doublets 4 and 7, which are most obviously attached to the PFR (Fig. 4B) were missing in only 4.7% of axonemes, whereas doublets 5 and 6 were absent in only 2.6% and 2.1% of axonemes, respectively (Fig. 4C).

Outer-doublet microtubule number decreases towards the distal tip of the flagellum

Variability in the number of missing doublets raised the possibility that there could be a variation in the number of missing doublets along the length of an individual axoneme in TbPACRG AB RNAi-induced cells. To determine if fewer outer doublets were present at either the distal end of the flagellum or the proximal end, we quantified the number of outer doublets present at various positions along the axoneme (Fig. 5). As the flagellum of *T. brucei* is attached to the cell body, which has different widths and morphology along its length, it is possible to position an axonemal profile in any given electron micrograph to a particular region of the

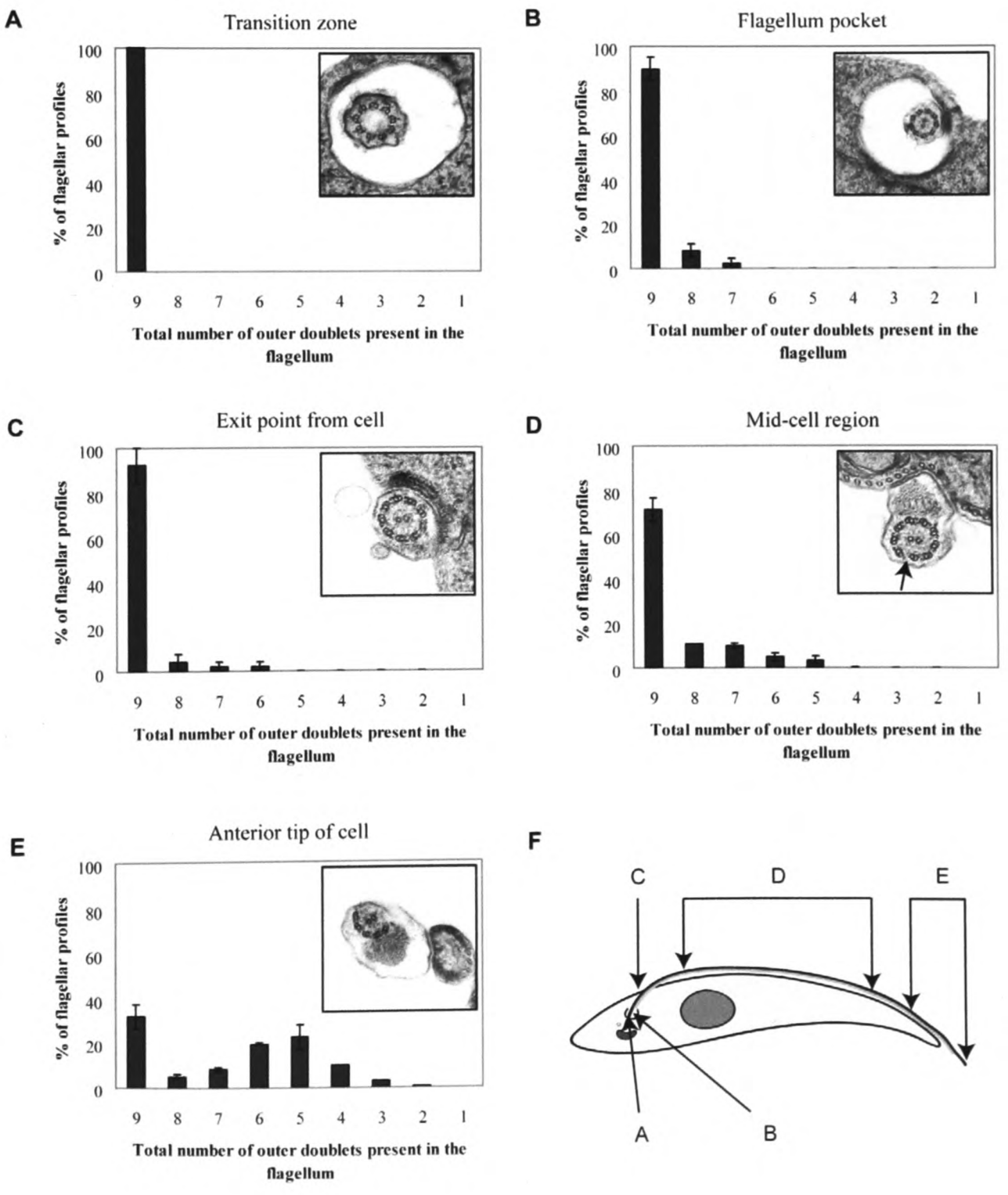


Fig. 5. Multiple outer-doublet loss occurs more frequently at the anterior of the cell. (A-E) The number of outer doublets was quantified at various positions along the axoneme. Graphs show the number of outer doublets present plotted against the frequency of occurrence in flagella profiles observed. Inset images show representative micrographs of flagella profiles at each position. The arrow in D indicates the break between two outer doublets that is observed prior to doublet loss. (F) Drawing of a *T. brucei* cell indicating the positions along the flagellum quantified in A-E.

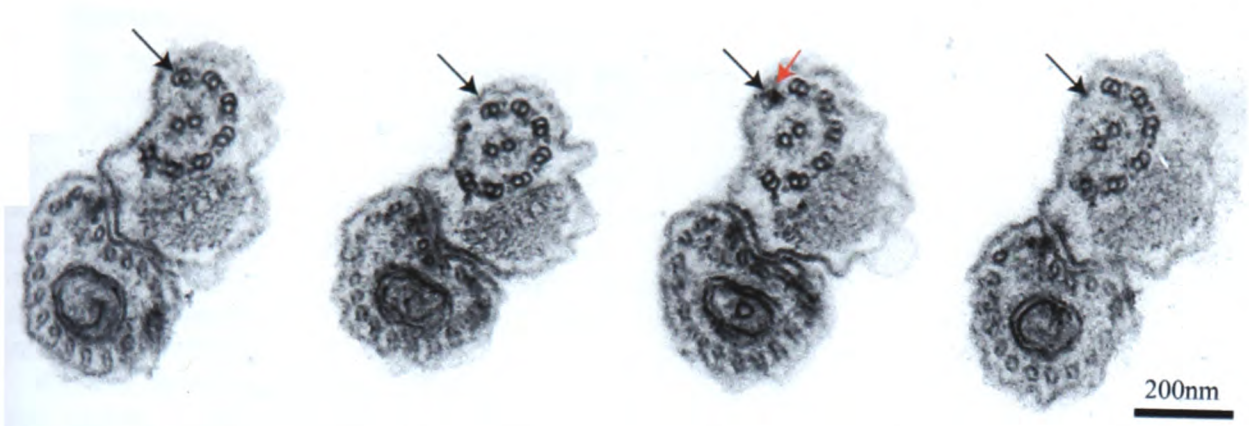


Fig. 6. The A and B tubules terminate simultaneously. Serial electron micrographs (left to right) showing loss of an outer doublet along a single axoneme. The black arrows indicate the position of the doublet that will be lost. Note the electron-dense lumen in the A tubule (red arrow) immediately prior to doublet loss. Bar, 200 nm.

flagellum. We characterised flagellar profiles into five subsets according to the adjacent cellular structures: transition zone, flagellum pocket, exit point of flagellum from cell, mid-cell region and anterior tip of cell. The basal bodies (data not shown) and transition zones (Fig. 5A) of RNAi-induced flagella appeared normal. Over 90% of axonemes found within, or just exiting the flagellar pocket had nine outer doublets, with only a minority having up to three doublets missing (Fig. 5B,C, respectively). However, the number of outer doublets decreased significantly from then on along the length of the cell body (Fig. 5D), such that at the distal tip of the flagellum only 32% of axonemes exhibited a 9+2 configuration, with 55% composed of six or fewer outer doublets (Fig. 5E).

We next examined serial thin-section micrographs to establish whether the missing doublets resulted from doublet termination. We focussed on the region close to the distal tip of the flagellum, where little or no cell body was visible, as this was where most doublets appeared to be lost (Fig. 5E). Serial sectioning through the distal tip region revealed that both the A and B tubules of a doublet terminated simultaneously (Fig. 6, black arrows show the doublet that is lost). An electron-dense lumen was observed only in the A tubule (Fig. 6, red arrow) immediately prior to the loss of that doublet, similar to that observed in capped *Chlamydomonas* flagella (Dentler, 1980), suggesting that the doublet may be capped prior to termination.

GFP-TbPACRG fusion proteins localise to the axoneme

To localise each of the two TbPACRG proteins within *T. brucei*, one copy of the two endogenous genes (*T. brucei* is diploid) was replaced with a GFP-TbPACRG fusion. Strains were constructed individually expressing GFP-TbPACRG A or GFP-TbPACRG B. In both instances, live cells exhibited a fluorescent flagellum. We performed immunofluorescence on detergent-extracted cytoskeletons using anti-GFP polyclonal antibody (Invitrogen) and antibodies against the paraflagellar rod (L8C4) (Kohl et al., 1999) or against the distal end of the basal body (BBA4) (Woods et al., 1989). The anti-GFP staining ran along the entire length of the flagellum in cells expressing either TbPACRG A, (Fig. 7A,B) or TbPACRG B (Fig. 7C,D). We investigated to which subcompartment of the flagellum TbPACRG A was localised using dual labelling with antibodies to both the basal body and the PFR. The anti-GFP signal (Fig. 7F, green, arrow) extended beyond that of the PFR (Fig. 7F, red), suggesting that GFP-PACRG is localised to the axoneme and not the PFR. No staining was apparent in the basal body (Fig. 7H, red staining marks the distal end of the basal body), suggesting that TbPACRG appears in the flagellum distal to this structure. These localisation experiments were performed independently for both TbPACRG A and TbPACRG B, with identical results.

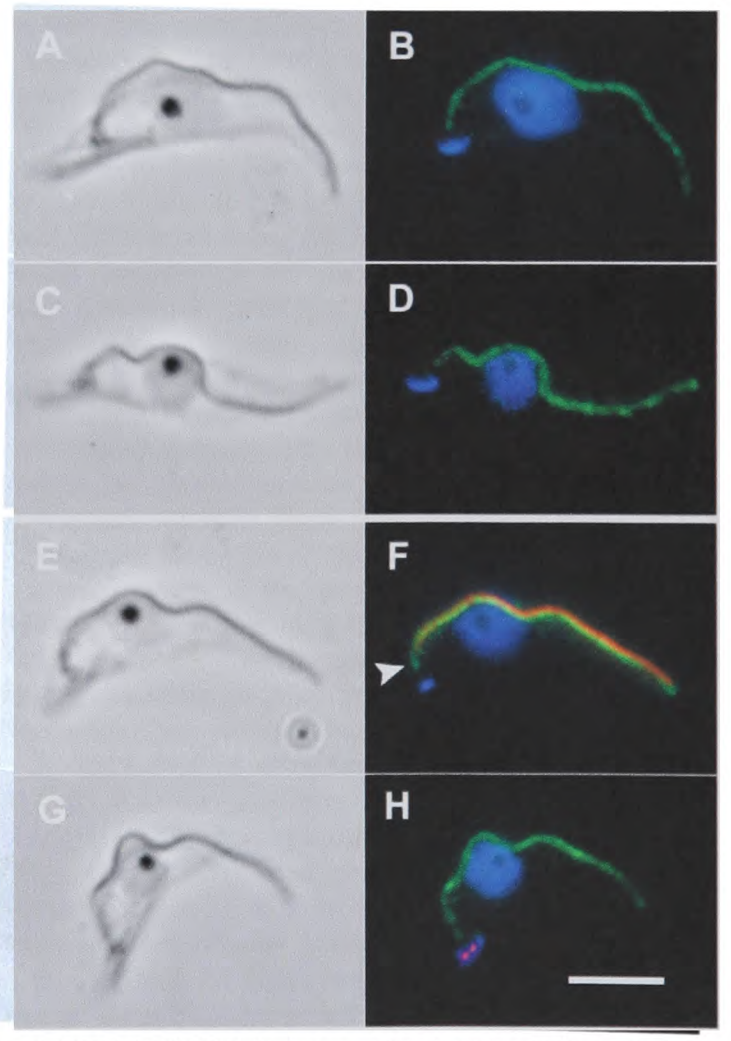


Fig. 7. GFP-TbPACRG fusion proteins localise to the axoneme. Phase-contrast microscopy (A,C,E,G) and fluorescence (B,D,F,H) images of detergent-extracted trypanosome cytoskeletons. DNA is labelled with DAPI (blue), and GFP is identified by anti-GFP polyclonal antibody (green). (A,B) Cells expressing GFP-TbPACRG A. (C,D) Cells expressing GFP-TbPACRG B. (E,F) Cells expressing GFP-TbPACRG A where the PFR is identified by the L8C4, anti-PFR, monoclonal antibody (red). Note the GFP signal extends proximal to the PFR staining (F, arrow). (G,H) Cells expressing GFP-TbPACRG A where the distal end of the basal body is identified by the BBA4 monoclonal antibody (red). Bar, 5 μm.

Journal of Cell Science

Discussion

Our aim in this work was to characterise the location and function of the evolutionarily conserved protein PACRG. We have shown that TbPACRG A and TbPACRG B localise to the axoneme of the eukaryotic flagellum and that simultaneous ablation of TbPACRG A and B expression produces a dramatic motility phenotype caused by loss of outer-doublet microtubules. Taken together, our results identify a novel axonemal protein that we suggest plays a role in outer-doublet microtubule stability.

We have shown using bioinformatics that *T. brucei* possesses two closely related PACRG paralogues. Both are equally similar to mammalian PACRG and are most conserved in the C-terminal region. Two other kinetoplastid protozoa, *T. cruzi* and *L. major*, also possess two PACRG paralogues, indicating the situation in *T. brucei* is not the result of a recent gene duplication. To date we have no evidence to suggest functional differences between the two proteins. Although very similar at the protein level and therefore likely to have the same function, they are different enough at the nucleic acid level for us to select between them with RNAi. We find no obvious evidence of PACRG splice variants in the mammalian EST databases (data not shown); this cannot therefore explain the expansion of PACRG genes in kinetoplastids. Our data point to functional redundancy within the PACRG family in these organisms.

RNAi of TbPACRG A and B produces a major motility phenotype. Despite the lack of cell locomotion, the flagellum is built and at the light microscope level extends to essentially the same length as that observed in non-induced controls. There are, in addition, detectable cellular consequences for cell morphogenesis. First, the adversely affected new flagellum is associated with a mispositioning and/or malsegregation of the replicated mitochondrial genome, the kinetoplast. Kinetoplast position and segregation is known to be dependent upon basal body/flagellum connections and integrity (Ogbadoyi et al., 2003; Ploubidou et al., 1999; Robinson and Gull, 1991; Robinson et al., 1995). The kinetoplast mispositioning effect is likely to result from flagellum positioning/motility defects deriving from the absence of a full axoneme structure. The absence of this prevents effective function of motility and interaction with the connector that interlinks the tip of the new flagellum and the lateral aspect of the old. We have previously shown the importance of the flagella connector in trypanosome procyclic cell morphogenesis, and hypothesised that force applied by the new flagellum via connector attachment to the old is responsible for kinetoplast segregation in procyclic trypanosomes (Briggs et al., 2004; Moreira-Leite et al., 2001). Our present evidence shows that impairment of motility and flagellar connector action produces an ineffective movement of the new basal body/kinetoplast. Ultimately, such defects in cellular morphogenesis appear to accumulate and become compounded such that cell growth is affected.

A previous study has shown that mouse Pacrg was present in the sperm flagellum (Lorenzetti et al., 2004) but its localisation to a flagellar compartment or function was not elucidated. We used GFP-PACRG fusion proteins to confirm this general localisation in trypanosome flagella. We then examined to which subcompartment of the flagellum TbPACRG A and TbPACRG B localised. Our results show that both TbPACRG A and B localise along the full length of the axoneme but not to the basal body or PFR. Furthermore, TbPACRG A and B are both present in a preparation of the detergent-insoluble flagellar fraction (our unpublished proteomic observations). One other protein is known to cause immotile sperm because of outer-doublet loss (Sampson et al., 2001). However, this protein, a voltage-dependent anion channel called VDAC3, localises to the outer dense fibres of sperm (Hinsch et al., 2004) rather than the axoneme and loss of only a single outer-doublet microtubule has been observed (Sampson et al., 2001). The presence of TbPACRG A and TbPACRG B along the whole length of the axoneme suggests that they are not required for outer-doublet initiation. Further evidence for this comes from the apparent absence of TbPACRG A and B from the basal body and transition zone regions, which appear normal by electron microscopy in TbPACRG AB RNAi-induced cells.

It is known that flagellar paralysis can result from loss of structures such as the PFR (Bastin et al., 1998), axonemal radial spokes and central pair (McKean et al., 2003; Smith and Lefebvre, 1997; Warr et al., 1966; Witman et al., 1978), however all these structures are present in TbPACRG AB RNAi-induced cells. The central pair remains present until more than four outer doublets have been lost, suggesting that this is a secondary effect of loss of multiple outer doublets. The presence of a *PACRG* homologue in the *C. elegans* genome, and EST evidence from mouse and human tissues containing primary (9+0) cilia (data not shown) support the idea that TbPACRG A and B are involved in the formation of outer-doublet microtubules but not the central pair.

In the majority of dividing cells, both the old and new flagella exhibited outer-doublet loss. This suggests that an affected old axoneme does not immediately stop morphogenesis of new axonemal/cytoskeletal architecture. This finding also demonstrates that the new axoneme starts to show doublet abnormalities before cytokinesis has occurred, during its late morphogenesis.

We tested whether there was variation in outer-doublet number along the length of an individual flagellum and found that it was normal at the proximal end of the flagellum and varied at the distal end, suggesting that axoneme formation is initiated normally. We do not yet know whether the outer-doublet microtubules grow to full length or are terminated prematurely. One possibility for PACRG function could be a role in outer-doublet extension. Depletion of PACRG would therefore lead to premature termination of outer-doublet microtubules, an idea supported by the capped A tubule seen in Fig. 6 prior to disappearance of that doublet. This explanation would fit with the observed increase in the number of missing microtubules along the flagellum, as observed in Fig. 5. The lack of random doublet termination around the axoneme would be explained by the fact that those doublets attached to the PFR would be preferentially stabilised by this connection. Alternatively, the microtubule outer doublets might be extended to their full length and then undergo partial catastrophe. Again, firmer linkages between doublets adjacent to the PFR could lead to their preferential stabilisation.

We have been unsuccessful at localising TbPACRG A or TbPACRG B at the ultrastructural level; nevertheless, aspects of the phenotype suggest possibilities for its sub-axonemal localisation. A likely candidate for its localisation would be the nexin interdoublet links (Fig. 4B). The interdoublet or nexin linkages have long been defined (Gibbons, 1965; Olson and

Journal of Cell Science

Linck, 1977; Stephens, 1970; Stephens and Edds, 1976; Warner, 1976) as an electron-dense band connecting the A tubule of one doublet to the B tubule of the adjacent doublet. It is proposed that these are elastic structures (Minoura et al., 1999) that enable the sliding of the doublets, yet their molecular identity remains unknown. It has been proposed that nexin links are in fact the dynein regulatory complex (DRC) (Woolley, 1997), a complex of six polypeptides (Huang et al., 1982; Piperno et al., 1992) of which only one has been characterised (Rupp and Porter, 2003). It is therefore possible that PACRG is a novel part of the DRC. A second study has localised the DRC to the junction between the radial spokes and the inner dynein arms (Gardner et al., 1994).

Various aspects of the TbPACRG AB RNAi phenotype support these ideas. Weakening of the nexin or other intermicrotubule linkages would be expected to lead to flagellar paralysis as the dynein-mediated interdoublet sliding that results in motility would be compromised. Premature termination of doublets could occur as a result of these weakened interdoublet linkages. We have observed axonemes containing nine outer-doublet microtubules where there is an apparent break in the connection between two adjacent doublets (e.g. inset in Fig. 5D, arrow indicates break), suggesting the integrity of the linkages may be compromised. One feature of the phenotype was the preferential loss of specific outer doublets. Those furthest from the PFR (9, 1 and 2) were most frequently lost, suggesting that the PFR may play a stabilising role. The physical connection between the PFR and doublets 4 and 7 is expected to reduce strain on the ring structure in this region by restricting lateral movement of the associated doublets, and hence stabilise the axoneme at this point. Further stabilisation here is likely to come from the linkage between doublets 5 and 6, which previous studies in other systems suggest are more stable than other interdoublet linkages (reviewed by Lindemann and Kanous, 1997). Loss of the intact ring structure of the axoneme would be expected to promote further loss of adjacent doublets owing to increased strain on the doublets located either side of the gap.

Although PACRG is predominantly expressed in the testis (Lorenzetti et al., 2004), EST evidence suggests a wider tissue distribution. Owing to the co-regulation of *PACRG* and *Parkin* in mammals, one study examined the role of PACRG in neurodegenerative disorders (Imai et al., 2003). In neuronal tissue, PACRG is found in neurodegenerative inclusions, where it is thought to form part of a complex that includes members of the chaperonin and heat shock protein (HSP) families including HSP70, HSP90 and various TCP1 members (Imai et al., 2003). It remains to be seen if PACRG has similar binding partners in the axoneme, but it is worth noting that cilia and flagella are known to contain an HSP70 family member (Bloch and Johnson, 1995; Stephens, 1997; Stephens and Lemieux, 1999; Williams and Nelsen, 1997), an HSP90 family member (Stephens and Lemieux, 1999; Williams and Nelsen, 1997) and a chaperonin of the TCP1 family (Cyrne et al., 1996; Soares et al., 1994; Stephens and Lemieux, 1999). In addition, an HSP40 family member has recently been identified as a component of the radial spoke complex (Satouh et al., 2005; Yang et al., 2005).

The repertoire of putative flagellar proteins of unknown function has recently been expanded by the application of comparative genomics and proteomics technologies. Our work identifies PACRG as a novel and evolutionarily conserved axonemal component that plays a role in axonemal stability. The evolutionary conservation of PACRG highlights its importance in the axoneme and suggests it plays a fundamental role in axoneme stability in many eukaryotic organisms and cell types exhibiting both motile and sensory flagella. Although we have demonstrated its importance in motility in this work, we predict that PACRG is also necessary for the functioning of primary cilia. A challenge for the future will be to firmly identify the axonemal compartment where PACRG is located and to elucidate the molecular mechanisms that underlie its function.

We are grateful to Laura Briggs for early bioinformatic analyses and Steven Kelly for assistance with GFP tagging. We would also like to thank Dick McIntosh and members of the Gull lab for helpful discussions. This work was supported by the BBSRC and Wellcome Trust and a BBSRC studentship (H.F.). K.G. is a Wellcome Trust Principal Research Fellow.

References

Altschul, S. F., Madden, T. L., Schäffer, A. A., Zhang, J., Zhang, Z., Miller, W. and Lipman, D. J. (1997). Gapped BLAST and PSI-BLAST: a new generation of protein database search programs. *Nucleic Acids Res.* **25**, 3389-3402.

Avidor-Reiss, T., Maer, A. M., Koundakjian, E., Polyanovsky, A., Keil, T., Subramaniam, S. and Zuker, C. S. (2004). Decoding cilia function: defining specialized genes required for compartmentalized cilia biogenesis. *Cell* **117**, 527-539.

Bastin, P., Sherwin, T. and Gull, K. (1998). Paraflagellar rod is vital for trypanosome motility. *Nature* **391**, 548.

Bloch, M. A. and Johnson, K. A. (1995). Identification of a molecular chaperone in the eukaryotic flagellum and its localization to the site of microtubule assembly. *J. Cell Sci.* **108**, 3541-3545.

Briggs, L. J., McKean, P. G., Baines, A., Moreira-Leite, F., Davidge, J., Vaughan, S. and Gull, K. (2004). The flagella connector of Trypanosoma brucei: an unusual mobile transmembrane junction. *J. Cell Sci.* **117**, 1641-1651.

Brun, R. and Schonenberger, M. (1979). Cultivation and in vitro cloning or procyclic culture forms of Trypanosoma brucei in a semi-defined medium. *Acta Trop.* **36**, 289-292.

Cyrne, L., Guerreiro, P., Cardoso, A. C., Rodrigues-Pousada, C. and Soares, H. (1996). The Tetrahymena chaperonin subunit CCT eta gene is coexpressed with CCT gamma gene during cilia biogenesis and cell sexual reproduction. *FEBS Lett.* **383**, 277-283.

Dentler, W. L. (1980). Structures linking the tips of ciliary and flagellar microtubules to the membrane. *J. Cell Sci.* **42**, 207-220.

El Zein, L., Omran, H. and Bouvagnet, P. (2003). Lateralization defects and ciliary dyskinesia: lessons from algae. *Trends Genet.* **19**, 162-167.

Gadelha, C., Wickstead, B., de Souza, W., Gull, K. and Cunha-e-Silva, N. (2005). Cryptic paraflagellar rod in endosymbiont-containing kinetoplastid protozoa. *Eukaryot. Cell* **4**, 516-525.

Gardner, L. C., O'Toole, E., Perrone, C. A., Giddings, T. and Porter, M. E. (1994). Components of a "dynein regulatory complex" are located at the junction between the radial spokes and the dynein arms in Chlamydomonas flagella. *J. Cell Biol.* **127**, 1311-1325.

Gibbons, I. R. (1965). Chemical dissection of cilia. *Arch. Biol. (Liege)* **76**, 317-352.

Gull, K. (1999). The cytoskeleton of trypanosomatid parasites. *Annu. Rev. Microbiol.* **53**, 629-655.

Hinsch, K. D., De Pinto, V., Aires, V. A., Schneider, X., Messina, A. and Hinsch, E. (2004). Voltage-dependent anion-selective channels VDAC2 and VDAC3 are abundant proteins in bovine outer dense fibers, a cytoskeletal component of the sperm flagellum. *J. Biol. Chem.* **279**, 15281-15288.

Huang, B., Ramanis, Z. and Luck, D. J. (1982). Suppressor mutations in Chlamydomonas reveal a regulatory mechanism for Flagellar function. *Cell* **28**, 115-124.

Imai, Y., Soda, M., Murakami, T., Shoji, M., Abe, K. and Takahashi, R.

(2003). A product of the human gene adjacent to parkin is a component of Lewy bodies and suppresses Pael receptor-induced cell death. *J. Biol. Chem.* **278**, 51901-51910.

Kohl, L., Sherwin, T. and Gull, K. (1999). Assembly of the paraflagellar rod and the flagellum attachment zone complex during the Trypanosoma brucei cell cycle. *J. Eukaryot. Microbiol.* **46**, 105-109.

Li, J. B., Gerdes, J. M., Haycraft, C. J., Fan, Y., Teslovich, T. M., May-Simera, H., Li, H., Blacque, O. E., Li, L., Leitch, C. C. et al. (2004). Comparative genomics identifies a flagellar and basal body proteome that includes the BBS5 human disease gene. *Cell* **117**, 541-552.

Lindemann, C. B. and Kanous, K. S. (1997). A model for flagellar motility. *Int. Rev. Cytol.* **173**, 1-72.

Lockhart, P. J., O'Farrell, C. A. and Farrer, M. J. (2004). It's a double knock-out! The quaking mouse is a spontaneous deletion of parkin and parkin co-regulated gene (PACRG). *Mov. Disord.* **19**, 101-104.

Lorenzetti, D., Bishop, C. E. and Justice, M. J. (2004). Deletion of the Parkin coregulated gene causes male sterility in the quaking(viable) mouse mutant. *Proc. Natl. Acad. Sci. USA* **101**, 8402-8407.

McKean, P. G., Baines, A., Vaughan, S. and Gull, K. (2003). Gamma-tubulin functions in the nucleation of a discrete subset of microtubules in the eukaryotic flagellum. *Curr. Biol.* **13**, 598-602.

Minoura, I., Yagi, T. and Kamiya, R. (1999). Direct measurement of inter-doublet elasticity in flagellar axonemes. *Cell Struct. Funct.* **24**, 27-33.

Moreira-Leite, F. F., Sherwin, T., Kohl, L. and Gull, K. (2001). A trypanosome structure involved in transmitting cytoplasmic information during cell division. *Science* **294**, 610-612.

Ogbadoyi, E. O., Robinson, D. R. and Gull, K. (2003). A high-order trans-membrane structural linkage is responsible for mitochondrial genome positioning and segregation by flagellar basal bodies in trypanosomes. *Mol. Biol. Cell* **14**, 1769-1779.

Olson, G. E. and Linck, R. W. (1977). Observations of the structural components of flagellar axonemes and central pair microtubules from rat sperm. *J. Ultrastruct. Res.* **61**, 21-43.

Ostrowski, L. E., Blackburn, K., Radde, K. M., Moyer, M. B., Schlatzer, D. M., Moseley, A. and Boucher, R. C. (2002). A proteomic analysis of human cilia: identification of novel components. *Mol. Cell Proteomics* **1**, 451-465.

Piperno, G., Mead, K. and Shestak, W. (1992). The inner dynein arms I2 interact with a "dynein regulatory complex" in Chlamydomonas flagella. *J. Cell Biol.* **118**, 1455-1463.

Ploubidou, A., Robinson, D. R., Docherty, R. C., Ogbadoyi, E. O. and Gull, K. (1999). Evidence for novel cell cycle checkpoints in trypanosomes: kinetoplast segregation and cytokinesis in the absence of mitosis. *J. Cell Sci.* **112**, 4641-4650.

Robinson, D. R. and Gull, K. (1991). Basal body movements as a mechanism for mitochondrial genome segregation in the trypanosome cell cycle. *Nature* **352**, 731-733.

Robinson, D. R., Sherwin, T., Ploubidou, A., Byard, E. H. and Gull, K. (1995). Microtubule polarity and dynamics in the control of organelle positioning, segregation, and cytokinesis in the trypanosome cell cycle. *J. Cell Biol.* **128**, 1163-1172.

Rupp, G. and Porter, M. E. (2003). A subunit of the dynein regulatory complex in Chlamydomonas is a homologue of a growth arrest-specific gene product. *J. Cell Biol.* **162**, 47-57.

Sampson, M. J., Decker, W. K., Beaudet, A. L., Ruitenbeek, W., Armstrong, D., Hicks, M. J. and Craigen, W. J. (2001). Immotile sperm and infertility in mice lacking mitochondrial voltage-dependent anion channel type 3. *J. Biol. Chem.* **276**, 39206-39212.

Satouh, Y., Padma, P., Toda, T., Satoh, N., Ide, H. and Inaba, K. (2005). Molecular characterization of radial spoke subcomplex containing radial spoke protein 3 and heat shock protein 40 in sperm flagella of the ascidian Ciona intestinalis. *Mol. Biol. Cell* **16**, 626-636.

Sherwin, T. and Gull, K. (1989). The cell division cycle of Trypanosoma brucei brucei: timing of event markers and cytoskeletal modulations. *Philos. Trans. R. Soc. London B Biol. Sci.* **323**, 573-588.

Sidman, R. L., Dickie, M. M. and Appel, S. H. (1964). Mutant mice (quaking and jimpy) with deficient myelination in the central nervous system. *Science* **144**, 309-311.

Smith, E. F. and Lefebvre, P. A. (1997). The role of central apparatus components in flagellar motility and microtubule assembly. *Cell Motil. Cytoskeleton* **38**, 1-8.

Soares, H., Penque, D., Mouta, C. and Rodrigues-Pousada, C. (1994). A Tetrahymena orthologue of the mouse chaperonin subunit CCT gamma and its coexpression with tubulin during cilia recovery. *J. Biol. Chem.* **269**, 29299-29307.

Stephens, R. E. (1970). Isolation of Nexin – The linkage protein responsible for the maintenance of the nine-fold configuration of flagellar axonemes. *Biol. Bull.* **139**, 438.

Stephens, R. E. (1997). Synthesis and turnover of embryonic sea urchin ciliary proteins during selective inhibition of tubulin synthesis and assembly. *Mol. Biol. Cell* **8**, 2187-2198.

Stephens, R. E. and Edds, K. T. (1976). Microtubules: structure, chemistry, and function. *Physiol. Rev.* **56**, 709-777.

Stephens, R. E. and Lemieux, N. A. (1999). Molecular chaperones in cilia and flagella: implications for protein turnover. *Cell Motil. Cytoskeleton* **44**, 274-283.

Thompson, J. D., Gibson, T. J., Plewniak, F., Jeanmougin, F. and Higgins, D. G. (1997). The CLUSTAL X windows interface: flexible strategies for multiple sequence alignment aided by quality analysis tools. *Nucleic Acids Res.* **25**, 4876-4882.

Warner, F. D. (1976). Ciliary inter-microtubule bridges. *J. Cell Sci.* **20**, 101-114.

Warr, J. R., McVitte, A., Randall, J. and Hopkins, J. M. (1966). Genetic control of flagellar structure in Chlamydomonas reinhardtii. *Genet. Res.* **7**, 335-351.

West, A. B., Lockhart, P. J., O'Farell, C. and Farrer, M. J. (2003). Identification of a novel gene linked to parkin via a bi-directional promoter. *J. Mol. Biol.* **326**, 11-19.

Wickstead, B., Ersfeld, K. and Gull, K. (2002). Targeting of a tetracycline-inducible expression system to the transcriptionally silent minichromosomes of Trypanosoma brucei. *Mol. Biochem. Parasitol.* **125**, 211-216.

Williams, N. E. and Nelsen, E. M. (1997). HSP70 and HSP90 homologs are associated with tubulin in hetero-oligomeric complexes, cilia and the cortex of Tetrahymena. *J. Cell Sci.* **110**, 1665-1672.

Wirtz, E., Leal, S., Ochatt, C. and Cross, G. A. (1999). A tightly regulated inducible expression system for conditional gene knock-outs and dominant-negative genetics in Trypanosoma brucei. *Mol. Biochem. Parasitol.* **99**, 89-101.

Witman, G. B., Plummer, J. and Sander, G. (1978). Chlamydomonas flagellar mutants lacking radial spokes and central tubules. Structure, composition, and function of specific axonemal components. *J. Cell Biol.* **76**, 729-747.

Woods, A., Sherwin, T., Sasse, R., MacRae, T. H., Baines, A. J. and Gull, K. (1989). Definition of individual components within the cytoskeleton of Trypanosoma brucei by a library of monoclonal antibodies. *J. Cell Sci.* **93**, 491-500.

Woolley, D. M. (1997). Studies on the eel sperm flagellum. I. The structure of the inner dynein arm complex. *J. Cell Sci.* **110**, 85-94.

Yang, C., Compton, M. M. and Yang, P. (2005). Dimeric novel HSP40 is incorporated into the radial spoke complex during the assembly process in flagella. *Mol. Biol. Cell* **16**, 637-648.

Journal of Cell Science

ETTERS

lagellar motility is required for the viability of the loodstream trypanosome

hard Broadhead[1]*, Helen R. Dawe[2]*, Helen Farr[2]*, Samantha Griffiths[2]*, Sarah R. Hart[3]*, Neil Portman[2]*, chael K. Shaw[2], Michael L. Ginger[2], Simon J. Gaskell[3], Paul G. McKean[1] & Keith Gull[2]

e 9+2 microtubule axoneme of flagella and cilia represents one the most iconic structures built by eukaryotic cells and organ-s. Both unity and diversity are present among cilia and flagella the evolutionary as well as the developmental scale. Some cilia motile, whereas others function as sensory organelles and can iously possess 9+2 and 9+0 axonemes and other associated uctures[1]. How such unity and diversity are reflected in molecu-repertoires is unclear. The flagellated protozoan parasite *panosoma brucei* is endemic in sub-Saharan Africa, causing astating disease in humans and other animals[2]. There is little pe of a vaccine for African sleeping sickness and a desperate d for modern drug therapies[3]. Here we present a detailed teomic analysis of the trypanosome flagellum. RNA inter-ence (RNAi)-based interrogation of this proteome provides ctional insights into human ciliary diseases and establishes t flagellar function is essential to the bloodstream-form try-nosome. We show that RNAi-mediated ablation of various oteins identified in the trypanosome flagellar proteome leads a rapid and marked failure of cytokinesis in bloodstream-form t not procyclic insect-form) trypanosomes, suggesting that pairment of flagellar function may provide a method of disease ntrol. A postgenomic meta-analysis, comparing the evolutiona-y ancient trypanosome with other eukaryotes including mans, identifies numerous trypanosome-specific flagellar oteins, suggesting new avenues for selective intervention.

Flagellum-mediated migration between the gut and salivary nds of its tsetse fly vector is essential for progression of the panosome life cycle. However, the necessity for motility in an tracellular bloodstream-form trypanosome is unclear. In both ms, a single attached flagellum emerges from a posterior flagellar cket (Fig. 1a) and comprises a membrane-bound axoneme and sociated paraflagellar rod (PFR; Fig 1b). We isolated the structural oneme and associated PFR and basal body from procyclic trypano-mes by a well-characterized procedure of detergent and high-salt atment[4]. Bands and spots were cut from one- (Fig. 1c) and two-mensional gels and digested with trypsin, and the resulting ptides analysed by reverse-phase high-performance liquid chroma-graphy coupled with tandem mass spectrometry. Bands and spots cised from ten representative gels were analysed, resulting in the ntification of 522 nonredundant proteins.

Further manual mass spectrometric validation confirmed 380 oteins (see Supplementary Methods and Supplementary Fig. 1 peptide numbers and coverage). Highly basic proteins are known contaminate microtubule preparations owing to charge inter-ions[4], and we noted some highly basic ribosomal proteins as cognizable contaminants. To limit contamination, we filtered the ta by using an isolectric point (pI) value of 10.2 as a cut-off (the pI of the most acidic ribosomal protein), and placed 49 proteins (30 of which were ribosomal proteins) in a separate pool undoubtedly containing some genuine flagella components (for example, TbDIP13). The remaining 331 proteins constitute a *T. brucei* flagellum proteome (TbFP) characterized by both the inclusion of many known flagellar proteins and a lack of proteins from other subcellular compartments.

We subjected the TbFP to an *in silico* screen, testing which of these 331 proteins (and the pI-filtered set) were encoded in genomes of flagellated and non-flagellated eukaryotes (Supplementary Fig. 1). The TbFP is characterized by the absence of homologues in the genomes of non-flagellated eukaryotes (land plants, fungi and red algae; Fig. 1d). Shared components, such as α- or β-tubulin, are expected. We found that many TbFP proteins have homologues in the related trypanosomatid parasites *Trypanosoma cruzi* (312) and *Leishmania major* (286). Conservation of homologues between trypanosomatids and other flagellates reflects known structural differences among flagella of evolutionarily divergent organisms, being highest in *Tetrahymena*, human and *Chlamydomonas* (Fig. 1d). We found a much reduced proportion of homologues shared with *Plasmodium*, *Caenorhabditis* and *Drosophila*, which build motile or sensory cilia that are divergent in aspects of axoneme or basal body structure or formation[5]. We found that 208 TbFP proteins (Fig. 1d) are trypanosomatid-specific and probably represent organism-specific flagellar structures and functions. Although these most obviously include the PFR, some are likely to be axonemal.

Several studies have sought to identify components of the eukaryotic flagellum by proteomic[6–9] or bioinformatic[10,11] strategies. Although highly informative, bioinformatic and comparative genomic approaches exclude genuine conserved flagella components that have homologues and orthologues in non-flagellates. Similarly, occurrence of a protein in proteomes reflects the biochemical nature of the purified material. The TbFP, the *Tetrahymena thermophila* ciliome[9] and the axonemal fraction of the *Chlamydomonas* flagellar proteome[8] are data sets derived from comparable preparations of insoluble flagellar architectures, with shared and organism-specific structures. To carry out a meta-analysis of these three data sets (Fig. 1e), we devised a stringent reciprocal BLASTP protocol that necessitated reanalysis of each data set to acquire the most current gene models available. After unification by applying the pI filter to all data sets, we undertook three reciprocal pairwise comparisons. We found that the TbFP contains the largest number of proteins in any of the three data sets. The presence of the PFR, an extra-axonemal, trypanosome-specific structure might explain the large number of proteins not encoded in the genomes of the other two organisms (indeed, the TbFP contains all of the known PFR proteins). However,

partment of Biological Sciences, Lancaster University, Lancaster LA1 4YQ, UK. [2]Sir William Dunn School of Pathology, University of Oxford, South Parks Road, Oxford 3RE, UK. [3]Michael Barber Centre for Mass Spectrometry, School of Chemistry, University of Manchester, Sackville Street, Manchester M60 1QD, UK.
ese authors contributed equally to this work.

© 2006 Nature Publishing Group

the *Chlamydomonas* and *Tetrahymena* pairwise axoneme-only comparisons revealed correspondingly large cohorts not represented in e genome of the opposing organism. Thus, the structural homogeneity of the 9+2 axoneme seems to be dependent on a relatively few evolutionarily conserved proteins and masks considerable organism-specific elaborations that go beyond the presence of obvious extra-axonemal structures.

Present in the conserved subset are proteins with implications for human inherited diseases. Ciliary diseases are characterized by clinical presentations such as retinal degeneration, primary ciliary dyskinesia, hydrocephalus, polycystic kidney disease and polydactyly[1]. In addition to all three axonemal dyneins known to cause primary ciliary dyskinesia[12], interrogation of the TbFP identified homologues of a further seven proteins directly implicated in diseases of human, mouse or zebrafish (Supplementary Fig. 2a). This list includes Hydin[13], PACRG[14] and Scorpion[15]; two of these, TbHydin and TbPACRG, are validated functionally here for the first time to our knowledge. We determined the human chromosomal locus for every homologue represented in the TbFP, which identified 34 genes mapping to 25 loci where diseases with a clinical spectrum suggestive of ciliary dysfunction have been mapped genetically, but where the causal gene has not been identified. We suggest that these 34 genes (Supplementary Fig. 2b) represent candidates underlying syndromes including primary ciliary dyskinesia, polycystic kidney disease, macular and cone-rod dystrophies, retinitis pigmentosa, Rieger and BRESEK (see http://www.ncbi.nlm.nih.gov/entrez/query.fcgi?db=OMIM for syndrome details).

We subjected the orthologue of the cryptic hydrocephalus-inducing protein Hydin to functional analysis by using inducible RNAi in procyclic trypanosomes. This resulted in a severe motility defect, revealing an impairment of ciliary function as a likely explanation for the aetiology of this disease model (Fig. 2). A further ten TbFP proteins were interrogated by this RNAi approach (Fig. 2a), eight of which (including the trypanosome-specific proteins PFR2 and HERTS) showed a flagellar phenotype on ablation (Fig. 2a). All mutants were viable except one in which flagellar detachment caused pleiotropic effects[16]. Two genes (*TbPACRGA* and *TbPACRGB*) comprise a gene family in *T. brucei* and gave no phenotype on individual ablation. Simultaneous knockdown, however, produced paralysed flagella, suggesting functional redundancy.

The high success rate of the RNAi interrogation provides experimental evidence for the integrity of the TbFP. These phenotypes extend the catalogue of trypanosome flagellar RNAi mutants, which have all been made in the procyclic form[16–19], and show that motility can be severely compromised while proliferation remains unaffected. We extended our functional interrogation by carrying out RNAi against five proteins in our TbFP validation set in bloodstream-form trypanosomes (Supplementary Fig. 3a). Unexpectedly, we found that all five RNAi analyses resulted in bloodstream-form trypanosomes that did not complete cytokinesis, yielding monstrous cells with an inability to proliferate (Fig. 3 and Supplementary Fig. 3b–h). This striking contrast to the viable RNAi phenotypes produced in

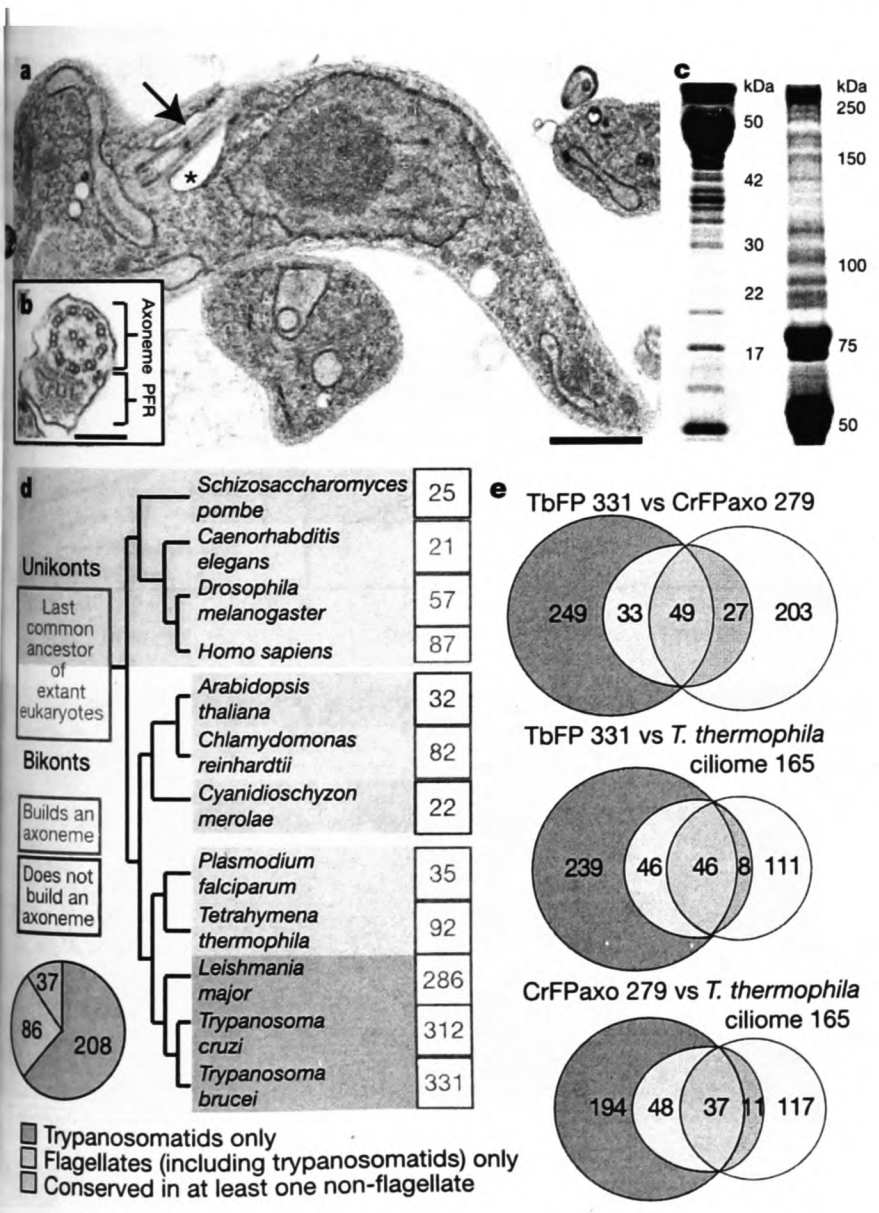


Figure 1 | The *T. brucei* flagellar proteome. **a**, Transmission electron micrograph showing the flagellum (arrow) and flagellar pocket (asterisk). **b**, The 9+2 axoneme and the PFR. **c**, One-dimensional electrophoretic separation of isolated flagella. **d**, Distribution of TbFP protein homologues. **e**, Comparison of the *T. brucei*, *Chlamydomonas reinhardtii* (CrFPaxo) and *T. thermophila* flagellar proteomes. For each comparison, green indicates present in both; orange/red indicates present in opposing genome but not opposing proteome; blue/yellow indicates no homologue in opposing genome. Homology determined by alignment to each genome with reciprocal alignment by BLASTP. Scale bars, 1 μm (**a**); 200 nm (**b**).

a

Accession number	Name	*T. brucei*	*T. cruzi*	*L. major*	*C. merolae*	*A. thaliana*	*S. pombe*	*H. sapiens*	*C. reinhardtii*	*D. melanogaster*	*C. elegans*	*T. thermophila*	*P. falciparum*	Procyclic RNAi phenotypes: Motility defect?	Flagellum made?	Cytokinesis defect?
Tb927.4.2140	TbMBO2	+	+	+	x	x	x	+	+	x	x	+	x	Yes	Yes	No
Tb927.8.5000	PFR2	+	+	+	x	x	x	x	x	x	x	x	x	Yes	Yes	No
Tb11.01.0680	HERTS	+	+	+	x	x	x	x	x	x	x	x	x	Yes	Yes	No
Tb927.6.4670	TbCMRP	+	+	+	x	+	x	x	+	+	+	+	+	Yes	Yes	No
Tb11.01.2670	MENG	+	+	+	x	x	x	+	+	+	x	+	x	Yes	Yes	No
Tb927.4.3130	TbSpef1	+	+	+	x	x	x	+	+	+	x	+	+	Yes	Yes/detached	Severe
Tb927.8.4870	DIGIT	+	+	+	x	x	x	+	+	+	x	+	+	Yes	Yes	No
Tb927.6.3150	TbHydin	+	+	+	x	x	x	+	+	x	x	+	x	Yes	Yes	Minor
Tb09.211.1790	TAX-1	+	+	+	x	x	x	+	+	x	x	x	x	Yes	Yes	No
Tb927.3.2310	TbPACRGA	+	+	+	x	x	x	+	+	+	x	+	x	No	Yes	No
Tb09.211.1470	TbPACRGB	+	+	+	x	x	x	x	x	x	x	x	x	No	Yes	No
Tb927.3.2310 & Tb09.211.1470	TbPACRGA and TbPACRGB simultaneous ablation													Yes	Yes	Minor

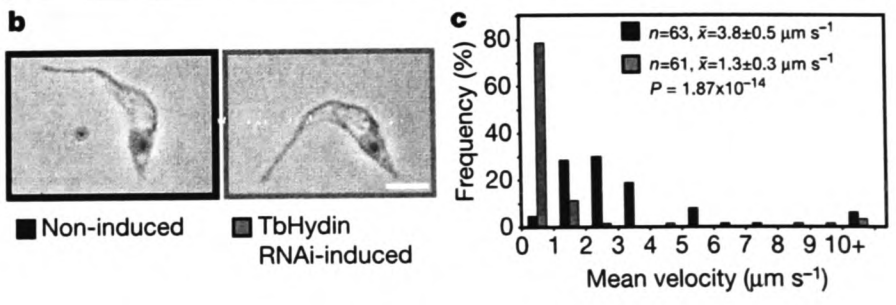


Figure 2 | Biological verification of the *T. brucei* flagellar proteome. **a**, Biological validation of the TbFP by RNAi of procyclic trypanosomes, showing phylogenetic distribution and RNAi phenotype. '+' indicates presence of homologues; 'x' indicates absence of homologues. **b**, **c**, Phenotype of *T. brucei* Hydin (TbHydin). On RNAi induction the flagellum is built (**b**), but motility is severely compromised in individual cells and the cell population (**c**). Scale bar, 5 μm (**b**). Blue indicates non-induced control; red indicates TbHydin RNAi-induced. *P* value determined by Mann–Whitney *U*-test. Population statistic given as the mean ± s.e.m.

© 2006 Nature Publishing Group

cyclic cells is shown in Fig. 3a–c. In each case, RNAi induction led n inhibition of cytokinesis.

rypanosomes have one kinetoplast (mitochondrial DNA) and nucleus (1K1N), and replicate these once during a cell cycle[20]; on Ai induction, however, bloodstream cells ceased dividing but tinued to progress through the cell cycle. Cells initiated new rounds ; phase and mitosis, leading to large contorted cells containing ltiple kinetoplasts and nuclei (Fig. 3d, i, j). At 24 h after induction, RNAi-induced population of 'monsters' contained large numbers 4K4N and 8K8N cells (Fig. 3d).

included in the bloodstream RNAi set were newly identified gellar proteins such as TAX-1, TbPACRGA and DIGIT in addition an orthologue (TbMBO2) of a *Chlamydomonas* protein known to ulate motility[21]. Given the implications of these observations, we ted whether the well-characterized procyclic *snl* mutant pheno-e[17,18] (paralysed but viable) of the *T. brucei* specific PFR2 protein s different in the bloodstream form. We found that this mutant o produced a rapid, lethal and unusual phenotype with pro-ction of monstrous cells. Notably, the same construct expressed procyclic cells reproduced the published paralysed, but viable, enotype (Fig. 2a).

A very particular phenotype led to the death of bloodstream cells. induced cells had a normal morphology (Fig. 3e), producing a w flagellum during the cell cycle before cytokinesis, with the gellum emerging from the flagellar pocket and extending along trypanosome. On RNAi induction, cells produced new flagella but l not complete division and lost all normal morphogenetic axes, coming monstrously contorted and multiflagellated (Fig. 3f–h). in-section electron microscopy showed that the cell periphery s highly convoluted; multiple nuclei were present and some gella were attached to the outside of the cell, while others were located in a highly enlarged flagellar pocket (Fig. 3i, j and Supplementary Fig. 3b, c, f, g). There were also many flagella with two axonemes, which could be either parallel or antiparallel, indicative of a total loss of morphogenetic patterning (Supplementary Fig. 3d, e). These characteristics are also found in the TbMBO2 and DIGIT phenotypes (Supplementary Fig. 3f, g). Examination of the flagellar pockets indicated that although large they still showed clathrin-coated pits, suggesting that endocytotic processes were operating to some extent (for example, in the TAX-1 phenotype; Supplementary Fig. 3h).

The explanation for the lethal phenotype in bloodstream cells is that cytokinesis fails as a primary event in the absence of correct flagellar motility. Subsequent rounds of the cell cycle compound these events as new flagella and pockets are formed at inappropriate locations. The lack of precise morphogenetic axes in the resulting 'monstrous cells' leads to pleiotropic effects compromising membrane–cytoskeletal balance during morphogenesis of the pocket structure. Examination of endocytosis shows that the multiple pockets are active and can facilitate entry of antibodies and lectins. However, there is much variation in their individual capacity for vectorial internalization to nearby endomembrane compartments (Supplementary Fig. 4). An imbalance in the known high flux of endocytosis in the bloodstream form[22], coupled with a focus of the secretory pathway on particular pockets in a multiflagellated cell, will lead to the large flagellar pocket phenotype as a secondary event.

In summary, we have shown that flagellum function cannot be compromised and is essential in the bloodstream trypanosome. The severity of the phenotype, its rapid onset, its lethality and its occurrence after the ablation of proteins of diverse function and location in either the axoneme or the trypanosome-specific PFR is highly significant. Coupled with our identification of a set of trypanosome-specific proteins in the TbFP, this suggests that impair-

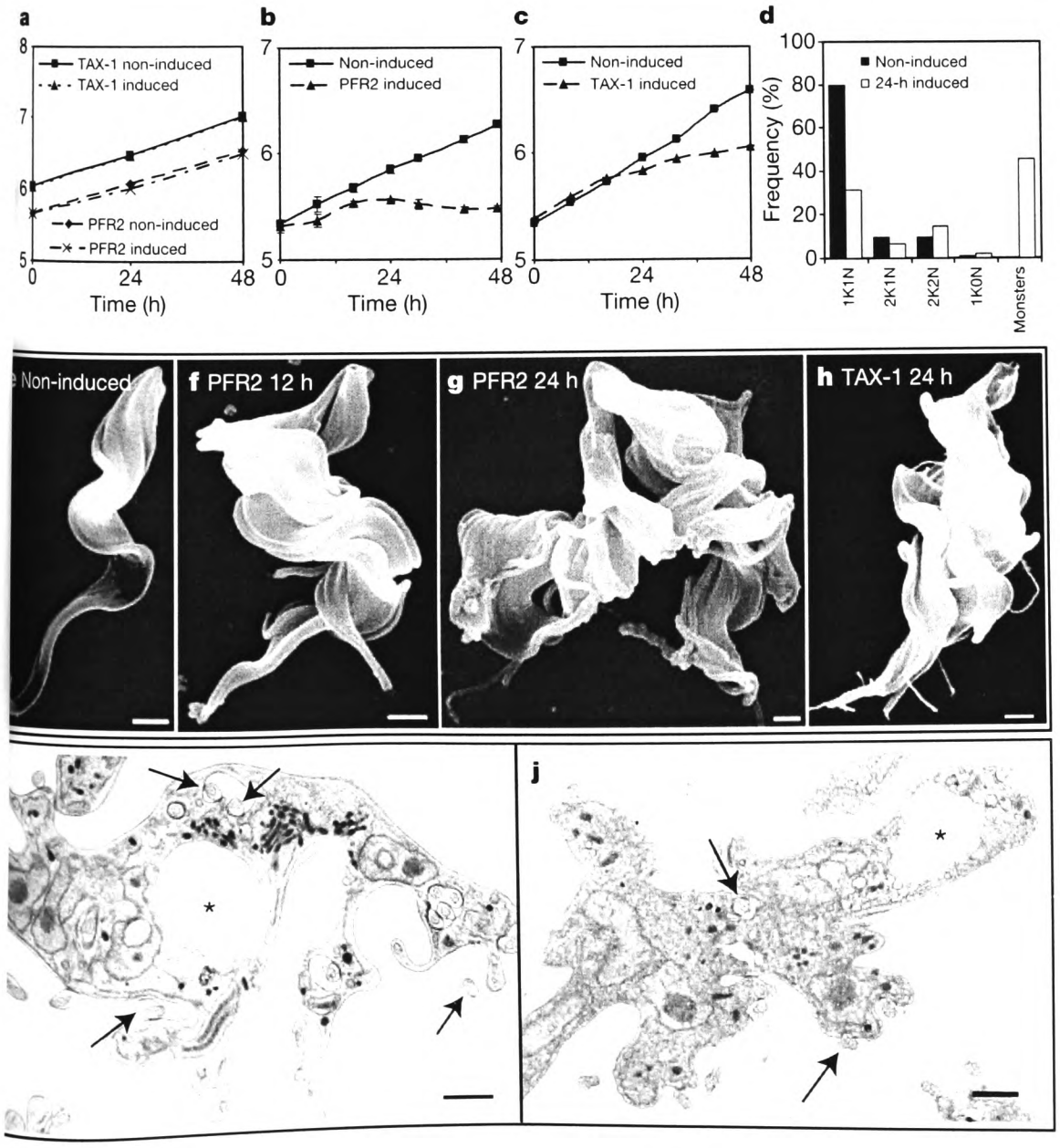


Figure 3 | Flagellar motility is essential for bloodstream trypanosomes. **a–c**, Ablation of PFR2 and TAX-1 affects growth in bloodstream (**b**, **c**), but not procyclic (**a**), forms. **d**, Numbers of cells with multiple nuclei and kinetoplasts increase after ablation of TAX-1 in bloodstream forms. **e–h**, Scanning electron micrograph showing bloodstream-form morphogenesis before (**e**) and after (**f–h**) ablation of PFR2 and TAX-1 flagellar proteins. **i, j**, Transmission electron microscopy analysis of PFR2 (**i**) and TAX-1 (**j**) ablation in bloodstream forms. Arrows denote axonemes; asterisks denote flagellar pockets (**i**, **j**). Scale bar, 1 μm.

© 2006 Nature Publishing Group

pent of flagellar function may provide an avenue for disease control n African sleeping sickness.

METHODS

Preparation of flagella proteins for mass spectrometry. Procyclic *T. brucei* cells were collected by centrifugation (800*g*, 10 min), washed once in PBS containing 1 μM E-64d, and resuspended in PEME (100 mM PIPES, 2 mM EGTA, 0.1 mM EDTA and 1 mM $MgSO_4$; pH 6.9) containing 1% Nonidet P40, 1× Focus protease-arrest mix (Calbiochem), 7.5 μM Pepstatin A and 5 μM E-64d. Cytoskeletons were collected by centrifugation and subjected to two rounds of salt extraction with PEME containing 1 M NaCl, 200 μg ml^{-1} of DNaseI, 50 μg ml^{-1} RNaseA, 1× Focus protease-arrest mix, 7.5 μM Pepstatin A and 5 μM E-64d at 4 °C for 10 min. Flagella pellets were collected by centrifugation (16,000*g*, 15 min, 4 °C), washed twice in PEME and resuspended in Laemmli buffer[23]. Proteins from 6×10^8 cell equivalents were resolved by one-dimensional SDS–PAGE (using standard protocols) and two-dimensional SDS–PAGE (see Supplementary Methods) and visualized by staining with Coomassie blue. Regions, bands and spots were excised, digested with trypsin and analysed by mass spectrometry. Verification of the goodness of fit of putative matches to predicted protein sequences was done manually (see Supplementary Methods). All data that yielded information used to construct the TbFP will be uploaded to the EBI Proteomics Identification database (http://www.ebi.ac.uk/pride/), a public data repository. This resource is freely available for use by the proteomics community.

Analysis of the TbFP. A detailed description of the reciprocal BLASTP[24] protocol used in comparative analysis is given in Supplementary Methods. Genetic loci containing human homologues of TbFP proteins were identified and compared to the following: first, loci implicated in known cilia-related diseases and diseases of unknown cause where the clinical presentation suggests a defect in cilia or flagella function (derived from OMIM: http://www.ncbi.nlm.nih.gov/entrez/query.fcgi?db=OMIM&itool=toolbar); second, the RetNet database of retinal disorders (http://www.sph.uth.tmc.edu/Retnet/); third, human orthologues of mouse infertility models[25]; and last, genes that cause polycystic kidney disease in zebrafish[15].

Trypanosome cell culture and RNAi. Procyclic (427, 29-13 and derivatives) and bloodstream (90-13 and derivatives) cell lines were maintained and transfected by standard methods[26]. Cell growth was monitored by a CASY1 cell-counter and analyser system (Schärfe System GmbH). RNAi studies were carried out with 400–600 base-pair fragments of *T. brucei* coding sequence, which were amplified by PCR from genomic DNA and cloned into the inducible RNAi vector p2T7-177 (ref. 27). Primer sequences are given in Supplementary Methods. For counts of nuclei and kinetoplast number, cells were fixed in 3.6% paraformaldehyde in PBS and dried onto microscope slides. 4,6-Diamidino-2-phenylindole (DAPI) was used to visualize DNA. We counted 500 cells at each time point. Motility analyses were done essentially as described[28]: time-lapse sequences were captured every 2 s for 40 s by using phase-contrast microscopy at ×10 magnification and 22 °C. Mean velocities were determined for individual cells and for each cell line collectively. Statistical significance was tested by a two-tailed Mann–Whitney *U*-test because samples varied in size and distributions were not suited to parametric testing. All analyses showed significance at $\alpha = 0.01$ with the exception of TbPACRGA and TbPACRGB single knockdowns, which were not significant at this level.

Electron microscopy. For thin-section electron microscopy, cells were fixed in 2.5% glutaraldehyde, 2% paraformaldehyde and 0.1% picric acid in 100 mM phosphate (pH 6.5) for 2 h at 4 °C followed by post-fixation in 1% osmium tetraoxide in 100 mM phosphate buffer (pH 6.5) with 50 mM sucrose for 1 h at 4 °C. The fixed material was stained *en bloc* with 2% aqueous uranyl acetate for 2 h at 4 °C, dehydrated, and embedded in epon resin. For scanning electron microscopy, samples were prepared essentially as described[29].

Received 8 November; accepted 14 December 2005.

1. Afzelius, B. A. Cilia-related diseases. *J. Pathol.* **204**, 470–477 (2004).
2. Sternberg, J. M. Human African trypanosomiasis: clinical presentation and immune response. *Parasite Immunol.* **26**, 469–476 (2004).
3. Steverding, D. & Tyler, K. M. Novel antitrypanosomal agents. *Expert Opin. Invest. Drugs* **14**, 939–955 (2005).
4. Robinson, D., Beattie, P., Sherwin, T. & Gull, K. Microtubules, tubulin, and microtubule-associated proteins of trypanosomes. *Methods Enzymol.* **196**, 285–299 (1991).
5. Briggs, L. J., Davidge, J. A., Wickstead, B., Ginger, M. L. & Gull, K. More than one way to build a flagellum: comparative genomics of parasitic protozoa. *Curr. Biol.* **14**, R611–R612 (2004).
6. Ostrowski, L. E. *et al.* A proteomic analysis of human cilia: identification of novel components. *Mol. Cell. Proteomics* **1**, 451–465 (2002).
7. Padma, P. *et al.* Identification of a novel leucine-rich repeat protein as a component of flagellar radial spoke in the Ascidian *Ciona intestinalis*. *Mol. Biol. Cell* **14**, 774–785 (2003).
8. Pazour, G. J., Agrin, N., Leszyk, J. & Witman, G. B. Proteomic analysis of a eukaryotic cilium. *J. Cell Biol.* **170**, 103–113 (2005).
9. Smith, J. C., Northey, J. G., Garg, J., Pearlman, R. E. & Siu, K. W. Robust method for proteome analysis by MS/MS using an entire translated genome: demonstration on the ciliome of *Tetrahymena thermophila*. *J. Proteome Res.* **4**, 909–919 (2005).
10. Avidor-Reiss, T. *et al.* Decoding cilia function: defining specialized genes required for compartmentalized cilia biogenesis. *Cell* **117**, 527–539 (2004).
11. Li, J. B. *et al.* Comparative genomics identifies a flagellar and basal body proteome that includes the *BBS5* human disease gene. *Cell* **117**, 541–552 (2004).
12. Chodhari, R., Mitchison, H. M. & Meeks, M. Cilia, primary ciliary dyskinesia and molecular genetics. *Paediatr. Respir. Rev.* **5**, 69–76 (2004).
13. Davy, B. E. & Robinson, M. L. Congenital hydrocephalus in *hy3* mice is caused by a frameshift mutation in *Hydin*, a large novel gene. *Hum. Mol. Genet.* **12**, 1163–1170 (2003).
14. Lorenzetti, D., Bishop, C. E. & Justice, M. J. Deletion of the Parkin coregulated gene causes male sterility in the *quaking(viable)* mouse mutant. *Proc. Natl Acad. Sci. USA* **101**, 8402–8407 (2004).
15. Sun, Z. *et al.* A genetic screen in zebrafish identifies cilia genes as a principal cause of cystic kidney. *Development* **131**, 4085–4093 (2004).
16. Moreira-Leite, F. F., Sherwin, T., Kohl, L. & Gull, K. A trypanosome structure involved in transmitting cytoplasmic information during cell division. *Science* **294**, 610–612 (2001).
17. Bastin, P., Ellis, K., Kohl, L. & Gull, K. Flagellum ontogeny in trypanosomes studied via an inherited and regulated RNA interference system. *J. Cell Sci.* **113**, 3321–3328 (2000).
18. Bastin, P., Sherwin, T. & Gull, K. Paraflagellar rod is vital for trypanosome motility. *Nature* **391**, 548 (1998).
19. Hill, K. L. Biology and mechanism of trypanosome cell motility. *Eukaryot. Cell* **2**, 200–208 (2003).
20. Woodward, R. & Gull, K. Timing of nuclear and kinetoplast DNA replication and early morphological events in the cell cycle of *Trypanosoma brucei*. *J. Cell Sci.* **95**, 49–57 (1990).
21. Tam, L. W. & Lefebvre, P. A. The *Chlamydomonas MBO2* locus encodes a conserved coiled-coil protein important for flagellar waveform conversion. *Cell Motil. Cytoskeleton* **51**, 197–212 (2002).
22. Field, M. C. & Carrington, M. Intracellular membrane transport systems in *Trypanosoma brucei*. *Traffic* **5**, 905–913 (2004).
23. Laemmli, U. K. Cleavage of structural proteins during the assembly of the head of bacteriophage T4. *Nature* **227**, 680–685 (1970).
24. Altschul, S. F. *et al.* Gapped BLAST and PSI-BLAST: a new generation of protein database search programs. *Nucleic Acids Res.* **25**, 3389–3402 (1997).
25. Liska, F. Selected genetic aspects of male infertility—what animal models tell us. *Folia Biol. (Praha)* **49**, 129–141 (2003).
26. Wirtz, E. & Clayton, C. Inducible gene expression in trypanosomes mediated by a prokaryotic repressor. *Science* **268**, 1179–1183 (1995).
27. Wickstead, B., Ersfeld, K. & Gull, K. Targeting of a tetracycline-inducible expression system to the transcriptionally silent minichromosomes of *Trypanosoma brucei*. *Mol. Biochem. Parasitol.* **125**, 211–216 (2002).
28. Gadelha, C., Wickstead, B., de Souza, W., Gull, K. & Cunha-e-Silva, N. Cryptic paraflagellar rod in endosymbiont-containing kinetoplastid protozoa. *Eukaryot. Cell* **4**, 516–525 (2005).
29. Sherwin, T. & Gull, K. The cell division cycle of *Trypanosoma brucei brucei*: timing of event markers and cytoskeletal modulations. *Phil. Trans. R. Soc. Lond. B* **323**, 573–588 (1989).

Supplementary Information is linked to the online version of the paper at www.nature.com/nature.

Acknowledgements We thank the genome centres, particularly GeneDB at the Sanger Institute, and our laboratory colleagues, especially S. Gordon and P. Taylor, for access to unpublished data and constructive discussions. This work was funded by the Biotechnology and Biological Sciences Research Council, the Wellcome Trust, the Royal Society and the Edward P. Abraham Trust. M.L.G. is a Royal Society University Research Fellow; K.G. is a Wellcome Trust Principal Research Fellow.

Author Contributions The first six authors contributed equally to this work and are listed alphabetically. Individual contributions were as follows: R.B. proteomics and bioinformatic analysis; H.R.D. proteomics, bioinformatic and functional analyses; H.F. and S.G. functional analysis; S.R.H. proteomics; N.P. proteomics, bioinformatic and functional analyses.

Author Information Reprints and permissions information is available at npg.nature.com/reprintsandpermissions. The authors declare no competing financial interests. Correspondence and requests for materials should be addressed to K.G. (keith.gull@path.ox.ac.uk).

© 2006 Nature Publishing Group

Centriole/basal body morphogenesis and migration during ciliogenesis in animal cells

Helen R. Dawe*,‡, Helen Farr* and Keith Gull

Sir William Dunn School of Pathology, University of Oxford, South Parks Road, Oxford, OX1 3RE, UK

*These authors contributed equally to this work

‡Author for correspondence (e-mail: helen.dawe@path.ox.ac.uk)

Accepted 26 September 2006
Journal of Cell Science 120, 7-15 Published by The Company of Biologists 2007
doi:10.1242/jcs.03305

Summary

Cilia, either motile or immotile, exist on most cells in the human body. There are several different mechanisms of ciliogenesis, which enable the production of many kinds of cilia and flagella: motile and immotile, transient and long-lived. These can be linked to the cell cycle or associated with differentiation. A primary cilium is extended from a basal body analogous to the mitotic centrioles, whereas the several hundred centrioles needed to form the cilia of a multi-ciliated cell can be generated by centriolar or acentriolar pathways. Little is known about the molecular control of these pathways and most of our knowledge comes from ultrastructural studies. The increasing number of genetic diseases linked to dysfunctional cilia and basal bodies has renewed interest in this area, and recent proteomic and cell biological studies in model organisms have helped to shed light on the molecular components of these enigmatic organelles.

Key words: Cilia, Centriole, Flagellum, Primary cilium, Epithelia, Cell cycle, Basal body

Introduction

Cilia are found on virtually all cells in the human body; yet despite the importance of these organelles many aspects of their formation and function remain enigmatic. Cell biology textbooks usually pronounce that cilia and flagella are highly conserved structures containing a 9+2 microtubule axoneme made up of nine outer doublet microtubules and two single central pair microtubules (Fig. 1A) surrounded by a ciliary membrane. While it is true that this basic structure is well conserved throughout eukarya, and that 9+2 and 9+0 (lacking the central pair) axonemes are the most common, there are many variations in either the axoneme itself or in the presence of extra-axonemal structures that allow cilia, either motile or non-motile, and flagella to perform specialised functions in diverse organisms and cell types (Afzelius, 2004)[1].

The terms cilia and flagella are sometimes used interchangeably but there are differences: first, only one or two flagella are usually present on cells whereas motile cilia are usually found in higher multiples. This is a generalisation, however, because the sperm of the fern *Marsilea* and the gymnosperm Ginkgo are multiflagellate, displaying up to a thousand flagella (Myles, 1975; Vaughn and Renzaglia, 2006).

[1]Some exceptions to the canonical axoneme structure. The sperm of certain insects have complex axonemes: A 9+9+2 configuration made up of an outer ring of nine singlet microtubules surrounding nine doublets and a central pair is common [e.g. in honey bees (Lino-Neto et al., 2000), fire ants (Lino-Neto and Dolder, 2002) and stick insects (Afzelius, 1988; Afzelius et al., 1990)]. A 9+7 configuration is found in caddis flies whereas mosquitos of *Culex* spp have a 9+9+1 arrangement (Phillips, 1969). Limpet cilia contain nine outer doublets with five to ten central microtubules (Hackney et al., 1983; Phillips, 1979). The sperm flagellum of the gall midgefly is an extreme case: the axoneme is formed from up to 2500 doublets arranged in a double spiral (Mencarelli et al., 2000). Each doublet has only an outer dynein arm and there is no central pair. Extra-axonemal accessory structures are often found: examples include the outer dense fibres of many sperm (Fouquet and Kann, 1994) and the paraflagellar rod of kinetoplastid protozoa (Maga and LeBowitz, 1999).

Second, cilia move with a characteristic ciliary beat that is distinguished by an effective stroke followed by a recovery stroke, whereas flagellar motility usually consists of successive waves originating at either the base or the tip of the flagellum and propagated along its length. Again, there are exceptions to this: the single-celled parasitic protozoan *Trypanosoma brucei* is capable of both flagellar and ciliary beating (our unpublished observations). Third, cilia are often all of one developmental state whereas multiple flagella in the same cell may often be at different stages of development. Fourth, the term cilium is usually used to describe structures shorter than flagella. Fifth, rows of cilia can fuse to form specialised cirri or membranelles.

Flagella often move individual cells, such as mammalian sperm and protists. Cilia can be motile or non-motile and occur singly or in multiples. Multiple cilia are generally motile. They move single-celled protists such as *Tetrahymena* and, in metazoa, material such as mucosal fluids past epithelial cell layers. Single cilia are normally non-motile – the primary cilia on the surface of most mammalian cells are the most common (Wheatley et al., 1996), and much evidence suggests these play pivotal roles in normal tissue homeostasis and disease (reviewed by Davenport and Yoder, 2005), with cilium-generated Hedgehog and Wnt signalling being critical during development (reviewed by Scholey and Anderson, 2006). Certain tissues contain specialised cilia, including motile and non-motile nodal cilia (which are found exclusively in the embryonic node), the transient non-motile kinocilium of the inner ear and the highly modified non-motile connecting cilium of the retina.

As stated above, most axonemes consist of a ring of nine outer doublet microtubules held together by nexin linkages (Fig. 1); this is the basic structure of the primary cilium. Motile

cilia and flagella generally additionally have two singlet central pair microtubules, radial spokes and dynein arms, which are the molecular motors that enable microtubule sliding and consequent ciliary or flagellar beating. The dynein arms are attached to the A-tubule of each doublet such that their motor head domains are in close proximity to the B-tubule of the neighbouring doublet (Gibbons and Gibbons, 1973; Gibbons and Rowe, 1965). With the exception of early ultrastructural observations of cilia and flagella, much of the work on these has been carried out in single-celled organisms, particularly the green alga, *Chlamydomonas reinhardtii* (reviewed by Dutcher, 1995; Silflow and Lefebvre, 2001). Until recently the molecular composition of cilia and flagella was largely obscure. A combination of forward genetic mutational analysis and electrophoresis the *C. reinhardtii* flagella led to predictions that they to contain ~250 polypeptides (reviewed by Dutcher, 1995). More recent studies on a variety of model organisms have used proteomic (Andersen et al., 2003; Broadhead et al., 2006; Keller et al., 2005; Ostrowski et al., 2002; Pazour et al., 2005; Smith et al., 2005), transcriptomic (Blacque et al., 2005; Stolc et al., 2005) and genomic (Avidor-Reiss et al., 2004; Efimenko et al., 2005; Li et al., 2004) approaches and to suggest that the number is much greater. A database of cilia/flagella and basal body components identified in these studies can be found at the Ciliary Proteome Web Server at http://www.ciliaproteome.org/ (Gherman et al., 2006).

Studies primarily in algae have led to a model of ciliary/flagellar motility in which coordinate action of the central pair, radial spokes and dynein arms enable motility. It has been proposed that the central pair signals through the radial spokes to provide an asymmetric stimulus to the dynein motors associated with each of the outer doublet microtubules that enables a flagellar bend to be generated. One hypothesis for how this stimulus is generated relies on the rotation of the central pair microtubules observed in *Chlamydomonas* and *Paramecium* (Mitchell, 2003; Omoto and Kung, 1979; Omoto and Kung, 1980). However, this paradigm does not work for all systems: central pair rotation is not found in all organisms (Gadelha et al., 2006; Sale, 1986; Tamm and Tamm, 1981), which raises the question of how the central pair regulates motility in these systems.

All cilia are extended from a basal body. The Henneguy-Lenhossek theory, first postulated in 1898 and generally accepted today, proposed that these basal bodies are analogous to the mitotic centrioles (Henneguy, 1898; Lenhossek, 1898). Indeed the primary cilium is extended from a single basal body analogous to the pre-existing mature centriole in the cell. By contrast, in multi-ciliated epithelia, ciliogenesis begins with centriole multiplication that yields up to several hundred basal bodies. In both cases migration of the centrioles to the apical cell surface and acquisition of accessory structures follows. Once a centriole has docked with the cell membrane, it is known as a basal body. Finally, an axoneme is extended to form a cilium. Despite the overall similarities there are distinct differences in the mechanisms of formation of single cilia and cilia of multi-ciliated cells in terms of cell cycle regulation and control of centriole number. Our knowledge of the molecular mechanisms of ciliogenesis is largely restricted to intraflagellar transport (IFT), the bidirectional movement of particles along the doublet microtubules, which elongates and maintains the cilium. Many excellent reviews on IFT are available (e.g. Rosenbaum and Witman, 2002; Scholey, 2003). Here, we

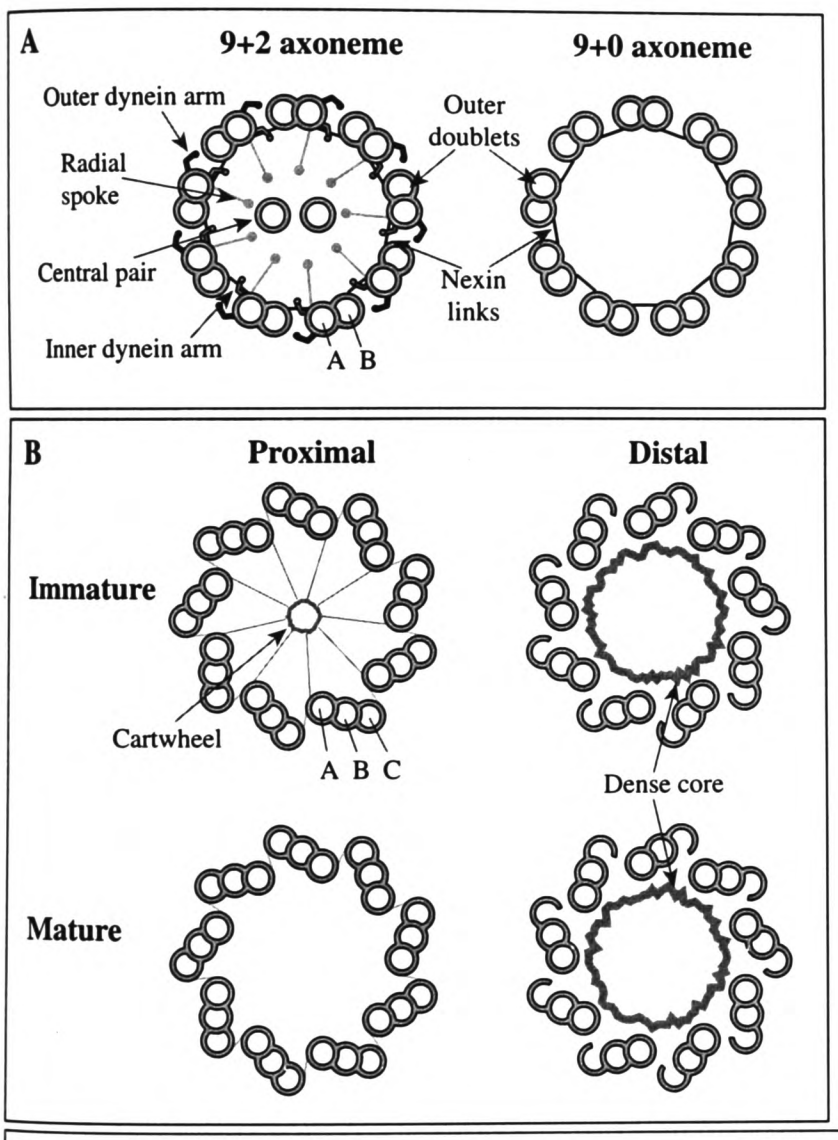


Fig. 1. Structures of centrioles and cilia. (A) The structure of the canonical motile 9+2 axoneme and its most common variation, the immotile 9+0 axoneme. (B) Schematic of a transverse section through the immature and mature centrioles. (C) Schematic of a longitudinal view of the mature centriole, showing the appendages, and a basal body with accessory structures.

instead focus on the earlier stages of ciliogenesis, comparing the ultrastructural details and molecular events that occur during formation of ciliated epithelia and solitary primary cilia.

Multiple pathways of ciliogenesis

At least six mechanisms for generation of cilia and flagella exist and the resulting cilia or flagella can be transient or long-lived (Anderson and Brenner, 1971; Brenner and Anderson, 1973; Flock and Duvall, 1965; Lemullois et al., 1988; Sherwin and Gull, 1989; Sobkowicz et al., 1995; Sorokin, 1968). These enable the production of many kinds of cilia, as well as sperm flagella (Fig. 2). They require various mechanisms for accurate control of centriole number, and there are variations in cell cycle control, in the timing of cilium production in the cell cycle, in the timing of centriole maturation and in whether a probasal body is associated with the cilium or flagellum basal body. Our focus here is on the five major mechanisms for formation of cilia; sperm flagella will not be dwelt upon further.

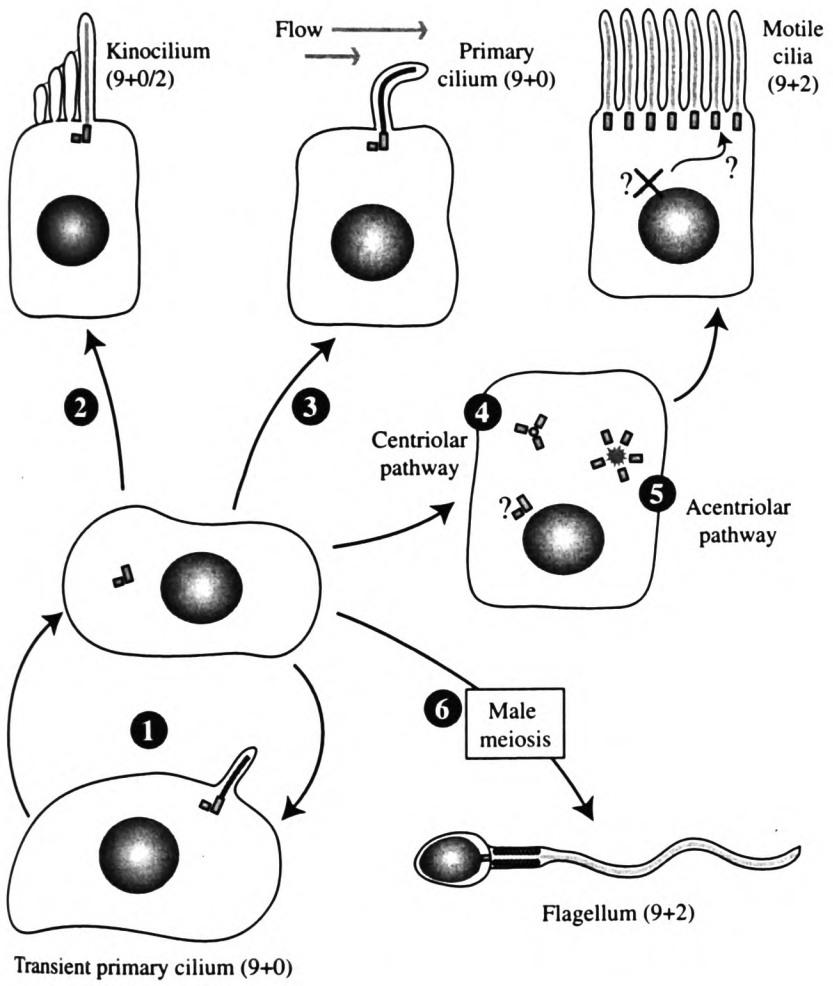


Fig. 2. Multiple pathways of ciliogenesis. Quiescent somatic cells use a single pre-existing mature centriole to subtend a transient primary cilium (Fig. 1 and ❶) lacking central pair microtubules, which is lost as the cell re-enters the cell cycle. In differentiated cells, several different types of single cilia can be produced from a mature centriole, such as the temporary (9+2 or 9+0) kinocilium (❷), which may or may not possess the central pair microtubules (Flock and Duvall, 1965; Sobkowicz et al., 1995) and the primary (9+0) cilium produced on the luminal epithelium of kidney tubules (❸). The pathways that produce several hundred cilia in epithelial cells in the mammalian airway are depicted at ❹ and ❺. Here, hundreds of centrioles are produced, duplicated either using the pre-existing centriole as a template (❹), or formed via a non-templated method (❺). The sperm flagellum produced in male meiosis is depicted at ❻. Green denotes 9+2 axonemes; dark blue denotes 9+0 axonemes; centrioles are shown in red; the deuterosome is shown in purple.

Centriole production

The centriole is a cylindrical structure 0.4 μm long and 0.2 μm in diameter, composed of microtubule triplets that display ninefold radial symmetry. The triplets are positioned around a cylindrical core with a slight twist and are composed of heterodimers of α- and β-tubulin. The immature centriole has a unique feature called the cartwheel (Vorobjev and Nadezhdina, 1987), which is made up of a central rod linked to the inner (A) tubule of each triplet by spokes (Fig. 1B). The mature centriole also has distinct appendages at the distal and subdistal regions (Fig. 1C) (Paintrand et al., 1992). The two centrioles are closely associated, usually in an orthogonal configuration, and surrounded by an amorphous mass of pericentriolar material (PCM) to form the centrosome.

Most differences between ciliogenesis in primary cilia and the cilia of multi-ciliated epithelia are observed in centriologenesis: a primary cilium forms from a pre-existing centriole whereas cilia of multi-ciliated epithelia require de novo production of many centrioles. Multi-ciliated epithelial cells are terminally differentiated. Primary cilia can be formed in quiescent somatic cells or in proliferating populations that make a primary cilium in G1. For cells that will form a primary cilium (Fig. 2, ❶-❸), centriole duplication is cell cycle related. The centriole pair duplicates once per cycle at S phase and maturation (see below) occurs later (Hinchcliffe et al., 1998; Lange and Gull, 1996; Sluder and Hinchcliffe, 1998; Vorobjev and Chentsov Yu, 1982). By contrast, centriole multiplication in cells that will become multi-ciliated (Fig. 2, ❹ and ❺) is differentiation related and often independent of the pre-existing centrioles (Anderson and Brenner, 1971; Dirksen, 1991). In this case, the centrioles that are made mature as they form.

Once formed, centrioles of ciliated cells migrate to the cell surface. For cells that form a primary cilium (Fig. 2, ❶ and ❸), the centriole remains associated with its procentriole daughter throughout ciliogenesis (Alieva and Vorobjev, 2004; Hagiwara et al., 2002; Jensen et al., 2004; Sorokin, 1968); those in multi-ciliated epithelia and the centriole subtending the kinocilium of the inner ear do not have associated procentrioles (Abughrien and Dore, 2000; Anderson and Brenner, 1971; Dirksen, 1971; Hagiwara et al., 1992; Kalnins et al., 1972; Sobkowicz et al., 1995; Sorokin, 1968). During maturation, centrioles acquire additional appendages such as transitional fibres and basal feet that stabilise the centriole/basal body, and IFT extends and maintains the axoneme. This occurs in both primary cilia and cilia of multi-ciliated cells (Rosenbaum and Witman, 2002).

Centriole duplication

During the cell division cycle the centrosome duplicates just before S phase; duplication requires the immature centriole-associated protein centrobin (Zou et al., 2005). Several serine/threonine kinases are implicated in the process, including Polo-like and Aurora kinases (Berdnik and Knoblich, 2002; Hannak et al., 2001; Lane and Nigg, 1996). A procentriole (Andre and Bernhard, 1964; Gall, 1961; Mizukami and Gall, 1966; Renaud and Swift, 1964) forms from the side of each centriole and elongates throughout S phase so that the cell possesses two pairs of centrioles as it

enters G2 phase. Only the mature centriole can produce a cilium. Maturation occurs over 1.5 cell cycles, the maturing centriole acquiring the unique fibrous distal and subdistal appendages mentioned above. Several protein components of these appendages have been identified, including ninein (Mogensen et al., 2000), ϵ-tubulin (Chang et al., 2003), centriolin (Gromley et al., 2003) and CEP110 (Ou et al., 2002). Cenexin is found exclusively at the mature mother centriole and its acquisition at the G2-M transition is a marker for maturation (Lange and Gull, 1995) and essential for appendage production (Ishikawa et al., 2005).

Centrioles are inherited by daughter cells in a semi-conservative manner (Kochanski and Borisy, 1990). Centrosome duplication and DNA regulation are coordinated by a complex pathway involving cyclin-E–Cdk2 (Hinchcliffe et al., 1999; Karsenti, 1999; Meraldi et al., 1999). Centrosome duplication is stimulated by Cdk2. Factors required for entry into S phase, such as Cdk2 and E2F, are required for centrosome duplication, and phosphorylation of the tumour suppressor Rb is also needed (Meraldi et al., 1999). Unduplicated G1 centrosomes are duplication competent, whereas G2 centrosomes placed under identical experimental conditions are not. This strongly suggests the centrosome itself blocks further centrosome duplication (Wong and Stearns, 2003); this might involve a physical connection between the mature and immature centrioles that prevents duplication until after mitosis (Tsou and Stearns, 2006). In most cell lines the centrosome will not re-duplicate during S phase, even in cells treated with hydroxyurea to prolong S phase (Balczon et al., 1995; Meraldi et al., 1999). However, in certain cell lines containing a mutant p53 tumour suppressor, extended cell cycle arrest leads to centrosome accumulation (D'Assoro et al., 2004), which suggests that centrosome duplication is uncoupled from cell division checkpoints in these cells.

Centriole multiplication

Multi-ciliated epithelial cells such as those in the mammalian trachea can each produce 200-300 centrioles during ciliogenesis. Two mechanisms of centriole production have been identified: the centriolar and acentriolar pathways, both of which can occur in a single cell (reviewed by Beisson and Wright, 2003). In contrast to centriole duplication during the cell division cycle, these pathways are linked to differentiation rather than proliferation, and multiple procentrioles are produced simultaneously, making this process distinct from the centriole duplication described above. In the centriolar pathway (Fig. 2, ❹), new centrioles are produced around an existing centriole. Unlike cell-cycle-dependent centriole duplication, however, more than one procentriole may be produced around a single centriole (Anderson and Brenner, 1971; Chang et al., 1979; Hagiwara et al., 1992; Sorokin, 1968; Steinman, 1968). Variations in the number of procentrioles observed could be attributable to the plane of the electron micrograph: among several procentrioles surrounding a centriole, two or three are seen only in glancing section (Sorokin, 1968); serial thin-section electron microscopy will be necessary to resolve the exact number of procentrioles formed in the centriolar pathway. The origin of the core centriole that produces these procentrioles is unclear. Neither the cartwheel, a marker for immature centrioles, nor appendages, present around mature centrioles, appear to be present. Thus the identity of the core centriole is unknown.

In the acentriolar pathway (Fig. 2, ❺), centrioles form around intermediary structures rather than an existing centriole (Anderson and Brenner, 1971; Chang et al., 1979; Dirksen, 1971; Dirksen and Crocker, 1966; Hagiwara et al., 1992; Kalnins et al., 1972; Lemullois et al., 1988; Sorokin, 1968; Sorokin and Adelstein, 1967; Steinman, 1968). The terminology for these intermediary structures is confused in the literature. We use the nomenclature system of Chang et al. (Chang et al. 1979) for the granular structures observed at the first stage of the acentriolar pathway. So-called dense granules (Fig. 3A) form clusters that can be associated with the existing centriole. Some molecular components of these dense granules have been identified: PCM-1 has been detected in them (Kubo et al., 1999) in addition to the striated rootlet protein p195 (Hagiwara et al., 2000). Centrin proteins localise close to granules in ciliogenic epithelial cells, which suggests that they are involved in an early stage of the acentriolar pathway (Laoukili et al., 2000). Dense granule clusters may condense to produce deuterosomes (Fig. 3B, arrowheads), around which

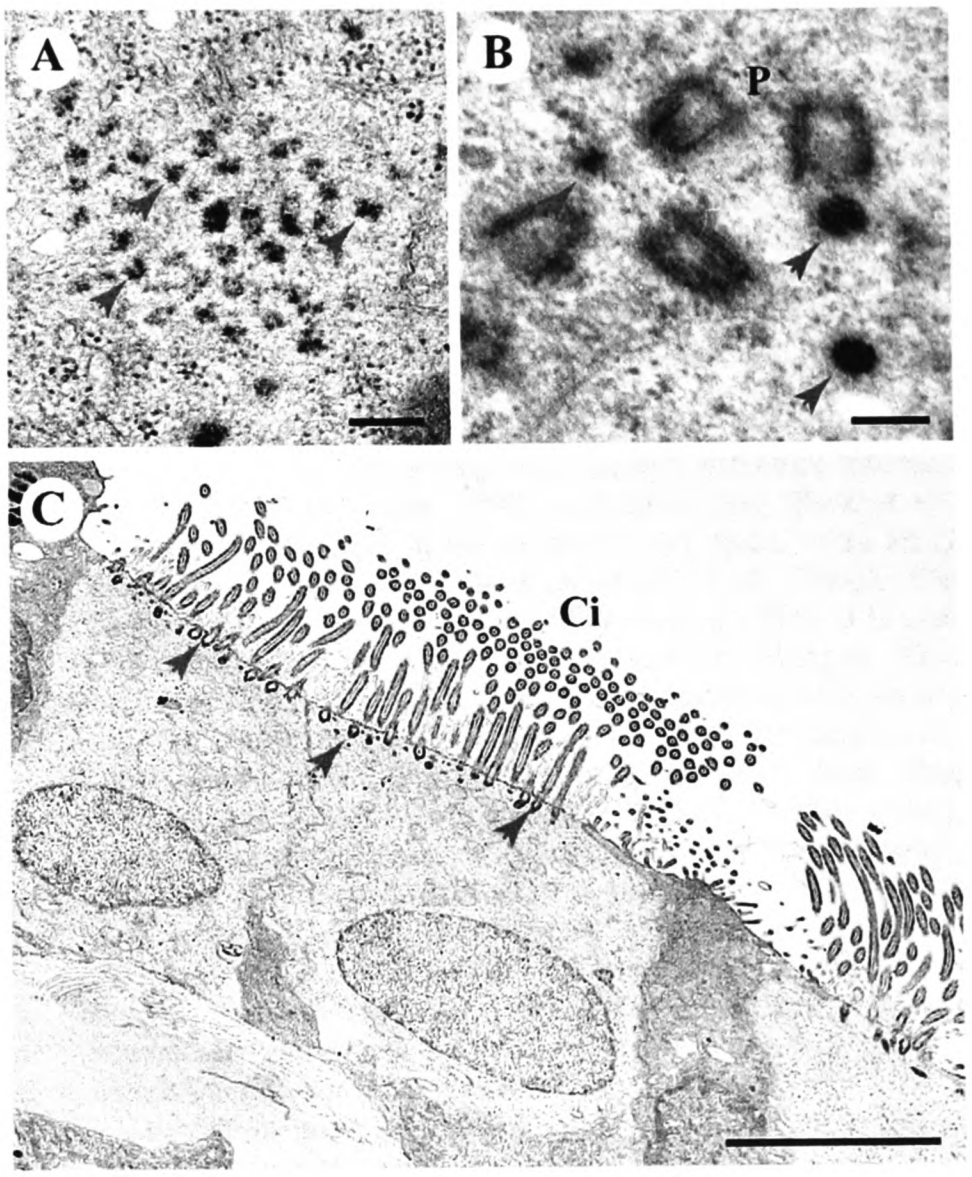


Fig. 3. Ciliogenesis in rat trachea. (A) The first visible stage in the acentriolar pathway is the appearance of dense granules (arrowheads). (B) Procentrioles (P) form around deuterosomes (arrowheads). (C) Mature ciliated cells. The procentrioles have docked with the apical membrane to become basal bodies (arrowheads) and have extended cilia (Ci). Scale bars (A) and (B)=200 nm; (C)=5 μm.

procentrioles (labelled P in Fig. 3B) develop. Two types of deuterosome exist, classified as solid or hollow on the basis of their ultrastructural appearance; there are organismal and size differences between the two (Dirksen, 1971; Dirksen, 1991; Hagiwara et al., 1992; Sorokin, 1968). The number of procentrioles around a deuterosome correlates with its size (Anderson and Brenner, 1971; Chang et al., 1979; Hagiwara et al., 1992; Kalnins et al., 1972; Sorokin, 1968). Serial thin-section electron microscopy reveals different numbers of procentrioles in each section (Anderson and Brenner, 1971). Thus the centriolar pathway may also produce more procentrioles than are seen in a single section, and there may be less variability in procentriole number in both the centriolar and acentriolar pathways in vivo than previously thought.

What happens to the pair of centrioles initially present in the cell during centriole multiplication? Several possible scenarios exist. First, the centriole pair could migrate to the surface and extend one of the motile cilia. This would imply that all centrioles are identical and that global control of ciliogenesis exists. Second, the two centrioles could migrate to the surface and extend a distinct, primary cilium prior to centriole multiplication and subsequent generation of the multiple motile cilia. This would suggest that an individual cell can form both 9+0 and 9+2 cilia, albeit at slightly different times. This phenomenon has been observed (Anderson and Brenner, 1971; Brenner and Anderson, 1973; Lemullois et al., 1988; Sorokin, 1968), and the presence of developing procentrioles around the mature basal body subtending a primary cilium (Anderson and Brenner, 1971; Sorokin, 1968) makes it probable that the same cell goes on to produce multiple cilia. In this case, the primary cilium is probably only transient, because none has been found in mature ciliated cells (Lemullois et al., 1988); it may function to pattern the apical surface in preparation for formation of motile cilia. The ultimate fate of its basal body – whether it later subtends a motile cilium or returns deeper into the cytoplasm – is unknown, but if it goes on to subtend a 9+2 cilium it is probable that the information needed to template a 9+0 cilium versus a 9+2 cilium does not lie within the centriole. Third, the mature centriole could remain in the cytoplasm. This would imply that existing centrioles are different from those produced by the centriolar and acentriolar pathways and that ciliogenesis is controlled at the level of individual centrioles. Although several studies have failed to observe isolated centrioles in ciliated cells (Anderson and Brenner, 1971; Lemullois et al., 1988; Lenhossek, 1898), one study has observed a centriole deep in the cytoplasm of a ciliated cell (Kalnins et al., 1972). Final resolution of these important questions will require tracking of individual centrioles in live cells during ciliogenesis.

Is cell-cycle-dependent duplication or centriole multiplication the default pathway in cells? Given the deleterious consequences of uncontrolled centriole proliferation, it could be argued that cell-cycle-dependent centriole duplication represents the default pathway. However, whereas most cells lacking centrioles undergo cell cycle arrest (Hinchcliffe et al., 2001), HeLa cells in which the centrosome has been surgically removed can produce multiple centrioles throughout the cytoplasm (La Terra et al., 2005). This implies that an existing centriole prevents production of further centrioles, and that newly synthesised centriole precursors destined for the existing centrosome will, in its absence, form multiple foci throughout the cytoplasm that produce centrioles independently of each other. This suggests that increased centriole production might be the default pathway for cells and that this is suppressed by an existing centriole. However, it is apparent that centriole production in HeLa cells must be uncoupled from the cell cycle and thus these cells do not necessarily represent the in vivo state.

Centriole migration and acquisition of accessory structures

How centrioles migrate during primary cilium formation remains unresolved, although the cytoskeleton is probably involved. Microtubules position the interphase centrosome (Burakov et al., 2003). The Rho-associated protein kinase p160ROCK maintains the position of the mature centriole (Chevrier et al., 2002); however, the upstream and downstream events remain unknown. In multi-ciliated cells, duplicated centrioles migrate towards the apical surface, where they dock to become basal bodies. Much evidence implicates the actin-myosin network in centriole migration in these cells. Actin and myosin are associated with centrioles or centriolar material (Klotz et al., 1986; Lemullois et al., 1988; Lemullois et al., 1987), and treatment of ciliogenic oviducts with agents that inhibit actin polymerisation (Boisvieux-Ulrich et al., 1990) or myosin function (Boisvieux-Ulrich et al., 1987) prevents centriole migration. Conversely, drugs that target the microtubule network do not directly stop migration (Boisvieux-Ulrich et al., 1989). In the ctenophore *Beroe*, centrioles are associated with parallel bundles of actin microfilaments arising in the basal cytoplasm and oriented towards the cell surface (Tamm and Tamm, 1988). They might therefore be pushed to the surface along actin tracks akin to the 'rocket-like' motility of intracellular bacteria (see Gouin et al., 2005; Machesky, 1999).

The signalling events regulating these processes also remain obscure. The planar cell polarity effectors inturned (*in*) (Collier and Gubb, 1997) and fuzzy (*fy*) (Park et al., 1996) are implicated in the control of an apical actin array essential for basal body docking (Park et al., 2006). The forkhead/winged helix family of transcription factors is also implicated in centriole migration and/or docking. One member, *Foxj1*, is expressed in ciliated epithelia (Blatt et al., 1999; Hackett et al., 1995; Lim et al., 1997; Pelletier et al., 1998; Tichelaar et al., 1999). *Foxj1*-null mice have situs defects and impaired ciliogenesis (Brody et al., 2000); centriologenesis appears unimpaired but centriole migration fails. The cysteine protease calpain, acting on the cytoskeletal linker protein ezrin, may regulate membrane anchoring (Gomperts et al., 2004), which suggests a need for localised regulation of cytoskeletal proteolysis. By contrast, factors regulating centriole migration during primary cilium development are unknown.

Directional control of centriole migration during formation of single or multiple cilia remains an open question. The Rho family GTPase Cdc42 has a central role in establishment of cell polarity and localisation of the PAR3-PAR6-atypical protein kinase C complex (reviewed by Suzuki and Ohno, 2006) to the membrane in diverse polarity pathways (Etienne-Manneville and Hall, 2001; Joberty et al., 2000). Re-orientation of the centrosome is one step in this process, and

he complex might thus function in centriole/basal body novements. A second complex, comprising the ransmembrane protein Crb3 and the apical proteins Pals1 and Patj, is also involved in mammalian epithelial polarity (Roh et al., 2003) (reviewed by Margolis and Borg, 2005). Moreover, the two complexes interact in epithelia (Hurd et al., 2003) and are required for ciliogenesis, interacting with the anterograde IFT motor KIF3 (Fan et al., 2004). Such associations between polarity determinants and the ciliogenesis machinery are intriguing and it is tempting to speculate that polarity complexes provide signals for centriole migration.

After migration, centrioles attach to the membrane and serve as basal bodies for ciliary elongation. Ultrastructural analysis has uncovered a plethora of accessory structures that are associated with centrioles and basal bodies (Fig. 1C), including centriolar satellites, transitional fibres, striated rootlets and basal feet, that are associated with both primary cilia and multi-ciliated epithelia. The timing of acquisition of these structures is unclear: transitional fibres and/or basal feet are found associated with migrating centrioles in some studies (Anderson and Brenner, 1971; Lemullois et al., 1988) but not in others (Frisch and Farbman, 1968; Hagiwara et al., 1992). However, when centriole migration is perturbed (Boisvieux-Ulrich et al., 1990), the centrioles that remain cytoplasmic acquire accessories. Subcellular location is therefore not the determining factor.

Diseases associated with dysfunctional ciliogenesis

An increasing number of genetic diseases are associated with defects in ciliogenesis or ciliary function (reviewed by Afzelius, 2004; Badano et al., 2006; Badano et al., 2005). These comprise a diverse group of pathologies including cystic kidney disease, infertility, retinal degeneration, hydrocephalus, laterality defects and chronic respiratory problems. Recent work has also identified cilia and basal body dysfunction as the underlying cause of various systemic diseases, including Bardet-Biedl, Alstrom, Orofaciodigital and Meckel syndromes (Andersen et al., 2003; Ansley et al., 2003; Kyttala et al., 2006; Romio et al., 2004), and these have expanded the range of ciliopathy phenotypes to include obesity, diabetes, hypertension and cardiac abnormalities (Badano et al., 2006). The affected tissues vary between diseases but all have motile or immotile cilia.

Most of the gene products implicated in the ciliopathies affect ciliary function (e.g. motility or signalling) rather than cilium formation. Others affect ciliogenesis itself. As discussed above, mice lacking the transcription factor FoxJ1 have laterality defects and a loss of cilia (Chen et al., 1998) due to a failure in centriole migration (Brody et al., 2000; Gomperts et al., 2004). A second protein, Seahorse, is implicated in polycystic kidney disease (Sun et al., 2004) and is required to regulate basal body duplication in *Trypanosoma brucei* (Morgan et al., 2005). Seahorse (also known as TbLRTP) localises to the distal part of the trypanosome basal body. Whereas overexpression of the protein suppresses flagellum assembly, RNA-interference experiments result in excess basal bodies; this suggests that Seahorse is a negative regulator of basal body duplication. Polycystic kidney disease and Bardet-Biedl syndrome can be caused by a failure in IFT (Blacque et al., 2004; Li et al., 2004; Ou et al., 2005; Pazour et al., 2000), the final stage of ciliogenesis. Finally, mice lacking the orofaciodigital syndrome gene *OFD1* show defective cilium formation (Ferrante et al., 2001). Based on the phenotypic overlap with Bardet-Biedl syndrome, a role for OFD1 in IFT has been proposed (Ferrante et al., 2001); however, because OFD1 is a centrosomal/basal body protein (Romio et al., 2004), it could also function in earlier stages of ciliogenesis.

Much work on elucidating the biology of cilia disease genes has been carried out in model organisms (e.g. Blacque et al., 2004; Dawe et al., 2005; Pazour et al., 2000; Sun et al., 2004). However, the question of why the defect affects some tissues and not others in mammalian systems is difficult to address in single-celled models. Presumably tissue-specific transcriptional control plays a part. Mice lacking the polycystic kidney disease gene product polycystin 1 have polycystic kidneys but no laterality defects, which correlates with the absence of polycystin 1 in nodal cilia (Karcher et al., 2005). Turnover is also likely to be important. Ciliary tubulin continually turns over (Stephens, 1999); however, the rate varies between tissues. The stability of the cilium and/or the cell probably also varies from tissue to tissue. Comparison of published flagellar proteomes (Broadhead et al., 2006; Ostrowski et al., 2002; Pazour et al., 2005; Smith et al., 2005) from a number of model organisms reveals a surprising diversity despite overall structural conservation (Broadhead et al., 2006). This suggests the canonical axonemal structure is dependent on a central cohort of conserved proteins plus organism, cell and tissue type elaborations. This diversity could contribute to tissue-specific functional specialisation.

Perspectives and conclusions

Despite recent advances, our knowledge of ciliogenesis is still largely confined to ultrastructural observations and scattered information on various proteins. A number of challenges remain. The signals that trigger assembly and disassembly of cilia in tissues are not well understood. It is probable that molecules that control the cell cycle will be involved, at least in cells that form a primary cilium, because the cilium is present in only a limited cell cycle window. Tight control of transcription and translation may be required because many cilia proteins bind or regulate cytoskeletal elements and may have a detrimental effect if released in large quantities into the cytosol.

The paucity of information on the protein constituents of cilia and basal bodies has hampered research. While several recent studies have sought to address this, so that there are now a number of flagellar (Broadhead et al., 2006; Ostrowski et al., 2002; Pazour et al., 2005; Smith et al., 2005) and centrosomal/centriolar (Andersen et al., 2003; Keller et al., 2005) proteomes from evolutionarily diverse organisms, primary cilia have not yet been subjected to proteomic analysis. The composition of the primary cilium is therefore unknown, although it is likely to contain several hundred proteins, including core components shared with motile cilia.

A major challenge is to elucidate the structure and function of the cellular networks that underlie ciliogenesis. Comparative genomics provides one approach to study this. Subtraction of the genomes of organisms that do not build cilia or flagella from those of flagellate organisms yields a dataset that should include regulatory factors as well as structural components (Avidor-Reiss et al., 2004; Li et al., 2004). Importantly, this approach will not identify proteins with cytosolic functions in

addition to roles in ciliogenesis (most obviously tubulin). Work with single-celled model organisms cannot, however, distinguish the mechanisms underlying primary cilium formation from those that organise a multiciliated epithelium.

Finally, altough the list of diseases associated with impaired cilia or basal body function is expanding at a tremendous rate, biology and physiology have not kept pace with the clinical genetics and we do not yet understand why defective cilia or basal bodies lead to such wide-ranging pathologies. Cilia and basal bodies are increasingly implicated in 21st century diseases such as heart disease, obesity and hypertension; yet the underlying mechanisms remain an open question. If we are to treat these diverse pathological conditions, we must focus our efforts on understanding the biology of these iconic but still rather cryptic organelles.

We thank Alison Faragher for electron micrographs of rat trachea. Work in our laboratory is funded by The Wellcome Trust, the BBSRC and the E. P. Abraham Trust. H.D. is a Beit Memorial Research Fellow; K.G. is a Wellcome Trust Principal Research Fellow.

References

Abughrien, B. M. and Dore, M. A. (2000). Ciliogenesis in the uterine tube of control and superovulated heifers. *Cells Tissues Organs* **166**, 338-348.

Afzelius, B. A. (1988). Microtubules in the spermatids of stick insects. *J. Ultrastruct. Mol. Struct. Res.* **98**, 94-102.

Afzelius, B. A. (2004). Cilia-related diseases. *J. Pathol.* **204**, 470-477.

Afzelius, B. A., Bellon, P. L. and Lanzavecchia, S. (1990). Microtubules and their protofilaments in the flagellum of an insect spermatozoon. *J. Cell Sci.* **95 (Pt 2)**, 207-217.

Alieva, I. B. and Vorobjev, I. A. (2004). Vertebrate primary cilia: a sensory part of centrosomal complex in tissue cells, but a "sleeping beauty" in cultured cells? *Cell Biol. Int.* **28**, 139-150.

Andersen, J. S., Wilkinson, C. J., Mayor, T., Mortensen, P., Nigg, E. A. and Mann, M. (2003). Proteomic characterization of the human centrosome by protein correlation profiling. *Nature* **426**, 570-574.

Anderson, R. G. and Brenner, R. M. (1971). The formation of basal bodies (centrioles) in the Rhesus monkey oviduct. *J. Cell Biol.* **50**, 10-34.

Andre, J. and Bernhard, W. (1964). The centriole and the centriolar region. *Excerpta Med. Int. Cong. Ser.* **77**, 9.

Ansley, S. J., Badano, J. L., Blacque, O. E., Hill, J., Hoskins, B. E., Leitch, C. C., Kim, J. C., Ross, A. J., Eichers, E. R., Teslovich, T. M. et al. (2003). Basal body dysfunction is a likely cause of pleiotropic Bardet-Biedl syndrome. *Nature* **425**, 628-633.

Avidor-Reiss, T., Maer, A. M., Koundakjian, E., Polyanovsky, A., Keil, T., Subramaniam, S. and Zuker, C. S. (2004). Decoding cilia function: defining specialized genes required for compartmentalized cilia biogenesis. *Cell* **117**, 527-539.

Badano, J. L., Teslovich, T. M. and Katsanis, N. (2005). The centrosome in human genetic disease. *Nat. Rev. Genet.* **6**, 194-205.

Badano, J. L., Mitsuma, N., Beales, P. L. and Katsanis, N. (2006). The Ciliopathies: An Emerging Class of Human Genetic Disorders. *Annu. Rev. Genomics Hum. Genet.* **7**, 125-148.

Balczon, R., Bao, L., Zimmer, W. E., Brown, K., Zinkowski, R. P. and Brinkley, B. R. (1995). Dissociation of centrosome replication events from cycles of DNA synthesis and mitotic division in hydroxyurea-arrested Chinese hamster ovary cells. *J. Cell Biol.* **130**, 105-115.

Beisson, J. and Wright, M. (2003). Basal body/centriole assembly and continuity. *Curr. Opin. Cell Biol.* **15**, 96-104.

Berdnik, D. and Knoblich, J. A. (2002). Drosophila Aurora-A is required for centrosome maturation and actin-dependent asymmetric protein localization during mitosis. *Curr. Biol.* **12**, 640-647.

Blacque, O. E., Reardon, M. J., Li, C., McCarthy, J., Mahjoub, M. R., Ansley, S. J., Badano, J. L., Mah, A. K., Beales, P. L., Davidson, W. S. et al. (2004). Loss of C. elegans BBS-7 and BBS-8 protein function results in cilia defects and compromised intraflagellar transport. *Genes Dev.* **18**, 1630-1642.

Blacque, O. E., Perens, E. A., Boroevich, K. A., Inglis, P. N., Li, C., Warner, A., Khattra, J., Holt, R. A., Ou, G., Mah, A. K. et al. (2005). Functional genomics of the cilium, a sensory organelle. *Curr. Biol.* **15**, 935-941.

Blatt, E. N., Yan, X. H., Wuerffel, M. K., Hamilos, D. L. and Brody, S. L. (1999). Forkhead transcription factor HFH-4 expression is temporally related to ciliogenesis. *Am. J. Respir. Cell Mol. Biol.* **21**, 168-176.

Boisvieux-Ulrich, E., Laine, M. C. and Sandoz, D. (1987). In vitro effects of benzodiazepines on ciliogenesis in the quail oviduct. *Cell Motil. Cytoskeleton* **8**, 333-344.

Boisvieux-Ulrich, E., Laine, M. C. and Sandoz, D. (1989). In vitro effects of colchicine and nocodazole on ciliogenesis in quail oviduct. *Biol. Cell* **67**, 67-79.

Boisvieux-Ulrich, E., Laine, M. C. and Sandoz, D. (1990). Cytochalasin D inhibits basal body migration and ciliary elongation in quail oviduct epithelium. *Cell Tissue Res.* **259**, 443-454.

Brenner, R. M. and Anderson, R. G. W. (1973). Endocrine control of ciliogenesis in the primate oviduct. In *Handbook of Physiology*, Vol. 2 (eds R. O. Greep and E. B. Astwood), pp. 123-139. Baltimore: Williams & Wilkins.

Broadhead, R., Dawe, H. R., Farr, H., Griffiths, S., Hart, S. R., Portman, N., Shaw, M. K., Ginger, M. L., Gaskell, S. J., McKean, P. G. et al. (2006). Flagellar motility is required for the viability of the bloodstream trypanosome. *Nature* **440**, 224-227.

Brody, S. L., Yan, X. H., Wuerffel, M. K., Song, S. K. and Shapiro, S. D. (2000). Ciliogenesis and left-right axis defects in forkhead factor HFH-4-null mice. *Am. J. Respir. Cell. Mol. Biol.* **23**, 45-51.

Burakov, A., Nadezhdina, E., Slepchenko, B. and Rodionov, V. (2003). Centrosome positioning in interphase cells. *J. Cell Biol.* **162**, 963-969.

Chang, J. P., Mayahara, H., Yoloyama, M., Ubukata, A. and Moller, P. C. (1979). An ultrastructural study of morphogenesis of fibrogranular complex and centriole in ductuli efferentes of Chinese hamster. *Tissue Cell* **11**, 401-412.

Chang, P., Giddings, T. H., Jr, Winey, M. and Stearns, T. (2003). Epsilon-tubulin is required for centriole duplication and microtubule organization. *Nat. Cell. Biol.* **5**, 71-76.

Chen, J., Knowles, H. J., Hebert, J. L. and Hackett, B. P. (1998). Mutation of the mouse hepatocyte nuclear factor/forkhead homologue 4 gene results in an absence of cilia and random left-right asymmetry. *J Clin. Invest.* **102**, 1077-1082.

Chevrier, V., Piel, M., Collomb, N., Saoudi, Y., Frank, R., Paintrand, M., Narumiya, S., Bornens, M. and Job, D. (2002). The Rho-associated protein kinase p160ROCK is required for centrosome positioning. *J. Cell Biol.* **157**, 807-817.

Collier, S. and Gubb, D. (1997). Drosophila tissue polarity requires the cell-autonomous activity of the fuzzy gene, which encodes a novel transmembrane protein. *Development* **124**, 4029-4037.

D'Assoro, A. B., Busby, R., Suino, K., Delva, E., Almodovar-Mercado, G. J., Johnson, H., Folk, C., Farrugia, D. J., Vasile, V., Stivala, F. et al. (2004). Genotoxic stress leads to centrosome amplification in breast cancer cell lines that have an inactive G1/S cell cycle checkpoint. *Oncogene* **23**, 4068-4075.

Davenport, J. R. and Yoder, B. K. (2005). An incredible decade for the primary cilium: a look at a once-forgotten organelle. *Am. J. Physiol. Renal. Physiol.* **289**, F1159-F1169.

Dawe, H. R., Farr, H., Portman, N., Shaw, M. K. and Gull, K. (2005). The Parkin co-regulated gene product, PACRG, is an evolutionarily conserved axonemal protein that functions in outer-doublet microtubule morphogenesis. *J. Cell Sci.* **118**, 5421-5430.

Dirksen, E. R. (1971). Centriole morphogenesis in developing ciliated epithelium of the mouse oviduct. *J. Cell Biol.* **51**, 286-302.

Dirksen, E. R. (1991). Centriole and basal body formation during ciliogenesis revisited. *Biol. Cell* **72**, 31-38.

Dirksen, E. R. and Crocker, T. T. (1966). Centriole replication in differentiating ciliated cells of mammalian respiratory epithelium. An electron microscope study. *J. Micr.* **5**, 639-644.

Dutcher, S. K. (1995). Flagellar assembly in two hundred and fifty easy-to-follow steps. *Trends Genet.* **11**, 398-404.

Efimenko, E., Bubb, K., Mak, H. Y., Holzman, T., Leroux, M. R., Ruvkun, G., Thomas, J. H. and Swoboda, P. (2005). Analysis of xbx genes in C. elegans. *Development* **132**, 1923-1934.

Etienne-Manneville, S. and Hall, A. (2001). Integrin-mediated activation of Cdc42 controls cell polarity in migrating astrocytes through PKCzeta. *Cell* **106**, 489-498.

Fan, S., Hurd, T. W., Liu, C. J., Straight, S. W., Weimbs, T., Hurd, E. A., Domino, S. E. and Margolis, B. (2004). Polarity proteins control ciliogenesis via kinesin motor interactions. *Curr. Biol.* **14**, 1451-1461.

Ferrante, M. I., Giorgio, G., Feather, S. A., Bulfone, A., Wright, V., Ghiani, M., Selicorni, A., Gammaro, L., Scolari, F., Woolf, A. S. et al. (2001). Identification of the gene for oral-facial-digital type I syndrome. *Am. J. Hum. Genet.* **68**, 569-576.

Flock, A. and Duvall, A. J., 3rd. (1965). The ultrastructure of the kinocilium of the sensory cells in the inner ear and lateral line organs. *J. Cell Biol.* **25**, 1-8.

Fouquet, J. P. and Kann, M. L. (1994). The cytoskeleton of mammalian spermatozoa. *Biol. Cell* **81**, 89-93.

Frisch, D. and Farbman, A. I. (1968). Development of order during ciliogenesis. *Anat. Rec.* **162**, 221-232.

Gadelha, C., Wickstead, B., McKean, P. G. and Gull, K. (2006). Basal body and flagellum mutants reveal a rotational constraint of the central pair microtubules in the axonemes of trypanosomes. *J. Cell Sci.* **119**, 2405-2413.

Gall, J. G. (1961). Centriole replication: a study of spermatogenesis in the snail, *Viviparus*. *J. Biochem. Biophys, Cytol.* **10**, 163-209.

Gherman, A., Davis, E. E. and Katsanis, N. (2006). The ciliary proteome database: an integrated community resource for the genetic and functional dissection of cilia. *Nat. Genet.* **38**, 961-962.

Gibbons, B. H. and Gibbons, I. R. (1973). The effect of partial extraction of dynein arms on the movement of reactivated sea-urchin sperm. *J. Cell Sci.* **13**, 337-357.

Gibbons, I. R. and Rowe, A. J. (1965). Dynein: a protein with adenosine triphosphatase activity from cilia. *Science* **149**, 424-426.

Gomperts, B. N., Gong-Cooper, X. and Hackett, B. P. (2004). Foxj1 regulates basal body anchoring to the cytoskeleton of ciliated pulmonary epithelial cells. *J. Cell Sci.* **117**, 1329-1337.

Gouin, E., Welch, M. D. and Cossart, P. (2005). Actin-based motility of intracellular pathogens. *Curr. Opin. Microbiol.* **8**, 35-45.

Gromley, A., Jurczyk, A., Sillibourne, J., Halilovic, E., Mogensen, M., Groisman, I.,

Blomberg, M. and Doxsey, S. (2003). A novel human protein of the maternal centriole is required for the final stages of cytokinesis and entry into S phase. *J. Cell Biol.* **161**, 535-545.

Hackett, B. P., Brody, S. L., Liang, M., Zeitz, I. D., Bruns, L. A. and Gitlin, J. D. (1995). Primary structure of hepatocyte nuclear factor/forkhead homologue 4 and characterization of gene expression in the developing respiratory and reproductive epithelium. *Proc. Natl. Acad. Sci. USA* **92**, 4249-4253.

Hackney, C. M., McCrohan, C. R. and Hawkins, S. J. (1983). Putative sense organs on the pallial tentacles of the limpet, Patella vulgata (L.). *Cell Tissue Res.* **231**, 663-674.

Hagiwara, H., Shibasaki, S. and Ohwada, N. (1992). Ciliogenesis in the human oviduct epithelium during the normal menstrual cycle. *J. Electron. Microsc. (Tokyo)* **41**, 321-329.

Hagiwara, H., Aoki, T., Ohwada, N. and Fujimoto, T. (2000). Identification of a 195 kDa protein in the striated rootlet: its expression in ciliated and ciliogenic cells. *Cell Motil. Cytoskeleton* **45**, 200-210.

Hagiwara, H., Harada, S., Maeda, S., Aoki, T., Ohwada, N. and Takata, K. (2002). Ultrastructural and immunohistochemical study of the basal apparatus of solitary cilia in the human oviduct epithelium. *J. Anat.* **200**, 89-96.

Hannak, E., Kirkham, M., Hyman, A. A. and Oegema, K. (2001). Aurora-A kinase is required for centrosome maturation in Caenorhabditis elegans. *J. Cell Biol.* **155**, 1109-1116.

Henneguy, L. F. (1898). Sur les rapports des cils vibratiles avec les centrosomes. *Archives d'Anatomie Microscopique* **Tome 1**, 481-496.

Hinchcliffe, E. H., Cassels, G. O., Rieder, C. L. and Sluder, G. (1998). The coordination of centrosome reproduction with nuclear events of the cell cycle in the sea urchin zygote. *J. Cell Biol.* **140**, 1417-1426.

Hinchcliffe, E. H., Li, C., Thompson, E. A., Maller, J. L. and Sluder, G. (1999). Requirement of Cdk2-cyclin E activity for repeated centrosome reproduction in Xenopus egg extracts. *Science* **283**, 851-854.

Hinchcliffe, E. H., Miller, F. J., Cham, M., Khodjakov, A. and Sluder, G. (2001). Requirement of a centrosomal activity for cell cycle progression through G1 into S phase. *Science* **291**, 1547-1550.

Hurd, T. W., Gao, L., Roh, M. H., Macara, I. G. and Margolis, B. (2003). Direct interaction of two polarity complexes implicated in epithelial tight junction assembly. *Nat. Cell. Biol.* **5**, 137-142.

Ishikawa, H., Kubo, A., Tsukita, S. and Tsukita, S. (2005). Odf2-deficient mother centrioles lack distal/subdistal appendages and the ability to generate primary cilia. *Nat. Cell. Biol.* **7**, 517-524.

Jensen, C. G., Poole, C. A., McGlashan, S. R., Marko, M., Issa, Z. I., Vujcich, K. V. and Bowser, S. S. (2004). Ultrastructural, tomographic and confocal imaging of the chondrocyte primary cilium in situ. *Cell Biol. Int.* **28**, 101-110.

Joberty, G., Petersen, C., Gao, L. and Macara, I. G. (2000). The cell-polarity protein Par6 links Par3 and atypical protein kinase C to Cdc42. *Nat. Cell. Biol.* **2**, 531-539.

Kalnins, V. I., Chung, C. K. and Turnbull, C. (1972). Procentrioles in ciliating and ciliated cells of chick trachea. *Z. Zellforsch. Mikrosk. Anat.* **135**, 461-471.

Karcher, C., Fischer, A., Schweickert, A., Bitzer, E., Horie, S., Witzgall, R. and Blum, M. (2005). Lack of a laterality phenotype in Pkd1 knock-out embryos correlates with absence of polycystin-1 in nodal cilia. *Differentiation* **73**, 425-432.

Karsenti, E. (1999). Centrioles reveal their secrets. *Nat. Cell. Biol.* **1**, E62-E64.

Keller, L. C., Romijn, E. P., Zamora, I., Yates, J. R., 3rd and Marshall, W. F. (2005). Proteomic analysis of isolated chlamydomonas centrioles reveals orthologs of ciliary-disease genes. *Curr. Biol.* **15**, 1090-1098.

Klotz, C., Bordes, N., Laine, M. C., Sandoz, D. and Bornens, M. (1986). Myosin at the apical pole of ciliated epithelial cells as revealed by a monoclonal antibody. *J. Cell Biol.* **103**, 613-619.

Kochanski, R. S. and Borisy, G. G. (1990). Mode of centriole duplication and distribution. *J. Cell Biol.* **110**, 1599-1605.

Kubo, A., Sasaki, H., Yuba-Kubo, A., Tsukita, S. and Shiina, N. (1999). Centriolar satellites: molecular characterization, ATP-dependent movement toward centrioles and possible involvement in ciliogenesis. *J. Cell Biol.* **147**, 969-980.

Kyttala, M., Tallila, J., Salonen, R., Kopra, O., Kohlschmidt, N., Paavola-Sakki, P., Peltonen, L. and Kestila, M. (2006). MKS1, encoding a component of the flagellar apparatus basal body proteome, is mutated in Meckel syndrome. *Nat. Genet.* **38**, 155-157.

La Terra, S., English, C. N., Hergert, P., McEwen, B. F., Sluder, G. and Khodjakov, A. (2005). The de novo centriole assembly pathway in HeLa cells: cell cycle progression and centriole assembly/maturation. *J. Cell Biol.* **168**, 713-722.

Lane, H. A. and Nigg, E. A. (1996). Antibody microinjection reveals an essential role for human polo-like kinase 1 (Plk1) in the functional maturation of mitotic centrosomes. *J. Cell Biol.* **135**, 1701-1713.

Lange, B. M. and Gull, K. (1995). A molecular marker for centriole maturation in the mammalian cell cycle. *J. Cell Biol.* **130**, 919-927.

Lange, B. M. and Gull, K. (1996). Structure and function of the centriole in animal cells: progress and questions. *Trends Cell. Biol.* **6**, 348-352.

Laoukili, J., Perret, E., Middendorp, S., Houcine, O., Guennou, C., Marano, F., Bornens, M. and Tournier, F. (2000). Differential expression and cellular distribution of centrin isoforms during human ciliated cell differentiation in vitro. *J. Cell Sci.* **113 (Pt 8)**, 1355-1364.

Lemullois, M., Klotz, C. and Sandoz, D. (1987). Immunocytochemical localization of myosin during ciliogenesis of quail oviduct. *Eur. J. Cell Biol.* **43**, 429-437.

Lemullois, M., Boisvieux-Ulrich, E., Laine, M. C., Chailley, B. and Sandoz, D. (1988). Development and functions of the cytoskeleton during ciliogenesis in metazoa. *Biol. Cell* **63**, 195-208.

Lenhossek, M. (1898). Ueber Flimmerzellen. *Verhandl. der Anat. Gesel.* **12**, 106-128.

Li, J. B., Gerdes, J. M., Haycraft, C. J., Fan, Y., Teslovich, T. M., May-Simera, H., Li, H., Blacque, O. E., Li, L., Leitch, C. C. et al. (2004). Comparative genomics identifies a flagellar and basal body proteome that includes the BBS5 human disease gene. *Cell* **117**, 541-552.

Lim, L., Zhou, H. and Costa, R. H. (1997). The winged helix transcription factor HFH-4 is expressed during choroid plexus epithelial development in the mouse embryo. *Proc. Natl. Acad. Sci. USA* **94**, 3094-3099.

Lino-Neto, J. and Dolder, H. (2002). Sperm structure and ultrastructure of the fire ant Solenopsis invicta (Buren) (Hymenoptera, Formicidae). *Tissue Cell* **34**, 124-128.

Lino-Neto, J., Bao, S. N. and Dolder, H. (2000). Sperm ultrastructure of the honey bee (Apis mellifera) (L) (Hymenoptera, Apidae) with emphasis on the nucleus-flagellum transition region. *Tissue Cell* **32**, 322-327.

Machesky, L. M. (1999). Rocket-based motility: a universal mechanism? *Nat. Cell. Biol.* **1**, E29-E31.

Maga, J. A. and LeBowitz, J. H. (1999). Unravelling the kinetoplastid paraflagellar rod. *Trends Cell. Biol.* **9**, 409-413.

Margolis, B. and Borg, J. P. (2005). Apicobasal polarity complexes. *J. Cell Sci.* **118**, 5157-5159.

Mencarelli, C., Lupetti, P., Rosetto, M. and Dallai, R. (2000). Morphogenesis of the giant sperm axoneme in Asphondylia ruebsaameni Kertesz (Diptera, Cecidomyiidae). *Tissue Cell* **32**, 188-197.

Meraldi, P., Lukas, J., Fry, A. M., Bartek, J. and Nigg, E. A. (1999). Centrosome duplication in mammalian somatic cells requires E2F and Cdk2-cyclin A. *Nat. Cell. Biol.* **1**, 88-93.

Mitchell, D. R. (2003). Orientation of the central pair complex during flagellar bend formation in Chlamydomonas. *Cell. Motil. Cytoskeleton.* **56**, 120-129.

Mizukami, J. and Gall, J. G. (1966). Centriole replication II: sperm formation in the fern *Marsilea*, and the Cycad *Zamia*. *J. Cell Biol.* **29**, 97-111.

Mogensen, M. M., Malik, A., Piel, M., Bouckson-Castaing, V. and Bornens, M. (2000). Microtubule minus-end anchorage at centrosomal and non-centrosomal sites: the role of ninein. *J. Cell Sci.* **113 (Pt 17)**, 3013-3023.

Morgan, G. W., Denny, P. W., Vaughan, S., Goulding, D., Jeffries, T. R., Smith, D. F., Gull, K. and Field, M. C. (2005). An evolutionarily conserved coiled-coil protein implicated in polycystic kidney disease is involved in basal body duplication and flagellar biogenesis in Trypanosoma brucei. *Mol. Cell. Biol.* **25**, 3774-3783.

Myles, D. G. (1975). An ultrastructural study of the spermatozoid of the fern, Marsilea vestita. *J. Cell Sci.* **17**, 633-645.

Omoto, C. K. and Kung, C. (1979). The pair of central tubules rotates during ciliary beat in Paramecium. *Nature* **279**, 532-534.

Omoto, C. K. and Kung, C. (1980). Rotation and twist of the central-pair microtubules in the cilia of Paramecium. *J. Cell Biol.* **87**, 33-46.

Ostrowski, L. E., Blackburn, K., Radde, K. M., Moyer, M. B., Schlatzer, D. M., Moseley, A. and Boucher, R. C. (2002). A proteomic analysis of human cilia: identification of novel components. *Mol. Cell Proteomics* **1**, 451-465.

Ou, G., Blacque, O. E., Snow, J. J., Leroux, M. R. and Scholey, J. M. (2005). Functional coordination of intraflagellar transport motors. *Nature* **436**, 583-587.

Ou, Y. Y., Mack, G. J., Zhang, M. and Rattner, J. B. (2002). CEP110 and ninein are located in a specific domain of the centrosome associated with centrosome maturation. *J. Cell Sci.* **115**, 1825-1835.

Paintrand, M., Moudjou, M., Delacroix, H. and Bornens, M. (1992). Centrosome organization and centriole architecture: their sensitivity to divalent cations. *J. Struct. Biol.* **108**, 107-128.

Park, T. J., Haigo, S. L. and Wallingford, J. B. (2006). Ciliogenesis defects in embryos lacking inturned or fuzzy function are associated with failure of planar cell polarity and Hedgehog signaling. *Nat. Genet.* **38**, 303-311.

Park, W. J., Liu, J., Sharp, E. J. and Adler, P. N. (1996). The Drosophila tissue polarity gene inturned acts cell autonomously and encodes a novel protein. *Development* **122**, 961-969.

Pazour, G. J., Dickert, B. L., Vucica, Y., Seeley, E. S., Rosenbaum, J. L., Witman, G. B. and Cole, D. G. (2000). Chlamydomonas IFT88 and its mouse homologue, polycystic kidney disease gene tg737, are required for assembly of cilia and flagella. *J. Cell Biol.* **151**, 709-718.

Pazour, G. J., Agrin, N., Leszyk, J. and Witman, G. B. (2005). Proteomic analysis of a eukaryotic cilium. *J. Cell Biol.* **170**, 103-113.

Pelletier, G. J., Brody, S. L., Liapis, H., White, R. A. and Hackett, B. P. (1998). A human forkhead/winged-helix transcription factor expressed in developing pulmonary and renal epithelium. *Am. J. Physiol.* **274**, L351-L359.

Phillips, D. M. (1969). Exceptions to the prevailing pattern of tubules (9 + 9 + 2) in the sperm flagella of certain insect species. *J. Cell Biol.* **40**, 28-43.

Phillips, D. W. (1979). Ultrastructure of sensory cells on the mantle tentacles of the gastropod Notoacmea scutum. *Tissue Cell* **11**, 623-632.

Renaud, F. L. and Swift, H. (1964). The development of basal bodies and flagella in *Allomyces arbusculus*. *J. Cell Biol.* **23**, 339-354.

Roh, M. H., Fan, S., Liu, C. J. and Margolis, B. (2003). The Crumbs3-Pals1 complex participates in the establishment of polarity in mammalian epithelial cells. *J. Cell Sci.* **116**, 2895-2906.

Romio, L., Fry, A. M., Winyard, P. J., Malcolm, S., Woolf, A. S. and Feather, S. A. (2004). OFD1 is a centrosomal/basal body protein expressed during mesenchymal-epithelial transition in human nephrogenesis. *J. Am. Soc. Nephrol.* **15**, 2556-2568.

Rosenbaum, J. L. and Witman, G. B. (2002). Intraflagellar transport. *Nat. Rev. Mol. Cell. Biol.* **3**, 813-825.

Sale, W. S. (1986). The axonemal axis and Ca^{2+}-induced asymmetry of active microtubule sliding in sea urchin sperm tails. *J. Cell Biol.* **102**, 2042-2052.

Scholey, J. M. (2003). Intraflagellar transport. *Annu. Rev. Cell Dev. Biol.* **19**, 423-443.

Scholey, J. M. and Anderson, K. V. (2006). Intraflagellar transport and cilium-based signaling. *Cell* **125**, 439-442.

Sherwin, T. and Gull, K. (1989). The cell division cycle of Trypanosoma brucei brucei: timing of event markers and cytoskeletal modulations. *Philos. Trans R. Soc. Lond. B. Biol. Sci.* **323**, 573-588.

Silflow, C. D. and Lefebvre, P. A. (2001). Assembly and motility of eukaryotic cilia and flagella. Lessons from Chlamydomonas reinhardtii. *Plant Physiol.* **127**, 1500-1507.

Sluder, G. and Hinchcliffe, E. H. (1998). The apparent linkage between centriole replication and the S phase of the cell cycle. *Cell Biol. Int.* **22**, 3-5.

Smith, J. C., Northey, J. G., Garg, J., Pearlman, R. E. and Siu, K. W. (2005). Robust method for proteome analysis by MS/MS using an entire translated genome: demonstration on the ciliome of Tetrahymena thermophila. *J. Proteome Res.* **4**, 909-919.

Sobkowicz, H. M., Slapnick, S. M. and August, B. K. (1995). The kinocilium of auditory hair cells and evidence for its morphogenetic role during the regeneration of stereocilia and cuticular plates. *J. Neurocytol.* **24**, 633-653.

Sorokin, S. P. (1968). Reconstructions of centriole formation and ciliogenesis in mammalian lungs. *J. Cell Sci.* **3**, 207-230.

Sorokin, S. P. and Adelstein, S. J. (1967). Failure of 1100 rads X-radiation to affect ciliogenesis and centriolar formation in cultured rat lungs. *Radiation Res.* **31**, 748-759.

Steinman, R. M. (1968). An electron microscopic study of ciliogenesis in developing epidermis and trachea in the embryo of *Xenopus laevis*. *Am. J. Anat.* **122**, 19-56.

Stephens, R. E. (1999). Turnover of tubulin in ciliary outer doublet microtubules. *Cell Struct. Funct.* **24**, 413-418.

Stolc, V., Samanta, M. P., Tongprasit, W. and Marshall, W. F. (2005). Genome-wide transcriptional analysis of flagellar regeneration in Chlamydomonas reinhardtii identifies orthologs of ciliary disease genes. *Proc. Natl. Acad. Sci. USA* **102**, 3703-3707.

Sun, Z., Amsterdam, A., Pazour, G. J., Cole, D. G., Miller, M. S. and Hopkins, N. (2004). A genetic screen in zebrafish identifies cilia genes as a principal cause of cystic kidney. *Development* **131**, 4085-4093.

Suzuki, A. and Ohno, S. (2006). The PAR-aPKC system: lessons in polarity. *J. Cell Sci.* **119**, 979-987.

Tamm, S. L. and Tamm, S. (1981). Ciliary reversal without rotation of axonemal structures in ctenophore comb plates. *J. Cell Biol.* **89**, 495-509.

Tamm, S. and Tamm, S. L. (1988). Development of macrociliary cells in Beroe. I. Actin bundles and centriole migration. *J. Cell Sci.* **89 (Pt 1)**, 67-80.

Tichelaar, J. W., Wert, S. E., Costa, R. H., Kimura, S. and Whitsett, J. A. (1999). HNF-3/forkhead homologue-4 (HFH-4) is expressed in ciliated epithelial cells in the developing mouse lung. *J. Histochem. Cytochem.* **47**, 823-832.

Tsou, M. F. and Stearns, T. (2006). Mechanism limiting centrosome duplication to once per cell cycle. *Nature.* **442**, 947-951.

Vaughn, K. C. and Renzaglia, K. S. (2006). Structural and immunocytochemical characterization of the Ginkgo biloba L. sperm motility apparatus. *Protoplasma* **227**, 165-173.

Vorobjev, I. A. and Nadezhdina, E. S. (1987). The centrosome and its role in the organization of microtubules. *Int. Rev. Cytol.* **106**, 227-293.

Vorobjev, I. A. and Chentsov, Yu, S. (1982). Centrioles in the cell cycle. I. Epithelial cells. *J. Cell Biol.* **93**, 938-949.

Wheatley, D. N., Wang, A. M. and Strugnell, G. E. (1996). Expression of primary cilia in mammalian cells. *Cell Biol. Int.* **20**, 73-81.

Wong, C. and Stearns, T. (2003). Centrosome number is controlled by a centrosome-intrinsic block to reduplication. *Nat. Cell. Biol.* **5**, 539-544.

Zou, C., Li, J., Bai, Y., Gunning, W. T., Wazer, D. E., Band, V. and Gao, Q. (2005). Centrobin: a novel daughter centriole-associated protein that is required for centriole duplication. *J. Cell Biol.* **171**, 437-445.